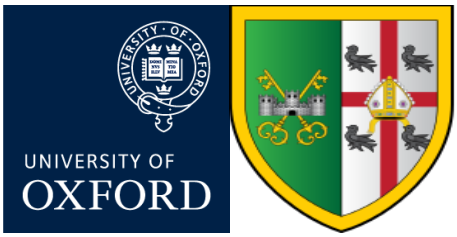
DIELECTRIC MEASUREMENTS AND CATALYTIC CRACKING OF HEAVY OILS USING ADVANCED MICROWAVE TECHNOLOGIES

Afrah Mohammed Aldawsari

St. Peter's College, University of Oxford



A thesis submitted to the Department of Chemistry, University of Oxford for the Degree of Doctor of Philosophy in Inorganic Chemistry

Supervisor

Prof. Peter P. Edwards FRS ML

Trinity Term 2016

The work described in this thesis was performed in the Inorganic Chemistry Laboratory, University of Oxford from October 2012 until September 2016, under the complete supervision of Professor Peter P. Edwards. All of the work is my own unless otherwise stated and has not been submitted previously for any other degree at this or any other university.

Afrah M. Aldawsari

October 2016

Acknowledgements

First and foremost I would like to acknowledge God for the strength, inspiration, and encouragement given to me from the initial phases to the completion of this thesis. I would like to extend my deepest gratitude to my supervisor, Professor Peter P. Edwards who has patiently supported me with his skills and knowledge throughout the progress of my research work. Without his continuous encouragement and support, this study would not be completed.

I would like to thank Professor Hamid Al-Megren for encouraging me throughout my research and for the advice on both types of research as well as on future career; his contribution is priceless.

It is an honour for me to be part of the King Abdulaziz City for Science and Technology (KACST) projects and for this I would like to take the opportunity to express my special appreciation and thanks to H.H. Prince Dr. Turki bin Saud bin Mohammed Al-Saud for all the help and the generous support he provided to KOPRC to move forward and reach what we have achieved today.

I would like to extend my words of appreciation to Dr. Vladimir Kuznetsov, Dr. Tiancun Xiao, Dr. Liam France and Dr. Mohammed Al-Kinany for always being there and for their support, guidance, and valuable advice during the research experiment.

I attribute the level of my DPhil. degree to the encouragement and effort I have been receiving from Dr. Daniel Slocombe and Dr. Sergio Gonzalez-Cortes. Without you, all this thesis would not have been completed. Thanks to Dan for all the knowledge he shared with me and being patient with all my questions about microwave. Thanks to Sergio for all the knowledge he shared with me about catalysts and refinery process, and for all the great times, all the talks, scientific discussions, and laughs that lighted up my time in Oxford lab.

I would like to express my deepest appreciation to professor Michael Mingos for all the insightful comments and helpful discussions.

My deepest heartfelt appreciation goes to Mrs. Linda Webb I cannot ever thank you enough for all you have done for me during the entire period of the study.

I would like to thank my friends Nazanin Rashidi and Nurul Akmal for making the office such a lovely place as a second home.

I am indebted to my KOPRC colleagues: Mr. Bonan Liu, Mr. Pirzada Pirzada, Mr. Xian Du, Mr. Zhaoxi Zhango, Dr. Himanshu Jain, and Dr. Benzhen Yao, thank you for all the great times and fun we have had in the last few years.

I am also indebted to Alex Vai, Andrew Seel, Josh Makepeace for their kind help while I was accomplishing this project.

Great amount of appreciation goes to the university mechanical workshop people for all the help in fabricating and fixing all the microwave cavities Samuel Davies, and Charles Evans.

I would like to gratefully acknowledge the help and support I have received form my Nottinghamian friends Raghad Allwihan and Dr Mazen Mansouri.

My Oxonion friends, Mrs Aljawhara Alquhaidan, Hanan Alqarashi, Maha Alurimi, Charline Alfodari and her lovely family, Mr Alaa Mansour, Amanda, Madoka, and Wie Ze You made my life here truly memorable experience and your friendships are invaluable to me.

Dearest dad Mohammad, Beloved mom Huda, your endless support, your love, and faith in me is what has brought me here today.

My older sister and brother Ashwaq and Fahad, my soul mates, your hand in my hand, makes my dreams come true.

My younger sister and brother Nosa and Badr, your love and continuous support have meant a lot to me.

Last and not least, My UK journey friends, Nouf Abuhadi, Hasna Alqahtani, Sarah Taj, Shereen Jamalalddeen, I'm so grateful to the place that brought us together and even if we go back to different countries, I know that I have sisters for life.

Afrah Aldawsari

2016

To my beloved parents..

and my wonderful siblings..

DIELECTRIC MEASUREMENTS AND CATALYTIC CRACKING OF HEAVY OILS USING ADVANCED MICROWAVE TECHNOLOGIES

Afrah Aldawsari, St Peter's College

A thesis submitted to the Department of Chemistry, University of Oxford for the Degree of Doctor of Philosophy in Inorganic Chemistry

Abstract

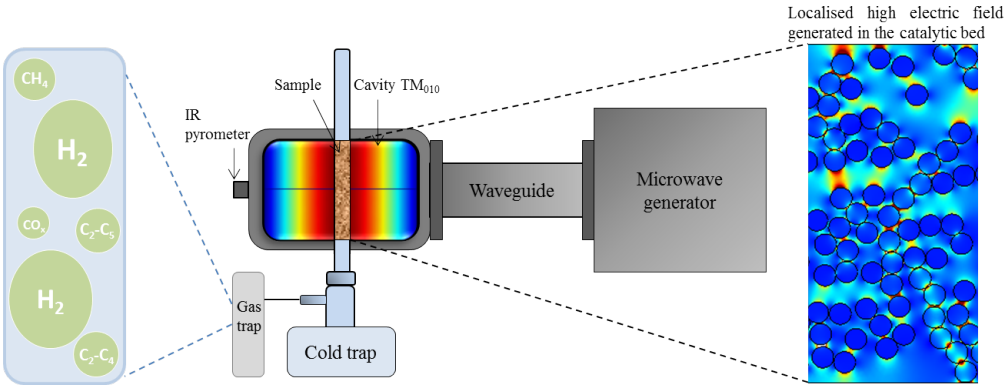
The continuously growing world demands of petroleum to service the domestic and industrial electricity, transportation sectors, and its contribution to Climate Change, places onus on researchers to find more efficient methods for heavy oil (petroleum) processing. Given the enormous quantities of petroleum processed in the world, and the general prevalence of high energy cost and high carbon footprint processing technologies, there is strong interest in development of more efficient and improved unconventional processing methods. This thesis contributes to the field of unconventional processing methods for petroleum. We investigate the utility of microwave irradiation for efficient chemical activation for the processing of petroleum to useful products, and demonstrate that the selective and targeted dissipation of microwave energy has great potential to deliver shorter reaction times compared to conventional cracking processes driven by thermal energy.

Heavy bunker oil, which is the starting feedstock for petroleum processing, is a thick and viscous material. Furthermore, it is not a good absorber of microwave energy due to the presence of non-polar heavy fractions such as hydrocarbons, sulphur, and nitrogen compounds. Such characteristics make microwave processing of petroleum especially challenging. As the essential first step, the elucidation of microwave response properties of petroleum is one of the key outcomes of this thesis. This was accomplished by a systematic investigation of dielectric properties of model chemical compounds and oil samples using the cavity perturbation technique at 2.45 GHz.

The zeolite HZSM-5 is widely recognized among the best catalysts for the production of high value light products from petroleum, and was employed for our studies. The dielectric properties of the zeolite were evaluated at room, and at higher temperatures up 500°C to gain insight into the behaviour of the sample (catalyst and oil) in a microwave energy driven catalytic cracking reaction. Generally, we found that the permittivity of the zeolite increases as the temperature increases. We attribute this to the enhancement in polarisation, as well as to a temperature dependent microwave conductivity, which occurs via proton hopping mechanism.

We have systematically explored libraries of dielectric materials to understand the materials interaction with microwave energy. This has allowed us to investigate the variation of microwave energy dissipation and cracking reactions for various catalyst-petroleum systems.

The optimisation of microwave applicator parameters using a model compound (decane) was performed. This indicated a clear difference in product distribution between thermal and microwave processing and an enhanced fraction of hydrogen and olefins were observed under microwave irradiation. We ascribe this observation to the difference in heat generation mechanism between the two modes. The microwave applicator was used to study heavy oil cracking it was found it is possible to conduct an efficient cracking reaction over appropriately modified zeolite. We should particularly highlight our results, whereby we demonstrate the production of large fraction of hydrogen over metal oxide doped HZSM-5 zeolite.



It was found that the cracking reactions of the heavy oil over zeolite are influenced by the high electric field, which can result in highly localised superheating within the catalytic material. The heavy oil impregnated metal oxide-zeolite displayed significant temperature gradients between the catalyst particles hotspot and the surrounding domains compared to the non-modified zeolite. Thus, the dehydrogenation process and the release of hydrogen were found to be enhanced in the decomposition of metal oxide-HZSM-5 zeolite compared to the pure HZSM-5.

Further enhancement of our system to a continuous flow reaction was performed in order to assess the potential for industrial applications of heavy oil cracking processes using microwave technology. This would be a critical step to demonstrate the scalability of our techniques. However, the results presented in this thesis reliably demonstrate that a significantly enhanced performance at lab scale system in shorter reaction times could be achieved through the cracking of heavy oil to hydrogen and high value light products.

Contents

Declaration ii

Acknowledgements iii

Abstract vi

Glossary 11

Symbols 13

1 INTRODUCTION TO HEAVY OIL 14

1.1 Historical Background 14

1.2 Crude Oil Classifications 15

1.2.1 Heavy Oil Chemistry 17

1.3 Conventional Methods for Heavy Oil Processing 19

1.3.1 Cracking 21

1.3.1.1 Thermal Cracking 21

1.3.1.2 Hydrocracking 21

1.3.1.3 Catalytic Cracking 21

1.4 Microwave Technology in the Petrochemical Industry 22

1.5 Thesis Objectives 26

2 THE INTERACTION OF MICROWAVES WITH MATTER 33

2.1 Introduction 33

2.2 The Electromagnetic Field . . . 34
2.2.1 Electric and Magnetic Fields . . . 36
2.3 Microwave Interaction with Materials . . . 39
2.4 Microwave Heating Mechanisms . . . 40
2.4.1 Polarisation . . . 43
2.4.1.1 Electronic Polarisation . . . 45
2.4.1.2 Orientational Polarisation . . . 45
2.4.1.3 Ionic Polarisation . . . 45
2.4.1.4 Interfacial Polarisation . . . 46
2.5 Penetration Depth . . . 47
2.6 Dielectric Measurement Techniques . . . 48
2.6.1 Transmission Techniques . . . 49
2.6.2 Open Coaxial Probe Techniques . . . 49
2.6.3 Resonant Cavity Techniques . . . 50
2.7 Microwave Heating Applicators . . . 50
2.7.1 Single-Mode System . . . 50
2.7.2 Multi-Mode System . . . 51

3 INTRODUCTION TO ZEOLITES 57

3.1 Structure and Properties of the Zeolite . . . 57
3.2 The Structure and Properties of ZSM-5 Catalyst . . . 60
3.3 Zeolite in Industry . . . 61
3.4 ZSM-5 Catalyst for Olefin Production . . . 62

4 EXPERIMENTAL METHODS 67

4.1 Cavity Perturbation Technique . . . 67
4.1.1 Introduction and Background . . . 67
4.1.2 Cavity Resonator Fields and Analysis . . . 68
4.1.3 General Aspects of Designing the Cavity . . . 72
4.1.3.1 Resonant Frequency . . . 72
4.1.3.2 Finite Element Modelling using COMSOL Multiphysics® . . . 73

4.1.3.3 TM_{010} Mode . . . 74
4.1.4 Quality Factor of the Cavity . . . 76
4.1.5 Sample Depolarisation . . . 78
4.1.6 Instrumentation for Dielectric Measurements . . . 81
4.1.6.1 Calibrations and Corrections . . . 85
4.2 Single Mode Applicator for Microwave Heating System . . . 87
4.2.1 Equipment Design Requirements . . . 88
4.2.1.1 Microwave Power Supplied/Absorbed . . . 88
4.2.1.2 Pulse Width Modulation . . . 89
4.2.1.3 Field Distributions and Field Uniformity . . . 90
4.2.1.4 Temperature Control and Ramp Rate . . . 91
4.2.1.5 Temperature Measurements . . . 91
4.2.1.6 Applicator Design . . . 92
4.2.1.7 Command and Control . . . 93
4.2.1.8 Microwave Design Safety Issues . . . 94
4.2.2 Microwave System Specification and Build . . . 94
4.2.2.1 Configuration and Details . . . 94
4.2.2.2 Microwave System Technical Details and Specifications . . . 95
4.2.2.3 Software . . . 97
4.2.2.4 Calibration and Testing . . . 101
4.3 X-Ray Diffraction - XRD . . . 102
4.3.1 Basic Theory of XRD and Bragg's Law . . . 103
4.3.2 Instrumentation . . . 104
4.3.3 Data Collection . . . 105
4.4 Thermogravimetric Analysis (TGA) . . . 105
4.4.1 Instrumentation . . . 106
4.5 Gas Chromatography (GC) . . . 107
4.5.1 Detectors . . . 108
4.5.1.1 Flame Ionisation Detector (FID) . . . 108
4.5.1.2 Thermal Conductivity Detector (TCD) . . . 108

4.5.2 Instrumentation . . . 109
4.6 Gas Chromatography/Mass Spectrometry (GC/MS) . . . 109
4.6.1 Introduction . . . 109
4.6.2 Detectors . . . 110
4.6.3 Instrumentation . . . 110
4.7 Scanning Electron Microscopy (SEM) . . . 111
4.7.1 Introduction . . . 111
4.7.2 Principle of SEM . . . 111
4.7.3 Instrumentation . . . 112
4.8 Transmission Electron Microscopy (TEM) . . . 113
4.8.1 Principle of TEM . . . 113
4.8.2 Instrumentation . . . 115

5 DIELECTRIC MEASUREMENTS AT ROOM TEMPERATURE 122

5.1 Introduction . . . 122
5.2 Experimental . . . 124
5.2.1 Materials . . . 124
5.2.2 Dielectric Measurements . . . 125
5.2.3 Microwave Heating . . . 125
5.3 Results and Discussion . . . 125
5.3.1 Linear Alkanes and Heavy Oil . . . 125
5.3.2 Oil Samples . . . 145
5.3.3 Zeolite Samples . . . 150
5.4 Conclusions and Future Work . . . 156

6 STUDY OF DIELECTRIC PROPERTIES AT HIGH TEMPERATURES 163

6.1 Microwave Measurement . . . 164
6.1.1 Setup . . . 164
6.1.2 Procedure . . . 165
6.2 Results and Discussion . . . 167
6.2.1 Heavy Oil Sample . . . 169

6.2.2 HZSM-5 Zeolite . . . 172
6.2.3 Heavy Oil Impregnated into HZSM-5 (Fresh Sample) . . . 177
6.2.4 Heavy Oil Impregnated into ZSM-5 (Spent Sample) . . . 180
6.3 Conclusions and Future Outlook . . . 183

7 STUDY FOR CONTROLLING SINGLE-MODE APPLICATOR IN MICROWAVE HEATING REACTIONS 188

7.1 Introduction . . . 189
7.2 Materials and Method . . . 190
7.3 Result and Discussion . . . 191
7.3.1 Effect of Microwave Parameters . . . 192
7.3.1.1 Microwave versus Conventional Heating . . . 192
7.3.1.2 Power Input Level . . . 197
7.3.1.3 Heating Rate . . . 198
7.3.1.4 Microwave Power Delivery Using Pulsing and Continuous Irradiation . . . 200
7.3.2 Effect of Sample Parameters . . . 204
7.4 Conclusions and Future Work . . . 208

8 MICROWAVE-ASSISTED HEAVY OIL UPGRADING 213

8.1 Introduction . . . 213
8.2 Experimental . . . 215
8.2.1 Catalyst Preparation . . . 215
8.2.2 Experimental Setup . . . 216
8.2.3 Gas Chromatography (GC) . . . 217
8.2.4 Dielectric Measurements . . . 217
8.2.5 X-Ray Diffraction (XRD) . . . 218
8.2.6 Thermogravimetric Analysis (TGA) . . . 218
8.2.7 Scanning Electron Microscopy (SEM)/ Transmission Electron Microscopy (TEM) . . . 218
8.3 Results and discussion . . . 218

8.3.1 Heavy Oil Processing using HZSM-5 Catalyst . . . 218
8.3.2 HZSM-5 Catalyst Impregnated with Transition Metal Oxides . . . 228
8.3.3 The Impregnation of Lanthanum Oxide into HZSM-5 . . . 244
8.3.4 Enhanced Batch Reactor System for Catalytic Activity Evaluation . . . 250
8.3.5 Adopting a Continuous Flow System into Microwave Reactor . . . 252
8.4 Conclusions and Future Work . . . 256

9 CONCLUSIONS AND FUTURE WORK 262
9.1 Conclusions . . . 262
9.2 Future Work . . . 267
9.2.1 High Temperature Dielectric Measurements . . . 267
9.2.2 Microwave Single Mode Applicator . . . 267
9.2.3 Purification of the Produced Hydrogen . . . 268
9.2.4 Catalyst Configuration and Regeneration . . . 268
9.3 Scaling Up Considerations . . . 269

A THE CHEMICAL PROPERTIES OF MODEL COMPOUNDS AND HEAVY OIL 273
A.1 1-Model compounds . . . 273
A.2 2-Oil samples analyses . . . 275
A.2.1 Bunker oil . . . 275
A.2.2 Crude oil . . . 275
A.2.3 Pyrolysis oil . . . 276

B PRODUCT DISTRIBUTION IN VOL.% 277

C TGA ANALYSIS FOR COKE CONTENT 280

D CALCULATIONS 282
D.1 Mass balance calculations . . . 282
D.2 Error calculations . . . 282

List of Figures

1.1 Schematic representation of the crude oil in terms of density in addition to a mixture of components which might be all included an oil sample and can be separated into these and other products in oil refinery. Reproduced from Ref. [14]. 16

1.2 Shows the density and sulphur content of different classifications of crude oil around the world [20]. 17

1.3 World Oil Demand [27]. 19

1.4 Typical distillation column in oil refinery [28]. 20

2.1 The components of the electromagnetic wave [15]. 35

2.2 The electromagnetic spectrum, showing the scale of the wavelengths that corresponding to the microwave frequency in meter [17]. 36

2.3 Illustrating the charge separation in two parallel conducting plates causing an internal electric field [20]. 37

2.4 Magnetic field lines for a coil of a current loop [22]. 38

2.5 The interaction between microwaves and different types of materials. 40

2.6 The dipole rotation and ionic conduction mechanisms after introducing microwave to the sample. Image reproduced from Ref. [30]. 41

2.7 The different types of polarisation mechanisms (top), and a schematic representation of various polarisation mechanisms verses frequency (bottom) [38]. 44

2.8 Schematic representation of the single mode microwave system [59]. 51

2.9 Schematic example of multi-mode microwave system [59]. 52

3.1 Basic Structure of the zeolite. 57
3.2 Three different cases of shape selectivity mechanisms: (1) Reactant shape, (2) Transition state shape, (3) Product shape selectivity [14]. 60
3.3 Schematic diagram of the channels structure in HZSM-5 [15]. 61

4.1 Cylindrical coordinate system. 69
4.2 The Resonant Mode Chart for a Cylindrical Cavity Resonator [27]. 73
4.3 COMSOL simulations of the Electric (red) and Magnetic (blue) Fields distribution in Cylindrical Cavity for the (a)TM_{010}, and (b) TE_{011} Mode. 75
4.4 Transmission peak of a TM_{010} empty cavity describing the Q-factor calculation. . . . 77
4.5 Sample depolarisation. Reproduced from Ref. [38]. 80
4.6 The (a) Copper, and (b) Aluminium host cavities showing the central hole where samples are introduced along the axis of the electric field. 81
4.7 Front panel and input keys of the VNA 8753E. 82
4.8 (a) Schematic of the dielectric measurements system with a vector network analyzer, (b) A 3D COMSOL generated representation of the field distribution in the resonator cavity of the TM_{010}. 84
4.9 Resonant curve before (red) and after (blue) inserting the sample. 87
4.10 Schematic representation of different PWM waveforms; with with low (10%) and high (90%) duty cycle. 90
4.11 Schematic of the high power microwave system, showing the microwave electric field distribution of the TM_{010} mode in the applicator generated using COMSOL Multiphysics. 95
4.12 The reflected power measurement system connected to the isolator dummy load. . . 96
4.13 Microwave system a) Microwave head and isolator components, where microwaves are being generated and directly reflected to the dummy load and crystal detector, b) Pulsed mode oscilloscope trace, c) tunable waveguide section with a single movable tuning stub, d) generator, e) Applicator chain with 3-stub tuning section, sliding short, quartz window and resonant applicator section. 97

4.14 User interface of Labview control panel. The software monitors (top screen) views all power where the white line is assigned to the input power and the red line is assigned to the reflected power; and (bottom screen) temperature meters; and (right panel) all parameters that control the microwave generator. 98
4.15 User interface of Labview control panel for temperature control program and pulsing mode. 99
4.16 Faults code command panel. 100
4.17 Heating profile for a typical oil-catalyst mixture starting at room temperature, where the red denotes the measured forward power and black denotes the power absorbed by the sample (forward power minus reflected power). 101
4.18 102
4.19 Schematic diagram of Bragg's law. 104
4.20 An example of typical Calcium Carbonate TGA curve [59]. 106
4.21 Schematic diagram of the SEM [69]. 112
4.22 Schematic diagram of the TEM [69]. 114

5.1 The change in the bandwidth and the shift in resonance frequency of the linear alkanes in comparison to the heavy bunker oil. 127
5.2 The real permittivity (ε') vs. the density of the hydrocarbon materials and bunker oil, as a function of increasing the chain length. 129
5.3 The real permittivity (ε') and the imaginary permittivity (ε'') for linear alkanes in comparison to the heavy bunker oil sample. 131
5.4 The change in the resonance peak positions in sulphur compounds. 134
5.5 The change in the bandwidth and the shift in the frequency values in sulphur compounds. 135
5.6 The real permittivity (ε') and the imaginary permittivity (ε'') for sulphur compounds. 136
5.7 The shift in the resonance peak and the broadening in the bandwidth for nitrogen compounds. 139
5.8 The change in the bandwidth and frequency for nitrogen compounds. 139

5.9 The real permittivity and the imaginary permittivity of the nitrogen compounds. . 140
5.10 The shift in the resonance peak of some cycloparaffins and cycloaromatic compounds. 143
5.11 The change in the bandwidth and the shift in the frequency values. 143
5.12 The real permittivity and the imaginary permittivity of the cycloparaffins and cycloaromatics. 144
5.13 (a) the resonance peak positions, and (b) the change in the bandwidth and frequency values of heavy (heavy bunker, light crude, and pyrolysis oil samples. 146
5.14 Dielectric properties of the oil samples. 148
5.15 The variation in heating profiles of the oil samples at fixed input power of 300 W. . 150
5.16 Zeolite structure. 151
5.17 Dielectric properties of zeolite samples. 151
5.18 The microwave conductivity of zeolite samples. 153
5.19 Library of dielectric loss tangent (tanδ) for a group of sulphur compounds, nitrogen compounds, cyclo and linear paraffinic compounds, heavy oil samples and zeolitic catalysts, nitrogen compounds are presented separately in the top corner as they are exhibiting higher loss value comparing to the rest of the compounds. 155
5.20 Overview of the increase in microwave susceptibility within the model compounds. . 156

6.1 High-temperature dielectric measurements setup (1) Copper TM_{010} cavity showing the E-field distribution within in the centre simulated using finite element modelling COMSOL software (2) stainless steel rigid coaxial cables (3) Cylindrical furnace (4) Coaxial cables (5) Vector network analyser (VNA). 165
6.2 The Q-factor values of the unloaded copper cavity as a function of temperature. . . 167
6.3 The shift in frequency to lower frequencies of the unloaded cavity as the temperature increasing. 168
6.4 Experimental results for detecting the change in oil volume as the temperature increasing. 169
6.5 (a) The temperature dependent properties of heavy bunker oil using the TM_{010} mode (b) the TGA profile representing the weight loss of the heavy bunker oil with increasing temperature. 170

6.6 The temperature dependence of the effective loss tangent of the heavy oil. 172
6.7 (a) the dielectric properties, and (b) the TGA profile of the HZSM-5. 174
6.8 The microwave conductivity measurements of the HZSM-5 zeolite as a function of temperature. 176
6.9 The change in the effective loss tangent of the HZSM-5 with increasing temperature. 177
6.10 (a) the dielectric properties, and (b) the TGA profile of oil /zeolite pre-reacted (fresh) sample. 178
6.11 Microwave electrical conductivity (left) and loss tangent (right) of the impregnated zeolite with heavy bunker oil (fresh catalyst). 180
6.12 The dielectric properties (a) and the TG analysis profile (b), of the the oil/HZSM-5 spent catalysis. 181
6.13 Electric conductivity of the impregnated zeolite with heavy bunker oil (spent) sample. 182
6.14 The change in loss factor value of the oil/HZSM-5 (spent) catalyst with increasing temperature. 183

7.1 Comparison of the effect of thermal and microwave processing of decane over HZSM-5 zeolite on the individual vol.% of the gaseous products. 193
7.2 Chromatograph showing the gas products of the (a) FID channel specifically operated for hydrocarbon analysis and (b) TCD channel for general analysis of decane cracking over zeolite. 194
7.3 Chromatograph showing the gas products of the (a) FID channel specifically operated for hydrocarbon analysis and (b) TCD channel for general analysis from the microwave cracking of decane over zeolite. 195
7.4 Effect of thermal and microwave processing of decane/ZSM-5 cracking on the vol.% of the olefins fractions $C_2^{\smile}C_4^{=}$, illustrating a clear increase in the olefin production under microwave compared to the thermal method. 197
7.5 Effect of power level on the microwave heating behaviour of HZSM-5 representing the change in heating rate as the input power increases. 198
7.6 Comparison of the products distribution at different heating rates of the decane/HZSM-5 cracking reaction (50, 200, 500°C/min). 199

7.7 The absorbed power and heating profile in a continuous irradiation mode for decane cracking over HZSM-5 reaction. 200

7.8 The absorbed power and heating profile in a microwave pulse modulated irradiation and a duty cycle of 20% of decane over HZSM-5 cracking reaction. 201

7.9 Product distribution of decane/HZSM-5 cracking under pulsing vs. continuous microwave irradiation. 202

7.10 Comparison of the olefin distribution of decane/HZSM-5 cracking under pulsing and continuous irradiation. 203

7.11 Model of general hydrocarbon cracking process, where the reaction favours the breakge of C-H over C-C under micorwave irreadiation compared to the theraml process where the oppisit case is ocurring. 204

7.12 The effect of varying particle size on the heating behaviour of Fe_2O_3 in a microwave applicator at fixed applied power. The particles distribution was in the range of 50-100 nm, 125-250 μm, and 500-710 μm. 205

7.13 Variation in heating profiles of different carbon black loading over zeolite at fixed applied power. 206

8.1 Schematic representation of the experimental setup. 217

8.2 Microwave heating profile of HZSM-5 impregnated with 25 wt.% of heavy oil during the microwave cracking reaction. 219

8.3 The volume of the gaseous products resulting from the heavy oil cracking over HZSM-5 zeolite. 220

8.4 Chromatograph showing the gas products of the (a) FID channel and (b) TCD channel from the heavy oil cracking over zeolite. 222

8.5 XRD patterns of the pristine HZSM-5 before and after microwave irradiation compared to the spent oil/catalyst after microwave irradiation at 450°C. 225

8.6 Change in dielectric properties of the HZSM-5/oil sample before and after the microwave reaction. 226

8.7 SEM images (a,b) of the pristine HZSM-5 before reaction, (c,d) spent sample after washing with toluene indicating some particle aggregation and loss in crystallinity after microwave treatment. 227
8.8 XRD patterns of different samples HZSM-5, 5 wt % FeO_x/HZSM-5, and 20 wt% FeO_x/HZSM-5, (*) indicates the presence of the iron oxide species. 229
8.9 The volume of the produced gas from the heavy oil cracking over different iron loadings into HZSM-5 catalysts in comparison to the cracking over the parent HZSM-5. 230
8.10 The dehydrogenation and coke formation mechanism under microwave irradiation. . 231
8.11 XRD patterns of different iron/zeolite spent catalyst after microwave irradiation, the (o) might be attributed to the iron carbide peaks. 233
8.12 Dielectric properties of the fresh and spent catalysts for the 5, 10, 20 wt.% FeO_x/HZSM-5. 234
8.13 TGA profiles of the spent FeO_x/HZSM-5 catalysts before toluene washing. 235
8.14 SEM images from the 20 wt% of FeO_x/HZSM-5-heavy oil samples treated at (a) and (b) 490-500°C, (c) and (d) around 900-1000°C. 236
8.15 TEM images of the 20 wt% of FeO_x/HZSM-5-heavy oil samples (a) and (b) treated at 490-500°C, (c) and (d) showing the core-shell structure of the iron-zeolite surrounded by the carbon nanotubes of treated at 900-1000°C. 237
8.16 XRD analysis of 5 wt.% and 20 wt.% CoO_x/HZSM-5, (*) indicates the presence of the cobalt oxides species 239
8.17 Volume of different gas compositions produced from the heavy oil cracking reaction over CoO_x/HZSM-5 catalysts with different loading of cobalt and 25 wt% of heavy oil. 240
8.18 XRD pattens of the spent cobalt samples, illustrating a clear decease in the peaks intensity as result of coke formation 243
8.19 The XRD patterns of the parent HZSM-5 and the LaO_x/HZSM-5 with three different loading levels of lanthanum. 245
8.20 The volume of the produced gas composition from the catalytic processing of 25 wt% of heavy oil over 5, 10, 20 wt% of LaO_x/HZSM-5 compared with the pure zeolite. . 247

8.21 XRD patterns of different LaO_x doping levels into zeolite after microwave cracking reaction of heavy oil. 249

8.22 Evaluation of the gas compositions for the (a) 5 wt%, (b) 10 wt%, (c) 20 wt% of FeO_x/HZSM-5 heavy oil impregnated samples under batch operation conditions as a function of time on stream at 450°C. 251

8.23 Schematic design of the continuous flow system representing a COMSOL simulated high field distribution of the generated electromagnetic field in the catalyst bed. . . 253

8.24 Gas composition of the proceed crude oil over 20 wt% FeO_x/HZSM-5 under continuous flow operation conditions. 254

8.25 Qualitative analysis of the GC–MS data for the collected liquid product of the processed crude oil under microwave irradiation, the top corner image shows the liquid product obtained after completing the reaction. 255

9.1 Comparison between (a) thermal heating and (b) microwave heating, where heat is transferred from the atmosphere to the bulk material in thermal heating and generated from the centre of the material in microwave heating. 263

9.2 Schematic diagram summarising the performed dielectric measurements accompanied with the explored library of dielectric properties of the model compounds, oil samples, and zeoltic materials. 264

9.3 Schematic diagram represents the catalytic cracking process of heavy oil over pure and modified zeolites, the result indicated an enhanced hydrogen production in case of metal oxide doping compared to the non-modified zeolite. 266

9.4 The initial design of the larger scale cavity operated at 900 MHz. 270

B.1 Gas composition of heavy oil cracking over HZSM-5 zeolite in vol.% 277

B.2 The gas composition concentration in vol.% of the heavy oil cracking over different iron loadings into HZSM-5 catalysts in comparison to the parent HZSM-5 278

B.3 Gas composition of the heavy oil cracking reaction over Co/HZSM-5 catalysts with different loading of cobalt and 25 wt% of heavy oil 278

B.4 Typical analysis of gas composition of a catalytic processing 25 wt% of heavy oil over 5, 10, 20 wt% of La @ HZSM-5 compared with the pure zeolite 279

C.1 The TGA profile of the spent sample after toluene washing for the 5, 10, 20 wt.% FeOx/ZSM-5 280
C.2 TGA plot of the cobalt spent catalysts CoOx/ZSM-5 281
C.3 TGA analysis of the LaOx/ZSM-5 spent samples 281

List of Tables

4.1 Values of P_{nm} for TM Modes of a Circular Waveguide [24]. 71

4.2 The real permittivity values applied for the calibration of the resonant cavity [42]. . 86

5.1 The Physical properties of the linear hydrocarbons. 126

5.2 Summary of the analysis of the dielectric data for some of the pure liquids and experimental values. 132

5.3 The physical properties of sulphur compounds. 133

5.4 The physical properties nitrogen compounds. 138

5.5 The physical properties cycloparaffinic and aromatic compounds. 142

8.1 The product distribution (wt%) of the heavy oil cracking over unmodified HZSM-5 zeolite. 224

8.2 Product distribution (wt.%) of HZSM-5 modified zeolite with iron oxide. 232

8.3 Product distribution (wt%) of HZSM-5 doped with different levels of cobalt oxides. 241

8.4 Product distribution (wt%) of the heavy oil cracking reactions over La oxide modified HZSM-5. 248

A.1 The Physical Properties of the linear hydrocarbons bought from Sigma Aldrich . . . 273

A.2 Sulphur Compounds 274

A.3 Nitrogen Compounds 274

A.4 Cycloparaffinic and Aromatic Compounds 274

Glossary

AC	Activated carbon
API gravity	American petroleum Institute's, it is an arbitrary scale expressing the gravity or density of liquid petroleum products
Alkylation	Transferring an alkyl group from one molecule to another
Asphaltene	Is the most heavy and polar components in crude oil
Applicator	The device where the microwave interaction with materials occur
BEA	Beta polymorph A zeolite
Barrel	A unit of volume measurement used for petroleum and its products
Bunker oil	Type of fuel oil used aboard ships and also commonly called heavy fuel oil
CHA	Type of zeolite with a pore size of 0.37 × 0.42 nm
Crude Oil	A general term for unrefined petroleum or liquid petroleum
CNT	carbon nanotubes
COMSOL Multiphysics	Modeling and simulating scientific and engineering software
Conductivity	A property of materials that determines the magnitude of the electric current density when an electric field is impressed on the material.
dB	Decibel
Dehydration	The process of losing water
Dehydrogenation	The process of losing hydrogen
DMO	Domestic microwave oven
Desulphurisation	The process of losing sulphure
EM	Electromagnetic
FCC	Fluid catalytic cracking
FID	Flame ionisation detector for hydrocarbon analysis
GC	Gas chromatographer
GC/MS	Gas chromatography-mass spectrometry
ID	Internal diameter
IR	Infrared
ISM	Industrial, scientific and medical. internationally approved radio band for radio frequency (RF) energy
MCR	Microwave cavity resonator
MMBD	Million Barrels Per Day
MFI	The framework type of the ZSM-5

MTH	Methanol to hydrocarbon conversion
MTG	Methanol-to-gasoline
MTO	Methanol-to-olefin
MTP	Methanol-to-propylene
m/z in (GC-MS)	M stands for mass and Z stands for charge number of ions.
Naphthenes	Group of cyclic aliphatic hydrocarbons (e.g. cyclohexane)
Naphtha	Any of several liquid mixtures of hydrocarbons made by refining petroleum
Octan number	A measure of a fuel ability to resist 'knock
OD	Outer diameter
Olefins	Unsaturated hydrocarbons
Paraffins	Waxy solid consisting of a mixture of saturated hydrocarbons
PID	A proportional–integral–derivative and it is is the most common control algorithm specially in temperature Controlling
PNA	Information represents the percentage of the paraffinic-naphthenic -aromatic compounds in the oil
PTFE	Polytetrafluoroethylene, Teflon
PWM	Pulse width modulation
Pyrolysis oil	Biocrude or biooil,and it is a distillation product of biomass
RF	Radio frequency
Reservoirs	A storage space for fluids
RSM	Response Surface Methodology
(SBU)	Secondary building units
Si/Al ratio	The distribution of Si to Al within the zeolite framework
TCD	Thermal conductivity detector for inorganic gases analysis
TEM	Transmission electron microscopy
Thermal effect	Any effect of electromagnetic energy on a body that is not a heat-related effect.
TE	Transverse Electric
TGA	Thermogravimetric analysis
TM	Transverse Magnetic
TOS	Time on stream
S_{11}	Reflection coefficient (port 1)
S_{21}	Transmission coefficient (from port 1 to port 2)
SMA	Sub miniature version A is a connector that is semi-precision coaxial RF connectors
VNA	Vector Network Analyser
XRD	X-ray diffractometry

List of Symbols

A	Angstroms 10^{-10} m
bbl	Barrel
B	Magnetic flux Tesla (T)
C	Degree(s) Celsius
	Dielectric loss tangent
c	m/s
C_1–C_5	Paraffins
C_2–$C_4^=$	Olefins
Dp	The penetration depth (cm)
$\triangle f$	The change in frequency
$\triangle BW$	The change in bandwidth
	Permittivity of free space
E	Electric field
E'	Electric field experienced by the dipole ($\mathbf{V}\mathrm{m}^{-1}$)
E_{app}	Externally applied electric field ($\mathbf{V}\mathrm{m}^{-1}$)
H	Magnetic field
h	Hour(s)
g	Gram(s)
$\varepsilon*$	Complex permittivity
ε'	Dielectric constant/ real permittivity
ε''	Dielectric loss/ imaginary permittivity
ε_r	Relative dielectric constant
ε_0	Permittivity of free space
$\tan\delta$	Loss factor
σ	Electrical conductivity
ν-f	Frequency (Hz)
I	Electrical current
MHz	Megahertz
min	Minute(s)
mL	Millilitre(s)
MW	Molecular weight
μ_0	Magnetic permeability in a vacuum Hm^{-1}
μ_r	Permeability of the air
μ	Permeability
N'	Number of dipole moments
P	Polarisation
α_t	total polarisability of a material
Q	Quality factor
ω	the angular frequency
wt. %	weight percentage
λ	wavelength (m)

Chapter 1

INTRODUCTION TO HEAVY OIL

1.1 Historical Background

Petroleum is a very old discovery; however, it is not exactly known when it was first used by mankind. Many thousand years ago, ancient peoples used petroleum in various forms for lightning and medicinal purposes [1]. Also, asphalt and bitumen forms were utilised in the construction of walls of both Egyptian pyramids [2] and the towers of Babylon [3, 4]. Additionally, it was also used as a waterproof agent when building boats.

Regarding the oil recovery process, in 347 BC the earliest recognised well was dug in China [5], where the oil was used to burn and produce salt by evaporating brine. In the 8th century, the utilisation of heavy residue was found in Baghdad where it was applied to the pavement of new streets. In the 9th Century, in Baku, Azerbaijan, the first known people were reported to distil petroleum for producing naphtha, which was later used for generating the incendiary Greek fire [6, 7].

The earliest known discovery of petroleum in America was reported in 1595 as a lake of asphaltene. This was followed by several more discoveries in 1632 and 1854 [7].

The first refinery was built in Baku, Azerbaijan, in 1861 by Meerzoedd. Subsequently, the first well which was established for commercial purposes was drilled in North America in 1858. Afterwards, the industrialisation of petroleum started in 1859 by Edwin Drakes in Pennsylvania who led the drilling of wells for the Seneca Oil Company, which used to produce 25 barrels per day

[7].

In Saudi Arabia, the first drilling work was conducted in 1935 by California Arabian Standard Oil Company (CASOC) and the first discovered well was in Dammam city, which only contained very little amount of oil. However, in 1938, the 7th drilled well in Dammam brought a significant change to the history of the country with an oil flow rate of 3,810 barrels per day. Several more discoveries were made in the area since then, and the name of CASCO changed to Arabian American Oil Company (ARAMCO) in 1944. The share of the Saudi government in ARAMCO started to increase, and in 1980 the company became 100% owned by the Saudi government [8, 9]. In 1970, crude oil was produced at a rate of 4 million barrels per day (MMBD) , which, in turns, reached 10.2 MMBD in 2015 [10].

As a summary, petroleum can be found in many countries and the industry grew through the 19th century onwards. The current top oil producing countries are Saudi Arabia, Russia, the United States, Iran, and China [11]. To conclude, petroleum has become a vital aspect of the daily activities of humans, and will remain so for the coming decades.

It is worth noting that fuels that are derived from petroleum contribute to over half of the total global supply of energy [12, 13], and their typical usage is as follows:

- Transportation: such as propane, diesel, gasoline, and jet fuel.
- Heating: such as heating oil, and natural gas.
- Sources of electricity: such as burning oil to generate electricity.
- Other petrochemicals from such as plastics, clothing, cosmetics, constructing and building materials, and more other products in different fields of life and science.

1.2 Crude Oil Classifications

Petroleum is a wide term covering a wide range of hydrocarbon materials that occur and accumulate in the geological strata over thousands of years. The term petroleum includes crude oil, heavy oil, extra-heavy oil and bitumen.

Figure 1.1 shows a scheme of the crude oil type with a mixture of components and possible products in refinery.

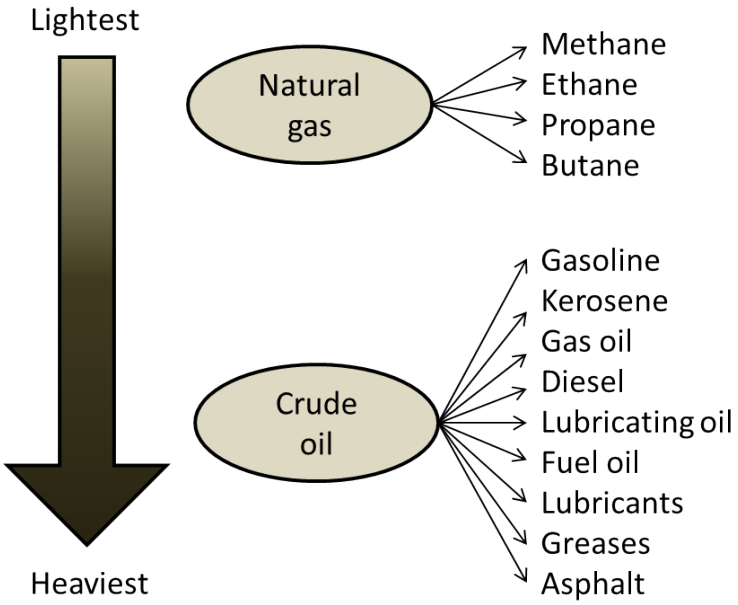


Figure 1.1: Schematic representation of the crude oil in terms of density in addition to a mixture of components which might be all included an oil sample and can be separated into these and other products in oil refinery. Reproduced from Ref. [14].

Many different classifications of crude oil can be found in the literature. The main sorts of classifications are light, heavy, sweet and sour crude oil. These are based on factors, such as chemical structures, distillation properties, crude oil properties and origin. In terms of chemical structure, oil can be called 'heavy' or 'extra heavy' based on its high viscosity and larger molecular structure. Moreover, opposite properties can be assigned to the lighter oil which is less viscous and has a lower molecular weight. As such, API gravity is a way of measuring the density of petroleum. If the API gravity value is lower than 22.3, the petroleum is defined as 'heavy'. In return, petroleum is called 'light' when the API gravity is greater than 31.1. An API gravity of less than 10.0 means that he petroleum is considered an 'extra heavy oil' [15, 16].

Another sorting of oil types is based on the amount of sulphur. If sulphur is present in high amount, the crude oil is described as 'sour'. However, and the opposite is true, it is described as

'sweet' for smaller quantities of sulphur [17–19]. Figure 1.2 represents various crude oils around the world with different densities and sulphur contents.

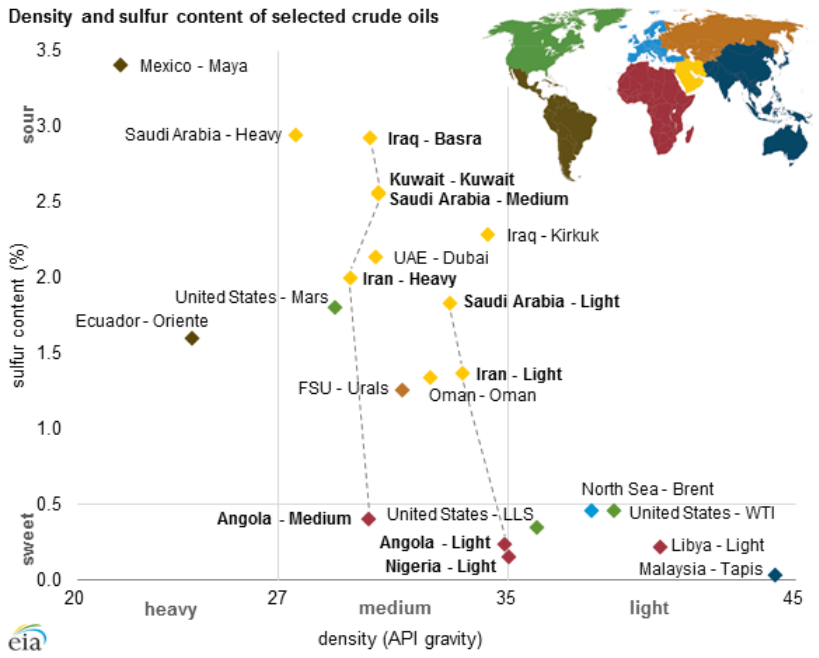


Figure 1.2: Shows the density and sulphur content of different classifications of crude oil around the world [20].

1.2.1 Heavy Oil Chemistry

Heavy crude oil is kind of petroleum that is viscous and composed of hundreds and thousands of naturally-occurring hydrocarbon compounds, non-hydrocarbons, organic compounds (comprising nitrogen, oxygen, and sulphur), as well as trace quantities of metallic constituents (e.g. iron, nickel, and vanadium) [21].

In general, heavy oils have a higher amount of high molecular weight fractions in comparison to low molecular weight and more volatile compounds. These high molecular weight compounds are mainly composed of a mixture of complex paraffins and asphaltene with greater melting points.

As the oil gets heavier, the level of asphaltene increases compared to the level of straight chain of paraffin constituents [17, 22].

Heavy oil is a relatively variable material, thus its physical and chemical characteristics can change with the age or location of the oil field, as well as the depth of the wells. Two adjacent wells may contain petroleum with distinct and different characteristics.

The term C_n is used to define hydrocarbons having equivalent 'n' carbon atoms. C_1 or methane is the simplest hydrocarbon in petroleum and is the main component of natural gas mixtures. C_2 and C_3 are ethane and propane, respectively. C_4 is a term for normal and iso-butanes, while C_5 stands for normal, iso-, and neo- pentane. As the number of carbon atoms increase above 6, the number of isomers also rapidly increases. Constituent compounds C_n ($n > 6$) components are generally placed in the following hydrocarbon chemical classes: paraffins, naphthenes, aromatics, and hetero compounds [23].

Paraffins are saturated hydrocarbons that have straight (normal) or branched (iso-paraffins) chains. Their carbon atoms have single covalent bonds.

Naphthenes are cycloparaffins, which have a saturated ring structure. This structure may have five, six, or sometimes seven carbon atoms (cyclopentanes, cyclohexanes, and cycloheptanes, respectively). A large majority of naphthenes found in petroleum bear paraffinic side chains, and may also have more than one ring in the molecule. These rings may or may not be fused, if they share more than one carbon atom.

Aromatics have at least one benzene ring. The different types of aromatics (monoaromatics, diaromatics, and triaromatics) are distinguished by the number of aromatic rings. Aromatics in petroleum generally have paraffinic side chains and/or may also have naphthenic rings. Both the aromatic and naphthenic rings may or may not be fused. Aromatic compounds' complexities increase greatly as the number of rings increases, as a result of the multiple iterations of the arrangements of naphthenic and aromatic rings and side chains [24].

Heterocompounds are a type of hydrocarbon from the aforementioned groups, in which at least one heteroatom (N, S, O, V, Ni, Fe) forms part of the molecule. The presence of heteroatoms and their functions contribute to the complexity of the structural framework of the hydrocarbon compounds. Heterocompounds generally belong to high molecular weight factions of petroleum. The percentage of the paraffinic, naphthenic, and aromatic components in a petroleum fluid is defined

as the PNA distribution. Higher amounts of paraffins and naphthenes are found in conventional light and medium oils, while aromatics and heterocompounds mostly occur in oils and bitumens [18, 23, 25].

1.3 Conventional Methods for Heavy Oil Processing

Production, transportation, and refining are the main three sectors of the petroleum industry supply chain. Heavy crude oil is taken to advanced refineries by ship, train, or pipeline after it is extracted and prepared for transport. Then in refineries it is turned into various useful products, e.g. fuel [17].

There is an ever-increasing global demand for oil production. An oil stockpile of 3 billion barrels could be sufficient to reach a comfortable supply to the world markets [26] (Figure 1.3). As stated by TOTAL, in 2035, global energy demand is projected to be more than 30% higher than it was in 2010. As oil and gas will continued to play a key role in meeting demand, there will be several major technical, economic, societal and environmental challenges to overcome in order to achieve a continued sustainable supply of energy [26].

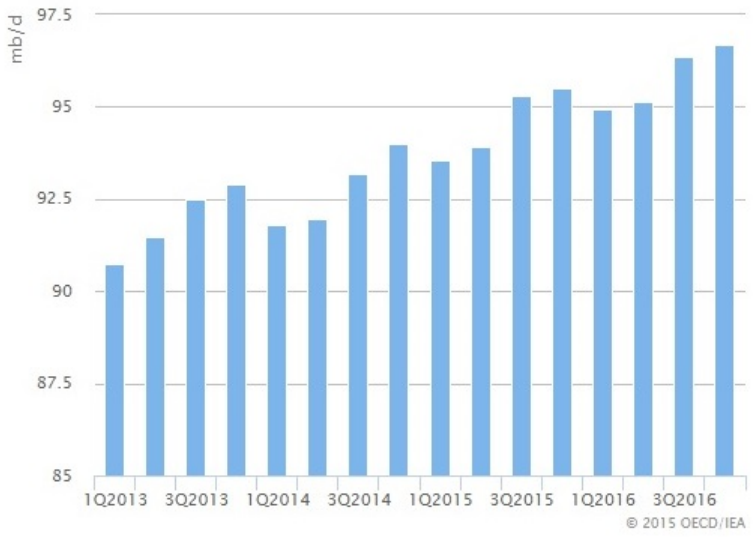


Figure 1.3: World Oil Demand [27].

Light and sweet crude oils with high API gravity and low sulphur content are the most wanted and highly priced type of oil, because it is easy and relatively cheap to produce gasoline and diesel fuel from light oils, and these are the most premium products that can be processed using less energy-intensive processes.

Heavy oil needs to be processed to synthetic oil of higher API, which requires additional treatment before it can be turned into valuable compounds. Figure 1.4 represents the typical distillation column in oil refinery.

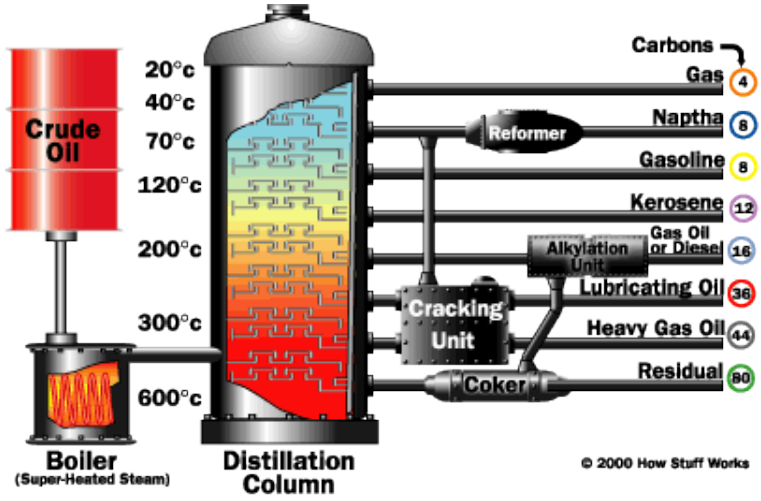


Figure 1.4: Typical distillation column in oil refinery [28].

Overall, in order for heavy crude oil to be processed into lighter materials, several steps must be taken. In general, macromolecules have to be removed, viscosity has to be lowered, the H/C ratio must be increased, and heteroatoms (O, N, and S) have to be taken out. The following section provides a description of the conventional cracking method in refining process for heavy oil [29].

1.3.1 Cracking

The process of converting heavy crude oil into lighter fractions is called cracking. Heat and pressure are used by refineries to break heavy hydrocarbons into lighter hydrocarbons. It can be done either with or without catalysts [30]. Cracking can be classified as follows.

1.3.1.1 Thermal Cracking

Thermal cracking began in 1913 [31]. It is the process of applying heat (~800°C) and pressure (~700kPa) to modify hydrocarbon molecules by breaking down and rearranging them. This originally took place in large drums in which heavy oil was cracked into smaller hydrocarbon molecules. The main problem facing this type of cracking is the formation of irreversible coke. Later on, different forms of thermal cracking were developed: steam cracking, visbreaking, and coking [3, 25].

In *steam cracking*, steam is used to break large hydrocarbon molecules into smaller ones. It is used to produce olefins such as ethylene or propene. These can be used by refineries to make light oil products. In *visbreaking*, the viscosity of heavy oil is reduced by thermally cracking its hydrocarbon molecules in a furnace between 400-550°C. The result is heating oil and diesel fuel. In *coking*, thermal cracking is used to turn heavy oil into useful coke that can be further processed [32].

1.3.1.2 Hydrocracking

In hydrocracking, hydrogen is used to crack heavy oil and catalysts are used to ensure faster and more selective conditions. The oil is cracked in the presence of hydrogen because this results in more useful oil products [33].

1.3.1.3 Catalytic Cracking

In catalytic cracking, various catalysts in the form of powders solid materials such as zeolite, aluminium hydrosilicate, bauxite, and silica-alumina, and metal are also introduced. Heavy oil is cracked in the presence of these catalysts at temperatures ranging from 450-550°C and pressures ranging from 10-20 psi [34–36]. This breaks the hydrocarbon into less complex products, which in turn can be refined to make gasoline, kerosene, and heating oil. There are three kinds of catalytic cracking: fluid catalytic cracking (FCC), moving-bed catalytic cracking, and thermo catalytic

cracking (TCC). There are also more catalytic processes such as dehydrogenation, hydrogenation, and isomerization [37].

Although thermal cracking was the first process used for reducing complex hydrocarbon into simpler forms of light oil, catalytic cracking, first developed by Eugene Houdry in the late 1920s [38], was responsible for producing the gasoline necessary for aircraft in World War II, particularly aircraft in the European theatre. In the 1930s, catalytic cracking continued to develop.

"Necessity is the mother of invention" is one explanation for technological innovation, and it still explains why various stakeholders in technology spend resources and make huge efforts towards meeting needs and making profits. The need for fuel has spurred the development of more efficient cracking processes that can take complex crude oil and convert it into a product that can be further refined into gasoline and other petroleum products. Previous methods of refining led to undesirable products such as waste coke, CO_2 emission, large energy consumption ; hence, better methods of processing were necessary. Early c, but research eventually led to the use of zeolite as a catalyst .

The aim of catalyst research in the 1950s was to find an efficient catalyst with internal pores that matched the size of the molecules desired in the cracking process [39]. In 1956, an amorphussilic-alumina matrix catalyst was used in a cracking test. In the 1960s, zeolite became a cracking catalyst, leading to more efficient refining processes [40, 41]. In particular, more efficient fluidized-bed technology replaced fixed-bed technology, which had both technological and economic ramifications. In terms of the technology, fluid catalytic cracking now took place in higher temperature reactors and required less contact time between heavy crude and the catalyst. In economic terms, the more efficient conversion of heavy crude into lighter products that could be further refined led to a more profitable and economically efficient refinery process. Two particular types of zeolite are desirable: ZSM-5 and Y-zeolite. These forms of zeolite resist the production of coke and can be used multiple times in the cracking furnace [40, 42, 43].

1.4 Microwave Technology in the Petrochemical Industry

Researchers have been looking at unconventional method for producing different temperature profiles for refining heavy oil, given that oil reserves are limited and demand is still high. Such methods include ultrasonic energy, electric fields, and magnetic fields [44]. These methods are very different

from traditional non-catalytic and catalytic methods used in the thermal industry as the thermal one requires a large amount of input energy.

Microwave technology became very popular and was considered to be a relatively breakthrough in the field, as it can speed up many chemical reactions with high efficiency [45, 46]. However the actual mechanism responsible for the enhancing in some of the microwave reactions remains unclear. According to some reports, it may be due to the "electromagnetic effect", a non-thermal effect which could be associated with the selective absorption of energy by polar molecules [44, 47].

From the early 1980s, one of the first experiments to use microwaves during refining included light hydrocarbons. The experiment involved a cracking of different types of gasoil over two groups of catalysts, the pre-irradiated and non-irradiated catalysts. It was found that the composition of the cracked naphtha was different from the non-irradiated catalyst. Moreover, the obtained naphthenes and isoalkanes were found to be higher in the pre-irradiated catalysts compared to the non-irradiated catalysts, which resulted from the decrease in the content of alkenes [48, 49]. This was an expensive procedure, but in the 1990s a new procedure was developed and it is called the (HEET) hydrocarbon enhancement electron-beam technology [50].

In more recent times, microwaves have been used to inspect coiled tubing and pipelines, measure multiphase flow, and mobilise asphaltic crude oil [49].

Microwave radiation was also used in oil recovery [51]. Chakma and Jha [52] used electromagnetic heating to heat a scaled, thin heavy oil reservoir. This was done by injecting gas in horizontal wells in order to reduce oil viscosity and attain a gas drive. It was found that electromagnetic heating accompanied with nitrogen injection of the wellbore vicinity in thin pay zones could be achieved. The process leads to a 45% oil recovery rate, compared to a 5% primary recovery rate. The combination of electromagnetic heating and gas injection led to higher recovery rates than either method alone. Gas injection pressure, heating rate, and electromagnetic frequency are possible factors that yielded the result of the combined method, according to Chakma and Jha [53].

In the industry of refinery studies they reported the use of microwaves in the demulsification of water in the oil process [54]. The demulsification process can be conducted by optimising the water percentage that is separated by microwave irradiation, as water is considered a good microwave absorber compared to oil. Then, the optimum conditions for every crude oil could be determined

using the Response Surface Methodology (RSM). This method has the advantages of saving time and is cost effective for the demulsification process [55].

More advantages of microwave technology, such as a selective and rapid heating was efficiently exploited for the recovery of crude oil in contaminated oil. The process was undertaken by proceeding the contaminated oil mixed with granular activated carbon under microwave irradiation. The enhancement of microwave heating resulted from the carbon additive and led to the oil recovery which can be carried out in a condensation system. The process helped in achieving a 91% recovery from the contaminated oil [56].

In more application of microwave in petrochemical industry, Gunal and Islam [57] they exposed asphaltenes to microwave irradiation and they noticed an increase in asphaltenes viscosity in addition to a permanent alteration of the molecules in the colloidal structures. This is happing due to the reorientation of molecular structures rather than thermal breakdown. Zaykina, *et al.* [58, 59] exposed the paraffinic oil to microwave and they reported the observation of branching and cracking of the paraffin chain during the irradiation time. Overall, microwave energy offers several benefits in processing heavy oil; it is efficient, heats rapidly, requires little start up time, and offers precise control over the process [60].

In another study, Hascakir *et al.* [61] used microwaves in gravity drainage on heavy oil samples from reservoirs in Turkey with different API levels (9.5 API; 12 API; and 18 API). They used specially designed novel graphite core holder packed with crushed limestone. to look at how microwave heating is affected by various factors, including the properties of rocks and fluids, waiting period, and heating time. They found that the increase in water salinity and saturation had a positive effect on the process. This is similar to the conclusion drawn by Chakma and Jha. Finally, Hascakir *et al.* posited several favourable conditions for high oil recovery rates, including wet conditions, large porosity, and permeability [54].

By itself, heavy oil is not a good receptor of microwave energy and cannot be heated directly by microwaves to reach sufficiently high temperatures. However, efficient heating of heavy oil might be possible if the oil is mixed with an effective catalyst that can absorb microwaves, such as carbon or metal oxides. Metal oxides have in fact been used in both microwave and non-microwave processes to enhance crude oil conversion. However, this can lead to contamination of the oil, which is mitigated by catalysts which are able to absorb microwaves [62].

For the processing of heavy crude oil, microwaves can be used to upgrade the heavy to lighter crude oil. The process was found to be time and energy saving, and moreover environmentally friendly. It was conducted by mixing the heavy oil with a good microwave absorber, such as carbon nano-catalysts, where the electron density of carbon varies greatly; thus, resulting in a higher dielectric constant. The experiment reported that a decrease in viscosity of 96% could be achieved in less than an hour at a fairly low temperature of 150°C [63].

In general, it was found that mixing heavy crude oil with good microwave absorbers, such as carbon materials [56] and metal oxides [53, 64] resulted in a significant improvement in microwave absorption and heating.

The upgrading of heavy crude oil to lighter crude was used not just as a batch process, but also in the production lines of an oil well. A scalable system where a pump is added, and the use of a microwave irradiation system have greatly reduced the viscosity of the recovered oil [65].

In terms of oil cracking process, microwave irradation was used in the desulfurisation of crude oil [66–69]. Several research teams reported the conduction of microwave heating for crude oil desulfurisation over various types of catalysts [70]. The desulfurisation experiment of an Arabian heavy sour crude oil was conducted with a desulfurisation agent under microwave treatment. The results indicated a decrease in the sulphur content after exposing the samples to microwave for different periods of time and input powers. It was found that the sulphur content decreased by 2.3% and 33.8% after microwave heating for 5 and 25 minutes, respectively [62].

Most of the approaches including the cracking of crude oil and the use of microwave irradiation were conducted in domestic microwave ovens. With the aim of heavy oil processing to light and high value chemicals using a specially designed microwave system, we have conducted an experimental study for measuring the dielectric properties of two types of oil samples [71]. The measurements of the dielectric properties of the oil were conducted at a single frequency of 2.45 GHz using the cavity perturbation method. The results indicated that although the dielectric properties of the oil samples were found to be small, it is possible to achieve decent microwave heating using the proper catalyst and a suitable design for the microwave reactor.

1.5 Thesis Objectives

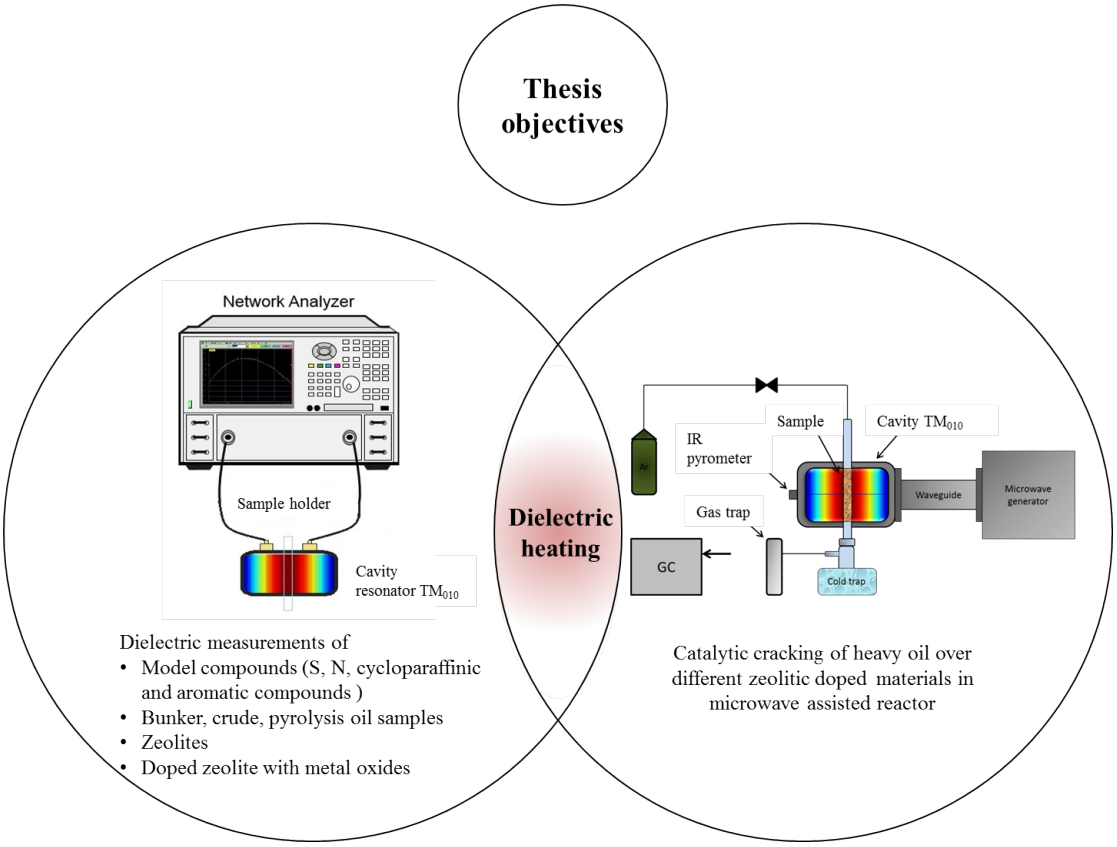
Petroleum is one of the major sources of energy for humanity and will remain for the foreseeable future. The ever present challenge of maintaining production volumes from oil reneries, given especially the depletion of extant oil wells, is a key driver for the development of unconventional methods for the processing of petroleum. The use of dielectric heat generated at-site from microwave energy has promises in many applications. Microwave heating has a number of advantages over other conventional heating processes as regards to selectivity and rapidity. In addition, the application of microwave heating in oil processing has become increasingly attractive due to the environmental concerns that arise with conventional heating methods.

Thus, the conducted project in this thesis aims to explore the potential application of microwave technology for the cracking reaction of heavy oil to high value light products. The project is mainly focused on gaining insight into the microwave interaction with oil/catalysts for obtaining the desired products. It brings the science of catalysis and materials chemistry together with microwave, physical and chemical engineering and can be divided into two main parts.

1. The development of a better understanding of microwave-material interaction based on the role of dielectric properties. The dielectric properties have been characterised using the cavity perturbation technique at 2.45 GHz and TM_{010} mode. The measurements were conducted on model compounds, oil samples, and zeolitic materials. The evaluated materials were explored to compile a comprehensive library of the dielectric properties, which will provide the knowledge of potential efficiency to generate heat in a microwave system designed for cracking process.

2. The design and parameters optimisation of a single-mode microwave applicator was performed based on dielectric heating compared to conventional heating process. The bench-top microwave system has been used to investigate the fundamental interactions of microwaves with oil and catalysts. The focused aim of this stage is to develop a processing method that can heat both catalysts and heavy oil in a single step, with a high degree of control over the applied conditions. Different metal oxides of Fe, Co, and La were loaded over HZSM-5 and then impregnated with heavy oil. The heavy oil-impregnated metal oxide-HZSM-5 composites were evaluated in the cracking reactions using microwave dielectric heating. The

product distributions of modified and non-modified HZSM-5 zeolite and the potential catalytic mechanisms related to the conversion process were investigated. Further development of the microwave reactor was conducted. This step has been conducted for the prospect of contribution to the development of future manufacturing technology with significant industrial applications. The schematic diagram below represents the two major objectives of this work.



Bibliography

[1] A. Demirbas. *Biohydrogen: for Future Engine Fuel Demands*. Springer Science and Business Media, 2009.

[2] Bricklayers, editor. *The Bricklayer, Mason and Plasterer*. ProQuest, 1932.

[3] V. Simanzhenkov and R. Idem. *Crude Oil Chemistry*. CRC Press, 2003.

[4] M. B. McElroy. *Energy: Perspectives, Problems, and Prospects*. Oxford University Press, 2010.

[5] E.R. Crain. A True Histor y of Oil and Gas Development. *Canadian Well Logging Society*, pages 9–12, 2000.

[6] C. Cobb and H. Goldwhite. *Creations Of Fire: Chemistry's Lively History from Alchemy to the Atomic Age*. Springer Science and Business Media, 2013.

[7] J.G. Speight. *Introduction to Enhanced Recovery Methods for Heavy Oil and Tar Sands*. Gulf Professional Publishing, 2016.

[8] M.S. Vassiliou. *Historical Dictionary of the Petroleum Industry*. Scarecrow Press, 2009.

[9] A.E.M. Nairn A.S. Alsharhan and A.E.M. Nairn. *Sedimentary Basins and Petroleum Geology of the Middle East*. Elsevier, 1997.

[10] Production and Reserves. Technical report, Saudi Aramco, 2015.

[11] S. Levine, G. Taylor, D. Arthur, M. Tolleth. Understanding Crude Oil and Product Markets. Technical report, American Petroleum Institute, 2014.

[12] A.Y. Huc. *Heavy Crude Oils: From Geology to Upgrading : an Overview*. Editions TECHNIP, 2010.

[13] I.A. Wiehe. *Process Chemistry of Petroleum Macromolecules*. Chemical Industries. CRC Press, 2008.

[14] A. Fagan. An Introduction to the Petroleum Industry. Government of Newfoundland and

Labrador: Department of Mines andEnergy, 1991.

[15] S. Chopra. *Heavy Oils: Reservoir Characterization and Production Monitoring*, volume 13. SEG Books, 2010.

[16] R.G. Santos, W. Loh, A.C. Bannwart, and O.V. Trevisan. An Overview of Heavy Oil Properties and its Recovery and Transportation Methods. *Brazilian Journal of Chemical Engineering*, 31:571 – 590, 2014.

[17] H. Devold. *Oil and Gas Production Handbook: An Introduction to Oil and Gas Production*. Lulu.com, 2013.

[18] J.G. Speight. *Heavy Oil Production Processes*. Gulf Professional Publishing, 2013.

[19] G. Falcone, G.F. Hewitt, and C. Alimonti. *Multiphase Flow Metering: Principles and Applications*. Elsevier, 2009.

[20] Crude Oils Have Different Quality Characteristics, 2013. Accessed: 2016.

[21] J. Ancheyta and J.G. Speight, editors. *Hydroprocessing of Heavy Oils and Residua*. CRC Press, 2007.

[22] J.G. Speight. *The Chemistry and Technology of Petroleum*. CRC Press, 5th edition, 2014.

[23] F.J. Hein, D. Leckie, S.R. Larter, and J.R. Suter. *Heavy-oil and Oil-sand Petroleum Systems in Alberta and Beyond: AAPG Studies in Geology*. AAPG Studies in Geology. American Association of Petroleum Geologists, 2013.

[24] K.H. Altgelt. *Composition and Analysis of Heavy Petroleum Fractions*. Chemical Industries. Taylor & Francis, 1993.

[25] C. Ovalles and C.E. Rechsteiner Jr. *Analytical Methods in Petroleum Upstream Applications*. CRC Press, 2015.

[26] Total, Oil and Gas, 2015. Accessed: December 2015.

[27] Internation energy agency. Oil Market Report, November 2015. Accessed: December 2015.

[28] G. Freudenrich. How Oil Refining Works. Accessed: 2016.

[29] Energy Economics Applied Optimization. An Introduction to Petroleum Refining and the Production of Ultra Low Sulfur Gasoline and Diesel Fuel. Technical report, icct the international council on clean transportation, 2011.

[30] N.S. El-Gendy and J.G. Speight. *Handbook of Refinery Desulfurization*, volume 140 of *Chemical Industries*. CRC Press, 2015.

[31] C.J. Cleveland and C.G. Morris. *Handbook of Energy: Chronologies, Top Ten Lists, and Word Clouds*. Elsevier, 2013.

[32] A. Chauvel and G. Lefebvre. *Petrochemical Processes*. Editions OPHRYS, 1989.

[33] A. Harta, G. Leekea, M. Greavesb, and J. Wood. Down-hole Heavy Crude Oil Upgrading by CAPRI: Effect of Hydrogen and Methane Gases upon Upgrading and Coke Formation. *Fuel*, 119:226–235, 2014.

[34] E. Fumoto, T. Tago, and T. Masuda. Recovery of Lighter Fuels from Petroleum Residual Oil by Oxidative Cracking with Steam over Zr-Al-FeOx Catalyst. *Chemistry Letters*, 35:998–999, 2006.

[35] E. Fumoto, A. Matsumura, S. Sato, and T. Takanohashi. Recovery of Lighter Fuels by Cracking Heavy Oil with Zirconia-Alumina-Iron Oxide Catalysts in A Steam Atmosphere. *Energy and Fuels*, 23:1338–1341, 2009.

[36] E. Fumoto, T. Tago, T. Tsuji, and T. Masuda. Recovery of Useful Hydrocarbons from Petroleum Residual Oil by Catalytic Cracking with Steam over Zirconia-Supporting Iron Oxide Catalyst. *Energy and Fuels*, 18:1770–1774, 2004.

[37] J.P. Favennec and R. Baker. *Petroleum Refining*. Editions OPHRYS, 2001.

[38] Houdry Process for Catalytic Cracking, April 13 1996. Accessed: Jun 2015.

[39] J.T. Richardson. *Principles of Catalyst Development*. Springer, 2013.

[40] D.N. Perkins and R.J. Weber. *Inventive Minds: Creativity in Technology*. Oxford University Press, 1992.

[41] D.R. Lide. *CRC Handbook of Chemistry and Physics*. CRC Press, 85th edition, 2004.

[42] D. Decroocq. *Catalytic Cracking of Heavy Petroleum Fractions*. Institut Francais du Petrole publications. Editions Technip, 1984.

[43] B.G. Reuben H.A. Wittcoff and J.S. Plotkin. *Industrial Organic Chemicals*. John Wiley and Sons, 2012.

[44] National Energy Technology Laboratory. A Literature Review on Cold Cracking of Petroleum Crude Oil. Technical report, United States Department of Energy, 2006.

[45] G. Whittaker. Microwave Chemistry. *School Science Review*, 85:87–94, 2004.

[46] M.B. Gawande, S.N. Shelke, R. Zboril, and R.S. Varma. Microwave-Assisted Chemistry: Synthetic Applications for Rapid Assembly of Nanomaterials and Organics. *American Chemical*

Society, 47:1338–1348, 2014.

[47] A. de la Hoz, A. Diaz-Ortiz, and A. Moreno. Microwaves in Organic Synthesis: Thermal and Non-thermal Microwave Effects. *Chemical Society Reviews*, 34(2):164–78, 2005.

[48] G.M. Panchenkov and V.V. Erchenkov. Radiation-chemical Processes. *Chemistry and Technology of Fuels and Oils*, 16:433–436, 1980.

[49] M.R. Khan and E.N. Al-Shafei. Microwave-Promoted Desulfurization of Crude Oil, August 19 2014. US Patent 8,807,214.

[50] Y.A. Zaykin, R.F. Zaykina, and G. Mirkin. On Energetics of Hydrocarbon Chemical Reactions by Ionizing Irradiation. *Radiation Physics and Chemistry*, 67:305–309, 2003.

[51] A. Esmaeili. Effects of Microwave Radiation on Oil Recovery. *American Institute of Physics*, 137:137–140, 2011.

[52] K. N. Jha and A. Chakma. Heavy-Oil Recovery from Thin Pay Zones by Electromagnetic Heating. *Energy Sources*, 21:63–73, 1999.

[53] A. Chakma. Heavy-Oil Recovery from Thin Pay Zones by Electromagnetic Heating. In *SPE Annual Technical Conference and Exhibition,*, Washington, D.C., 1992. Society of Petroleum Engineers.

[54] A. Mukhametshina and E. Martynova. Electromagnetic Heating of Heavy Oil and Bitumen: A Review of Experimental Studies and Field Applications. *Journal of Petroleum Engineering*, 2013:1–7, 2013.

[55] A.N.I. Anisa, A.H. Nour, and A.H. Nour. Destabilization of Heavy and Light Crude Oil Emulsions via Microwave Heating Technology: An Optimization Study. *J. Applied Sci*, 113:2898–2906, 2011.

[56] L. Da-Wei, Z. Yao-Bin, Q. Xie, and Z. Ya-Zhi. Microwave Thermal Remediation of Soil Contaminated with Crude Oil Enhanced by Granular Activated Carbon. *Huan Jing Ke Xue*, 30:557–562, 2009.

[57] O.G. Gunal and M.R. Islam. Alteration of Asphaltic Crude Rheology with Electromagnetic and Ultrasonic Irradiation. *Journal of Petroleum Science and Engineering*, 26:263–272, 2000.

[58] R.F. Zaykina, Y.A. Zaykin, G. Mirkin and N.K. Nadirov. Prospects for Irradiation Processing in the Petroleum Industry. *Radiation Physics and Chemistry*, 63:617–620, 2002.

[59] Yu.A. Zaykin, R.F. Zaykina and J. Silverman. Radiation-Thermal Conversion of Paraffinic

Oil. *Radiation Physics and Chemistry*, 69:229–238, 2004.

[60] A. Miadonye And B. MacDonald. Microwave Radiation Induced Visbreaking of Heavy Crude Oil. *Journal of Petroleum Science Research*, 3:130–135, 2014.

[61] B. Hascakir, C. Acar, and S. Akin. Microwave-Assisted Heavy Oil Production: An Experimental Approach. *Energy and Fuels*, 23:6033–6039, 2009.

[62] A. Miadonye, S. Snow, D. J. G. Irwin, and M. Rashid Khan. Desulfurization Of Heavy Crude Oil By Microwave Irradiation. *WIT Transactions on Engineering Sciences*, 63:1–11, 2009.

[63] K. Li, B.i Hou, L. Wang, and Y. Cui. Application of Carbon Nanocatalysts in Upgrading Heavy Crude Oil Assisted with Microwave Heating. *Nano Letters*, 14:3002–3008, 2014.

[64] P. Monsef-Mirzai, M. Ravindran, W.R. McWhinnie, P. Burchill. Rapid Microwave Pyrolysis of Coal Methodology and Examination of the Residual and Volatile Phases. *Fuel*, 74:7–20, 1995.

[65] K.A. Safinya. Apparatus and Process for Upgrading Crude Oil using Microwave Radiation, 2011.

[66] R. Lu , J. Yang , X. Xu, and J. Gao. Microwave-chemical Desulphurization of Sulfurous Crude Oil. *Petroleum Science and Technology*, 27:1789–1799, 2009.

[67] L. Lin, L. Hong, Q. Jianhua, X. Jinjuan. Progress in the Technology for Desulfurization of Crude Oil. *China Petroleum Processing and Petrochemical Technology*, 12:1–6, 2010.

[68] S.G. Jeon, N.S. Kwak, N.S. Rho, C.H. Ko, J.G. Na, K.B. Yi and S.B. Park. Catalytic Pyrolysis of Athabasca Bitumen in H_2 Atmosphere using Microwave Irradiation. *Chemical Engineering Research And Design*, 90:1292–1296, 2012.

[69] A.D. Mohammed, A.G. Isah, M. Umaru, S. Ahmed, and Y.N. Abdullahi. Comparative Study on Sulphur Reduction from Heavy Petroleum - Solvent Extraction and Microwave Irradiation Approach. *International Journal of Energy and Environment*, 3:949–960, 2012.

[70] N.E. Leadbeater, and M. Khan. Microwave-Promoted Desulfurization of Heavy and Sulfur-Containing Crude Oil. *Energy and Fuels*, 22:1836–1839, 2008.

[71] A. Porch, D. Slocombe, J. Beutler, P.P. Edwards, A. Aldawsari, T. Xiao, V. Kuznetsov, H. Almegren, S. Aldrees and N. Almaqati. Microwave Treatment in Oil Refining. *Applied Petrochemical Research*, 2:37–44, 2012.

Chapter 2

THE INTERACTION OF MICROWAVES WITH MATTER

2.1 Introduction

In 1864, The Scottish physicist James Clark Maxwell established the theory behind electromagnetic wave propagation [1]. This dynamical theory of electromagnetic fields remained a theory paper until Heinrich Hertz, the German physicist, experimentally verified Maxwell's equations [2]. He examined the wave propagation using huge equipment that operated at 50 MHz with dipole antenna. Many scientists around the world followed the Hertz example and conducted research and experiments. Indeed, the Indian physicist J. C. Bose verified the optical properties of electromagnetic waves using the Hertzian waves. He demonstrated his work at the Royal Institution in London in 1896 [3].

Microwaves were generally enhanced by radar experts during WWII. Modifying the properties of the composite materials has been essential to the creation and improvement of radar-absorbing materials. The first radar came into use during WWII, and microwaves were first used as communication devices during this period. The use of microwave energy as a way to heat materials was first discovered in 1950 [4, 5]. The development of microwaves had much input to achieve what the world looks like today. Television, radio, and microwave ovens are all share the same history with radar and microwave systems. Materials properties and the investigation of their properties at

microwave frequencies have led to the development in the fields of physics, electrical and electronic engineering, solid-state chemistry, and materials science [6].

A good understanding of the properties of materials interaction and functioning at microwave frequencies is needed in order to develop microwave-assisted systems. As such, the characterisation of materials properties is a vital aspect of microwave technology; important parameters include complex permittivity, conductivity, and material permeability [7].

The differences between microwave and conventional heating have encouraged researchers and scientists to investigate the industrial use of microwave heating. Despite the complications in explaining some microwave phenomena, such as the so called non-thermal effects, the use of microwave processing of materials is still receiving huge attention. One of the advantages that microwaves provide in materials processing is volumetric heating, which differs significantly from conventional heating in which the heat penetrates the material [8]. Microwave heating has been successfully used in several areas, including food tempering, heating, cooking and drying [9]. These procedures are mostly performed with relatively low temperatures. However, microwave heating of materials at high temperatures was increasingly explored during the late 1960s and applied in inorganic chemistry in late 1970s [10]. Microwave has been used in curing of polymers and synthesising polymeric materials as a rapid heating technique. After successful applications, microwaves were then validated as a possible heating mechanism meant to replace conventional heating methods in some processing areas. The benefits such as the volumetric and the rapid heating, also fast and homogeneous heating of some large homogeneous items and the selective heating of heterogeneous materials were able to attract a significant number of researchers into the field [11, 12]. However, there are many other unexplained phenomena that have been observed during microwave processing which can fall under the controversial term which is called "electromagnetic effect" [13].

2.2 The Electromagnetic Field

To examine the electromagnetic field effect, it is crucial to understand both electromagnetic waves and the electromagnetic spectrum. When an electric or magnetic charge changes its position in space, the corresponding field also changes in space. These changes in either field produce an oscillatory wave, which is called an electromagnetic wave. Electromagnetic waves are self-propagating

and are characterised by electric E and magnetic H field components. These two components oscillate perpendicular to each other, as well as to the direction of propagation as shown in Figure 2.1. Electromagnetic waves can also propagate in a vacuum or in matter, and possess traits that are relatively similar to other waves, such as absorption, interference, diffraction, and reflection. Electromagnetic waves are characterised by their frequency, velocity, and electric field strength [14].

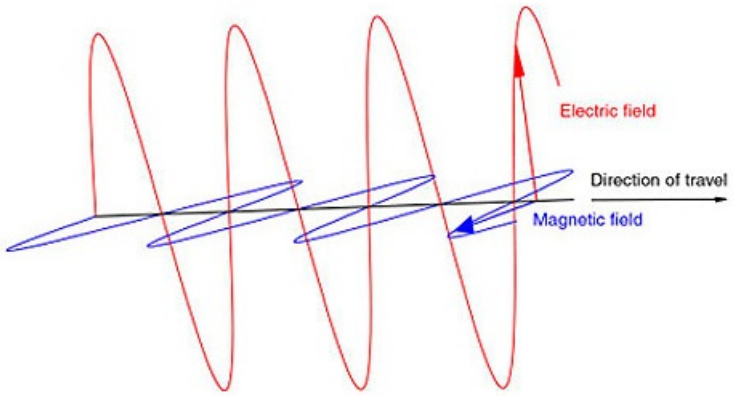


Figure 2.1: The components of the electromagnetic wave [15].

For electromagnetic waves, the general wave formula is given by the equation 2.1:

$$c = \lambda \cdot f \tag{2.1}$$

Where,

c= speed of light (3.0×10^8 m/s)

λ = wavelength in free space (m)

f = frequency (Hz)

differences in wavelength lead to the sub-categories (Figure 2.2), infrared, gamma rays, light waves, microwaves, radio waves, ultraviolet, and X-rays. Microwaves lie in the area between infrared and radio waves in the electromagnetic spectrum. They have a wavelength from 1 mm to 1 m, and a frequency band that ranges from 300 MHz to 300 GHz. In order to avoid interference between the wide range of microwave applications, specific frequencies are allocated for different purposes. A wide range of microwaves are used for communication applications, while only a certain frequencies are allocated for industrial, scientific, and medical (ISM) applications. For example, frequencies from 896 MHz to 2.45 GHz are used in the United Kingdom for ISM applications, which include domestic ovens and industrial heating [16].

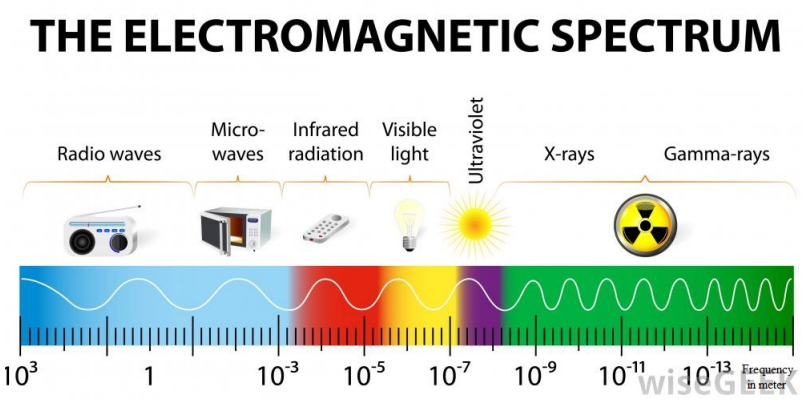


Figure 2.2: The electromagnetic spectrum, showing the scale of the wavelengths that corresponding to the microwave frequency in meter [17].

2.2.1 Electric and Magnetic Fields

Electric field strength can be determined easily by considering the potential difference of voltage V between two perfectly conducting plates. The plates are separated by a distance d (in meters), which is smaller than the plates size, and connected to a voltage source V (volts). So, the electric field strength E is simply V/d, or volts per meter. Figure 2.3 shows a simple schematic of the

plates arrangement. In a free space, the magnitude of the electric field differs inversely with the distance from the source. However, if the distance between these plates is doubled, the intensity of the electric field is halved, as shown by the following equation 2.2 [18, 19].

$$E = \frac{\triangle V}{d} \tag{2.2}$$

In this equation,

$\triangle V$ = the difference in voltage between two plates

d = the distance between the plates

So, according to the equation, if the potential difference is kept constant, the smaller the distance between the plates, the stronger the electric field becomes.

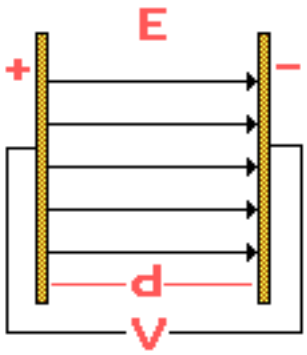


Figure 2.3: Illustrating the charge separation in two parallel conducting plates causing an internal electric field [20].

The strength of the *electric field* is based on electric voltage measured in volts, and the strength of the *magnetic field* is influenced by the intensity of the electric current, measured in amperes. The strengths of both fields decrease with increasing the distance from the source. Magnetic field

strength H is distinguished by magnetic force of the materials on other magnetic materials or moving electric charges. The simplest example representing the magnetic field of return path of the current can be explained by the circular loop example (Figure 2.4). The two equations below 2.3 and 2.4 define the strength of the magnetic field for an infinite straight conductor and at the centre of the loop respectively [21].

$$H = \frac{I}{2\pi r} \tag{2.3}$$

$$H = \frac{I}{2r} \tag{2.4}$$

Where,

I is the electrical current in the conductor

r is the distance between the conductor and the radius of the loop

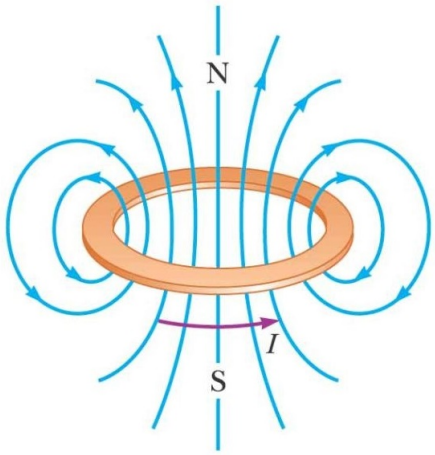


Figure 2.4: Magnetic field lines for a coil of a current loop [22].

At any specified point in the magnetic field, field strength is the force maintaining the magnetic flux and producing a specific value of the flux density at that point. The density of the magnetic flux B is equivalent to the strength of the magnetic field multiplied by the magnetic permeability in the space in which the field exists [23]. The unit of measurement for magnetic flux density is Tesla (T), and the relation between magnetic field strength and magnetic flux density is illustrated in the equation 2.5 below [24]:

$$B = \mu_0 \cdot H \tag{2.5}$$

The constant μ_0 has a value of $4\pi \times 10^{-7}$ when expressed in Henry per meter (Hm^{-1}). It refers to the magnetic permeability in a vacuum and in air, and also applies for all non-magnetic materials [24].

The absolute permeability of a magnetic material can be presented based on the value of its relative permeability and the permeability of the air or free space by the equation 2.6:

$$\mu = \mu_0 * \mu_r \tag{2.6}$$

Where μ_r is the relative permeability, which is defined by the ratio of the flux density produced by the material to that produced in a vacuum or non-magnetic core [19, 25].

2.3 Microwave Interaction with Materials

Materials vary in their responses to microwave radiation (Figure 2.5). They can be classified with respect to their interaction with the electric field component of the microwave field to: conductors, which reflect microwave energy and therefore are not effectively heated by electric field. The second type is the transparent, which microwaves pass through with little attenuation, and the absorbers.

Materials that absorb microwaves called dielectrics, have a high dissipation factor which represents the ability of the material to absorb microwaves and convert the energy into heat. Microwave heating of dielectric materials is also called the dielectric heating [26, 27].

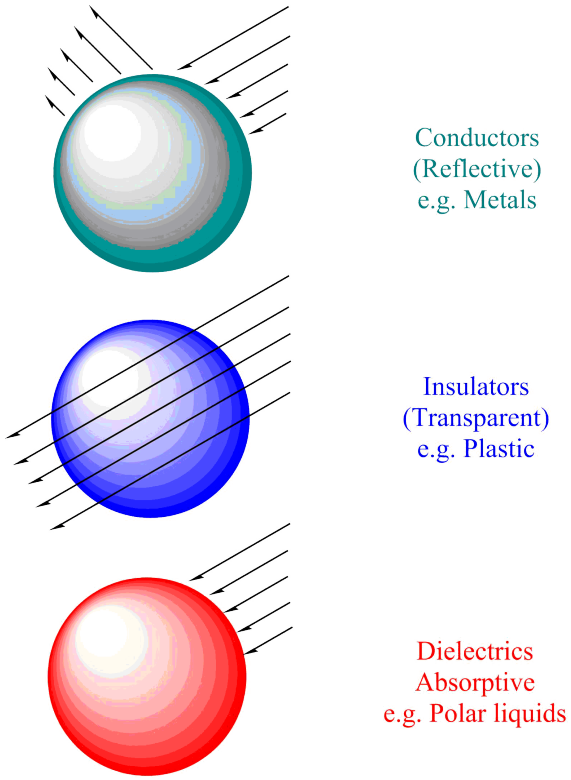


Figure 2.5: The interaction between microwaves and different types of materials.

2.4 Microwave Heating Mechanisms

There are several mechanisms that can explain microwave interaction with dielectric materials. In the microwave heating process, the main two mechanisms that contribute to dielectric heating are *dipolar polarisation* and *ionic conduction* (Figure 2.6). Other reported mechanisms, such as *interfacial polarisation,* are actually a combination of those two mechanisms [28]. When the electric

field is applied, the dipoles and the ions tend to align themselves in the direction of the electric. As the field oscillates, they keep realigning with it, resulting in molecular rotation and ion oscillation. The main mechanisms could occur simultaneously in many applications; for example, in a mixture of polar solvent molecules the dipoles follow the dipolar polarisation mechanism, whereas charged particles (ions) follow the ionic conduction mechanism. Ionic conduction occurs when an electromagnetic field is applied and results in the electrophoretic migration of ions. Furthermore, the solution experiences an increase in temperature when it resists the flowing ions, creating friction. The rearrangement of dipoles with the applied field results in dipole rotation and relaxation when the field is turned off [29, 30].

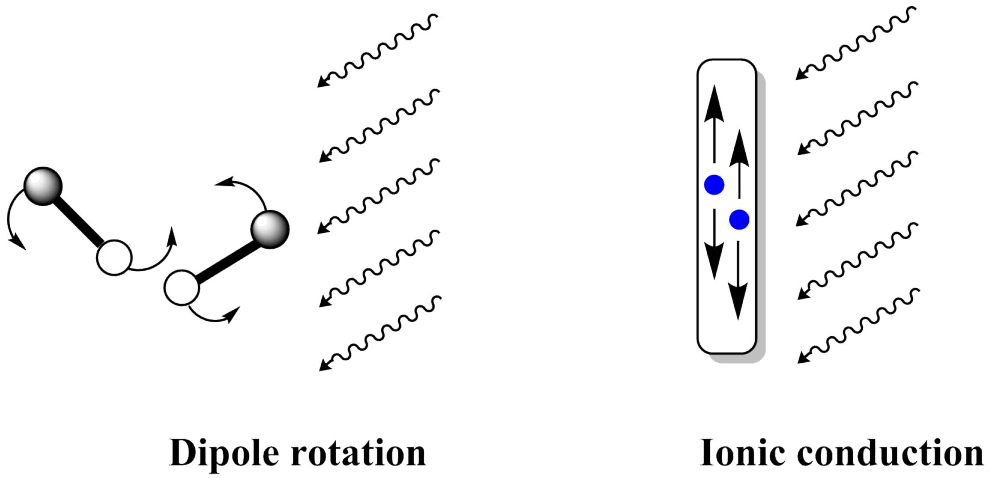


Figure 2.6: The dipole rotation and ionic conduction mechanisms after introducing microwave to the sample. Image reproduced from Ref. [30].

With the conventional process of heating, the transfer of energy to the material occurs through conduction, convection, or radiation through the external surfaces of the material. However, microwave heating involves delivering the microwave energy directly into the material. The molecular interactions of the material with the electromagnetic field, resulted in electromagnetic energy conversion into thermal energy. The most essential properties of the microwave process of dielectric mechanisms are complex permittivity (ε^*) and the dielectric loss tangent ($\tan\delta$). They are described

through the equations 2.7, 2.8, and 2.9 below [31, 32].

$$\varepsilon^* = \varepsilon' - j\varepsilon'' \tag{2.7}$$

$$\tan\delta = \frac{\varepsilon''}{\varepsilon'} \tag{2.8}$$

Where,

$$j = \sqrt{-1} \tag{2.9}$$

The permittivity of a material (ε) is associated with its interaction with electromagnetic energy. It is composed of two parameters, the real permittivity is ε', which measures how much energy is stored in the material (for a vacuum, ε'=1). The second parameter is the imaginary permittivity (or dielectric loss) is ε'', and determines the level of efficiency of the absorbed microwave energy that is converted into heat. The dielectric loss tangent ($\tan\delta$) serves as one of the most important characteristic in microwave processing. It determines the ability of the sample to take in microwave energy and spread the heat to the surrounding molecules, which also can represent microwave heating efficiency in a sample. A material with a high imaginary permittivity and dielectric loss permits the conversion of microwave energy into thermal energy [33]. The level of microwave absorption is generally proportional to the dielectric constant. The essential physical parameters involve dielectric constant and dissipation factors, the latter describing the capability of the material to dissipate microwave energy into heat [34, 35].

2.4.1 Polarisation

Under Electric Field: There are four different types of polarisation that could contribute to dielectric materials polarisation. These dipoles either already exist or are induced in the dielectric materials. Different polarisations are illustrated in Figure 2.7. These types are: electronic, ionic, orientation, and interfacial polarisation. The ability of a material to fall under a specific type of polarisation is defined by the *polarisability* α. The relation between the dielectric constant and the polarisation of the material is expressed in equation 2.10 [36, 37]:

$$P = (\varepsilon_r - 1)\varepsilon_0 E_{app} \tag{2.10}$$

Where,

P is the polarisation of the material

ε_r is the relative permittivity

E_{app} is the externally applied electric field ($\mathbf{V}\mathrm{m}^{-1}$)

ε_0 is the permittivity of free space

On a molecular scale, the dipole moment of the material volume unit can be expressed as follows:

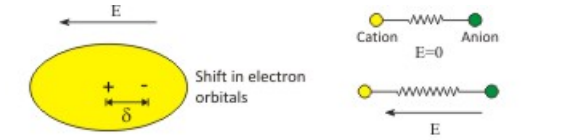
$$P = \alpha_t N' E' \tag{2.11}$$

Where,

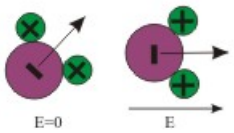
N' is the number of dipole moments

E' is the electric field experienced by the dipole ($\mathbf{V}\mathrm{m}^{-1}$)

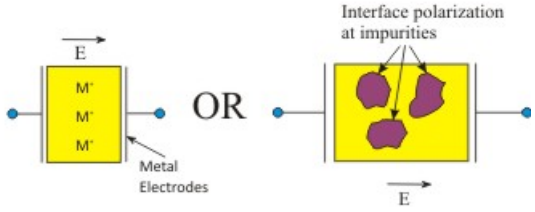
α_t is the total polarisability of a material



(a) Electronic Polarizaton in an atom (b) Ionic Polarization



(c) Dipolar or Orientation Polarization



(d) Interfacial Polarization

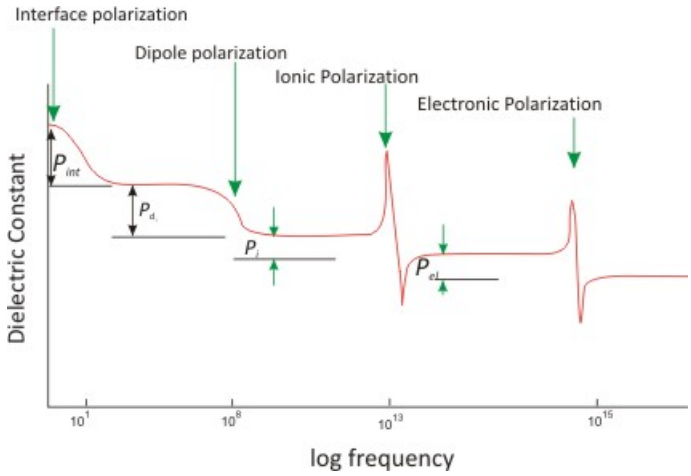


Figure 2.7: The different types of polarisation mechanisms (top), and a schematic representation of various polarisation mechanisms verses frequency (bottom) [38].

2.4.1.1 Electronic Polarisation

This type of induced polarisation is a result from the displacement of the centre of charge of electrons relative to the nucleus in each atom by the electric field. Therefore, the polarisation contributes only to the permittivity of a dielectric. This kind of polarisation only exists in the presence of an electric field, and is found in nonpolar and polar dielectric materials. The temperature of the electronic polarisation dependence is also inconsequential, with only a minor reduction in the material permittivity as the temperature rises due to thermal expansion and the subsequent decrease in the density of the material [39].

2.4.1.2 Orientational Polarisation

Orientational polarisation is based on a molecular rotational process, which is found in polar dielectrics which possess a permanent dipole moment. When atoms come together and share at least one electron, a molecule is formed. When the electrons rearranged this may result in an imbalance charge distribution, which creates this permanent dipole moment. These moments take up random orientations when there is no external electric field. When the electric field E is applied, each dipole will undergo a torque which will rotate them to align with the electric field, resulting in orientation polarisation. A change in the direction of the field will also lead to a change in the torque. According to the Debye interpretation the resulting friction that occurs with the orientation of the dipole leads to dielectric losses. The rotation of the dipole leads to a variation in both ε' and ε'' at the relaxation frequency, which commonly occurs in the microwave region [39]. When the field is turned off then the time for the dipoles to take up a random orientation is described as relaxation and the time taken for this is the relaxation time [40].

2.4.1.3 Ionic Polarisation

This occurs in materials which possesses free ions and are able to move under the effect of the dielectric field associated by the microwave radiation. The applied field disturb cations and moves them in one direction while anions move in the opposite direction, resulting in a net charge separation. As the temperature increases, so does polarisation as a result of the weakening elastic forces between the ions. However, it is also lessened by thermal expansion, which reduces the number of ions per unit volume. Due to microwave radiation, the induced dipoles will cause the sample

to heat up as a result of electrical resistance. If a material possesses a low electrical resistance, a large proportion of the microwave energy will not be able to penetrate the surface of the material. Despite this, there may still be high surface voltages induced, and these are what cause the arcing effects that are seen when metals are placed in microwave ovens [39]. Consequently, during this discharge process, a large amount of heat can be produced resulting in the formation of localised concentrated hot spots, which are plasma at a microscopic level. Mingos *et al.* used the dielectric heating of metal powders to heat them up and this led to the successfully synthesis of organometallic and coordination compounds [41–43].

2.4.1.4 Interfacial Polarisation

Interfacial polarisation results from the limited movement of charges leading to the alignment of charge dipoles under the applied electric field. It is a combination of the two dipolar polarisation, and ionic conduction mechanism [44].

Under Magnetic Field: Compared to the electric field heating effect, the magnetic heating of the H field has a lower number of published articles. However, due to the significant advantages when heating some materials using a magnetic field, this aspect started attracting significant attention. It has been found that in addition to dielectric heating generated from the E-field, the magnetic field (H-field) also contributed to some materials to generate heat. Magnetic loss heating, Joule heating are other types of microwave heating are generated by magnetic fields [45].

Eddy current loss is the Joule loss which results from the eddy current induced by an alternating magnetic field. It can be generated when the conductor material is exposed to an alternating magnetic field during the microwave heating process of metals. It can result either from the variation of the field with time or from the motion of the conductor and the field source. If the electric field is induced by the changing magnetic field, then the eddy current loss can be controlled by materials electrical resistivity. It can be considered the main mechanism of microwave heating based on the contributions of the magnetic field for many conductor and semiconductor materials [46].

Rosa *et al.* [47] described the contribution of the magnetic field interaction when heating ferromagnetic powders using microwaves. It has been shown that it can result in higher heating contribution when compared to an electric field. Nevertheless, more understanding of the mechanisms other than the dielectric heating is still required. However, developing this area of research

would create great opportunities for better understanding of microwave heating effects [48].

2.5 Penetration Depth

The penetration depth (Dp) is a term that describes the distance from the surface of the material to the level at which the power reduces to $1/e$ ($\sim 37\%$) of the power value of the surface. Assuming that there is zero energy reflected, the penetration depth equation 5.4 can be derived for a homogeneous material as follows [19],

$$D_p = \frac{1}{\omega \left\{ 2\mu_0 \mu' \varepsilon_0 \varepsilon' \left[\sqrt{1 + (\varepsilon''/\varepsilon') - 1} \right] \right\}^{\frac{1}{2}}} \tag{2.12}$$

Where,

μ_0 is the permeability of free space $= 4\pi \times 10^{-7}\text{H.m}^{-1}$

μ' is the permeability of the material (which is 1 for non-magnetic materials)

The penetration depth depends on the heated material and the applied frequency. It has a great influence on the way in which a sample absorbs and converts microwave energy.

Another term in microwave interaction with materials called 'skin depth' which describes the microwave propagation into metals. It can be defined as the depth at which the magnitude of the applied electric field decreases to 1/e of the original value at the surface [49]. It can be expressed as follows:

$$\delta = \frac{1}{(\nu \pi \mu \sigma)^{\frac{1}{2}}} \tag{2.13}$$

where,

(ν) is the microwave frequency ($\omega = 2\pi\nu$) and ω is the angular frequency

(σ) is the electrical conductivity.

Depending on the skin depth, the interaction of metal powders and pieces are different when

interacting with microwaves. In metal powders, rapid heating and localised hot spots can take place due to eddy currents and plasma effects. However, in bulk metals an electric discharge will occur when interacting with microwaves [50].

2.6 Dielectric Measurement Techniques

There are several factors that affect microwave heating; these are: heating applicator design, conductive losses, density, dielectric permittivity, field intensity, frequency, and temperature. Aside from their effect on dielectric heating, these factors are not independent and interact with each other. It can also depends on size and shape of the sample.

In order to generate heat within the material, microwaves must be able to penetrate the surface of the material and transmit energy. Both the real permittivity (ε') and the imaginary permittivity (ε'') measure the dielectric response capacitive and conductive components. These two components are defined in terms of the complex permittivity ($\varepsilon*$) through the equation 2.7 below [51]:

$$\varepsilon* = \varepsilon' - j\varepsilon'' \qquad (1.12)$$

The measurement of dielectric properties can be done safely without destroying the tested materials and it involves a number of techniques. Dielectric properties in the microwave region can be detected through a number of procedures, with the use of various sensors that measure the sample properties. The procedure employed depends on the type of target material and the frequency range of interest. The equipment that is used to measure dielectric properties and the design of the sample holder depend on the states of the material and the properties that will be measured, the available equipment, and the specific focus of research. Generally, the measuring equipment will include a Vector Network Analyzer (VNA), a relatively expensive but useful and versatile tool for controlling and displaying the measurements [52].

Many factors should be considered when choosing the method of measurement for any required application, including the electrical and physical nature of the dielectric material, the frequency of interest, and the required degree of accuracy. There are different types of instruments that provide reliable measurements of the dielectrical properties of unknown materials in a specific frequency range. However the challenge is measuring dielectric properties or permittivity accurately which is related to design of the sample holder [53]. Another challenge is ensuring that the circuit for reliable calculation of the permittivity obtained from the electrical measurements is modelled adequately. If the radio frequency circuit parameters are approximated correctly, the dielectric properties of a material at the specified frequency can be derived from equations that accurately describe how the material permittivity affects the parameters of the circuit [54, 55].

2.6.1 Transmission Techniques

Transmission line techniques involve placing the material of interest inside a transmission line that has been enclosed. The said transition line is generally a section of coaxial airline or rectangular waveguide.

Because the shape of the material must be a slab or annular, the said method is cumbersome. The sample size is somewhat large at 2450 MHz, and this is particularly true for oils and fats. The WR-284 is a common example of waveguide test equipment for 2450 MHz. The coaxial line technique is the sole method that is practical for 915 MHz measurements, because of the large required size of the waveguide. By using a sample holder at the end of a vertical transmission line, viscous-fluid foods and liquids can also be measured using this procedure [54].

2.6.2 Open Coaxial Probe Techniques

The open-ended coaxial probe is a part of transmission line that is cut off. The measurement of the material is done by submerging the probe into a liquid, or having it touch a flat surface of a material that is solid or powdery [54].

2.6.3 Resonant Cavity Techniques

Resonant cavity perturbation techniques involve a sample material that affects both the quality factor (Q) and the centre of frequency (f) of the cavity. Based on these parameters, the permeability ($\mu*$) or the complex permittivity ($\varepsilon*$) of the material may be derived at a single frequency. Various types of cavities and methods exist, with the cavity perturbation method being the most widely used. This procedure utilises a rectangular or cylindrical waveguide. A sample should be placed in a maximum electric field for a dielectric measurement. On the other hand, a sample should be placed in a maximum magnetic field for a magnetic measurement.

2.7 Microwave Heating Applicators

Over the last few decades, the use of microwave energy has been viewed as a suitable source for both the selective and volumetric heating of dielectric materials. Microwave energy has been successfully applied in many areas (e.g. commercial, domestic, industrial, and medical applications have been reported [56]. The efficiency and uniformity of the material heating are both governed by the design of these applications. The term 'applicator' refers to the component at which the interaction between the material and the microwave takes place in a controlled environment. Designing the suitable microwave heating applicator is a critical issue in microwave engineering, as the main goal is to achieve the efficient conversion of microwave energy into a heat which is related to the field distribution within the applicator. Usually, microwave heating systems consist of a microwave source (magnetron) which determines the frequency and output power of the microwave radiation. In addition to waveguides, travailing wave applicator, are used in either single or multi-mode cavities. Single mode and multi-mode are the two main types of microwave applicators [55, 57, 58].

2.7.1 Single-Mode System

The single mode applicator is a resonant cavity attached to the end of the waveguide power-feed line. Over the frequency range of the microwave source, there will be one specific electric or magnetic field distribution that can exist in the cavity. This leads to the formation of high electromagnetic field strength in the centre of the cavity. One of the main advantages of the single mode applicator over its multi-mode counterpart is the ability to regulate the amount of power that enters the

cavity. This also includes the forward power, which is the power leaving the generator tube and travelling down the line. Throughout the cavity, the distribution of the energy is homogeneous. However, this system may not be suitable for a number of applications, such as the processing of large bulk materials, despite the fact that this would lead to the centre being heated significantly. When designing and setting up the single mode applicator the cavity frequency, coupling aperture size and other considerations must be taken into account [57]. More details about the single mode applicator are presented in **Section 4.2.**

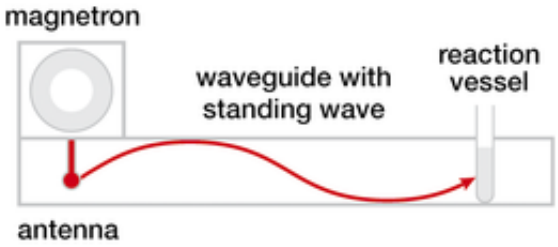


Figure 2.8: Schematic representation of the single mode microwave system [59].

2.7.2 Multi-Mode System

The microwave domestic oven is the best example of the multi-mode system. It produces a number of waves that are reflected around the cavity using a mode stirrer. This allows a large amount of material to be heated simultaneously without any constraints on the cavity size. However, because this process is relatively unsystematic and thus difficult to measure, it may be possible for 'hot' or 'cold' spots to exist in the microwave cavity. In these spots, the total wave function for overlapping waves at a particular point is either at the maximum or minimum level. For comparably simple applications, such as cooking, the effect is negligible. However, for relatively complex applications, such as the measurement of the heating rates of small samples, moving the sample a few millimetres produces significantly different conditions. This makes the characterisation of the reaction conditions more challenging [60].

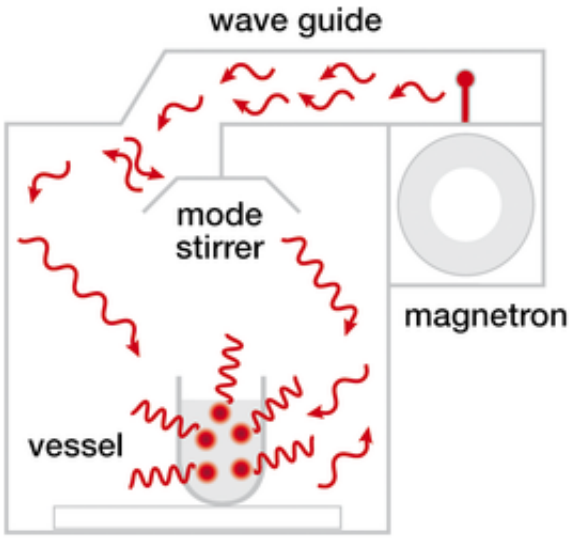


Figure 2.9: Schematic example of multi-mode microwave system [59].

Bibliography

[1] J.C. Maxwell. *A Treatise on Electricity and Magnetism*, volume 1 of *A Treatise on Electricity and Magnetism*. Clarendon Press, Oxford, 1873.

[2] R.A. Serway and J.W. Jewett. *Physics for Scientists and Engineers with Modern Physics*. Cengage Learning, 2008.

[3] T.A. Denidni and G. Augustin. *Ultrawideband Antennas for Microwave Imaging Systems*. Artech House antennas and propagation library. Artech House, 2014.

[4] C. Nelson. *High-Frequency and Microwave Circuit Design*. CRC Press, New York, 2007.

[5] T. Manning. *Microwave Radio Transmission Design Guide*. Artech House, Boston, 2009.

[6] I.H. Woodhouse. *Introduction to Microwave Remote Sensing*. Taylor & Francis, New York ; London, 2006.

[7] E.F. Knott, J. Shaeffer and M. Tuley. *Radar Cross Section*. SciTech Radar and Defense Series. SciTech Pub., 2nd edition, 2004.

[8] S. Grundas, editor. *Advances in Induction and Microwave Heating of Mineral and Organic Materials*. InTech, 2011.

[9] W. Cao, editor. *The Development and Application of Microwave Heating*. InTech, 2012.

[10] B. Hascakir, C. Acar, Schlumberger, B. Demiral and S. Akin. Microwave Assisted Gravity Drainage of Heavy Oils. In *International Petroleum Technology Conference*, volume 3, pages 1908–1916, 2008.

[11] D.R. Richard and D. Smith. Present and Future Uses of Microwave Power. *Materials Research Society*, 189, 1990.

[12] H.J. Kitchen, S.R. Vallance, J.L. Kennedy, N. Tapia-Ruiz, L. Carassiti, A. Harrison, A.G. Whittaker, T.D. Drysdale, S.W. Kingman, and D.H. Gregory. Modern Microwave Methods

in Solid-State Inorganic Materials Chemistry: From Fundamentals to Manufacturing. *Chem. Rev.*, 114:1170–1206, 2014.

[13] S. Miyake. *Novel Materials Processing by Advanced Electromagnetic Energy Sources.* Materials and Science Engineering, 2005.

[14] G. Barué. *Microwave Engineering: Land and Space Radiocommunications*, volume 9. J. Wiley & Sons, 2008.

[15] Electromagnetic Spectrum, 2015. Accessed: December 2015.

[16] P. Russer. *Electromagnetics, Microwave Circuit and Antenna Design for Communications Engineering.* Artech House, 2nd edition, 2006.

[17] Battery and Energy Technologies, 2005. Accessed: November 2015.

[18] D.I. Bower. *An Introduction to Polymer Physics.* Cambridge University Press, 2002.

[19] R.J. Meredith. *Engineers' Handbook of Industrial Microwave Heating.* Institution of Electrical Engineers, 1998.

[20] G.R. Delpierre, B.T. Sewell. Electronic Science Tutor, 2012. Accessed: November 2015.

[21] M. Gerloch. *Magnetism and Ligand-Field Analysis.* Cambridge University Press, 2009.

[22] Magnetic Fields. Accessed: November 2015.

[23] K. Sahay. *Basic Concepts of Electrical Engineering.* New Age International, 2006.

[24] A.V.Bakshi and U.A.Bakshi. *Electromagnetic Field Theory.* Technical Publications, 2009.

[25] K. Sahay. *Basic Concepts of Electrical Engineering.* New Age International, 2006.

[26] J.P. Hartnett. *Advances in Heat Transfer*, volume 33. Academic, 1999.

[27] C.A. Wilkie, G. Geuskens, V.M. de Matos Lobo, editor. *Handbook of Research on Functional Materials: Principles, Capabilities and Limitations.* CRC Press, 2016.

[28] G.B. Awuah, H.S. Ramaswamy, J. Tang, editor. *Radio-Frequency Heating in Food Processing: Principles and Applications.* CRC Press, 2014.

[29] T. Nyokong and V. Ahsen. *Photosensitizers in Medicine, Environment, and Security.* Springer, 2012.

[30] M.P. Ortega and I.C. Gil. *New Developments in Medicinal Chemistry.* Nova Science, 2009.

[31] A.S. Mujumdar. *Handbook of Industrial Drying.* CRC Press, Taylor & Francis Group, 4th edition, 2015.

[32] K.J. Klabunde and R. Richards. *Nanoscale Materials in Chemistry.* Wiley, 2nd edition, 2009.

[33] T. Varzakas and C. Tzia, editors. *Food Engineering Handbook: Food Process Engineering.* CRC Press, 2014.

[34] H. Schubert and M. Regier. *The Microwave Processing of Foods.* Woodhead, 2005.

[35] H.S. Ramaswamy G.B. Awuah and J. Tang. *Radio Frequency Heating in Food Processing: Principles and Applications.* CRC Press, Taylor & Francis, 2015.

[36] G.I. Torgovnikov. *Dielectric Properties of Wood and Wood-based Materials.* Springer-Verlag, 1993.

[37] B.S. Mitchell. *An Introduction to Materials Engineering and Science for Chemical and Materials Engineers.* John Wiley, 2004.

[38] I. Kanpur. Mechanisms of Polarization, June 2012. Accessed: December 2015.

[39] K.C. Kao. *Dielectric Phenomena in Solids: with Emphasis on Physical Concepts of Electronic Processes.* Academic Press, 2004.

[40] V.S. Yadav, D.K. Sahu, Y. Singh, D.C.Dhubkarya. The Effect of Frequency and Temperature on Dielectric Properties of Pure Poly Vinylidene Fluoride (PVDF) Thin Films. *IMECS*, 3:1–4, 2010.

[41] D.R. Baghurst, S.R. Cooper, D.L. Greene, D.M.P. Mingos, and S.M. Reynolds. Application of Microwave Dielectric Loss Heating Effects for the Rapid and Convenient Synthesis of Coordination Compounds. *Polyhedron*, 9:893–895, 1990.

[42] D.R. Baghurst, D.M.P. Mingos and M.J. Watson. Application of Microwave Dielectric Loss Heating Effects for the Rapid and Convenient Synthesis of Organometallic Compounds. *Journal of Organometallic Chemistry*, 368:C43–C45, 1989.

[43] D.R. Baghurst and D.M.P. Mingos. Design and Application of Application Reflux Modification for the Synthesis of Organometallic Compounds using Microwave Dielectric Loss Heating Effects. *Journal of Organometallic Chemistry*, 384:C57–C60, 1990.

[44] M. Chanda and S.K. Roy. *Plastics Technology Handbook.* Taylor & Francis, fourth edition, 2006.

[45] V. Singh R. Sanghi, editor. *Green Chemistry for Environmental Remediation.* John Wiley & Sons, 2012.

[46] Satoshi Horikoshi and Nick Serpone. *Microwaves in nanoparticle synthesis : fundamentals and applications.* Wiley-VCH, Weinheim, Germany, 2013.

[47] R. Rosa, P. Veronesi, A. Casagrande, and C. Leonelli. Microwave Ignition of the Combustion Synthesis of Aluminides and Field-Related Effects. *Journal of Alloys and Compounds*, 657:59–67, 2016.

[48] J. Sun, W. Wang, and Q. Yue. Review on Microwave-Matter Interaction Fundamentals and Efficient Microwave-Associated Heating Strategies. *Materials*, 9:1–25, 2016.

[49] R.E. Newham, S.J. Jang, M. Xu, and F. Jones. Fundamental Interaction Mechanisms Between Microwave and Matter. *Ceramic Transactions*, 21:50–67, 1991.

[50] U. Chandra, editor. *Microwave Heating*. InTech, 2011.

[51] A. Porch, D. Slocombe, J. Beutler, P.P. Edwards, A. Aldawsari, T. Xiao, V. Kuznetsov, H. Almegren, S. Aldrees and N. Almaqati. Microwave Treatment in Oil Refining. *Applied Petrochemical Research*, 2:37–44, 2012.

[52] J. Bird. *Electrical Circuit Theory and Technology*. Taylor & Francis, 5th edition, 2014.

[53] M.A. Rao, S.S.H. Rizvi, and A.K. Datta. *Engineering Properties of Foods*. Taylor & Francis, 4th edition, 2014.

[54] Agilent Technologies. Agilent Basics of Measuring the Dielectric Properties of Materials, 2006.

[55] M.S. Venkatesh and G.S.V. Raghavan. An Overview of Dielectric Properties Measuring Techniques. *Canadian Biosystems Engineering*, 47, 2005.

[56] D. Bogdal and A. Prociak. *Microwave-Enhanced Polymer Chemistry and Technology*. John Wiley & Sons, 2008.

[57] M. Mehdizadeh. *Microwave/RF Applicators and Probes for Material Heating, Sensing, and Plasma Generation: A Design Guide*. William Andrew, 2010.

[58] G.L. Robertson. *Food Packaging: Principles and Practice*. Taylor & Francis, 3rd edition, 2012.

[59] Instrument Types, Microwave Reactors. Accessed: November 2015.

[60] F. Chemat. *Microwave-Assisted Extraction for Bioactive Compounds : Theory and Practice*. Springer, 2012.

Chapter 3

INTRODUCTION TO ZEOLITES

The word "zeolite" comes from the Greek words for "boil" and "stone" - zein and lithos, respectively. The study of zeolite began over two centuries ago, when Axel F. Cronstedt identified zeolites as a new group of minerals [1]. After discovering stilbite in 1756, he found that zeolites are made up of hydrated aluminosilicates of alkali and alkaline earth [2, 3].

3.1 Structure and Properties of the Zeolite

Zeolites are commonly defined as crystalline aluminosilicate materials, which have distinct three-dimensional structures and pore sizes (3-13Å in diameter). All zeolites have distinct frameworks that are formed by combining oxide tetrahedral, [4] like SiO_4 and AlO_4 with different atomic ratios (Figure 3.1).

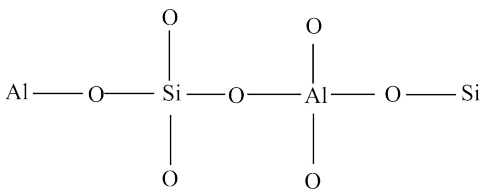


Figure 3.1: Basic Structure of the zeolite.

The existence of an Al^{+3} generates a negative charge that needs to be electro neutralised. Thus the negatively charged framework can be extended by an extra-framework cations through the exchange with different metal atom, such as B, Fe, Ga, Mg, Mn, Ti, and Zn into the tetrahedral positions within the structure. This can influence the ion-exchange chemistry and the adsorption properties of zeolites. The structural formula of a crystallographic unit cell of zeolite is [5]:

$$M_{x/n}[(AlO_2)_x(SiO_2)_y].wH_2O \tag{3.1}$$

Where,

M is the exchangeable cation of valence n

w is the number of water molecules,

The ratio y/x varies from 1 to ∞ depending on the structure, whereas, the sum (x+y) is the total number of tetrahedra in the unit cell. The part inside the bracket indicates the framework composition. The value of y/x must be equal to or greater than 1 according to the empirical Löwenstein rule [6].

The ratio of Si to Al can vary in a wide range between zeolites. It can start from one Al atom per Si atom as in zeolite X, to the amount of aluminium in the composition being zero in silica zeolite (silicalite) [7]. In ZSM-5 zeolite the silicate content is high compared to aluminium, while Y zeolite can be prepared with either high silicate or high aluminium form. In general, the presence of the aluminium in the framework can have a huge effect on the zeolite structure and properties.

Zeolite can become hydrophilic in case of high aluminium content and hydrophobic in case of high silicon content. Also, the presence of aluminium can influence the net negative charge which can be balanced by bonding the protons and the lone pairs of the bridging oxygens resulting in an acidic sites that are very important in influencing the catalytic activity [8].

The main building unit of zeolites is the TO_4 tetrahedron, which is three-dimensional. A combination of primary building units can create other structures, which include squares, pentagons, or octagons. These are called secondary building units (SBU), which are comprised of n-ring structures; where n is commonly 4, 5, 8, 10, or 12. The SBU linkages can create channels and cages

that are vital elements of all zeolite frameworks [9].

Zeolites are categorized by their framework type-codes, which only illustrate their framework topology; this is because of their wide diversity, and means that their structural composition, cell dimension, and tetrahedral atom distribution are not described. The International Zeolite established three-letter structure codes for zeolite and recognized more than 190 framework type-codes. For example, chabazite (CHA) has small pores from 8-membered rings, ZSM-5 (MFI) has medium pores from 10-membered rings, while beta zeolite (BEA) has large pores from 12- membered rings. The shape of various zeolites is primarily due to the variations in pore size, which permit the selective adsorption of particular reactants. These pore sizes also allow for desorption of particular materials that may promote or minimize the different reaction intermediates in catalytic reactions [10].

The catalytic activity in zeolite structures is due to five properties: molecular sieving ability, cation exchange, high surface area, variable acidity, and chemical and thermal stability. The first property explains zeolite shape-selective properties during catalysis [11]. Weisz and Frilette first discovered these properties, and since then Csicsery has identified three kinds of shape-selective behaviour during catalysis: reactant shape selectivity, product shape selectivity, and restricted transition-state shape selectivity, as illustrated in Figure 3.2. In reactant shape selectivity, reactant molecules are too large to enter the pores of zeolite. In product shape selectivity, different sizes of reactants form inside interior spaces of zeolite, and some of the reactants are too large for diffusion. This leads to blockage of the pores of zeolite, or sometimes to the reactants breaking down into smaller molecules [12, 13].

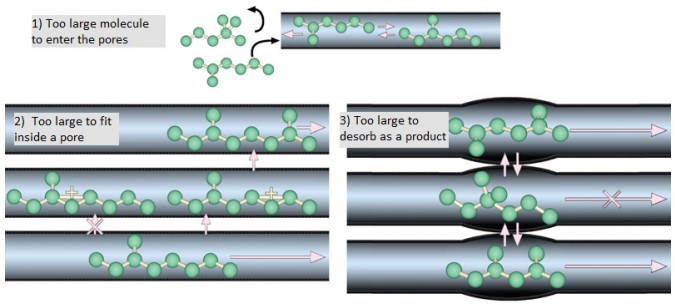


Figure 3.2: Three different cases of shape selectivity mechanisms: (1) Reactant shape, (2) Transition state shape, (3) Product shape selectivity [14].

3.2 The Structure and Properties of ZSM-5 Catalyst

From an industrial perspective, ZSM-5 is one if the most desirable forms of zeolite catalyst that can used in various applications. Examples include methanol to gasoline conversion, benzene alkylation, hydrodewaxing, and gas phase ethylation (the Mobil/Badger process). Moreover, ZSM-5 can be used in the catalysis of certain organic transformations under solvent-free conditions. ZSM-5 has a 10-membered oxygen ring and two types of channel systems with similar size: straight channels (5.3×5.6Å) and sinusoidal channels (5.1×5.5Å). These two different channels are perpendicular to each other and generate intersections with diameters of 8.9Å.

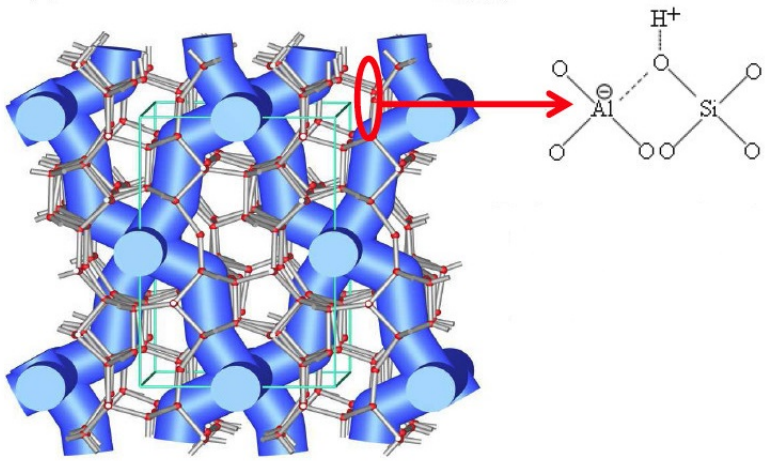


Figure 3.3: Schematic diagram of the channels structure in HZSM-5 [15].

The protonic form of ZSM-5 is known as HZSM-5 and is used widely in industrial chemical processes for acid catalysis. Because the external surfaces and pore mouth regions of HZSM-5 have non-selective acid sites, HZSM-5 zeolites have low selectivity. Pore-size engineering modifies the concentration of acid sites and other properties. Changing the zeolite from ZSM-5 to HZSM-5 can enhance the catalytic selectivity by influencing diffusion ability and overall catalytic properties. Transition metal doping into the zeolite framework can also help to arrange active site(s) required for specific reactions. Chemical modification of ZSM-5 zeolites by impregnation with acids (e.g. phosphoric/boric acid) enhanced their catalytic properties for the n-hexane cracking reaction, methanol to hydrocarbon (MTH) conversion. It can also be used in toluene alkylation with methanol, toluene disproportionation, and alkylation of benzene with ethanol [16].

3.3 Zeolite in Industry

Engineers and scientists continue to look for more efficient, potentially new methods of refining crude oil, especially given concerns about sustainability and the environment. Zeolite catalysis poses two key difficulties. First, there needs to be a direct way of converting alternative or poor-quality raw materials (e.g. coal or biomass) into useful products such as olefins. Currently, synthesis

gas can yield olefins, but the process is indirect. Second, stakeholders desire refining processes that are efficient and reduce the consumption of energy.

Nonetheless, zeolites are still important as the world transitions from a fossil-based economy to a sustainable one. Because zeolites are composed of silicon, aluminium, and oxygen, they are inexpensive and less environmentally toxic. Hence, they are still used in various chemical processes that require catalysis, including cracking, biomass conversion, and automotive catalysis [17, 18].

One important form of zeolite used in experiments is HZSM-5, the channel system of which is due to a well-ordered MFI-type framework. Zeolite frameworks consist of silica and alumina tetrahedra, which are linked by shared oxygen atoms. The solid-acid character of zeolites arises from negatively charged AlO_4- tetrahedra that are incorporated into the zeolite lattice [19]. Each of these tetrahedra produces a net negative charge on the framework, which needs to be compensated by a counter-cation. If the counter-cations are protons, strong Brønsted acid sites are formed [20]. If more aluminium is substituted in the framework, it leads to more acid sites. Therefore, the silicon to aluminium ratio (Si/Al) in the framework is an important parameter for zeolites. The combined shape selectivity and strong acidity of zeolites create the desired activities for the catalytic cracking of hydrocarbons [14].

Zeolites are primarily used as catalysts in cracking and oil-refining, but they are used as catalysts in other processes as well: alkylation of aromatics with oxygenates, conversion of (bio) alcohol to light olefins, dewaxing of hydrocarbons, aromatics and fuels, dehydrogenation of paraffins, the dehydration of (bio) alcohols, and in photocatalytic reactions. Zeolites can be used as catalysts for the future "green" conversion of hydrocarbon into useful products [19].

3.4 ZSM-5 Catalyst for Olefin Production

ZSM-5 has several desirable properties as a catalyst: shape selectivity, ion-exchanging properties, and special pore structures as well as large specific surface area [17]. These properties allows ZSM-5 to be the catalyst in cracking, aromatization of hydrocarbons, and other processes [21–23]. Steam cracking, however, is still the main procedure for the catalytic cracking of hydrocarbons and olefins [24].

Zeolite in the form of ZSM-5 makes successful the conversion of methanol to hydrocarbons,

leading to the production of olefins from methanol, this process was discovered in the late 1970s [25]. Hence, they have been used as catalysts in petroleum refining, and in the controlling of pollution. The methanol-to-hydrocarbon (MTH) procedure is considered an alternative to the coal chemical industry . Zeolites with different pore structures can serve as catalysts to convert methanol into various products through methanol-to-olefin (MTO) [26], methanol-to-propylene (MTP) and methanol-to-gasoline (MTG) conversions [27–29].

The catalytic cracking ability of ZSM-5 zeolites improves when treated with alkali, which introduces mesopores; this leads to better yields of light olefins [30]. Nonetheless, ZSM-5 requires frequent regeneration because it has low selectivity towards $C_5 - C_{10}$ alkanes and has high yields of aromatics and carbon deposition [31]. The properties of ZSM-5 zeolite, especially its framework Si/Al, which is related to the acidity of the catalyst, played a vital role in determining the nature of the product. To deactivate ZSM-5, steam pre-treatment at high temperatures (750-850^{o}C) is applied. When it is added as a catalyst, either in fresh form or having been deactivated by steam, the process will yield less gasoline and the yield of $C_3 - C_4$ unsaturated olefins will be affected. Because ZSM-5 is a typical acid function zeolitic catalyst, changes in the acidity of ZSM-5 caused by different initial Si/Al ratios, chemical dealumination, or steam deactivation will occur, along with the observed changes in octane number and product yields. The general role of zeolites in the production of olefins is to improve the efficiency of processes that are being developed. [21, 32, 33].

Bibliography

[1] J.L. Faria, M.M. Pereira, and J. Faria. *Catalysis from Theory to Application: An Integrated Course*. Coimbra University Press, 2008.

[2] R. Szostak and R.F.T. Stepto. *Molecular Sieves: Principles of Synthesis and Identification*. Springer, 1998.

[3] P.A. Jacobs, E.M. Flanigen and J.C. Jansen. *Introduction to Zeolite Molecular Sieves*. Elsevier, 2001.

[4] T. Ennaert, J.V. Aelst, J. Dijkmans, R. De Clercq, W. Schutyser, M. Dusselier, D. Verboekend, and B.F. Sels. Potential and Challenges of Zeolite Chemistry in the Catalytic Conversion of Biomass. *Chem.Soc.Rev.*, 45:584–611, 2015.

[5] A. García, C.M. López, L.V. García, J. Casanova, and M.R. Goldwasser. Improvements in the Synthesis of Zeolites with Low Si/Al Ratio from Venezuelan Sodium Silicate for an Environmentally Friendly Process. *Ingeniería e Investigación*, 36:62–69, 2016.

[6] W. Lutz. Zeolite Y: Synthesis, Modification, and Properties-a Case Revisited. *Advances in Materials Science and Engineering*, 2014:1–20, 2014.

[7] A. Primo, and H. Garcia. Zeolites as Catalysts in Oil Refining. *Chem.Soc.Rev.*, 43:7548–7561, 2014.

[8] H.F. Youssef, W.H. Hegazy, H.H. Abo-almaged, and G.T. El-Bassyouni. Novel Synthesis Method of Micronized Ti-Zeolite Na-A and Cytotoxic Activity of its Silver Exchanged Form. *Bioinorganic Chemistry and Applications*, pages 1–12, 2014.

[9] J.A. Boscoboinik, X. Yu, B. Yang, S. Shaikhutdinov, Hans-Joachim Freund. Building Blocks of Zeolites on an Aluminosilicate Ultra-thin Film. *Microporous and Mesoporous Materials*, 165:158–162, 2013.

[10] P. Parthasathi. *Asymptotic and Particle Methods in Nonlinear Transport Phenomena: Membrane Separations and Drop Dynamics*. PhD thesis, Chemical Engineering, 2008.

[11] Antonio Chica. Zeolites: Promised Materials for the Sustainable Production of Hydrogen. *ISRN Chemical Engineering*, 2013:1–19, 2013.

[12] K. Tanabe, M. Misono, H. Hattori and Y. Ono. *New Solid Acids and Bases: Their Catalytic Properties*. Elsevier, 1990.

[13] S. Lee, H. Kim, and M. Choi. Controlled decationization of X Zeolite: Mesopore Generation Within Zeolite Crystallites for Bulky Molecular Adsorption and Transformation. *Chem. A*, 1:12096–12102, 2013.

[14] B. Smit and T.L. Maesen. Towards a Molecular Understanding of Shape Selectivity. *Nature*, 451:671–678, 2008.

[15] S. Brandenberger, O. Krocher, A. Tissler and R. Althoff. Identification of the SCR Active Sites in Fe-ZSM-5. Accessed: January 2016.

[16] R. Isak , A. Rafique and A. Alamgir. H-ZSM-5 Zeolite Synthesis by Sourcing Silica from the Wheat Husk Ash: Characterization and Application as a Versatile Heterogeneous Catalyst in Organic Transformations Including Some Multicomponent Reactions. *Journal of Catalysis*, 2015:14, 2015.

[17] E.T.C. Vogt, and B.M. Weckhuysen. Fluid Catalytic Cracking: Recent Developments on the Grand Old Lady of Zeolite Catalysis. *Chem.Soc.Rev.*, 44:7342–7370, 2015.

[18] B. Silva, H. Figueiredo, O.S.G.P. Soares, M.F.R. Pereir, J.L. Figueiredo, A.E. Lewandowska, M.A. Banares, I.C. Neves, T. Tavares. Evaluation of Ion Exchange-modified Y and ZSM-5 Zeolites in Cr(VI) Biosorption and Catalytic Oxidation of Ethyl Acetate. *Applied Catalysi*, 117:406–413, 2012.

[19] H.E. Van Der Bij and B.M. Weckhuysen. Phosphorus Promotion and Poisoning In Zeolite-based Materials: Synthesis, Characterisation and Catalysis. *Chemical Society Reviews*, 44:7406–7428, 2015.

[20] Y. Li, H. Sun, R. Feng, Y. Wang, F. Subhan, Z. Yan, Z. Zhang, Z. Liu. Synthesis of ZSM-5 Zeolite from Diatomite for Fluid Catalytic Cracking (FCC) Application. *Applied Petrochemical Research*, 4:347–353, 2015.

[21] N. Rahimi and R. Karimzadeh. Catalytic Cracking of Hydrocarbons over Modified ZSM-5

Zeolites to Produce Light Olefins: A Review. *Applied Catalysis*, 398:1–17, May 2011.

[22] Z. Xie, Z. Liu, Y. Wang, Q. Yang, L. Xu, and W. Ding. An Overview of Recent Development in Composite Catalysts from Porous Materials for Various Reactions and Processes. *Int J Mol Sci.*, 11:2152–2187, 2010.

[23] C. Liu, Y. Deng, Y. Pan, Y. Gu, B. Qiao, and X. Gao. Effect of ZSM-5 on the Aromatization Performance in Cracking Catalyst. *Journal of Molecular Catalysis*, 215:195–199, 2004.

[24] R. Le Van Mao, A. Muntasar, H.T. Yan, and Q. Zhao. Catalytic Cracking of Heavy Olefins into Propylene, Ethylene and Other Light Olefins. *Catalysis Letters*, 130:86–92, 2009.

[25] P. Li, W. Zhang, X. Han, and X. Bao. Conversion of Methanol to Hydrocarbons over Phosphorus-modified ZSM-5/ZSM-11 Intergrowth Zeolites. *Catalysis Letters*, 134:124–130, 2010.

[26] P. Tian, Y. Wei, M. Ye, and Z. Liu. Methanol to Olefins (MTO): From Fundamentals to Commercialization. *ACS Catalyst*, 5:1922–1938, 2015.

[27] F.J. Keil. Methanol-to-Hydrocarbons: Process Technology. *Microporous and Mesoporous Materials*, 29:49–66, 1999.

[28] S. Ilias and A. Bhan. Mechanism of the Catalytic Conversion of Methanol to Hydrocarbons. *ACS Catalysis*, 3:18–31, 2013.

[29] Q. Wang, L. Wang, H. Wang, Z. Li, X. Zhang, S. Zhang, Suojiang, and K. Zhou. Effect of SiO_2/Al_2O_3 Ratio on The Conversion of Methanol to Olefins over Molecular Sieve Catalysts. *Frontiers of Chemical Science and Engineering*, 5:79–88, 2011.

[30] C. Xu L. Zhao, J. Gao and B. Shen. Alkali-treatment of ZSM-5 Zeolites with Different SiO_2/Al_2O_3 Ratios and Light Olefin Production by Heavy Oil Cracking. *Fuel and Energy*, 92:414–420, 2011.

[31] J. Biswas and I.E. Maxwell. Recent Process- and Catalyst-related Developments in Fluid Catalytic Cracking. *Applied Catalysis*, 93:197–258, 1990.

[32] J.S. Buchanan. The Chemistry of Olefins Production by ZSM-5 Addition to Catalytic Cracking Units. *Catalysis Today*, 55:207–212, January 2000.

[33] S M Sadrameli. Thermal / Catalytic Cracking of Hydrocarbons for the Production of Olefins : A State-of-the-art Review I : Thermal Cracking Review. *Fuel*, 140:102–115, 2015.

Chapter 4

EXPERIMENTAL METHODS

Overview

This chapter presents an overview of the experimental techniques used in this thesis. Design and technical analysis of both the cavity resonator and single mode heating systems will be described in detail. In addition, the implied characterisation techniques are also introduced.

4.1 Cavity Perturbation Technique

4.1.1 Introduction and Background

The cavity perturbation technique involves one of the most sensitive measurements for obtaining the complex microwave permittivity and permeability values [1]. The technique is usually employed for measuring dielectric properties, for couple of reasons: it is simple, accurate, and data some times could be easily produced and interpreted. The technique can also be used accurately on low dielectric loss materials, and is also sensitive to low loss tangents. An early description of the perturbation issue was given by Bethe and Schwinger in 1943 [2], Slater and Casimir in 1950-1952 [3]. The cavity resonator system has been in use for a long time, and continues to be used for dielectric measurements, for example by Horner *et al.* in 1945 [4], Sinha and Brown in 1960 [5], Li *et al.* in 1981 [6], and Martinelli *et al.* in 1985 [7]. The perturbation technique is based on the concept that when a dielectric or conducting material is placed into a resonant cavity, there is a

change in the shape of the frequency curve of the resonance and the Q factor of the cavity [8, 9].

Electromagnetic field orientation for two standard cavity modes could be either TM type (transverse magnetic) or TE type (transverse electric) mode of propagation [10]. The wave propagates along a single direction on the given waveguide and both electric and magnetic fields are always travelling together in the waveguide. Besides, they are always perpendicular to each other. In the case of the Transverse Electric (TE) mode, the electric field is transverse to the direction of propagation, whereas the magnetic field has a component in the direction of propagation. However, in the Transverse Magnetic (TM) mode, the magnetic field is transverse to the direction of propagation while the electric field has a component in the direction of propagation. [11, 12].

The TM_{0n0} cavities are used for dielectric measurements with samples, and are placed along the central axis of the cavity at the maximum area of the electric field. However, there are several limitations to this technique, such as the requirement for a very thin, small amount of sample. This drawback is especially crucial when considering high permittivity-loss materials that require needle-like samples. Parkash *et al.* [13] in 1979 built on the technique of classic cavity perturbation to comprise specimens that are thicker and whose length is less compared to the height of the cavity. Despite this, the volume of the material is still low and the accuracy of the measurement is diminished.

Variations in the width and centre frequency as a result of the sample insertion can be linked to the real permittivity [14]. Vector network analyzers (VNA) are employed to show the change in bandwidth and the shifts in frequency. Both Liao *et al.* [15] and Venkatesh [16], reported the details of measurement and information accuracy, as well as perturbation equations that are adjusted for the calculation of the real and imaginary permittivity. The resonant cavity limits the measurements to one frequency. Despite the need for calibration of each cavity, computations can be rapidly derived once calibration curves are found. The preparation of samples is not difficult, and many samples can be measured in a short amount of time [9].

4.1.2 Cavity Resonator Fields and Analysis

Figure 4.1 shows the cross-section of the infinite waveguide. There is an assumption that all dielectrics surrounding the centre of the sheath are concentric, and that the parameters for each one are constant. The two equations (by Maxwell) for a time harmonic field in a homogeneous free

space are [17]:

$$\nabla x\bar{E} = -j\omega\mu\bar{H} \tag{4.1}$$

$$\nabla x\bar{H} = j\omega\varepsilon\bar{E} \tag{4.2}$$

Where:

∇ is the vector curl, j is an imaginary unit = $\sqrt{-1}$

$\bar{E}$ is the vector electric field (V/m), and $\bar{H}$ is the vector magnetic field (A/m),

ω is the angular frequency

μ is the permeability, and ε is the permittivity

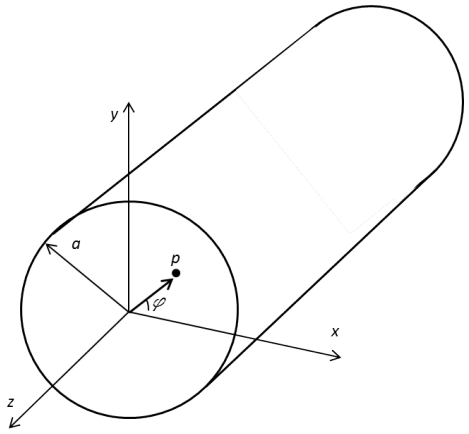


Figure 4.1: Cylindrical coordinate system.

The solution of the electromagnetic eigenvalue problem for a circular cylinder is shown in terms of the magnetic and electric fields, Q-values, and resonance frequencies [18]. There is an assumption

that the cavity has a homogeneous dielectric with permeability and permittivity. The cylindrical cavity resonators could be designed as either transverse electric or transverse magnetic modes [19]. The two equations for the two unknowns (E and H) can be solved for either the curl of E or H and the results of the equations 4.1 and 4.2 can give:

$$\nabla x \nabla x E = -j\omega\mu\nabla \times H = \omega 2\mu E \tag{4.3}$$

This result can be further simplified in terms of the vector identity for E,

$$\nabla^2 E + \omega 2\mu E = 0 \tag{4.4}$$

Because $\nabla \cdot E = 0$ in a region without a source.

The wave equation, or *Helmholtz* equation, is presented in equation 4.4. The same equation can be solved in terms of H vector in the same way

$$\nabla^2 E_z + k^2 E_z = 0 \tag{4.5}$$

where

E_z is the electric field of the z component

$k = \omega\sqrt{\mu\varepsilon}$ is defined as the propagation constant or wavenumber of the object, and its units are 1/m [20].

The general solution for solving for E_z using the wave equation for the TM modes of the circular waveguide in terms of the cylindrical coordinates (ρ, ϕ, z) is:

$$E_z(\rho, \phi) = (A\sin(n\phi) + B\cos(n\phi))J_n(k_c\rho) \tag{4.6}$$

where A and B are the amplitude constants associated with either the discrete TM or TE

modes.

k_c is the cutoff wavenumber.

J_n represents the Bessel function, and the solution to E_z must be periodic in φ, thus the integer n needs to be introduced.

The boundary conditions can be directly applied to E_z because:

$$E_z(\rho, \phi) = 0 \tag{4.7}$$

at $\rho = a$ where a is the radius of the cavity.

As a result, the equation is $J_n(k_c a) = 0$ or $k_c = \frac{P_{nm}}{a}$.

where P_{nm} roots of the Bessel function [21] of the first kind and the propagation parameters for the mth of the TM mode are constant. The values of P_{nm} are given in mathematical tables [22–24].

The first few values are listed in Table 4.1.

n	P_{n1}	P_{n2}	P_{n3}
0	2.405	5.520	8.654
1	3.832	7.016	10.174
2	5.135	8.417	11.620

Table 4.1: Values of P_{nm} for TM Modes of a Circular Waveguide [24].

The propagation constant of the TM_{nml} mode is,

$$\beta_{nm} = k^2 - k_c^2 = k^2 - (P_{nm}/a)^2 \tag{4.8}$$

and the cut off frequency is

$$fc_{nm} = k_c^2 \pi \sqrt{\mu} = p_{nm}^2 \pi a \sqrt{\mu} \tag{4.9}$$

As such, the first TM mode to propagate is the TM_{01} mode, such that $P_{01} = 2.405$. l is the length of the waveguide and it should be an integer number of half-wavelengths [17, 25, 26].

4.1.3 General Aspects of Designing the Cavity

4.1.3.1 Resonant Frequency

Special attention must be paid when designing a resonant cavity, in order to ensure that the operation is effective and optimum performance is achieved. Among the modes that are resonant inside the cavity at high frequency, the dominant frequency of the TM_{nm} mode is the TM_{010}. So, the cavity size must be planned to match the frequency of interest and to operate within the TM_{010} mode, as the relationship is inversely proportional (higher frequency, smaller cavity) [27]. The relationship between the resonant frequency and the dimension of the cavity with the sample is stated in the following equation:

$$f_{mnl} = \frac{c}{2\pi\sqrt{\mu_r \varepsilon_r}} \sqrt{\left\{\frac{P_{nm}}{a}\right\}^2 + \left\{\frac{l\pi}{d}\right\}^2} \tag{4.10}$$

where f_{mnl} represents the operation frequency of the cylindrical cavity, and c is the speed of light. μ_r and ε_r are the permeability and the permittivity of the tested sample respectively. a is the cavity radius and d represents the height of the cylindrical cavity resonator. l is the half wavelength long, and P_{nm} is the propagation parameters of the TM mode. Figure 4.2 shows the resonant frequencies for a number of low order modes against the cavity radius.

Each of the cavities is in needs of calibration. However, as each calibration curve is obtained, calculations become faster. The preparation of samples is comparatively easy, and the permittivities of large samples can be detrimental in a short amount of time [11, 22, 27].

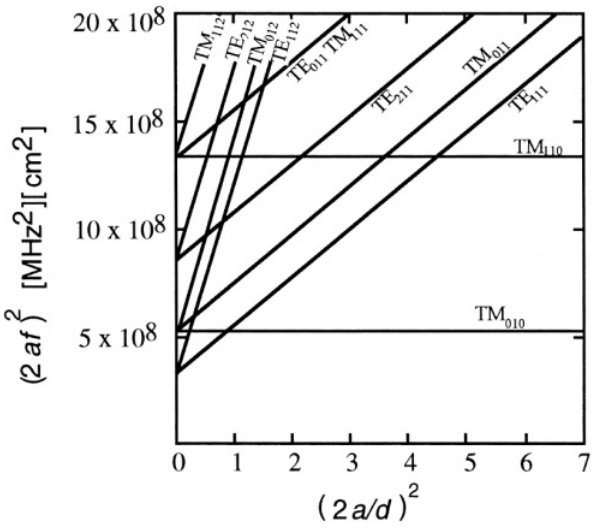


Figure 4.2: The Resonant Mode Chart for a Cylindrical Cavity Resonator [27].

4.1.3.2 Finite Element Modelling using COMSOL Multiphysics®

COMSOL is commercial computational software that can be used to construct and simulate models. Moreover, it can compute chemical reactions and physical phenomena. The computational modelling is based on the finite elements and mathematical methods to solve the physical equations [28]. COMSOL Multiphysics® 5.2 package with COMSOL RF-module has been used to simulate the electromagnetic field for the cases displayed in this thesis. The electromagnetic equation that was applied to simulate the TM waves mode is:

$$\nabla \mathrm{x} \left\{ \left[\varepsilon_r - \frac{j\sigma}{\omega \varepsilon_0} \right]^{-1} \nabla \mathrm{x} \overline{H} \right\} - \mu_r k_0^2 \overline{H} = 0 \tag{4.11}$$

Where ε_r is the relative permittivity

ε_0 is the permittivity of free space

σ is the material conductivity

H magnetic field intensity

μ_r is the relative permeability

k_0 is the input a wave vector

To solve a specific mode, COMSOL will compute the problems using a set of numerical advanced methods. After optimising the geometry, it will run the analysis and create a mesh together with an error control applying a numerical solver. All the steps that include the geometry optimisation, mesh applying, solver setting and results virtualisation will be recorded to create a sequence that allows for easier control over parameters and modification of any part of the system created [28].

Two and three dimension structures can be modulated using COMSOL. However, the 2D has the advantages of improving the accuracy of the model and the symmetry of the problems; whereas the 3D model can be more complicated and requires higher level of computational modelling.

COMSOL was used to generate the images provided in this thesis. The RF model and the microwave devices were used to generate the electromagnetic field within the resonant cavity in both the 2D and 3D structures. First, we were able to design and optimise the geometry of the cavity device. Then, by applying the electromagnetic equation, we were able to accurately and swiftly simulate a uniform distribution of the electric and magnetic fields propagation within the device. It was also possible to extend the simulation to provide a uniform distribution of the high electric field formation in the microwave reactor. Simulation was also conducted by computing the electric field in the microwave applicator and the field energy density distribution in the microwave applicator and in the catalyst bed.

4.1.3.3 TM_{010} Mode

TM_{010} or the monopole mode is the lowest frequency and the dominant TM mode (P_{01}=2.405). It can be characterised by a longitudinal electric field which is maximal at the centre of the cavity r =0. A schematic representation of both electric and magnetic field in the TM_{010} cavity can be seen in Figure 4.3. In this type of characterisation mode, the magnetic field and the cavity bottom are parallel, while the electric field is perpendicular to the latter. The energy density of the magnetic field increases from the centre of the cavity to the boundary, while the opposite is true for the electric field. The total energies of the two fields are also stored within the cavity, and consequently the power can be dissipated in the metal wall of the cavity resonator as well as the filled dielectric material [29].

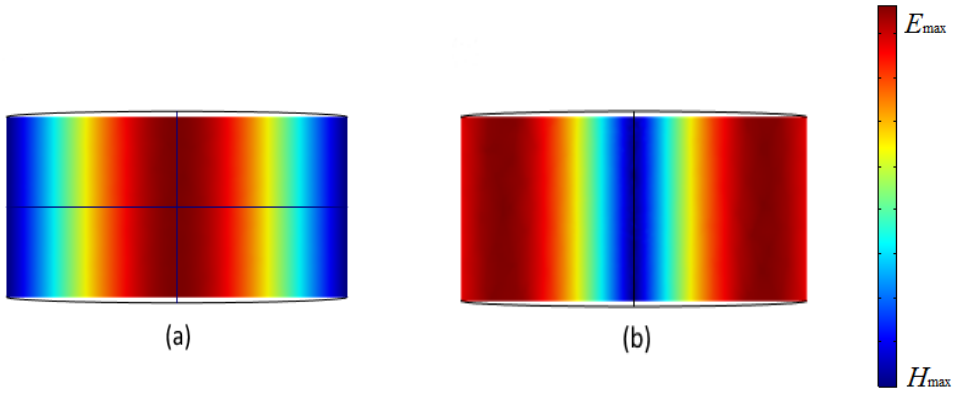


Figure 4.3: COMSOL simulations of the Electric (red) and Magnetic (blue) Fields distribution in Cylindrical Cavity for the (a)TM_{010}, and (b) TE_{011} Mode.

There are several advantages related to placing the sample in the central post of the cavity. In the TM_{010} mode, the electric field is at its maximum, resulting in an increased interaction between the signal and the sample. However, it falls to zero on the cylindrical sidewall, as required by the electrical boundary conditions. The fields strengths do not vary, as one goes from top to bottom along the cavity axis which results in a constant and uniform electric field over the sample. This is significantly important to the quality of the analysis. Specimens are generally in the form of rods or tubes, and these can be utilised as containers for liquid dielectrics. Specimens normally reach from the top of the cavity to its bottom, however this is not required [30].

The interpreting of resonance measurements involves measuring the shift in the frequency as well as the bandwidth of the mode that has been perturbed. The resonant circuit analysis illustrates that the resonance forms a Lorentzian line shape in the domain frequency. However, the presence of other modes in its vicinity distorts the said shape and can lead to inaccurate measurements. As such, the TM_{010} mode needs to be isolated from other frequencies. This must be accounted for when designing the dimensions of the cavity for the resonant frequency requirements. So, the cylindrical cavity is made with a radius a = 4.6 cm and height d= 4 cm. The length of the cavity does not have an effect on the resonance frequency for this mode; however, a longer cavity may lead to the deterioration of the mode, and this leads to ambiguity in the measurements [31].

4.1.4 Quality Factor of the Cavity

A general measurement for comparing cavities or resonators is Q, or the quality factor. The Q-value measures the efficiency of a cavity to dissipate the energy in its walls and the accuracy of the measurements. The Q-factor is also measured in terms of resonance techniques in order to ascertain the loss of dielectric specimens [32].

The definition of the Q factor in the frequency domain for resonating systems the ratio between the stored power in the cavity and the dissipated power in the walls and can be expressed as follows [20]:

$$Q = \frac{2\pi \text{xEnergy stored in the resonance}}{\text{Energy lost per cycle}} \tag{4.12}$$

In the resonators, the stored energy being referred to is the electromagnetic energy that is stored in the resonator fields. The lost energy is the electromagnetic energy that is lost from the wall currents, radiation and dielectric/magnetic absorption in the sample. The "per cycle" transferred to the cycle of the sinusoidal that resonates from the electromagnetic signal at the frequency present in the resonator [27, 33].

For a typical resonator, different sources of loss in the cavity should be considered, so the equation can be written as:

$$\frac{1}{Q_t} = \frac{1}{Q_{specimen}} + \frac{1}{Q_{resonator\ walls}} + \frac{1}{Q_{coupling}} \tag{4.13}$$

The Q specimen accounts for the dielectric loss of the sample, which is the parameter of interest in terms of measurement. The Q resonator walls account for the power that is lost in the resonator metal walls as a result of conduction losses. Q coupling refers to the power that is lost through

all coupling mechanisms into the resonators, loading effect, and power is lost through any coupling ports. In addition, there are other sources of loss in the resonators [20, 34].

A very simple way to calculate the Q factor is stated in the following equation,

$$Q = \frac{f_0}{\triangle f} \tag{4.14}$$

Where,

f_0 is the maximum frequency of a resonant peak, and $\triangle f$ the change in the width of the peak at the half maximum. As high the Q factor, the narrower and 'sharper' the peak would be. The calculation is illustrated in Figure 4.4 below.

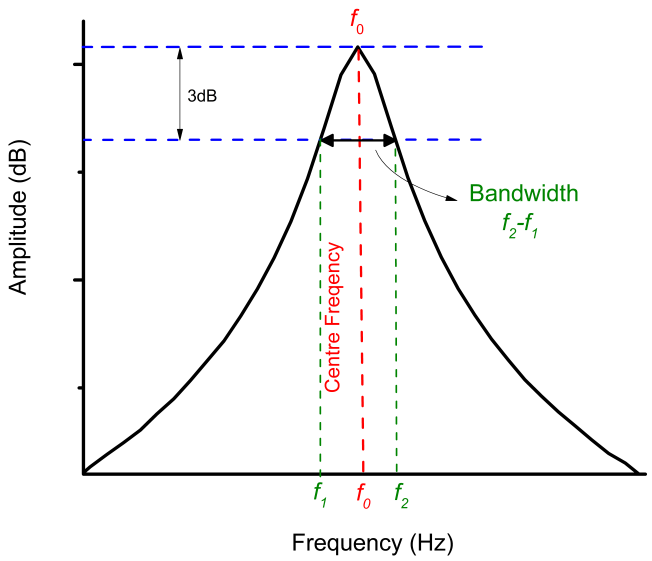


Figure 4.4: Transmission peak of a TM_{010} empty cavity describing the Q-factor calculation.

First order cavity perturbation theory refers to the shifts in the parameters of the resonator to the dielectric properties of the inserted sample (within the electric field antinode of the cavity). If

the sample inserted into a TM_{010} cavity, it is found to lessen the resonant frequency from f_0 to f_s, while the unloaded quality factor is reduced from Q_0 to Q_s, the variations can be linked to the permittivity values of the sample for the TM_{010} mode by the following equations:

$$\frac{\triangle f}{f_0} \approx (\varepsilon' - 1)\frac{V_s}{2V_{eff}} \tag{4.15}$$

$$\frac{\triangle f}{f_0} = \triangle(\frac{1}{Q}) \approx \varepsilon'' \frac{V_s}{V_{eff}} \tag{4.16}$$

f_0 is the start frequency and $\triangle f$ is the change in frequency of the cavity after inserting the sample.Vs refers to the volume of the sample, while V_{eff} is the cavity mode volume. These can be derived from the electric field distribution in the cavity. Because the V_{eff} has a critical role in determining resonator measurements from dielectric properties, it is also essential to substantiate the value of the cavity during experimentation, with the use of the perturbation technique. As a result, this can also be found by the calibration measurement of a material with known geometry [35, 36].

4.1.5 Sample Depolarisation

Under an applied electric field the sample become polarised, resulting in charge variations on the surface at the sample boundary of the dielectric material. The charges on the surface produce a depolarisation field that is opposite to the applied field. As a result, the net field within the sample is lessened, while it is constant for the field outside the sample. The interactions between the material and the field can be depicted by the relative permittivity (ε_r) of the material. This relates to the polarisation per unit volume *(P)* in terms of the internal electric field (E_{in}) through the relationship [22],

$$P = (\varepsilon_r - 1)\varepsilon_0 E_{in} \tag{4.17}$$

ε_r is the relative permittivity.

ε_0 is the permittivity of free space.

If a dielectric sample (powder or liquid) is introduced to the electric field (with a magnitude of E_0) of a resonator, the quality factor (Q) will be decreased because of the dielectric loss of the sample. On the other hand, the decrease in the resonance frequency is a result of the sample polarisation. These variations can be written using resonator perturbation analysis through the following equations [37]:

$$\triangle\left\{\frac{1}{Q}\right\} - \frac{I_m(\alpha)}{V_{eff}} \tag{4.18}$$

$$\frac{\triangle f_0}{f_0} \approx \frac{Re(\alpha)}{2V_{eff}} \tag{4.19}$$

In this equation,

f_0 is the unperturbed resonant frequency, the electric polarisability of the sample α which is defined by the induced electric I_m dipole moment, $p = \alpha\varepsilon_0 E_0$, and V_{eff} is the effective volume that is occupied by the energy of the electric field.

In order to make the sample have the most significant impact on the Q factor, the actuator must be designed such that the effects of depolarisation are mitigated.

This results in a consistently high electric field in the sample. Within the lossy dielectric, the average power that is dissipated is [38]:

$$W = \frac{1}{2}\omega_0\varepsilon_0\varepsilon'' E_{in}^2 V \tag{4.20}$$

In this case, V is the volume of the sample, while E_{in} is the internal electric field magnitude.ε_0 is the permittivity of the free space, ε'' is the imaginary permittivity, and ω_0 is the frequency band in vicinity.

The development of polarisation charges on dielectric surfaces perpendicular to the applied

electric field E_0 implies that $E_{in} < E_0$. This results in a significant decrease in the materials rate of heating, with large values of ε'. Figure 4.5 illustrates this, and it is assumed that a sample that has the shape of a cylinder is inserted into a microwave cavity that has an applied electric field E_0, at either parallel or perpendicular to the axis of the cylinder. The ratio of internal electrical fields to power dissipation in the two cases (with the assumption that the applied fields are the same) is [36–39]:

$$\frac{E_{in}^{\parallel}}{E_{in}^{\perp}} \approx \frac{1}{2}(\varepsilon + 1) \approx \frac{1}{2}((\varepsilon' + 1) - j\varepsilon'') \tag{4.21}$$

$$\frac{W_{\parallel}}{W_{\perp}} \approx \frac{1}{4}((\varepsilon' + 1)^2 + \varepsilon''^2) \tag{4.22}$$

where, ε is the complex permittivity, ε' is the real permittivity, and ε'' is the imaginary permittivity.

From the equations, it has been found that designing a cavity with an electric field that is parallel to the sample is greatly beneficial to enhance the power dissipation within the sample [38].

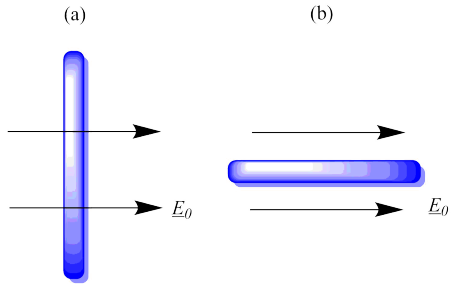


Figure 4.5: Sample depolarisation. Reproduced from Ref. [38].

4.1.6 Instrumentation for Dielectric Measurements

The cavity resonators that were utilised in this thesis were fabricated in the Oxford University's Mechanical Workshop. The aluminium and the copper cavities are illustrated in Figure 4.6. Both cavities are made with the same dimensions. The thickness of the wall is 1.5 cm, such that it can give sufficient strength to the structure. The internal length of the cavity is 4 cm and the external length is 5.5 cm. They have a small central hole with diameter of 1cm to allow the sample tube to fall in. The excitation of the cavity is done using two SMA copper connectors with pins extending into the cavity. Varying the length of each of the SMA pins inside the cavity allows the coupling strength to be controlled.

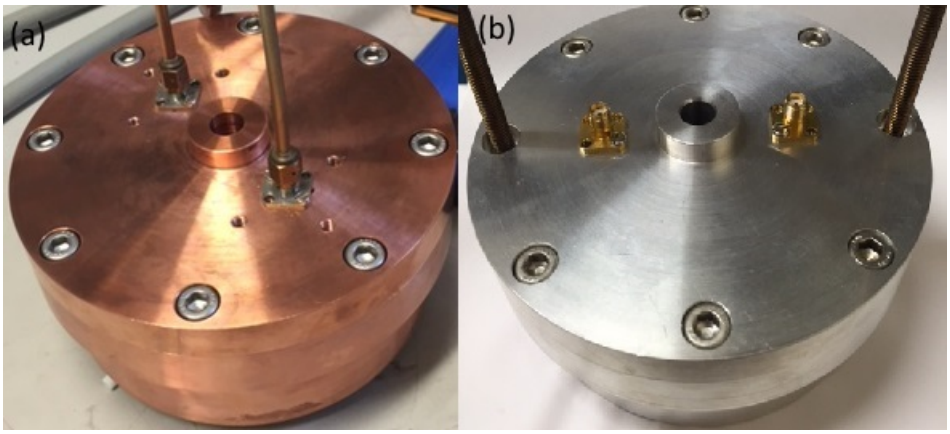


Figure 4.6: The (a) Copper, and (b) Aluminium host cavities showing the central hole where samples are introduced along the axis of the electric field.

The network analyzer is a measuring device which uses a two-port radio frequency that is connected to the cavity through two connection cables. It enables the user to measure the signal magnitude and phase at the input and/or output port of devices being tested. Different results can be shown based on set program for the desired parameters. Network analyzers that are commercially available function at different ranges of frequency; as such, care should be taken in order to make sure that the network analyzer operates at the cavity resonator frequency.

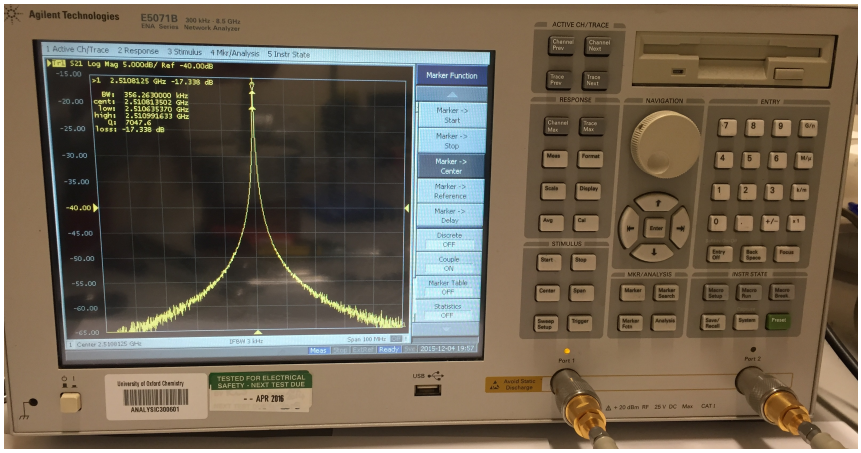


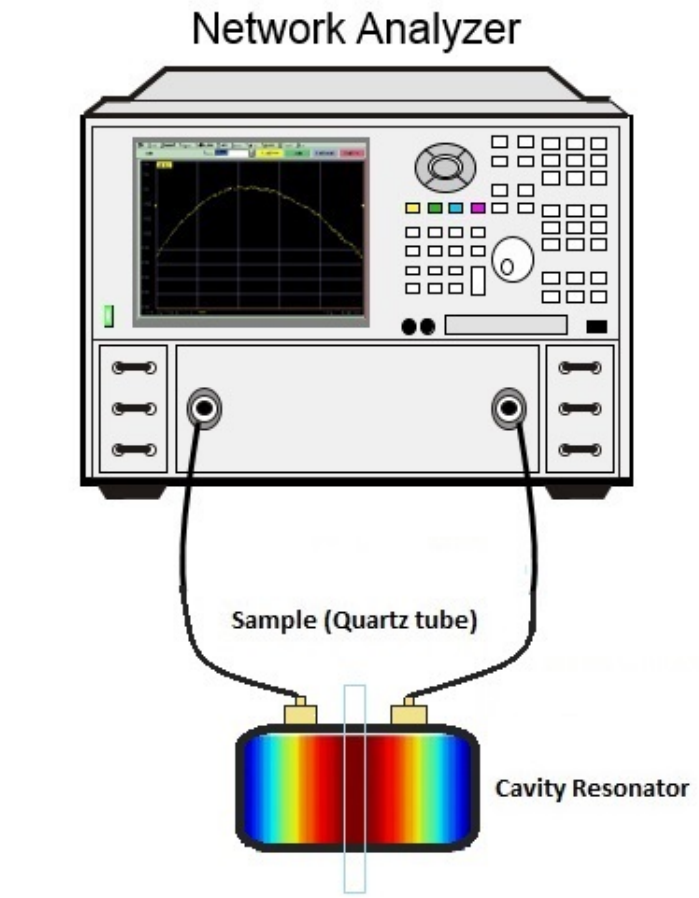
Figure 4.7: Front panel and input keys of the VNA 8753E.

Characteristics of resonance depend on the quality factor of the cavity, and the frequency of the resonance can also be observed to ascertain the dielectric parameters. The dielectric properties can be defined through the measurement of the quality factor and the resonant frequency of a cavity that is empty. Afterwards, the measurement is repeated after introducing the tested sample to the cavity [19, 40].

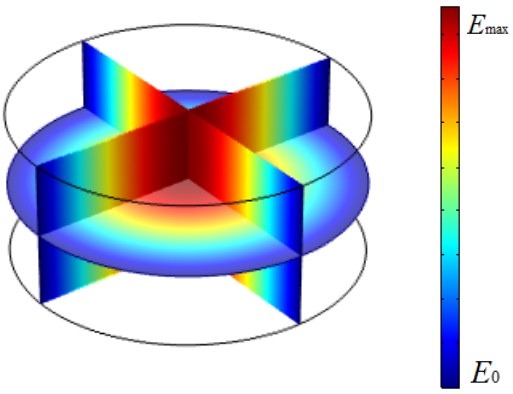
In order to set up the network analyzers for the dielectric measurements, there are several conditions that need to be satisfied. The S-parameter needs to be set to S_{21}, which represents the complex transmission coefficients from port 1 to 2, and is measured at room temperature as opposed to a fitted frequency of 2.45 GHz. The scale also needs to be revised by inputting arbitrary values in the Scale/Div, Reference Position, and Reference Value buttons. It is also necessary to load the measurements program file and the internal data as well as the results of the measurement (e.g. trace data) can be saved and display on the screen. After the cavity is positioned initially, the measurements will commence for the sample. The bandwidth and resonance frequency are recorded whilst the sample tube is empty. The empty tube measurements are taken first to allow for the calculation of the shift in frequency as the quartz tube will produce a very small perturbation when inserted in the field. Thus, for more accurate measurements the tube will be subtracted from the measurements. In these measurements, the sample tube is a quartz tube that has a 2 mm inner

diameter. The filled tube is then introduced axially in the centre of the cavity, and the resonance frequency and bandwidth are recorded once more. Using equation 4.16 and the calibrated V_{eff} value for the cavity configuration, the values of real permittivity (ε') and imaginary permittivity (ε'') for the sample are derived. Measurements need to be performed a minimum of three times for each sample in order to ensure repeatability.

COMSOL Multiphysics has been used to produce the electromagnetic field distribution in the cavity resonator. The initial dimensions of the TM_{010} cavity represented in Figure 4.8 (a) are d = 4 cm and a = 5 cm. The red colour indicates the strength of the electric field in the centre of the cavity at 2.294851 GHz.



(a)



(b)

Figure 4.8: (a) Schematic of the dielectric measurements system with a vector network analyzer, (b) A 3D COMSOL generated representation of the field distribution in the resonator cavity of the TM_{010}.

4.1.6.1 Calibrations and Corrections

The cavity perturbation technique is derived from the central idea that the insertion of a small sample into the maximum of the field will produce a shift in the Q factor and the cavity resonant frequency. These changes enable the calculation of the sample dielectric properties. By the term "small", it is meant that the volume is considerably smaller than the volume of the cavity. The amplitude and phase of the reflected microwave signals are measured for both the empty cavity and the cavity when it contains a sample. The cavity measurement with an empty quartz tube is needed, because quartz is not a perfect insulator. Several assumptions are made when using this technique: the first is that quality factors are measured at the same frequency; the second is that the difference is negligible between the cavity wall losses with and without a sample; the third is that the nature of the sample is homogeneous; the fourth is that the cavity is maintained at the same coupling condition as the external circuit; and the last assumption is that the sum of stored energy does not change when the sample is introduced.

If a sample is placed at the field antinode in the cavity, there is a greater amount of stored energy in the sample, for materials with real permittivity > 1. Using the sixth assumption from the previous paragraph, the electromagnetic energy at the cavity walls weakens, and as such the Q factor becomes greater and the loss lessens. As stated previously, the fourth assumption does not hold, because the quartz sample has a dielectric loss value, and is not a perfect insulator. In terms of practicality, assumption 3 is difficult to follow perfectly; despite this, only an effective permittivity of the mixture is being measured, and as such, the results can be processed to get the permittivities of the mixture constituents using well-established mixing laws. Treating these assumptions as correct simplifies the system and calculations that are needed to get ε' and ε'' values. Once the shift in Q factor and resonant frequency are recorded, the information can be placed in the equations below to obtain ε' and ε'' values.

$$(\varepsilon' - 1)AV_s = \frac{\triangle f}{f_0} \tag{4.23}$$

$$2\varepsilon'' A V_s = \frac{\triangle BW}{f_0} \tag{4.24}$$

In the above equations, $\triangle f$ is the change in frequency and f_0 is the start frequency. V_s is the sample volume and A is a constant that depends on the cavity geometry and size; calibration of the A constant values has been performed for both cavities. For the system utilised $A = 7.11\text{x}10^{-03}$, and $A = 7.55\text{x}10^{-03}$ for copper and aluminium cavities respectively . It has been determined using well known real permittivity values for PTFE rod and several alkanes. Table 4.2 illustrates the real permittivity values at room temperature and 2.45 GHz [41].

Sample	The real permittivity value ε' at 2.45 GHz
PTFE	2.1
Hexane	1.9
Decane	2.0

Table 4.2: The real permittivity values applied for the calibration of the resonant cavity [42].

This technique is very sensitive and accurate (within 5%); it only needs small sample quantities, and gives output data that can be converted by simply inputting the suitable information. However, the disadvantages include the fact that the technique can only be used in low and medium loss elements.

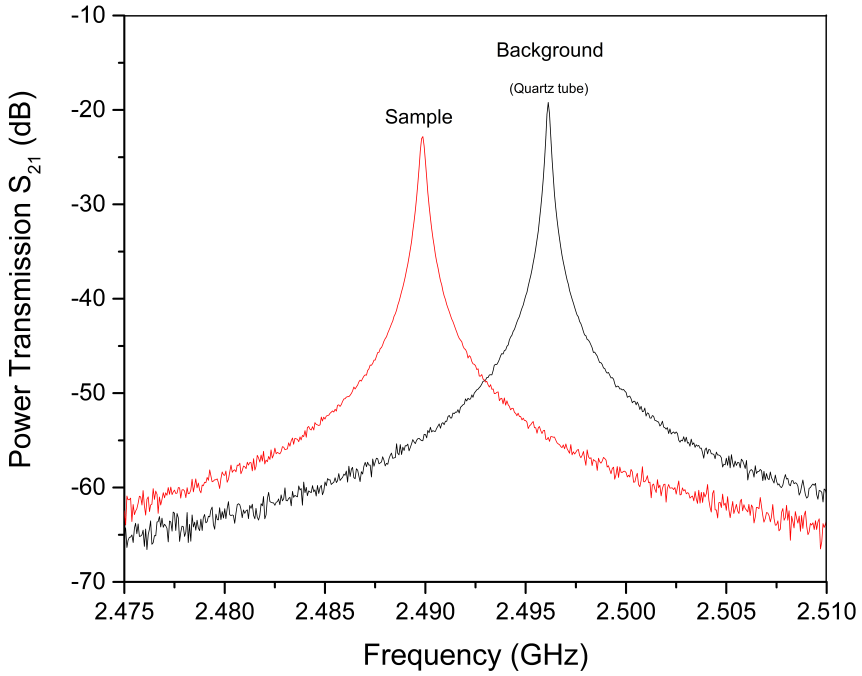


Figure 4.9: Resonant curve before (red) and after (blue) inserting the sample.

4.2 Single Mode Applicator for Microwave Heating System

Microwave reactors have been used in research and development for a number of years. They are also gaining massive importance in industry as an alternative to conventional heating systems, as microwaves can offer potentially significant energy reductions. Moreover, microwaves also offer greater yield and selectivity enhancement, in addition to the elimination of solvents and cleaner reactions which result in a number of other environmental benefits [43].

An important part of the microwave heating system is the applicator or cavity. In this thesis, all the microwave heating experiments have been conducted in a laboratory scale single-mode cylindrical microwaves applicator. The used Sairem kit (microwave generation and control chain) was a one-off design built by the French company Sairem Ltd. All applicators have been fabricated in

the mechanical workshop of the University of Oxford. The reactor, using a 2 kW microwave generator, has been built with a simple configuration and design for heavy oil and heating catalysts. For the purposes of this comprehensive project, the microwave equipment must be flexible, allowing control over every aspect of microwave interaction with the desired materials. As the single frequency systems can be adjusted for maximum throughput, the TM_{010} cavity can provide controlled high field strength at mode-specific locations within the cavity. The next section discusses the main requirements in equipment selection and design. It is also important to investigate the parametric variation for control and optimisation, and its implications for designing a versatile device to explore the possibilities of using microwaves in crude oil conversion into high value chemicals [44, 45].

4.2.1 Equipment Design Requirements

4.2.1.1 Microwave Power Supplied/Absorbed

The aim of microwave heating is to deliver the power from the microwave source to the sample; thus, it is important to define the amount of power dissipated inside the sample. The use of a single mode system that operates at one frequency allows for such an observation. This entails knowledge of the absolute value of the absorbed power in order to determine the rise in temperature; it is also important for the reproducibility and predictability of the data, which can be very difficult when using the multi-mode oven. Fully investigating the effects of the electromagnetic field strength requires using control programs to conduct the power profiles. The source will receive some of the energy supplied to the applicator; to find the amount of energy absorbed by the load being heated, it is necessary to calculate the amount of reflected energy. Power is reflected back to the source when it is not absorbed by either the system or the sample. The system is equipped with a circulator and dummy load to protect the power generator from reflected power. This prevents several possible problems with power being reflected back into the source: arcing decreased life of the magnetron, and lower efficiency of the microwave generator. Thus, the circulator redirects any reflected power into a water-cooled load; this couples well in the power generator frequency range. The sample absorbs power equal to some fraction of power that is not reflected; some power is radiated and some is absorbed by the cavity walls [46, 47].

4.2.1.2 Pulse Width Modulation

Pulse width modulation (PWM), a widely-used approach, controls the output power of the power switch by varying its (ON) and (OFF) times. The duty cycle is the ratio of (ON) time to the switching period time and will be examined parallel to the continuous microwave radiation in the reactor. Thus, it will achieve higher peak output power within a specified time period. It will also allow the separation of the effects of high-strength microwave fields and ambient temperature. The results of PWM can be compared to the results of the continuous mode.

The generator has to pulse microwaves at the required frequency and field strength (microwave power) with a preset duty cycle. Investigating temperature effects on a given field strength, as well as the field strength effects for a given temperature, requires controlling the duty cycle from 5% to 100% and controlling the power from 5% to 100%. This is significant because the main difference between microwave-driven processes and conventional heating is the presence of high strength magnetic fields. It is possible to study pulsed-power and continuous-power microwave processing in similar conditions. The system was only partially-processed with microwave radiation when the power was turned on and off. The results of pulsed-power processing may differ from continuous-power processing if there are non-thermal effects; that is, the preferential alignment of polar groups inside the electromagnetic field. An important question for several microwave-driven processes is whether or not the fields themselves modify the process, or simply induce heating rapidly and in a highly localised way [48].

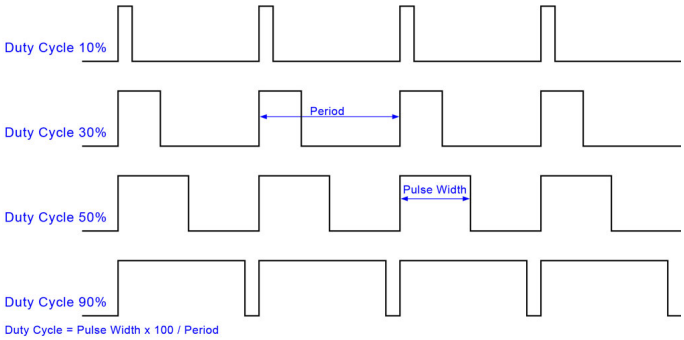


Figure 4.10: Schematic representation of different PWM waveforms; with with low (10%) and high (90%) duty cycle.

4.2.1.3 Field Distributions and Field Uniformity

The key issue in most microwave heating applications is obtaining uniform heating patterns in certain key regions of the applicator. Efficient microwave energy transfer is a function of many variables as processing occurs. Many of these variables relate to material type, density, and temperature, in addition to the applied electric field. Coupling is influenced by several other factors related to the applicator, cavity geometry, the excited mode in the cavity, and the size and frequency of the electromagnetic energy. Other factors include the relative size and shape of the material and the applicator, and the position of the material within the applicator.

Because it is an industrial, scientific, and medical (ISM) standard frequency of operation, 2.45 GHz will be the operation frequency of the proposed applicator. Moreover, 2.45 GHz creates wavelengths suitable for an experimental set-up on a bench-top. The frequency can be reduced for scale-up operations, while maintaining modes of operation and any required field distributions.

A versatile microwave configuration requires several applicators, providing a choice of field distributions most suited to the form of the sample in each experiment. In order to minimize resistive losses in the walls of the cavity, each applicator must be designed to account for depolarisation effects, coupling strength, material characteristics, and loaded frequency of operation.

The electromagnetic mode of operation will be chosen to investigate two forms of field heating: E-field heating, which is the applied form in this thesis, and H-field heating (using TE modes). Also, it could be chosen to minimize sample depolarisation, which would exclude the microwave field from the sample [49].

4.2.1.4 Temperature Control and Ramp Rate

A basic understanding of microwave dielectric heating effects and the use of appropriate temperature monitoring devices is necessary to accurately measure reaction temperatures in microwave-processing devices. Nonetheless, this process is more complex than it seems. Controlling the input microwave power in order to control the temperature and reaction conditions has been proved to be a reliable method for results reproducibility and has been developed in this reactor. This method created an automatic feed control system comprising the following: standard RF components, temperature sensor, data interfaces, and a computer with a Labview™ program to drive the applicator to achieve efficient EM fields in the heating region. The temperature in the loaded material is measured by an automatic, computer-controlled closed feedback loop that drives the microwave components to reach predetermined curing temperature cycles for efficient curing. A control loop algorithm controls the microwave source and measures the temperature at a certain acquisition rate; the microwave source is turned on or off based on the set temperature profile. The highly nonlinear microwave interaction with the samples leads us to anticipate challenges. For example, an increase in sample temperature may indicate an increase in permittivity and absorbed power, possibly leading to thermal runaways. Because the temperature will plateau at some level based on the supplied power, the control of the final sample temperature may not be a significant problem. There is another method, one that uses pulse width modulation to control the temperature. The benefit of this approach is that using constant field strength within the cavity will enable us to separate the field strength effects from ambient temperature effects.

4.2.1.5 Temperature Measurements

A reliable method for rapidly and accurately monitoring the reaction temperature online during the microwave irradiation process is necessary for controlling the temperature. The ability to detect the temperature is a very important step in the microwave-assisted reactions. A common method of measurement uses thermocouples or other sensing devices; however, this is not applicable to a microwave system. Therefore, the temperature measurement of the heated sample will be taken with an infrared pyrometer remaining outside of the resonant cavity. The type of pyrometer has to be able to measure temperatures over 600°C. Because of the nature of microwave heating, an infrared

pyrometer will not measure a temperature that is reflective of the temperatures occurring within the sample. This is one of the major drawbacks of using this detector; because the infrared pyrometer is focused on surfaces and not regions, it is therefore difficult to know the exact temperatures occurring throughout the sample. The distribution of temperatures must be taken into account, especially regarding any product distributions resulting from the experiments [45].

4.2.1.6 Applicator Design

Metal walls surround and enclose materials during microwave heating, and the space in which materials are enclosed is the microwave cavity. Our system has a single-mode cavity allowing for only one possible field pattern created by the standing wave between the walls of the cavity. Thus, the resonant cavity needs to be designed carefully to work effectively. The obvious concerns are the size and resonant frequency of the cavity, but there are more subtle factors involved in making sure that the cavity is fit for purpose and can achieve optimal performance. The TM_{010} mode will create a uniform electric field in the centre of the cavity, and a sample can be inserted and heated exclusively by the microwave electric field. Although this is ideal for heating in the region of the cavity axis, we have to be aware of the effect of other modes operating in the cavity.

To determine the causes behind the phenomena in this experiment, we want to separate the electric and magnetic fields. Modes other than the TM_{010} have different distribution fields, and if these modes couple to the sample, they may generate heating either through magnetic or electric fields. Hence, the TM_{010} mode should be isolated from the other modes, a fact that should be accounted for when specifying the dimensions of the cavity for the required resonant frequency. Moreover, the presence of the sample will itself modify the frequency at which each mode resides. This means that the applicator should be designed based on sample size, configuration, and permittivity. This is to guarantee that the fully-loaded cavity is still operating in the required field distribution.

Before a sample is placed into the cavity, it is packed in a quartz tube because the quartz reduces exclusion of microwave samples from the field. Then it is placed into the cavity along the axis at the point of high field intensity. The tube spans the cavity through two holes, and can be filled with various atmospheres. The holes have to be small enough to (1) avoid disturbing the electromagnetic fields and affecting the field distribution, and (2) avoid causing propagation

of the microwaves through the holes. This will reduce the escape of microwaves. To offset the distortion of the uniform electric fields in the cavity caused by the holes, the height of the cavity can be increased. This proportionally reduces the distortion effect in comparison to the length of the sample in the electric field. Moreover, it may change the resonant frequency or introduction more resonant modes into the frequency region of the TM_{010} mode.

Several modes will be present in the cavity. Thus, the design has to allow us to couple to the appropriate fields, that is, those that contribute to the electric field in which the measurement is being made. A material such as quartz, which is transparent to microwaves at a low level and can hold up at high temperatures, has been used to make the reactor tubes. The design of the cavity also has to account for the reactor affecting its resonant frequency. For TM modes the frequency of operation is given by:

$$f_{nml} = \frac{ck_{nml}}{2\pi} = \frac{c}{2\pi}\sqrt{\left(\frac{l\pi}{d}\right)^2 + \left(\frac{P_{nm}}{a}\right)^2} \tag{4.25}$$

and for TE modes

$$f_{nml} = \frac{ck_{nml}}{2\pi} = \frac{c}{2\pi}\sqrt{\left(\frac{l\pi}{d}\right)^2 + \left(\frac{P'_{nm}}{a}\right)^2} \tag{4.26}$$

Where$d$ is the cavity height, a is the cavity radius, c is the speed of light in free space, k_{nml} is the wavenumber and p_{nm} is the mth root of $Jn(x)$.

Detailed description of the cavity design was previously given in section 4.1

4.2.1.7 Command and Control

The microwave power, pulse mode, duty time, and start mode (overshoot or ramp) can be controlled with Labview. Power meters can measure the generation and reflection of microwave power, and we can monitor the power absorbed by the sample. Labview will collect the temperature and display it in real-time. The infrared pyrometer will be connected directly to the computer, and a proportional-integral-derivative approach will be used to write the control algorithms. This allows to manually control the applicator and to perform necessary maintenance at all times.

4.2.1.8 Microwave Design Safety Issues

Ensuring safety when designing the microwave equipment entails several precautions: safe and reliable equipment, high reproducibility, good reaction control, acceptable energy balance, acceptable cost, and the potential for mechanical breakdown. The system needs to be protected by constantly monitoring the inner part of the application to avoid plasma formation and arcing sensors. To avoid leaks, any new applicators have to include chokes and the appropriate flanges. Also, applicators should be checked for leaks with a microwave power density meter before operation. A power density level of 5 mW/cm^2 must not be exceeded. In general, using the microwave equipment requires diligent personal care [45].

4.2.2 Microwave System Specification and Build

4.2.2.1 Configuration and Details

One of the significant advantages of the applicator system used is that it can be changed for different reaction purposes. Also, it is able to investigate specific field distributions and different sample configurations. Moreover, it allows controlled interaction under a variety of ambient conditions. The microwave system comprises the following: power generator, microwave head, microwave circulator, dummy load, microwave power meters connected to transmission line (waveguide) sections, and the cylindrical cavity (applicator) in which the actual chemical reaction takes place.

Figure 4.11 shows the microwave system design in flow mode. The feedstock flows along the axis of the applicator at the antinode of the TM_{010} mode. In this region, there is minimal depolariation of the sample and maximum coupling to the electric field.

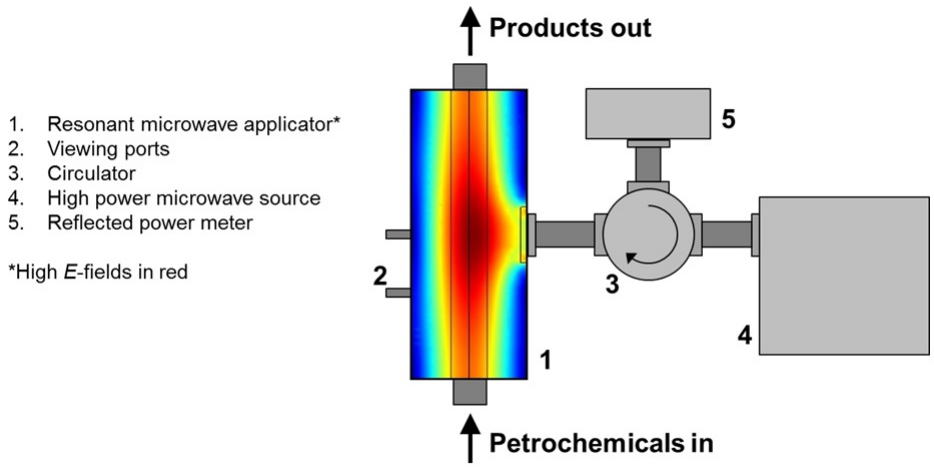


Figure 4.11: Schematic of the high power microwave system, showing the microwave electric field distribution of the TM_{010} mode in the applicator generated using COMSOL Multiphysics.

The microwave magnetic field extends around the outer part of the cavity and is separated from the feedstock. The sample is placed axially along the applicator, and the viewing ports allow different sections of the sample to be measured in terms of temperature. Thus, temperature gradients across the length of the sample can be identified. The applicator receives microwave fields along the waveguide section from a high-power microwave source. If microwave power is not absorbed by the sample, it is re-directed along the waveguide section to the reflected power meter and dummy load through a circulator.

4.2.2.2 Microwave System Technical Details and Specifications

The operating frequency of the system is 2450 MHz (±25 MHz) from 10% to 100% nominal power. The maximum output power is 2000W which is sufficient for lab scale work. The power has 1% stability from 10% to 100% maximum power after thirty minutes on. The microwave source is a magnetron with a ripple rate of $<$ 1% RMS from 10 % to 100%. The power rise time is about 100µs. With the isolator in place, there is no maximum reflected power.

Magnetron life in this system is from 2,000 to 10,000 hours. The magnetron preheating time is 30 seconds. The power generator is a high-efficiency resonant switching converter, with frequencies of 30 kHz up to 80 kHz, and an efficiency of 93% at nominal power. The power supply and microwave

head are both water and air cooled. Before starting the microwaves, a minimum cooling system water flow rate of 5 L/min is required, with a differential pressure of 1.9 bar. The microwave system will cease to operate below 3L/min and 0.7 bar.

The generator is controlled remotely via an RS232 MODBUS gateway. The reflected power measurement system is shown in Figure 4.12. The crystal detector is shown mounted onto the isolator load, with the level adapter box mounted onto the crystal detector.

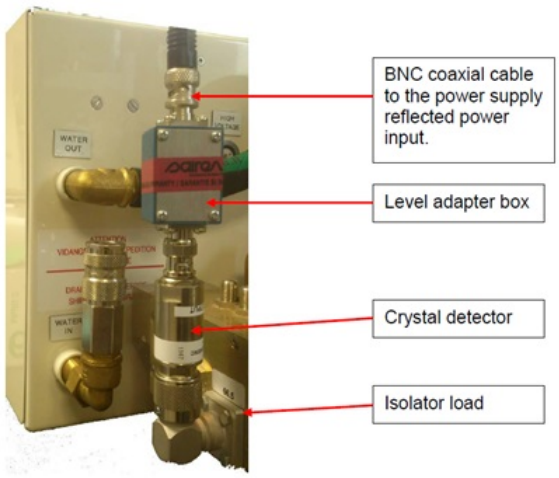


Figure 4.12: The reflected power measurement system connected to the isolator dummy load.

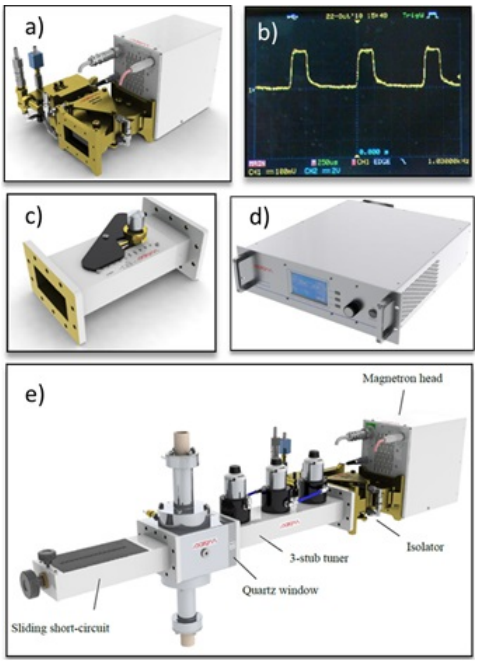


Figure 4.13: Microwave system a) Microwave head and isolator components, where microwaves are being generated and directly reflected to the dummy load and crystal detector, b) Pulsed mode oscilloscope trace, c) tunable waveguide section with a single movable tuning stub, d) generator, e) Applicator chain with 3-stub tuning section, sliding short, quartz window and resonant applicator section.

4.2.2.3 Software

The software which monitors all power and temperature meters and controls the microwave generator is called Labview. Figure 4.14 shows the control panel for the software. Forward and reflected microwave power can be observed on the graph, along with power absorbed by the sample. The sample temperature is also plotted, and all values are recorded in a data file for all experiments.

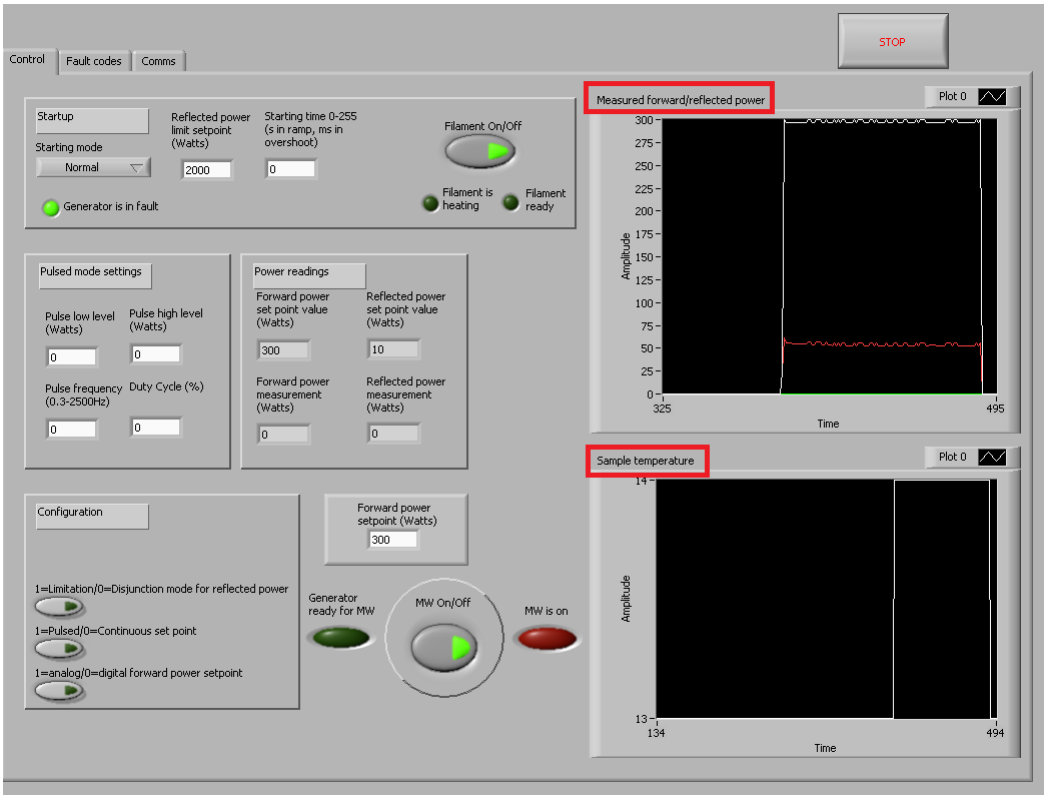


Figure 4.14: User interface of Labview control panel. The software monitors (top screen) views all power where the white line is assigned to the input power and the red line is assigned to the reflected power; and (bottom screen) temperature meters; and (right panel) all parameters that control the microwave generator.

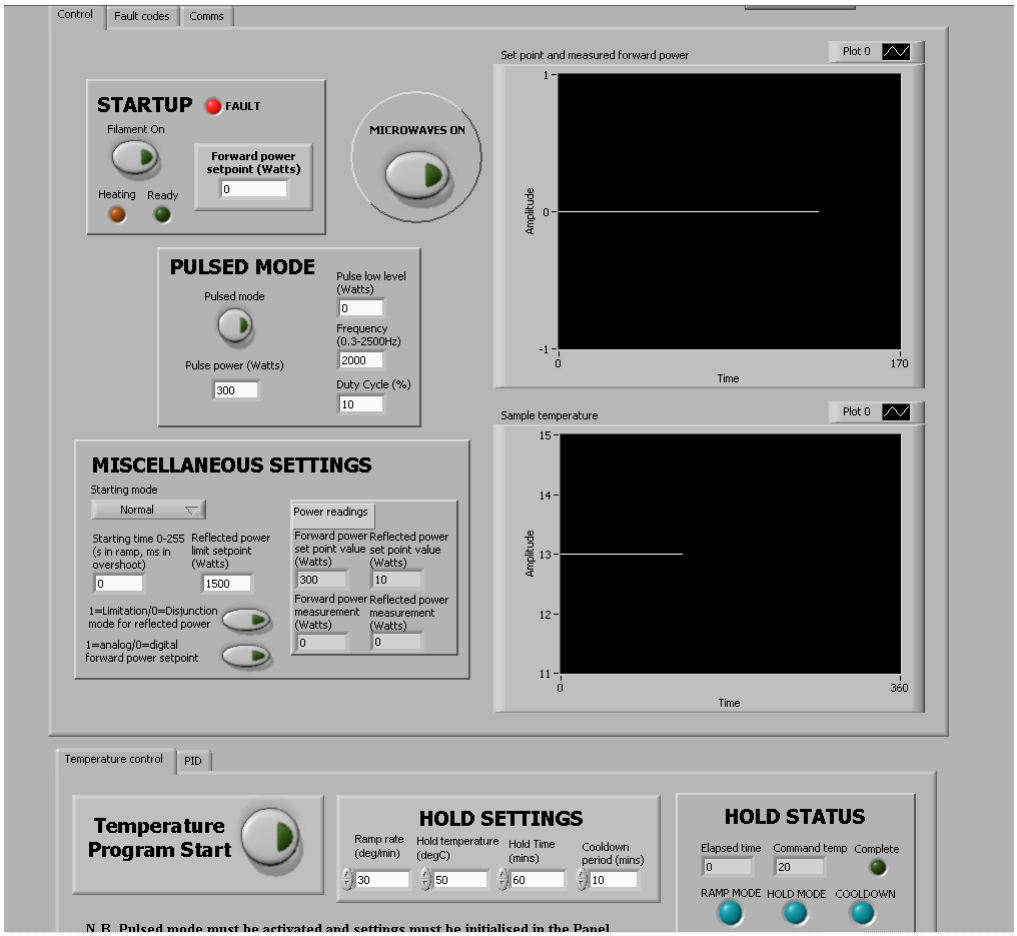


Figure 4.15: User interface of Labview control panel for temperature control program and pulsing mode.

The Fault codes tab indicates a fault warnings messages (illustrated in Figure 4.16). In case of having a fault warning we need to refer to the manual for an explanation of each fault code. The command tab is the tab for setting the communications protocols for the microwave system and infrared pyrometer respectively.



Figure 4.16: Faults code command panel.

At start up, the filament must first be heated for 30 seconds by pressing the button at the top of the control panel. The 'filament heating' warning light will come on followed by the 'filament ready' light. We will normally use 'normal' start-up mode, as this mode has a short ramp time.

For plasma applications, to strike the plasma often requires higher field strength than to maintain it. Thus, an overshoot option is available for start-up in which the power will initially rise above the set forward power level. The 'reflected power set-point' box refers to the maximum reflected power, before the microwaves will cut out, as set by the user. For the water and air cooled system used in this work, there is no upper limit for reflected power. A data file for the experiments records all values and sample temperatures, which are plotted.

4.2.2.4 Calibration and Testing

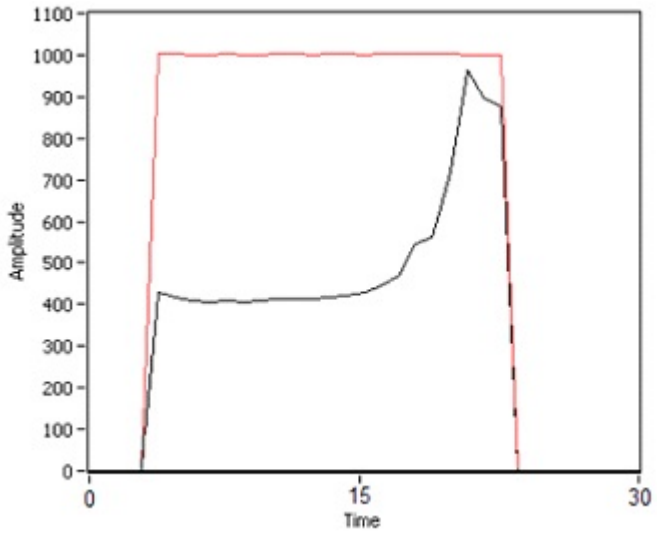


Figure 4.17: Heating profile for a typical oil-catalyst mixture starting at room temperature, where the red denotes the measured forward power and black denotes the power absorbed by the sample (forward power minus reflected power).

In Figure 4.17, the microwave power absorbed by a typical sample receiving microwave waves over ~20 seconds is shown. At first, the sample absorbs nearly 40% of the microwave power. In a properly-designed microwave system, this value is determined by (a) the complex permittivity of the sample and the intrinsic ability of the sample to absorb electromagnetic waves at the operating frequency, and b) the strength of the coupling of the electromagnetic waves into the cavity. Transferring the maximum amount of microwave power to the sample entails critical coupling, where coupling strength depends on sample configuration, geometry, permittivity, and coupling configuration. Moreover, coupling strength changes dramatically given different samples; thus, it is difficult to maintain strong coupling for different samples in a resonant system.

To maintain effective coupling during heating, a computer-controlled coupling can be used. Because the conducted research required more flexibility than the engineering specifications, coupling efficiency will not be explored at this stage. Rather we will increase or decrease the forward power to adjust the power absorbed. The significant power parameter in this project is the power absorbed by the sample, because we can infer the field strengths in the sample. More parameters testing and

calibration will be conducted in **Chapter 7.1.**

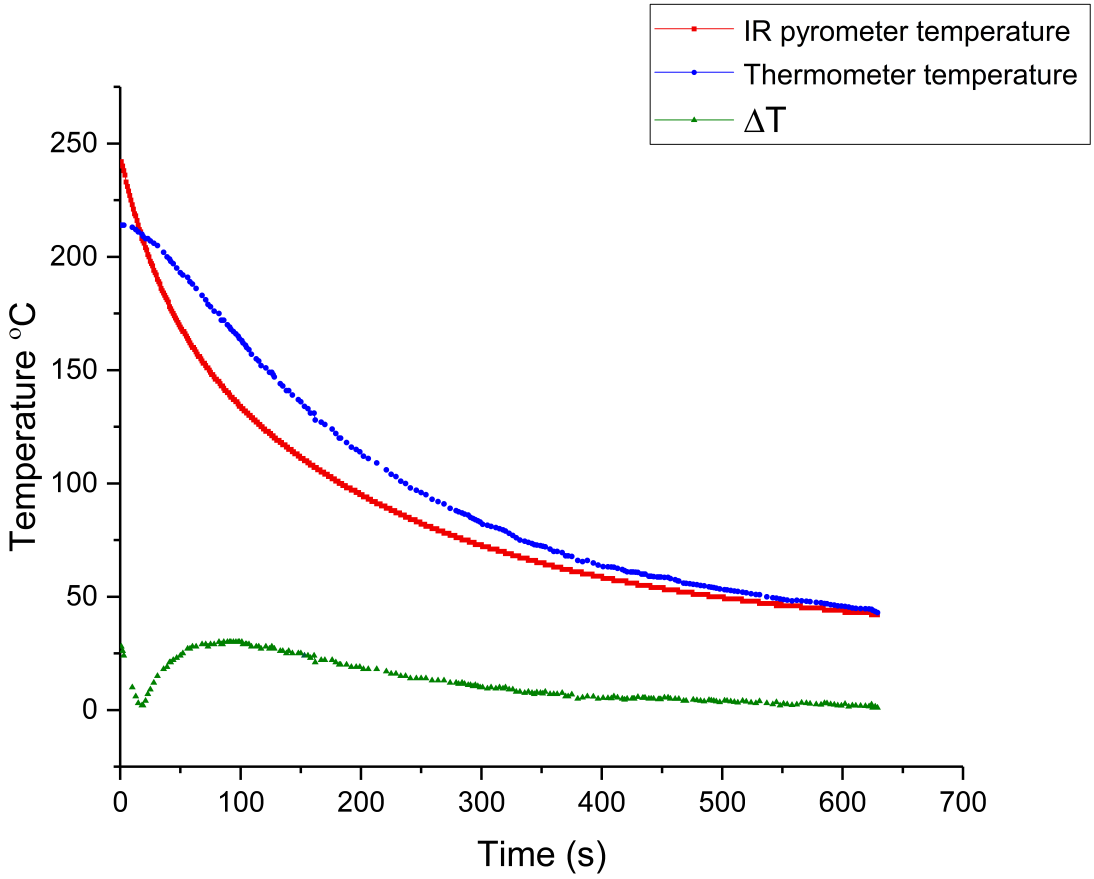


Figure 4.18

4.3 X-Ray Diffraction - XRD

X-ray diffraction is a powerful and versatile analytical technique that is used to investigate the properties and structure of materials. It can obtain information that ranges from basic phase identification from known structures, to relatively advanced framework solutions with the use of refinement techniques that help obtain suitable structural models. These can include the positions of framework and extra-framework atoms, and properties like particle shapes and sizes [50].

4.3.1 Basic Theory of XRD and Bragg's Law

X-rays were discovered by Wilhelm Röntgen in 1895 [51]. They are a type of electromagnetic radiation with wavelengths ranging from 0.01 to 10 nm. They are found between ultraviolet rays and γ rays in the electromagnetic spectrum [52].

Bragg was able to formulate a way of illustrating diffraction, where a crystal is considered as a layered construct that provides a recurring framework. Diffraction occurs when the perpendicular distance between the plains are proportional to the incident radiation wavelength (λ). As a result, the crystal serves as a diffraction grating [53].

A portion of the X-rays is reflected off the plane with the reflection angle equivalent to the incidence angle. However, the rest are diffused and then reflected by other planes. Reflection, however, is not the true physical process that occurs when a crystal is subjected to X-rays. Despite this, the procedure can be employed to approximate the diffraction geometry and come up with similar results. An example is the reflection of X-rays with a fixed wavelength from two contiguous lattice planes with an angle of incidence θ, and a perpendicular interplanar spacing d. The reflected beam deviation is denoted by 2θ, and $2dsin$ stands for the path difference. The equation below describes constructive interference [54].

$$n\lambda = 2d\sin\theta \tag{4.27}$$

Where

n = an integer in the "order" of reflection

λ= wavelength of the incident X-rays

d = distance between the crystal lattice planes

θ= angle of incidence

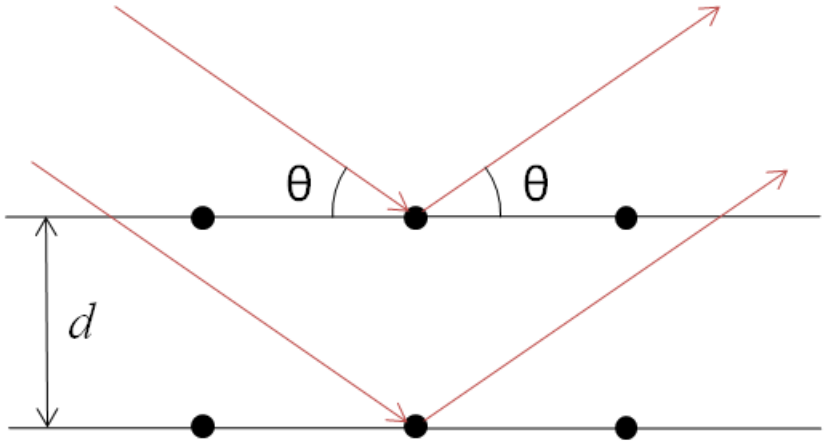


Figure 4.19: Schematic diagram of Bragg's law.

The ***Miller Indices*** (*hkl*) are three integers that define a plane orientation, regarding the three unit cell edges. The distance (d_{hkl}) between successive planes is defined by the lattice geometry. As such, this distance is a function of the unit cell parameters, in which V stands for the volume of the unit cell [26].

X-ray diffraction quantify a reflected intensities of specific area. Based on the findings, the crystal atomic-level distance can be derived. This can aid in further understanding the crystal structure of the substance. The determination of the degree of crystallisation may also be derived through the aid of X-ray diffractions [55]. Moreover, X-ray diffractions also help in distinguishing the various phases that have the same compositions, such as the state of atomic order. As a result of this versatility, X-ray diffractions are widely used in environmental science, materials science, and geology [56].

4.3.2 Instrumentation

X-ray diffractometers are comprised of three elements: the X-ray tube, the sample holder, and the X-ray detector. When the sample and X-ray detector rotate, the reflected X-rays intensity is recorded. When the incident X-ray geometry is able to satisfy the Bragg equation, there is

constructive interference and the intensity peaks. A cathode ray tube creates X-rays by producing electrons, which are made to accelerate by applying a voltage in order to bombard the material of interest. X-ray spectra are created when electrons have sufficient energy to displace electrons within the sample inner shell. These X-ray spectra have different components, with Kβ and Kα being common types. Kα1 and Kα2 compose Kα. Kα2 has a slightly longer wavelength than Kα1, but only half of its intensity. The particular wavelengths represent the characteristics of a sample.

The X-ray signal is then recorded and processed by a detector, which also converts it to a count rate. When Bragg's law is satisfied, constructive interference occurs, which results in a peak in intensity. This output generates the diffraction pattern. X-ray diffractometers may function in configurations relating to reflection or transmission. In the case of these two applications, the process involves placing the powder in a disc container, with its surface carefully flattened.

In the transmission or theta-theta configuration, the sample is made steady as the detector and X-ray tube rotate around it. The resulting angle that forms between the detector and the tube is 2θ. On the other hand, in the reflection configuration, the disc is placed on a diffractometer axis and tilted by an angle θ. A detector (scintillation counter) rotates around this on an arm at double this angle, and this configuration is called the Bragg-Brentano or $\theta - 2\theta$ configuration [57].

4.3.3 Data Collection

X-ray diffractometers are a non-destructive instrument, and have been used to study some of the prepared catalytic configurations. The sample has no special preparation requirements; it just needs to be ground into a fine power, and then put onto a metal disc (sample holder). The sample holder should then be placed on the rotating stage. The obtained data will be displayed in a series of lines with different intensities at various 2θ values, derived as the analyser crystal turns. X-ray diffractometer measurement has been carried out through a PW 3040/60 PanAlytical X'pert Pro diffraction system with a monochromatic CuKα source, operated at 40 keV and 30 mA.

4.4 Thermogravimetric Analysis (TGA)

Thermogravimetric analysis is a thermal analysis method that is performed to study materials thermal properties. TGA also measures the amount of weight changes in a material as a function

of temperature or time in a controlled environment. These measurements are then employed to draw conclusions about the composition and thermal stability of the material [58].

The material is generally observed in the condensed phase (as a solid or liquid); however, a change from liquid to gas or solid to gas may be observed. As such, the gas derived generally can escaped from the system. Analysis can be done in a controlled atmosphere, either in air, nitrogen or under inert gas (e.g. argon, helium). A typical example of a TGA curve is illustrated in Figure 4.20 [59, 60].

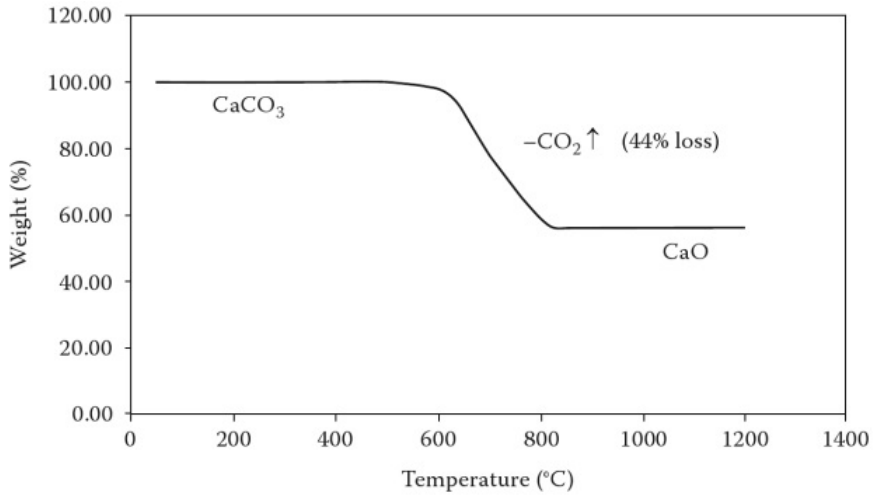


Figure 4.20: An example of typical Calcium Carbonate TGA curve [59].

Several common applications of thermogravimetric analysis include: the classification of various mineral compositions from broad mineral types; determining the purity of materials; and measuring evaporation rates, much like quantifying the volatile emissions of liquid mixtures.

4.4.1 Instrumentation

With a tweezers, a clean empty crucible is loaded into the wire basket that hangs down the TGA. This step should be done very carefully, as the hang-down wire is connected to a very expensive microbalance at the top of the instrument. After the crucible has been placed, the icon 'raise

furnace' should be pressed. The furnace will move into position to cover up the crucible. At this stage the weight of the empty crucible needs to be taken by pressing the 'zero balance' icon. The balance can be zeroed repeatedly until it stabilizes. Then we take the crucible out after moving the furnace off the sample. Only a small amount of sample is needed for this analysis (10-20 mg), as the balance can detect up to μg. When filling the crucible, the same steps need to be followed, however this time the sample weight needs to be taken.

Setting up the method can be done through the 'method editor' icon. This includes inputting information about the sample, and selecting the program method. The variation in mass is then recorded as the sample undergoes a heating sequence, or as it is maintained at a particular required temperature.

Thermogravimetric analysis for this work was carried out using (MSE-TGA) SIT. The samples were heated from 50°C to 950°C at a rate of 10°C under nitrogen, with a flow rate of 50 mL min-1. The resulting loss of weight and the temperatures for onset degradation for the samples were recorded.

4.5 Gas Chromatography (GC)

Introduction

Chromatography is considered as the most-used method of breaking down a mixture into its individual components. The process of separation allows each component to be distinguished qualitatively and measured quantitatively. There are different kinds of chromatographic methods, with consistent instruments. Among these methods is gas chromatography or GC. This is used for compounds that are thermally stable, but volatile. The fundamental principle of the method involves the evaporation of the mixture in a heated inlet port which results in the separation of the components, followed by the identification of each component with the use of a detector. The sample is then introduced into a stream of carrier gas, and is transferred through the column by the gas flow. Depending on the characteristics of the sample, the column can either be a capillary or packed column. As the gas flows through, the different components move at varying velocities. These are affected by the degree of their interaction with the column stationary phase. As a result, the various components separate. The column is generally placed in a thermally controlled oven, as the

processes are dependent on temperature [61].

4.5.1 Detectors

There are various detectors that are utilised in GC, and their use is dependent on the type of component that is being observed. These detectors include electron capture detectors (ECDs), flame ionisation detectors (FIDs), flame photometric detectors (FPDs), nitrogen/phosphorus detectors (NPDs), photoionisation detectors (PIDs), and thermal conductivity detectors (TCDs). In this section only the FID and the TCD detectors will be explored.

4.5.1.1 Flame Ionisation Detector (FID)

Flame ionisation detectors have both hydrogen or air flame and a collector plate. During the process of combustion, the collector electrode captures the ionised single-carbon intermediates. The electrometer measures the small microamp-level currents generated by the flow of ions. This is proportional to the number of carbon atoms present in the gas mixture. Because the operator knows which hydrocarbon component is eluting, the hydrocarbon species are known. As a result, the component concentration may be determined. The discharge from the GC passes through the flame, in which the organic molecules are broken down and ions are produced. These ions are then amassed in an electrode in order to create an electrical signal. The resulting current is proportional to the rate of ion formations, which depends on the hydrocarbon concentration in the sample. FID is generally used to detect hydrocarbons, such as methane, ethane, and acetylene [62].

4.5.1.2 Thermal Conductivity Detector (TCD)

Thermal conductivity detectors detect variations in the thermal conductivity of the column effluent, and transmit it into the reference gas. When the sample is removed from the gas chromatography column, the discharge thermal conductivity is lessened. As a result, a detectable signal is generated. This measure the thermal conductivity of the gas mixture as it passes over a filament. Typical TCDs utilise a Wheatstone Bridge circuit to measure a platinum filament resistance, as it is heated at a constant temperature. The temperature is lessened by an amount proportional to the thermal conductivity of the gas and the rate of gas-flow as the gas passes through the filament. The filament

resistance varies with the temperature. Gases of various compositions and thermal conductivities cool the said filament by varying amounts, at a constant flow rate [62].

4.5.2 Instrumentation

A Perkin-Elmer Clarus 580 GC was used in the chromatography process. The FID column is 30 m long and 0.53 mm diameter COL RT-Aumina. The temperature of the oven in the gas chromatograph was maintained to hold for 10 minutes at 80°C and then to increase from 80°C to 200°C at 25 °C/min, and then maintained to hold at 200°C for 3.90 minutes. The TCD temperature is 200°C and the helium carrier gas is set to a flow rate of 40 mL/min. The temperature of the FID is set to be 250°C and the flow rate of H_2 and Air are 45 mL/min, and 450 mL/min respectively.

4.6 Gas Chromatography/Mass Spectrometry (GC/MS)

4.6.1 Introduction

Gas chromatography mass spectrometry (GC/MS) is a method that is used to determine the different components from their mass spectra. Each compound has a distinct mass spectrum that may be compared and identified through the use of mass spectral databases [63]. Quantitation may also be possible through the use of standards. GC/MS analysis can also be employed to examine solids, liquids, and gases. For liquids, the analysed sample is injected directly. For gases, tight syringes are used to transfer components directly into the GC. The analysis process is done through outgassing, pyrolysis, or solvent extraction for solids [64]. In GC/MS, gas chromatography separates a sample components, while mass spectrometry distinguishes them individually. The analysed sample is dissolved and injected into the instrument. The gas chromatograph is the first step of the instrument. It is an oven that has long, narrow glass tubes coated with polymer. The sample passes through the column in a helium gas stream. The chemical components of the sample interact with the polymer coating. As such, these components arrive at the end of the column at different times. Each component comes out of the column and enters the detector, and is recorded as a peak. The size of the peak is relative to the abundance of the component in the sample [65].

In a GC/MS system, the sample is always a gas that is chemically homogeneous. This is created

by the GC component and can be directly introduced to the ioniser. After it has been ionised, the partitioned compound moves into the mass analyser where ions are transported through an electrical or magnetic field that classifies them according to their m/z ratios. The m/z ratios are the fragment mass divided by its charged, and is also termed mass-to-charge. The detector measures the beam of the newly-separated ions that have arrived at the end of the analyser. The detector also produces the mass spectrum from the changes in their intensity. The mass spectrum of a sample is then displayed, catalogued, and compared by a data system to a library of mass spectra [66].

4.6.2 Detectors

The mass spectrometer (MS) is the most widely used detector in GC/MS. Aside from categorising the separated components from the gas chromatography, the mass Spectrometry identifies them. In the MS, the chemical components are fragmented into ions. Because the manner by which each compound fragments varies, the range of fragmented ions and their relative abundance may be recorded as a mass spectrum from which these components can be distinguished. TCD, FID, are used used in GC/MS, in addition to NPD (Nitrogen–phosphorus), and ECD (Electron capture) detectors as well.

4.6.3 Instrumentation

Gas chromatograph-mass spectrometer (Shimadzu GC/MS-QP 2010 SE) was used to analyse the liquid product. The GC-MS is equipped with a capillary column (SHIM-5MS) 30m X 0.25 mm ID. The temperature of the oven was maintained to increase to 50°C and hold for 1 minute and then to increase to 100°C with rate of 5°/min and hold for 1 minute as well. Finally the temperature in maintained to raise to 200°C at rate of 20°/min and finish the programs. The ion source temperature is 250°C, interface temperature 250°C and detector voltage 0.7 kV.

4.7 Scanning Electron Microscopy (SEM)

4.7.1 Introduction

The scanning electron microscope (SEM) is a type of electron microscope that uses the electron to create an image, as opposed to light. SEMs have been used in medicine and the physical sciences since their development. SEMs use a focused beam of high-energy electrons to create different signals at the surface of a solid specimen. The signals that are obtained from the interactions with the electron-sample provide the sample information. This includes its chemical composition, the crystalline structure and orientation, and the external morphology of the materials that the sample comprises. Frequently, data are obtained in a specific portion of the surface of the sample, and an image that shows spatial variations in these characteristics is obtained. The SEM may also be employed to analyse a sample specified point locations; this is particularly important in determining crystalline structure, chemical compositions, and crystal orientations [67].

4.7.2 Principle of SEM

Accelerated electrons in an SEM have considerable kinetic energy, and this is dispelled as an assortment of signals that are produced by interactions between electrons and the sample during the point of the incident electrons deceleration in the solid sample. These signals include heat, photons (characteristics X-rays), diffracted backscattered electrons, visible light (cathodoluminescence-CL), backscattered electrons, and secondary electrons (that give SEM images). Both backscattered and secondary electrons are frequently employed for imaging samples, with the former displaying composition contrasts in multi-phase samples. On the other hand, secondary electrons are essential for displaying topography and morphology of samples. X-ray generation occurs when the electrons in discrete orbitals of atoms collide with incident electrons. Electrons produce X-rays of fixed wavelengths as they revert to their lower energy states from their excited state [68]. A schematic representation of the SEM is illustrated in Figure 4.21.

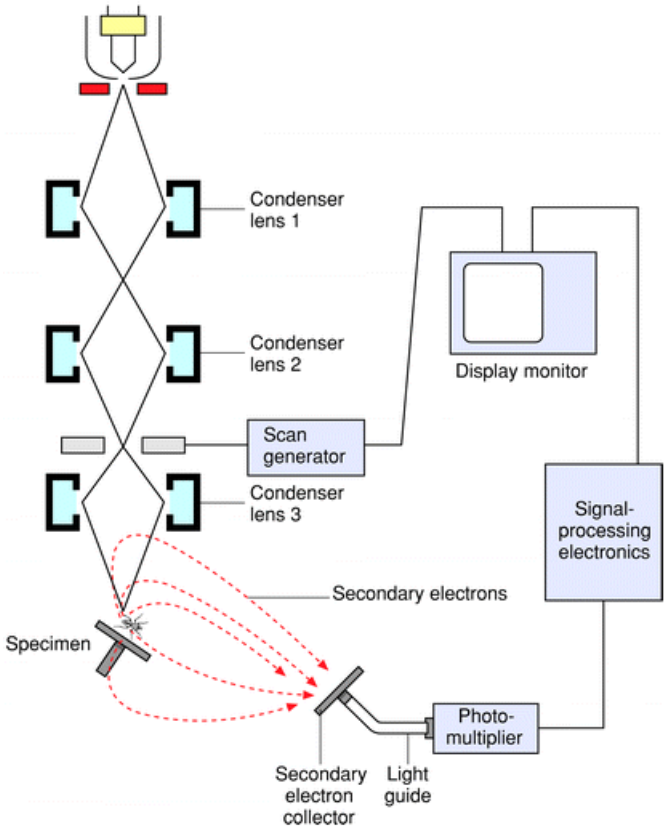


Figure 4.21: Schematic diagram of the SEM [69].

SEM analysis is non-destructive because the X-rays produced by electron interactions do not lead to volume loss, therefore repeated analysis is possible. SEM scanning electron microscopy applications are frequently employed to create high-resolution images of objects in order to illustrate spatial variations in chemical compositions. Furthermore, SEM is commonly used during the phase identification based on qualitative chemical analysis. Detailed measurements of minute objects (down to 50 nm) may also be taken through SEM. SEMs altered with diffracted backscattered electron detectors have also been employed to observe microfabrics and crystallographic orientation in materials.

4.7.3 Instrumentation

The employed SEM system in this thesis is a FESEM (Field Emission Scanning Electron Microscopy) Model = (JSM - 7100F). Catalysts used for the SEM characterisation were coated with

gold.

4.8 Transmission Electron Microscopy (TEM)

Transmission electron microscopy (TEM) is an imaging technique that focuses a beam of electrons onto a specimen, causing a larger version to appear on a fluorescent screen or layer of photographic film. TEM is generally used in metallurgy science, materials science, and life science research. TEM involves the process of an electron passing through a solid, and is consequently scattered several ways at varying times (multiple, plural, or single scattering); this scattering may be elastic or inelastic.

4.8.1 Principle of TEM

In TEM, a beam of electrons with a short wavelength is used as the illumination source. This beam of electrons is produced from a tungsten filament placed on top of a cylindrical column, with a height of around 2 m. The entire optical system of the microscope is enclosed by a vacuum. The air escaping from the column produces a vacuum that assists in preventing the electrons from scattering or colliding with air molecules. Magnetic coils that are found at specific intervals along the column act as an electromagnetic condenser lens system in order to focus the electron beam. The sample is stained with the use of a material that is dense with electrons. The specimen is put in the vacuum, where electron beams pass through it and are consequently dispersed by the internal structures. The heated filaments emit electrons, and in order to accelerate these electrons, the anode voltage is utilised. As the electrons become faster, their wavelength becomes shorter, and their resolution is increased. TEM involves a high-voltage electron beam that is produced by a cathode, and is formed by magnetic lenses. The electron beam that has been partially transmitted delivers information about the specimen structure. Magnetic lenses then magnify the resulting image up until it is recorded with a fluorescent screen, photographic plate, or light-sensitive sensor camera [67].

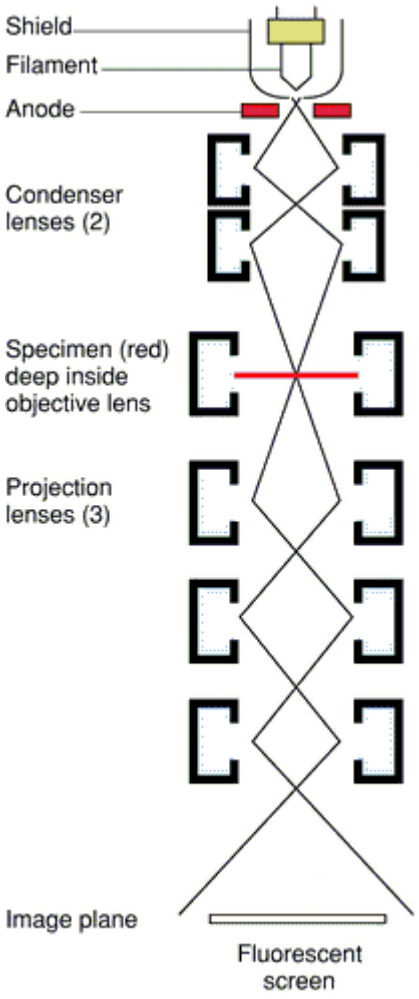


Figure 4.22: Schematic diagram of the TEM [69].

The TEM is composed of four parts: the imaging system, sample holder, electromagnetic lens system, and source of electrons. The source of electrons is an electron gun that contains a tungsten filament that emits electrons upon heating. The electromagnetic lens system focuses the beam of electrons onto the specimen, and the sample holder is a mechanical arm which holds the specimen. The imaging system contains a phosphorescent plate, and this illuminates when it is hit by the beam of electrons which has passed through the specimen. Figure 4.22, represents a diagram of the basic components making up the transmission (TEM). TEM is used in various fields, such as biological and material research, medical research, forensic analysis, gemmology and metallurgy,

among others. The process provides compositional, crystalline, topographical, and morphological information. This aids scholars in investigating samples from a molecular perspective, allowing the textural and structural examination of metals or crystals. TEM is also used in semiconductor analysis, as well as in the production and manufacturing of computer chips. Furthermore, TEM can be used to distinguish the position of atoms in materials; this method is vital to nanotechnology research, and to development in different fields (e.g. heterogeneous catalysis) [70].

4.8.2 Instrumentation

TEM experiments were carried out to determine the size, shape and location of the dispersed particles. The samples were examined at the Materials Department, using High resolution transmission electron microscopy experiments have been carried out on a JEOL 3000F field emission gun instrument. This instrument is equipped with an Oxford Instruments energy dispersive X-ray spectrometer (EDS) with a super atmospheric thin window (SATW) detector that allows chemical analysis of elements down to boron under suitable conditions. In addition a Gatan imaging filter (GIF) equipped with a 2k 794IF/20 MegaScan CCD camera allows chemical analysis using electron energy loss spectroscopy (EELS).

Bibliography

[1] M. Willert-Porada, editor. *Advances in Microwave and Radio Frequency Processing*. Springer Science & Business Media, 2007.

[2] H.A. Bethe and J. Schwinger. *Perturbation Theory for Cavities*. Cornell University, 1943.

[3] L.C. Maier Jr and J.C. Slater. Field Strength Measurements in Resonant Cavities. *J. Appl. Phys.*, 23:68, 1952.

[4] F. Horner, T. Taylor, R. Dunsmuir, J. Lamb and W. Jackson. Resonance Methods of Dielectric Measurement at Centimetre Wavelengths. *J.IEE*, XC111:53, 1945.

[5] J.K. Sinha and D. Brown. A New Cavity-resonator Method for Measuring Permittivity. *Proc.IEE*, 107:522, 1960.

[6] S. Li, C. Akyed and R.G. Bosisio. Precise Calculations and Measurements of The Complex Dielectric Constant of Lossy Materials using TM_{010} Cavity Perturbation Techniques. *IEEE Trans.Mic.The.Tech.*, 29:1041, 1981.

[7] M. Martinelli, P.A. Rolla and E. Tombari. A Method for Dielectric Loss Measurements by a Microwave Cavity in Fixed Resonance Condition. *IEEE Trans.Mic.Th.Tech*, MTT-33:779, 1985.

[8] Agilent Technologies. Agilent Basics of Measuring the Dielectric Properties of Materials. *Application Note*, 2006.

[9] S.N. Jha. *Nondestructive Evaluation of Food Quality: Theory and Practice*. Springer-Verlag, 2010.

[10] N. Marcuvitz. *Waveguide Handbook*. IET, 1951.

[11] M.A. Rao, S.S.H. Rizvi, and A.K. Datta. *Engineering Properties of Foods*. Taylor & Francis Group, 4th edition, 2014.

[12] N. Ida. *Engineering Electromagnetics*. Springer, 2015.

[13] A. Parkash, J.K. Vaid and A. Mansingh. Measurement of Dielectric Parameters at Microwave Frequencies by Cavity-perturbation Technique. *IEEE Transactions on Microwave Theory and Techniques*, 27:791–795, 1979.

[14] S.N. Jha, K. Narsaiah, A.L. Basediya, R. Sharma, P. Jaiswal, R. Kumar, and R. Bhardwaj. Measurement Techniques and Application of Electrical Properties for Nondestructive Quality Evaluation of Foods-a Review. *Journal of Food Science and Technology*, 48(4):387–411, 2011.

[15] J.L. Chen C. Liao and D.C. Yen. Theory of Planning Behavior (TPB) and Customer Satisfaction in the Continued use of e-service: An Integrated Model. *Computers in Human Behavior*, (23:6):2804–2822, 2007.

[16] V. Venkatesh, C. Speier and M.G. Morris. User Acceptance Enablers in Individual Decision Making About Technology: Toward an Integrated Model. *Decision Sciences*, pages 297–316, 2002.

[17] K. Zhang and D. Li. *Electromagnetic Theory For Microwaves and Optoelectronics*. Springer Science & Business Media, 2nd edition, 2013.

[18] M.A. Mushref. Matrix Solution to Electromagnetic Scattering by a Conducting Cylinder with an Eccentric Metamaterial Coating. *Journal of Mathematical Analysis and Applications*, 332:356–366, 2006.

[19] A. Kumar and S. Sharma. Measurement of Dielectric Constant and Loss Factor of the Dielectric Material at Microwave Frequencies. *Progress In Electromagnetics Research*, 69:47–54, 2007.

[20] R.J. Meredith. *Engineers' Handbook of Industrial Microwave Heating*. IET, 1998.

[21] G.S.N. Raju. *Electromagnetic Field Theory and Transmission Lines*. Pearson Education India, 2006.

[22] D. Slocombe. *The Electrical Properties of Transparent Conducting Oxide Composites*. PhD thesis, Cardiff University, Cardiff, 2012.

[23] N. Johan. *Modelling and Experiments of an Electromagnetic Measurement System for Fluidised Beds*. PhD thesis, Chalmers University of Technology, Goteborg, Sweden, 2012.

[24] M.L. Sisodia. *Microwaves: Introduction to Circuits, Devices and Antennas*. New Age International Publishers, 2007.

[25] D.M. Pozar. *Microwave Engineering*. John Wiley & Sons, Inc., 4th edition, 2011.

[26] P.P. Mondal and A. Diaspro. *Fundamentals of Fluorescence Microscopy : Exploring Life with Light*. Springer, 2014.

[27] R. Bansal. *Handbook of Engineering Electromagnetics*. Technology & Engineering, 2004.

[28] Booklet. Introduction to COMSOL Multiphysics 2015.

[29] Xiang Li and Yan Jiang. Design of a Cylindrical Cavity Resonator for Measurements of Electrical Properties of Dielectric Materials. Master's thesis, Master Thesis in Electronics/Telecommunications, 2010.

[30] R.J. Collier and A.D. Skinner. *Microwave Measurements*. IET, 2007.

[31] L.F. Chen, C.K. Ong, C.P. Neo, V.V. Varadan and V.K. Varadan. *Microwave Electronics: Measurement and Materials Characterization*. John Wiley & Sons, 2004.

[32] P.J. Petersan, and S.M. Anlage. Measurement of Resonant Frequency and Quality Factor of Microwave Resonators: Comparison of Methods. *J. Appl. Phys.*, 84(6):3392–3402, 1998.

[33] A. Das and S.K. Das. *Microwave Engineering*. Tata McGraw-Hill Education, 2nd edition, 2009.

[34] M.J. Lancaster. *Passive Microwave Device Applications of High-Temperature Superconductors*. Cambridge University Press, 2006.

[35] D. Slocombe, A. Porch, E. Bustarret, and O.A. Williams. Microwave Properties of Nanodiamond Particles. *Applied Physics Letters*, 102(24):1–5, 2013.

[36] J. Cuenca, E. Thomas, S. Mandal, O. Williams, A. Porch. Microwave Determination of sp^2 Carbon Fraction in Nanodiamond Powders. *Carbon*, 81:174–178, 2015.

[37] A. Porch, A. Masood, A.J. Naylon, A. Sulaimalebbe and D.A. Barrow. Sapphire Dielectric Resonators for Microfluidic Compositional Analysis. *14th International Conference on Miniaturized Systems for Chemistry and Life Sciences*, 2010.

[38] A. Porch, D. Slocombe, J. Beutler, P.P. Edwards, A. Aldawsari, T. Xiao, V. Kuznetsov, H. Almegren, S. Aldrees and N. Almaqati. Microwave Treatment in Oil Refining. *Applied Petrochemical Research*, 2:37–44, 2012.

[39] S. Donovan, O. Klein, M. Dressel, K. Holczer and G. Griiner. Microwave Cavity Perturbation Technique: Part II: Experimental Scheme. *International Journal of lnfrared and Millimeter Waves*, 14, 1993.

[40] Agilent Technologies Inc. *Agilent Basics of Measuring the Dielectric Properties of Materials*,

2005.

[41] Z. Fang and C.C. Xu. *Near-critical and Supercritical Water and Their Applications for Biorefineries*. Biofuels and Biorefineries. Springer Netherlands, 2014.

[42] D.R. Lide. *1998 Freshman Achievement Award*. CRC Press LLC, 87th edition, 1998.

[43] S. Horikoshi and N. Serpone. *Microwaves in Catalysis: Methodology and Applications*. Wiley, 2015.

[44] M.W. Lorence and P.S. Pesheck. *Development of Packaging and Products for Use in Microwave Ovens*. Elsevier, 2009.

[45] P.M. Gillespie. Microwave Chemistry: An Approach to the Assessment of Chemical Reaction Hazards. *IChemE*, 2004.

[46] G.L. Robertson. *Food Packaging: Principles and Practice*. Taylor & Francis, third edition, 2012.

[47] K. Gadamasetti and T. Braish. *Process Chemistry in the Pharmaceutical Industry: Challenges in an Ever Changing Climate*, volume 2. CRC Press, 2008.

[48] M. Mehdizadeh. *Microwave/RF Applicators and Probes: For Material Heating, Sensing, and Plasma Generation*. Elsevier, 2015.

[49] A.V. Starck, A. Mühlbauer and C. Kramer. *Handbook of Thermoprocessing Technologies: Fundamentals, Processes, Components, Safety*. Vulkan-Verlag, 2005.

[50] F. Smith. *Industrial Applications of X-Ray Diffraction*. CRC Press, 1999.

[51] R.F. Mould. *A Century of X-Rays and Radioactivity in Medicine: With Emphasis on Photographic Records of the Early Years*. CRC Press, 1993.

[52] Stanley R. Crouch Douglas A. Skoog, F. James Holler. *Principles of Instrumental Analysis*. Thomson Brooks/Cole, 2007.

[53] Y. Leng. *Materials Characterization: Introduction to Microscopic and Spectroscopic Methods*. John Wiley & Sons, 2013.

[54] M. Che and J.C. Vedrine. *Characterization of Solid Materials and Heterogeneous Catalysts: From Structure to Surface Reactivity*. Wiley, 2012.

[55] P. Bleuet, E. Welcomme, E. Dooryhée, J. Susini1, J. Hodeau, and P. Walter. Probing the Structure of Heterogeneous Diluted Materials by Diffraction Tomography. *Nature Materials*, 7:468–472, 2008.

[56] P.A. Jacobs. B. Delmon G. Poncelet and P. Grange. *Preparation of Catalysts: Scientific Bases for the Preparation of Heterogeneous Catalysts.* Studies in Surface Science and Catalysis. Elsevier Science, 1987.

[57] F.M. Ross R. Haight and J.B. Hannon. *Handbook of Instrumentation and Techniques for Semiconductor Nanostructure Characterization.* Materials and Energy. World Scientific Publishing Company Pte Limited, 2011.

[58] P. Gabbott. *Principles and Applications of Thermal Analysis.* John Wiley & Sons, 2008.

[59] G.M. Frame II J.W. Robinson, E.M.S. Frame. *Undergraduate Instrumental Analysis.* M. Dekker, 5th edition, 2004.

[60] E. Aulisa and D. Gilliam. *A Practical Guide to Geometric Regulation for Distributed Parameter Systems.* CRC Press, Taylor & Francis Group, 2016.

[61] R.L. Grob and E.F. Barry. *Modern Practice of Gas Chromatography.* Wiley, 2004.

[62] G. Meurant. *Detectors in Gas Chromatography.* Journal of Chromatography Library. Elsevier Science, 2011.

[63] G.S. Kriz D.L. Pavia, G.M. Lampman and J.A. Vyvyan. *Introduction to Spectroscopy.* Cengage Learning, 2014.

[64] Hans-Joachim Hübschmann. *Handbook of GC-MS.* Wiley-VCH, 2015.

[65] E. de Hoffmann and V. Stroobant. *Mass Spectrometry: Principles and Applications.* John Wiley & Sons, 2013.

[66] Z. Penton O.D. Sparkman and F.G. Kitson. *Gas Chromatography and Mass Spectrometry: A Practical Guide.* Academic Press, 2011.

[67] R.F. Egerton. *Physical Principles of Electron Microscopy: An Introduction to TEM, SEM, and AEM.* Springer ebook collection / Chemistry and Materials Science 2005-2008. Springer US, 2011.

[68] J. Humphreys P.J. Goodhew and R. Beanland. *Electron Microscopy and Analysis.* Taylor & Francis, 3rd edition, 2000.

[69] Optics & Binoculars. Scanning Electron Microscope Diagram, 2013. Accessed: December 2015.

[70] J. Boumendil G. Ehret J. Ayache, L. Beaunier and D. Laub. *Sample Preparation Handbook for Transmission Electron Microscopy: Methodology.* Springer, 2010.

Chapter 5

DIELECTRIC MEASUREMENTS AT ROOM TEMPERATURE

Overview

The aim of this chapter is to create a library of dielectric properties of heavy oils and model compounds to explore their susceptibility to interact with microwaves. The cavity perturbation technique has been used to perform the dielectric measurements at room temperature with TM_{010} mode and frequency of 2.45 GHz. Dielectric properties of the tested samples have been evaluated through the calculations of both the real permittivity (ε') and the imaginary permittivity (ε''). Where ε' determines the ability of the material to store the energy and ε'' represents the ability of the material to convert the energy into heat.

5.1 Introduction

The heating behaviour of any reacting materials under microwave radiation is mainly influenced by their dielectric properties. Studying dielectric properties is a very important parameter that can allow for the determination of the coupling and distribution of the electromagnetic field during the heating process. Dielectric measurements have been one of the most attractive subjects for researchers over the last couple of decades. In the 19^{th} century, Faraday (1838) published the initial

numerical dielectric measurements of the insulating materials [1]. It was based on the fact that the capacity of a condenser was influenced by the nature of the material separating the conducting surfaces. He initiated the use of the term (Specific inductive capacities), which indicates the ratio between the capacity of a specific condenser in two cases: when it is empty, and when it is filled with a dielectric. Currently, this is what is known as the real permittivity (ε') [2].

Dielectric phenomena then became more fundamental and general, as it originated from dielectric polarisation. Mossotti and Clausius both performed an investigation on dielectric properties of the materials [3, 4]. They tried to integrate Faraday's term (specific inductive capacity) with the microscopic structure of the material. This was followed by Lorentz who introduced the concept of the average field working on each individual particle in a system, which he called the internal field [2, 5].

During the start of the 20th century Debye [6] observed that a number of molecules had permanent electric dipole moments. This molecular dipole moment is a cause of a material's macroscopic dielectric properties. Debye was able to build on the theory of Mossotti and Clausius to consider the molecules permanent moments. This enabled Debye and others to determine the molecular dipole moment from the measurement of the real permittivity (ε') [6–8]. Onsager and Kirkwood extended Debye's theory, and agreed with experimental results for most polar solvents. Further major contribution by Debye to the dielectrics theory was his applying the concept of molecular permanent dipole moments to explicate Drude's observation of the real permittivity anomalous dispersion. In an alternating field, Debye realised that the lag time from the average orientation of the moments and the field is more apparent when field frequency is within the same order of magnitude as the reciprocal relaxation time. As a result, the process of molecular relaxation causes the dielectric relaxation [9, 10]. This is a macroscopic phenomenon in which the real permittivity disperses anomalously, and the electromagnetic energy is absorbed over a certain range of frequencies [11].

Studies conducted have shown that the nature and strength of molecular interaction plays an important role in interpreting the behaviour of the chemical compounds. The extent of recognition of the most strongly proven structures that involve chemical bonds and interactions is based on several quantitative and qualitative experiments [12, 13]. This mainly involves the exploration of theoretical and experimental methods that are typically known as "studies of electric permittivity". The dependence of dielectric parameters on properties such as viscosity, temperature, concentration,

and the applied frequency contributes to understanding the molecules behaviour. The permittivity depends on the polarisability of the material, as well as the frequency of the applied field [14]. The fall of polarisability can be linked to the decrease in permittivity as well as to the dielectric dispersion, in which electrical energy is absorbed. This is evidenced by the frequency-dependent dielectric measurements. The permittivity is a fundamental property and a dimensionless number, it significantly affects the values of melting point, boiling point, refractive index, and viscosity in pure materials [15–17]. It measures the interaction between a molecule and an oscillating electric field [18].

In order to optimise the microwave process for heavy oil cracking reactions, the knowledge of the dielectric properties for the evaluated materials is required. In this study, the dielectric measurements of three oil samples (heavy bunker, light crude, and pyrolysis) have been performed using the cavity perturbation technique. The oil samples were evaluated for the purpose of understanding the different dielectric properties of the oil, the corresponding heating profiles, and in turns, the correlation with their components. As heavy oil is composed of a large number of compounds, the dielectric measurements were also performed on various model compounds, such as paraffinic linear and cyclohydrocarbons, in addition to common aromatic and heterocyclic compounds that occur in heavy oil, in order to gain a better understanding of the molecular contribution of the dielectric heating.

Dielectric properties were studied in parallel with the electrical conductivity of the oil and zeolite samples in an attempt to explore these properties and its relation to their microwave activity. This study was carried out to establish a baseline for achieving an enhanced processing of heavy oil using microwave heating system.

5.2 Experimental

5.2.1 Materials

The heavy bunker oil and light crude oil sample was provided by Saudi ARAMCO, whereas the pyrolysis oil was provided by Future Blend LTD. The model compounds were bought from the Sigma Aldrich, Alfa Aesar, and ARCOS Companies. The chemical properties of the model compounds and the oil samples are presented in details in **Appendix A.** The zeolite samples were commercially

bought from Zeolyst International.

5.2.2 Dielectric Measurements

Cavity perturbation has been used to perform the dielectric measurements study. This technique was selected for its applicability for materials with low dielectric loss. The system is comprised of a cavity (with a cylindrical shape) that is connected to an 8735B Vector Network Analyzer (VNA). The VNA runs at a range of frequencies, 300 kHz - 8.5 GHz. This range is allocated for microwave industrial heating. Measurements were performed by obtaining the background values of the cavity with an empty sample-holder. The perturbation in the Q-factor, in addition to the shift in frequency and bandwidth values, were recorded once the sample is inserted into the cavity. The dielectric properties of the samples can be obtained with the use of the perturbation equations 5.1 and 5.2.

A number of straight-chain alkanes, sulphur, nitrogen and other compounds, in addition to the oil and zeolite samples, were filled in 2 mm diameter quartz tubes. The dielectric measurements of those samples were performed at room temperature in TM_{010} mode at 2.49436 GHz (in practice). The measurement of each sample was performed a minimum of three times and the average values were taken.

5.2.3 Microwave Heating

The oil samples were heated in a 2 kW 2.45 GHz single-mode applicator. The system specifications were explored in details in **Section 4.2.**

5.3 Results and Discussion

5.3.1 Linear Alkanes and Heavy Oil

Hydrocarbons are the major components of heavy oil, comprising more than 75% [19, 20]. Generally, it is difficult to determine the identity of hydrocarbons, particularly in the heavy oil fractions. However, it is well known that the hydrocarbons in heavy oil are composed of paraffinic, aromatic, and naphthenic groups. In these experiments, the dielectric properties were investigated in a series

of linear alkanes, and compared to the properties of the heavy oil [21]. Table 5.1 shows the physical properties of the evaluated hydrocarbons.

Table 5.1: The Physical properties of the linear hydrocarbons.

Sample	Chemical formula	Melting point °C	Boiling point °C
Hexane	C_6H_{14}	−96	69.1
Decane	$C_{10}H_{22}$	−29.7	174.1
Dodecane	$C_{12}H_{26}$	−9.6	216.3
Hexadecane	$C_{16}H_{34}$	18.2	286.8
Nonadecane	$C_{19}H_{40}$	32–34	330
Triacontane	$C_{30}H_{62}$	65.8	449.7
Pentatriacontane	$C_{35}H_{72}$	75	490

Studying the dielectric properties of hydrocarbons, especially those with longer chains and higher boiling fractions is very important, mainly for the production of high value compounds, such as hydrogen and light olefins, from large hydrocarbons fractions and heavy oil using microwave heating technology.

The cavity perturbation theory is based on the relationship between the changes in the parameters of the resonator to the dielectric properties tested when the sample is introduced to the electric field. The insertion of a small sample into the cavity would result in a reduction in the quality factor of the cavity from Q_0 to Q_s and a shift in the resonant frequency. The change in these parameters is directly related to the permittivity of the sample. The Q factor of an empty cavity is higher than the value of a loaded one, because the quality of the conducting walls have a great effect on the total value of the Q factor of a loaded cavity [22]. In general, a good dielectric material for heating can reduce the cavity Q factor as much as possible and this is directly related to the shift in frequency. For a well-known dielectric sample inserted into a cavity, the efficiency of the microwave cavity for a heating application is based on the greatest possible reduction of its Q-factor value. The greater the reduction in the Q-factor, the higher the conversion efficiency of the microwave energy [23].

Figure 5.1 illustrates the delta frequency, the shifted resonance peak from f_0 to f_s , and the

change in the bandwidth upon insertion the measured samples (alkanes/ oil) into the cavity.

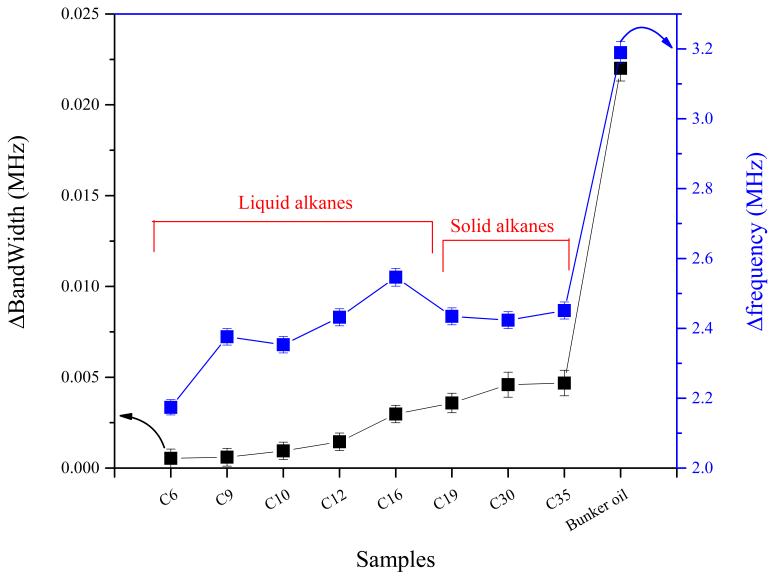


Figure 5.1: The change in the bandwidth and the shift in resonance frequency of the linear alkanes in comparison to the heavy bunker oil.

By recording the frequency and the bandwidth values, they can be used in the following set of equations to find the real and imaginary permittivities of the samples:

$$\frac{\triangle f}{f_0} = (\varepsilon' - 1)AV_s \tag{5.1}$$

$$\frac{\triangle BW}{f_0} = 2\varepsilon'' AV_s \tag{5.2}$$

It can be observed that there is no significant perturbation occurring within the cavity upon the insertion of the linear alkane samples. However, the heavy oil sample exhibits a higher ability

to perturb the electric field in the cavity, and indicates a greater reduction of the Q-factor value.

In the case of the non-polar hydrocarbons, the Clausius-Mossotti equation has been used for correlating the real permittivity and physical properties. However, it should be taken into account that this equation is designed to study the polarisability of the molecules at atomic level [24]:

$$\frac{\varepsilon_r - 1}{\varepsilon_r + 2}\frac{M}{\rho} = \frac{4\pi}{3}N\alpha \tag{5.3}$$

Where,

ε_r is the relative permittivity of the material (Macroscopic quantity)

M is the molecular weight

ρ is the density

N is Avogadro's number

α is the molecular polarisability (Microscopic quantity) F.m^2

It can be seen from the equation that the real permittivity value depends on both the molar volume of the material in vacuum and its polarisability [25].

Figure 5.2 shows the combined data of density and real permittivity values of linear alkanes.

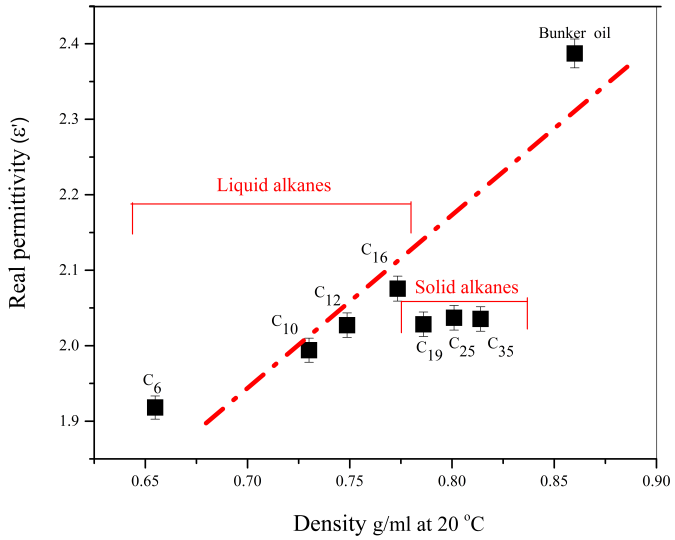


Figure 5.2: The real permittivity (ε') vs. the density of the hydrocarbon materials and bunker oil, as a function of increasing the chain length.

For the non-polar liquids (C_6 - C_{16}) it can be seen that the density measurement is a valid approach that can be used to characterise the ability of the material to be polarised in a microwave field. The change in the real permittivity is fairly constant, showing a notable increase with the increase in the number of carbon atoms of alkanes. However, the real permittivity becomes steady in case of heavier wax hydrocarbons, where the molecular rotation is restricted. Hence, for those compounds the reorientation under the applied field does not readily contribute to the permittivity. This can also indicate an important relationship between the permittivity and other physical properties of a material [26].

The correlation between an increase in the number of CH_2 units (real permittivity and polarisability) can be observed. The total effect of relatively weaker London dispersion forces of attraction that is involved with each CH_2 and CH_3 unit may be observed more in higher alkanes. In addition, as the polarisability becomes greater and the distance between non-polar alkanes is lessened, the standard enthalpies of vaporisation also become greater. Moreover, under the applied electric field, the electron cloud is experiencing a displacement from the nuclei to the reverse direction of the

electric field. As such, an electric dipole behaviour will result from the separation of the positive and negative charges. However, large liquid non-polar molecules will experience higher polarisability, as they have a greater number of electrons and a larger electron cloud. On the other hand, in small molecules the corresponding outer electrons are closer to the nuclei and have a tighter bond [5].

Introducing a material into a cavity where the maximum electric field is formed changes the electric flux density. This will also affect the storage and loss of energy. This can be presented through both permittivity parameters and the real permittivity (ε'), which is related to the stored energy within the material, in addition to the imaginary permittivity (ε''), which is related to energy lost from the material and dissipated into heat. The real permittivity (ε') that indicates energy storage within the material is associated with its dielectric polarisation.

Because polarisability is the capability of a molecule to be polarised, it is viewed as an important property. This is because the dynamical response of a material to external fields can be ascertained by its polarisability. It can give a better understanding and access into the internal structure of a molecule. Permittivity measures the resistance that occurs when an electric field is created in a tested sample in addition to the effect of the electric filed on the dielectric sample. The molecule permittivity also shows how much the electric field or flux is 'generated' per unit charge in the particular molecule. It is also important to study the polarisability of a dielectric material due to its direct relation to the energy storage within the material. In terms of energy, the high polarisability of a material allows the storage of large electric potential. For high energy storage dielectrics, it is necessary to increase polarisability as far as possible. Permittivity and polarisability are important properties of relative materials in the area of electrochemistry [27].

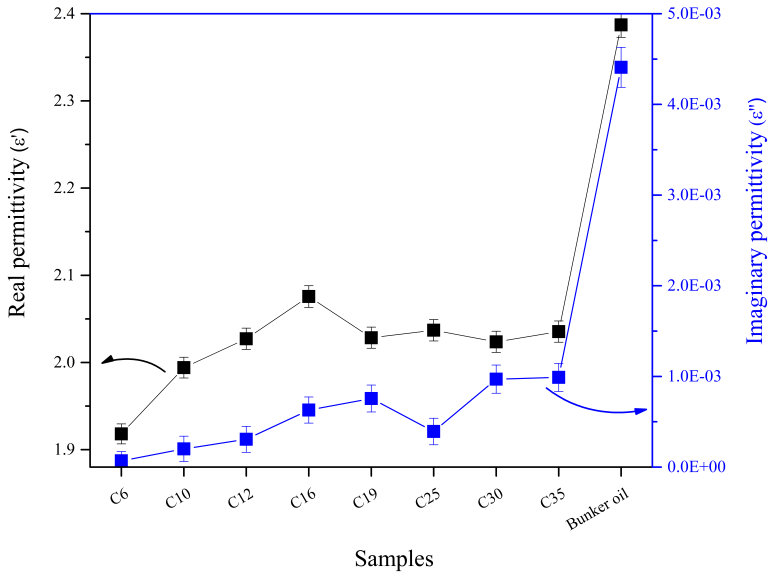


Figure 5.3: The real permittivity (ε') and the imaginary permittivity (ε'') for linear alkanes in comparison to the heavy bunker oil sample.

Figure 5.3 illustrates the real and imaginary permittivity for the n-alkane samples as a function of increasing the number of carbon atoms. The data for the imaginary permittivity shows predictable trends in the dielectric properties, where the ability of the alkanes to dissipate the energy into heat increases with chain length. The increase in the number of carbon atoms also leads to a greater imaginary permittivity and as well as higher real permittivity. Moreover, the heavy oil sample indicates a better ability than the linear alkanes to be heated by microwaves. This explains the overall low microwave susceptibility of the heavy oil due to the fact that hydrocarbon is the main component of the oil mixture. The fact that permittivity of the heavy oil is higher than the hydrocarbons can be attributed to the other components of aromatic, polar, organic and inorganic metal compounds. In general, the energy loss mechanisms in the material are related to the rapidly-oscillating applied electric field that resulted in an alignment of electric dipoles and any free electrons [28]. On the other hand, the polarisability behaviour of the n-alkanes can be rationalised to show an increase in polarisability with increasing the carbon chain length.

The real permittivity (ε') allows to define the nature of the constituent materials, whereas the

imaginary permittivity (ε'') helps to evaluate the interaction of the electromagnetic wave with the material.

In order to examine the validity of the measurements, the permittivity values of some basic n-alkanes were compared to the experimental values that we obtained using the cavity resonator. The real permittivity values for number of common solvents have been analysed and published in the literature [29] are illustrated with our experimental values in Table 5.2.

Table 5.2: Summary of the analysis of the dielectric data for some of the pure liquids and experimental values.

Compound	(ε') Literature values [1]	(ε') Experimental
Hexane	1.9	1.91
Octane	1.9	1.99
Dodecane	2	2.02
Hexadecane	2.14	2.07

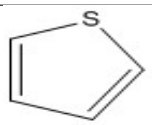
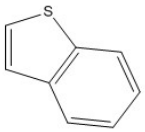
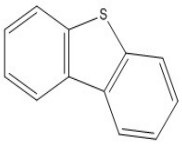
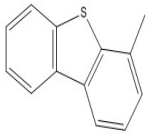
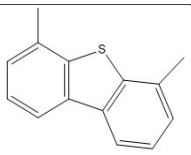
[1] Data have been taken from Ref. [29].

The experimental results of the real permittivity have been found to be fairly in agreement with the values found in the literature. The maximum error obtained between the theoretical and experimental results is less than 5%. This would support the validity of the measurements for other unknown materials, such as heavy oil and petrochemicals with the accuracy required to conduct a satisfactory measurement.

Heterocyclic and Aromatic Compounds

Sulphur compounds are considered as the most important non-hydrocarbon materials in petroleum and it can be found in different sorts of structures [30]. They can be found concentrated in a considerable number in the heavy fractions and residua. The proportion of sulphur increases with the boiling point of crude oil. Generally, it is hard to allocated a specific trend to the presence of compound types in different crude oils [31]. A group of chosen common sulphur compounds are listed in Table 5.3.

Table 5.3: The physical properties of sulphur compounds.

Sample	Structure	Melting point °C	Boiling point °C
Thiophene		-38	84
Benzothiophene		30	220
Dibenzothiophene		100	333
4-Methyldibenzothiophene		350	64-68
4,6-Dimethyldibenzothiophene		364.9	153-157

The change in the resonance peak of the sulphur compounds are presented in the Figure 5.4 below. In can be seen that the shift in frequency which is proportional to the real permittivity value is the highest in the case of thiophene and benzothiophene, whereas it is lower in the case of the other benzothiophene compounds.

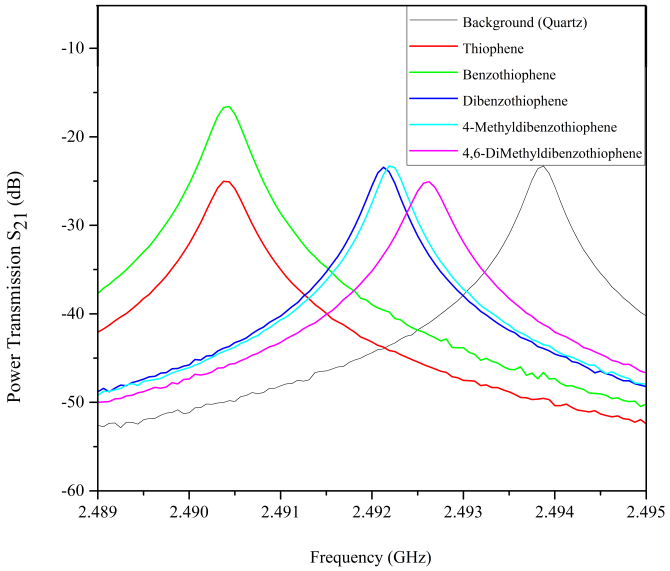


Figure 5.4: The change in the resonance peak positions in sulphur compounds.

Figure 5.5, represents the change in the bandwidth values occurring with increases in molecular size. The change in the bandwidth is related directly to the imaginary part of permittivity.

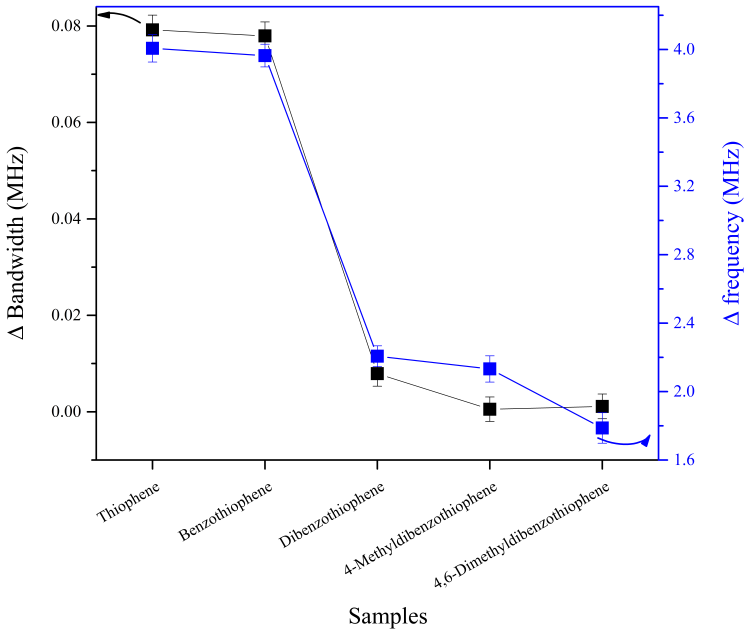


Figure 5.5: The change in the bandwidth and the shift in the frequency values in sulphur compounds.

The electron densities of the S atom in thiophene and its derivatives were found to be in the range of 5.696 D (for thiophene) to 5.760 D (for 4,6-dimethyledibenzothiophene) [31],[32]. It is obvious that thiophene has the lowest electron density. As the thiophene ring system becomes more condensed, the electron density on the sulphur increases in the following order: thiophene < benzothiophene < dibenzothiophene [32–34].

In the aromatic ring, one electron is donated by each carbon atom to the π-bond, whereas the sulphur atom is donating a pair of electrons to its aromatic ring [35]. However, in thiophene, the electron pair on the sulphur atom is not included in the electron cloud density, which means that it is not fully delocalised around the aromatic ring. However, in the case of benzothiophene and dibenzothiophene, the electron pair on the sulphur atom is fully delocalised around the aromatic ring. This results from the extra benzene ring that is fused to the thiophene structure, which greatly influences the π-electron cloud density in the case of an extra benzene ring fused to the thiophene. In addition, the extra benzene ring can lead to an increase in thermal stability of the molecule and reduce the reactivity of the compound. So, any additional benzene rings in the thiophene structure leads to a decrease in reactivity in the following order: thiophene > benzothiophene >

dibenzothiophene [36–38].

The real permittivity and imaginary permittivity values are presented in Figure 5.6.

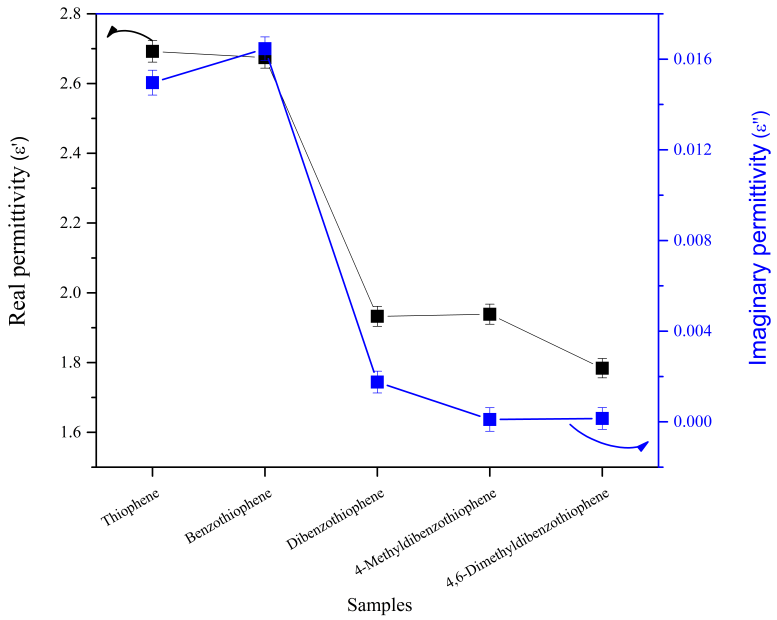


Figure 5.6: The real permittivity (ε') and the imaginary permittivity (ε'') for sulphur compounds.

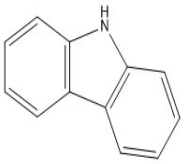
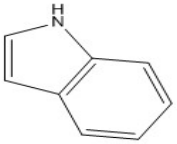
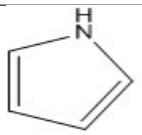
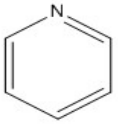
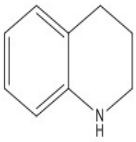
The susceptibility of the compounds to dissipate microwave energy follows the same order of reactivity from high (for thiophene) to low (for 4,6-dimethyldibenzothiophene). In the case of 4-methyldibenzothiophene and 4,6-dimethyldibenzothiophene, it can be observed that there is no significant difference in the real permittivity value from the dibenzothiophene. The slight decrease in real permittivity can be attributed to the substitutions near the sulphur atom (C_4 or C_6), resulting in a decrease in the dipole moment. The substituted methyl groups on the sulphur charge can cause a blocking effect which has a positive contribution on the dipole moment because both methyl groups are located on different aromatic rings however they are symmetrically positioned with respect to the sulphur atom [34, 39, 40].

Microwave frequencies induce specific bonds in reactive materials, and is more efficient at higher temperatures. The dielectric study of the sulphur compounds is very important in the field of pet-

roleum. The desulphurisation process by microwave heating is becoming a very attractive approach in the heavy oil upgrading process. Desulphurisation by microwaves is induced by the radical reaction mechanism, and microwaves are found to be more effective in weakening the C-S and C-H by activating the molecule. However, microwave heating could face lots of difficulties in meeting the requirements of chemical bond breaking energy due to the low susceptibility of the heavy sulphur compound to be heated by microwaves, particularly in the absence of microwave absorbers [5, 26, 35, 41].

The presence of **Nitrogen Compounds** in petroleum generally occurs in small amounts, almost less than 2%. Nitrogen compounds can be responsible for poisoning the catalysts, and they also contribute to gum formation in such products as domestic fuel oil [42]. The more asphaltic the oil, the greater the possibility of the nitrogen to occur as homologues of pyridine . The other common nitrogen compounds that can be found in the oil are: pyrrole, indole and carbazole types, they can occur in heavy fractions and residua. In addition, quinoline compounds can be found in the low boiling point fractions [32]. The list of the nitrogen compounds used in this study are introduced in Table 5.4.

Table 5.4: The physical properties nitrogen compounds.

Sample	Structure	Melting point °C	Boiling point °C
Carbazole		246.3	354.7
Indole		52 - 54	254
Pyrrole		-	129
Pyridine		-	115.2
1,2,3,4-tetrahydroquinoline		-	249

From Figures 5.7, and 5.8, an overall idea of the dielectric properties of the samples can be obtained. The large change in the bandwidth and the shift in frequency values upon the insertion of pyridine, pyrrole and 1,2,3,4-tetrahydroquinoline indicate an efficient ability to convert the microwave energy into heat. This can be seen from the significant broadening that occurs to these three peaks.

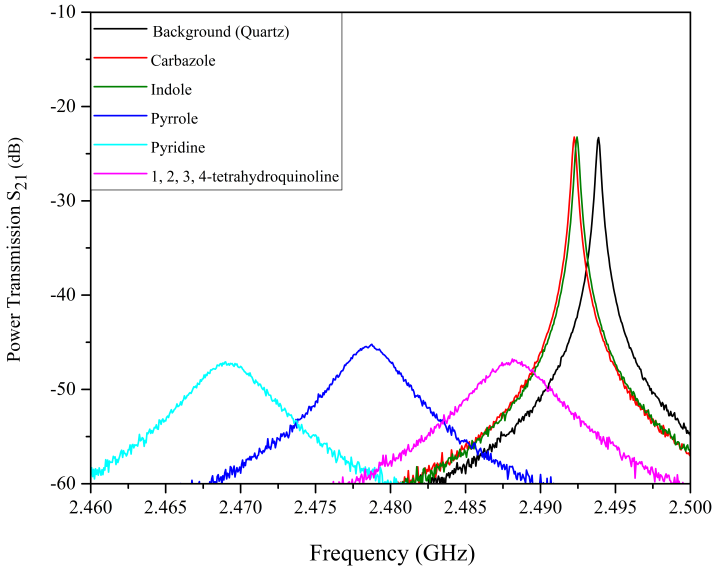


Figure 5.7: The shift in the resonance peak and the broadening in the bandwidth for nitrogen compounds.

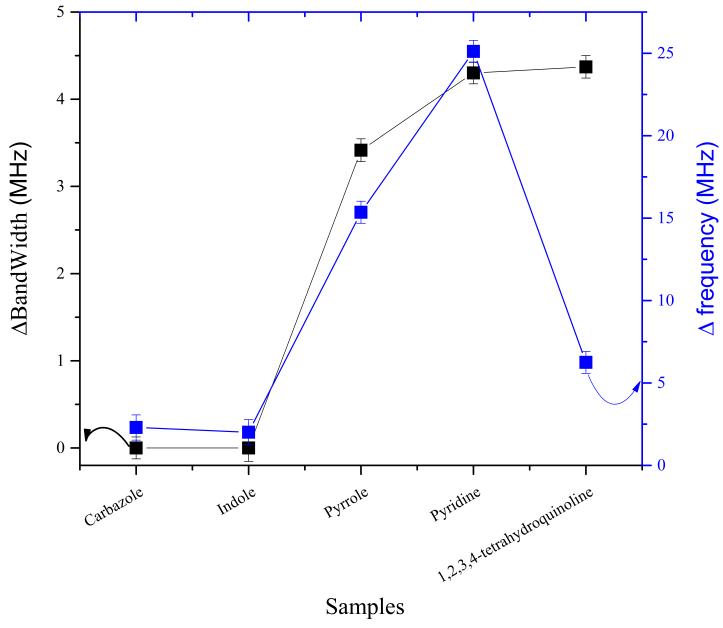


Figure 5.8: The change in the bandwidth and frequency for nitrogen compounds.

The simplest 6-membered ring of a nitrogen compound is pyridine, whereas the simplest 5-membered ring of a nitrogen compound is the pyrrole. From Figure 5.9, it can be seen that the polarisability of the pyridine is slightly higher than the pyrrole. This can be attributed to the delocalisation effect which resulted from the mesomeric interactions in the πelectrons in the pyridine ring.

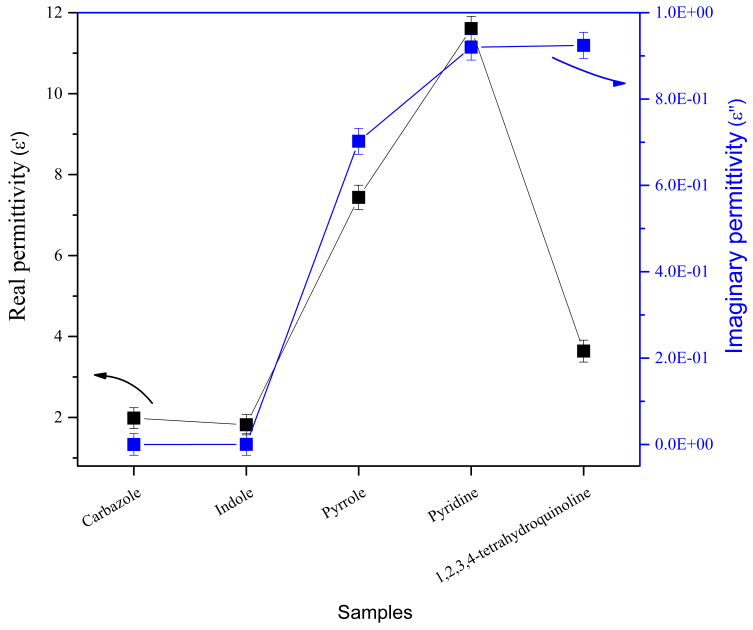


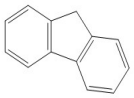
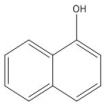
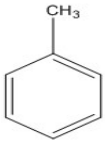
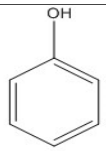
Figure 5.9: The real permittivity and the imaginary permittivity of the nitrogen compounds.

When comparing the compounds with 5-membered rings - indole, and carbazole - it can be noticed that they are fairly similar in their general physical properties. Since the 5-membered rings of nitrogen compounds have aromaticity which is indicating that higher π electron cloud and unsaturated bond formed in the compound itself. Moreover, in a similar behaviour to the sulphur compounds, the benzene ring that is attached to the five-membered ring of nitrogen compound results in an increase in the strength of their π electron cloud. So, the presence of the benzene ring in the indole and the two benzene rings in carbazole influenced the electrons' delocalisation and

increases the electron density of the molecule. This can explain the increase in real permittivity values from carbazole and indole to pyrrole which is more notable in the experimental values [32, 38]. The change in the compound's polarisability reflects the influence of the benzene ring on the real permittivity values. More benzene rings increase thermal stability, while decreasing the chemical reactivity in any environment due to the strength of unsaturated bonds, π electron density and higher aromaticity. However, this is not the case for the 1,2,3,4-tetrahydroquinoline where a high permittivity value is exhibited. This can be attributed to the free electron pair from the nitrogen atom, which is unshared in the delocalised π electron cloud of the fused benzene ring [40, 43, 44].

There are other important compounds which occur in heavy oils. These include naphthenes (cycloparaffins) such as cyclohexane, and aromatics in the form of cyclic hydrocarbons such as toluene, or in the form of oxygen compounds like phenol [44]. Compounds selected to represent the naphthenic and aromatic oxygen compounds are presented in Table 5.5.

Table 5.5: The physical properties cycloparaffinic and aromatic compounds.

Sample	Structure	Melting point °C	Boiling point °C
Fluorene		111-114	298
Naphthol		94-96	278-280
Biphenyl		69.2	255
Cyclohexane		-	80.74
Toluene		-	110.6
Phenol		-	181.7

Their shift in resonance peak in addition to the change in frequency and bandwidth values are presented in Figures 5.10 and 5.11.

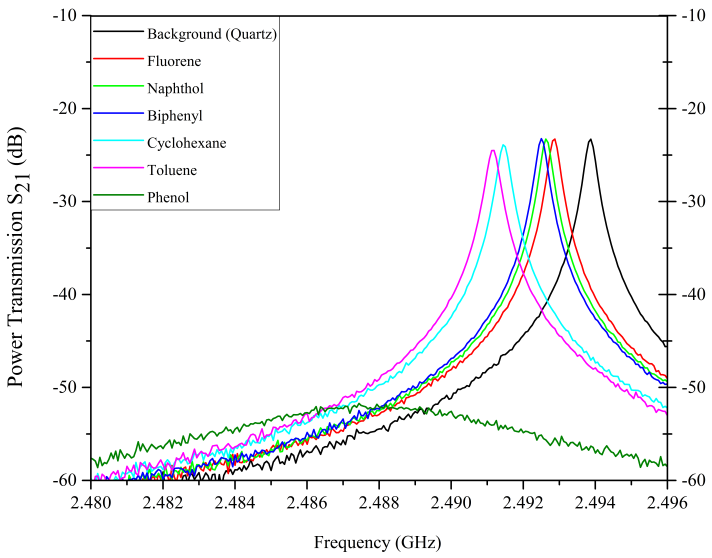


Figure 5.10: The shift in the resonance peak of some cycloparaffins and cycloaromatic compounds.

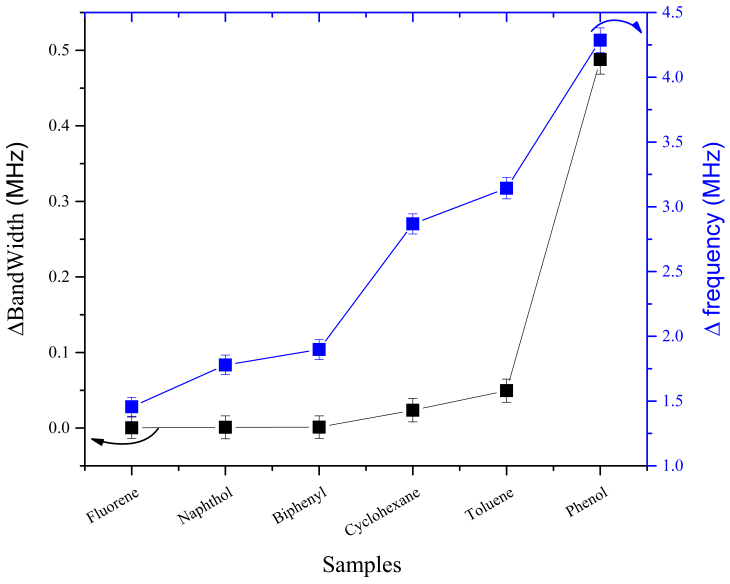


Figure 5.11: The change in the bandwidth and the shift in the frequency values.

In the case of the first three solid compounds, fluorene, naphthol, and biphenyl, the presence of the two benzene rings are influencing the high electron density. This can be attributed to the delocalisation of π as a general principle, the greater the spread of electrons in the molecule, the more stable it becomes. Additional measurements have been conducted on three other liquid compounds, cyclohexane, toluene, and phenol. Cyclohexane is a nonpolar solvent with a zero permanent electric dipole. However, when comparing toluene and phenol, we can see that phenol has a higher real permittivity value than toluene. The reason for this difference is related to the functional group and the dipole moment of the molecules (0.375 D and 1.224 D for toluene and phenol, respectively). The higher value for phenol is in part due to the permanent dipole-dipole attractions from the high electronegativity of the oxygen [45–47]. This can be seen in permittivity values of tested compounds (Figure 5.12)

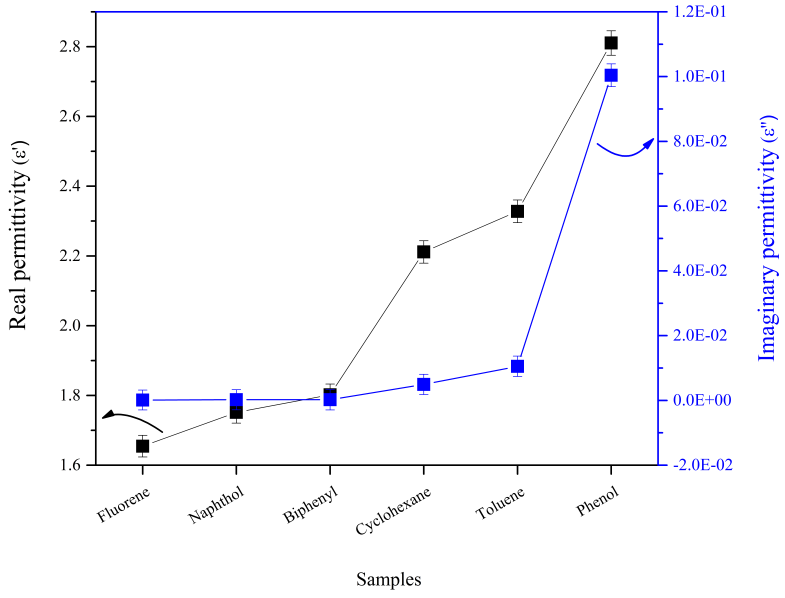


Figure 5.12: The real permittivity and the imaginary permittivity of the cycloparaffins and cycloaromatics.

Overall, it has been found that adding a benzene ring reduces the real permittivity in all the

tested cases. However, it has been found that the benzene ring reduces the dielectric loss in solid material cases only.

5.3.2 Oil Samples

The dielectric measurements have been performed to compare the dielectric behaviour of three oil samples. Heavy bunker oil, light crude oil, and pyrolysis oil have been analysed in the cavity resonator - additives and solvents free. It can be seen from Figure 5.13 that the pyrolysis oil is exhibiting a huge broadening in bandwidth whereas the bunker and crude oil shows the less broadening [23]. This can be attributed to the variation in the oils chemical properties **[Appendix A]**.

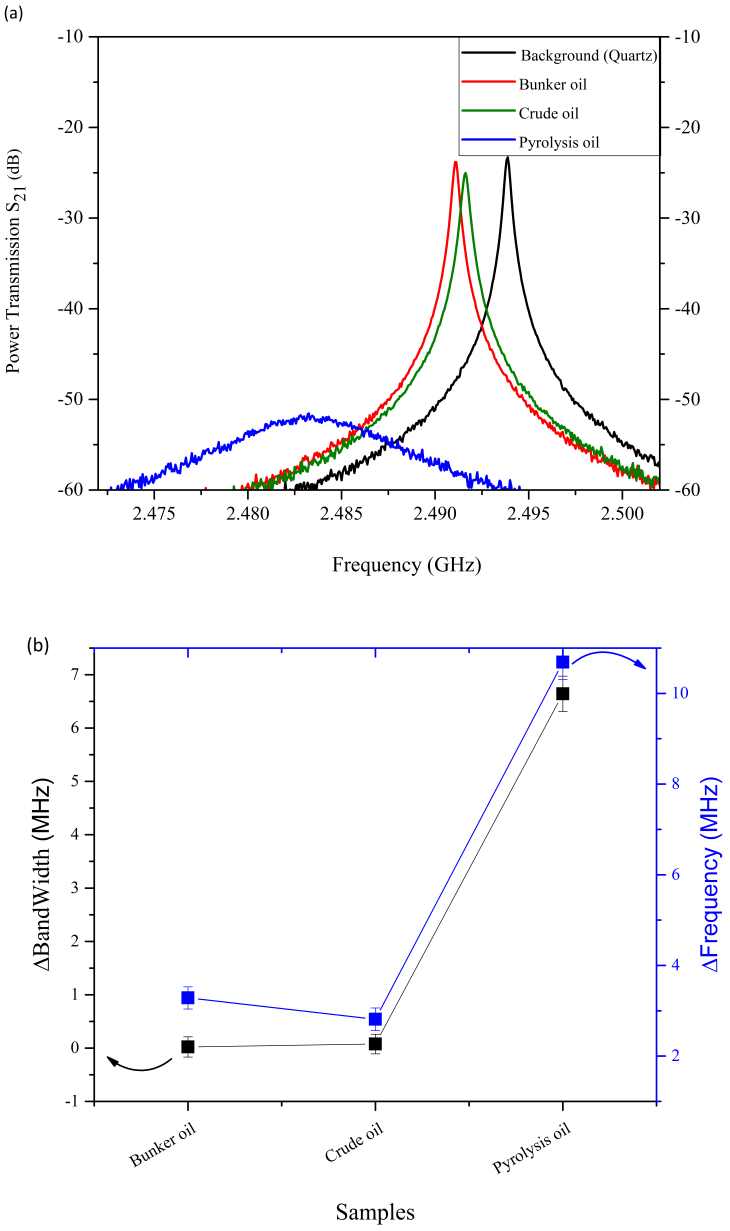


Figure 5.13: (a) the resonance peak positions, and (b) the change in the bandwidth and frequency values of heavy (heavy bunker, light crude, and pyrolysis oil samples.

Heavy bunker and light crude oil were found to contain approximately 84% by weight of carbon material. It is well known that bunker oil is composed of large amounts of heavy fractions with

high molecular weight, such as naphthenic and aromatic sulphur compounds compared to the lighter crude oil. The small changes in frequency and bandwidth value of bunker and crude oil are in agreement with the results obtained for the performed dielectric measurement of the model compounds, as alkanes, in general, are found to be exhibiting low dielectric properties. For the bunker oil, the heavier fractions of paraffinic and aromatics of sulphur and nitrogen compounds are also exhibiting low dielectric properties.

In case of pyrolysis oil, it often contains between 15-30 % of water [48]. However, the water, in any percentage, can significantly affect the dielectric properties of any material [49]. In the tested sample, the water percentage was found to be 28 wt.%, in addition to 52 wt.% of oxygenated compounds, such as hydroxyacetone, levoglucosan, acetic acid, methanol, and mostly ethanol. The dielectric nature of these compounds can be mainly attributed to the reorientation of the highly polar OH-group in liquids. As ethanol is the main constituent of the oxygenated compounds, it gives rise to the high dielectric properties of the pyrolysis oil, which in turn is due to its high polarity beside the molecular rotation and weak London dispersion force compared to other compounds, such as propanol.

The calculated real permittivity and imaginary permittivity values are presented in Figure 5.14.

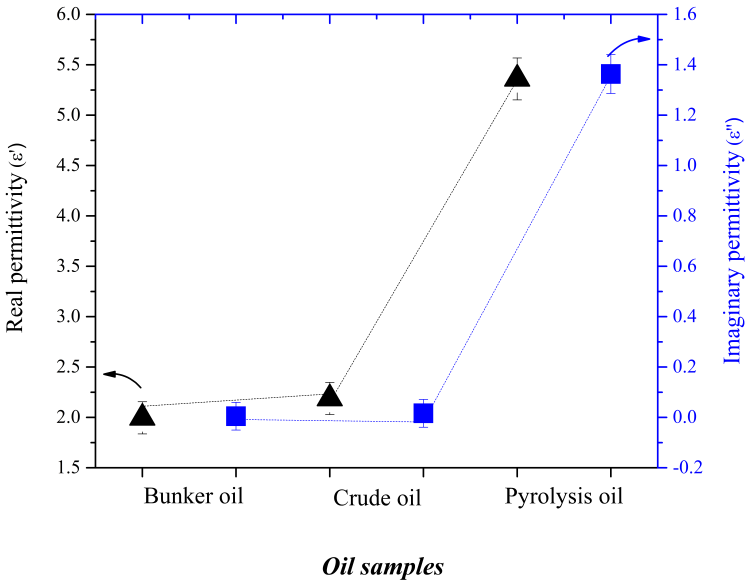


Figure 5.14: Dielectric properties of the oil samples.

As shown Figure 5.14, it is clear that the pyrolysis oil has a better susceptibility to interact with microwave in comparison to the bunker and crude oils. In general, the real permittivity values of the oil samples are considered relatively low. This can be attributed to the non-polar nature of the oil as the molecules cannot easily orientate under the applied electric field, also they cannot generate an effective dipole moment. This results in a decrease of both the polarisation and the real permittivity (ε').

It has been highlighted in the literature that water has a very high permittivity value of ε' =80.10 [29]. The symmetrical water molecule composed of one oxygen atom and two hydrogen atoms has a large susceptibility to polarise when an electric field is applied. In addition, the centre of the positive and negative charges does not coincide, resulting in a permanent dipole moment of the molecule. This phenomenon is called the orientational polarisation as the applied field tends to orientate each dipole. However, under a microwave field, the polar molecules will not be able to orient with the field due to the lack of sufficient time to do so. This resistance to rapidly changing polarity is molecularly expressed in the form of heat. The fact that pyrolysis oil is composed of a relatively large amount of water and OH-group compounds has a great contribution to its high

overall permittivity in comparison to the bunker and crude oil which can be seen in Figure 5.14.

Bunker and crude light oil samples are also composed of small number of ionic compounds that have a small contribution towards the possible dielectric heating behaviour which can be enhanced by the microwave additive dispersion within the oil sample [50, 51].

To evaluate the penetration of the electromagnetic waves when they are applied to the materials, the penetration depth of each oil sample has been calculated using the following equation [52]:

$$D_p = \frac{\lambda_0}{2\sqrt{2}\pi\{\varepsilon' \left[\sqrt{1 + (\varepsilon''/\varepsilon')^2}\right] - 1\}^{\frac{1}{2}}} \tag{5.4}$$

If the microwave heating device is operating at a frequency of 2.45 GHz, a wavelength of the radiation λ_0=12.24 cm at room temperature, the measured penetration depths of the oil samples are 5.94 m, 1.79 m, and 0.033 m for the heavy, crude, and pyrolysis oils, respectively. These values represent a decrease in the microwave field strength from the surface value by a factor of 1/e [53]. This decrease occurs due to varied loss mechanisms that arise within the material resulting in dielectric heat. In comparison to water, the penetration depth of the pure water was found to be in the range of 0.013 - 0.016 m at 2.45 GHz [52]. It can be concluded that the microwave penetrates more in the heavy oil with less interaction, followed by the lighter crude oil which exhibits a better interaction with microwave radiation. The penetration of the microwave within the pyrolysis oil is the shortest, which indicates an increase in its dielectric heating. The results of the penetration depth, are in agreement with the microwave heating profiles, which are illustrated in Figure 5.15.

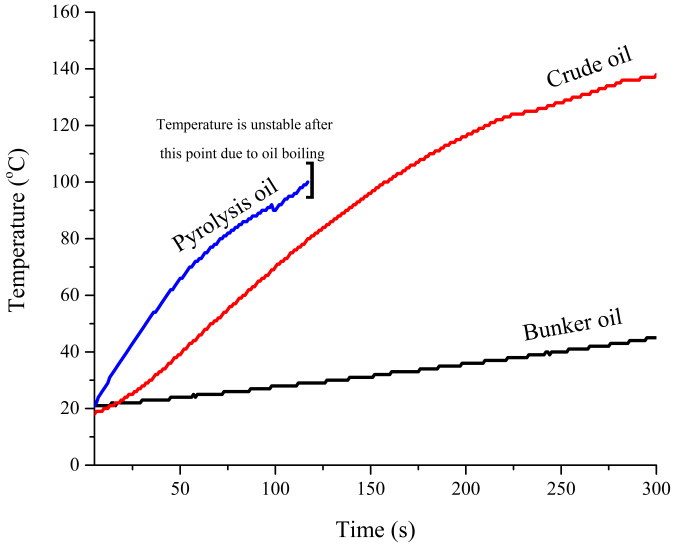


Figure 5.15: The variation in heating profiles of the oil samples at fixed input power of 300 W.

As the materials vary, they get heated up differently. This variation depends on their susceptibility to absorb the microwave and the ability to convert them to heat. When comparing oil samples it can be seen that they are all exhibiting dielectric heating ability, however, this ability is varying upon their dielectric properties.

5.3.3 Zeolite Samples

Zeolite is the main catalyst that will be utilised in this thesis. It has been chosen due its importance within different processes of the petrochemical industry. The shape-selectivity and acidic catalyst are the two main characteristics of the zeolite catalysts, and their activity is mainly resulting from the presence of Bronsted acidic sites, coming from the bridging OH groups, as exposed in Figure 5.16. Zeolites have different framework structures which can greatly vary according to their catalytic performance in different processes, but they still have these active sites in common [54].

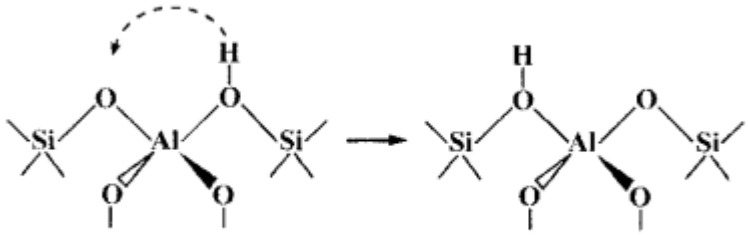


Figure 5.16: Zeolite structure.

The dielectric measurements have been performed to evaluate the dielectric properties of ZSM-5 zeolite. Figure 5.17 illustrates the real permittivity and imaginary permittivity values of NH_4ZSM-5, HZSM-5 Si/Al= 60 (before and after drying), in addition to ZSM-5 Si/Al=160.

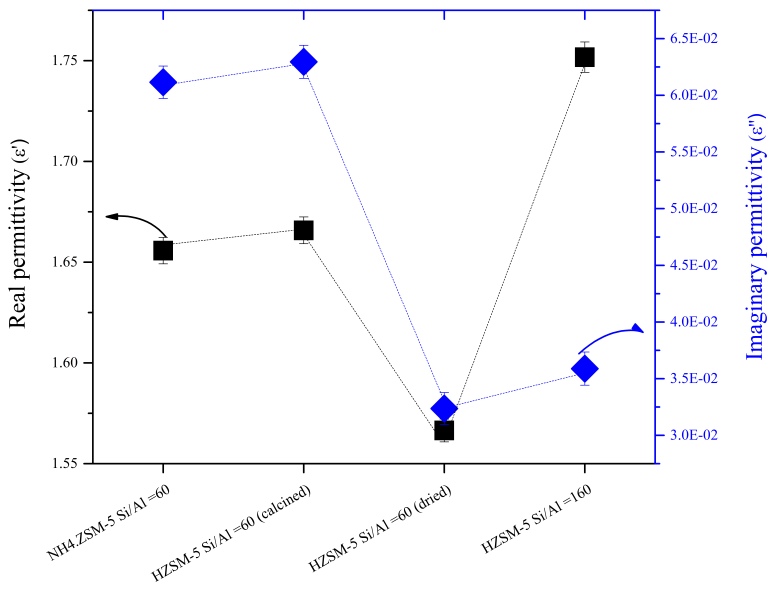


Figure 5.17: Dielectric properties of zeolite samples.

In general, zeolites are considered weak dielectric materials. Figure 5.17 shows that there is no significant difference in the dielectric properties values of all the zeolite samples. Zeolites have a porous nature and high tendency to absorb moisture within their pores. It can be seen that there is a slight decrease in real permittivity and imaginary permittivity when comparing the HZSM-5 before and after drying. This decrease can be an indication of the water loss from the zeolite pores after drying. However, there is no observed change in real permittivity when exchanging the H^+ with $NH_4{}^+$ [55, 56].

In terms of different Si/Al ratio, the electrical conductivity of the zeolite samples was evaluated using the following equation [18]:

$$\sigma = \omega \varepsilon_0 \varepsilon'' \tag{5.5}$$

where ω is the angular frequency and represented by $(2\pi f_0)$,

and ε_0 is the permittivity of the free space, 8.85×10^{-12} F/m.

The electrical conductivity of the zeolite samples are shown in Figure 5.18.

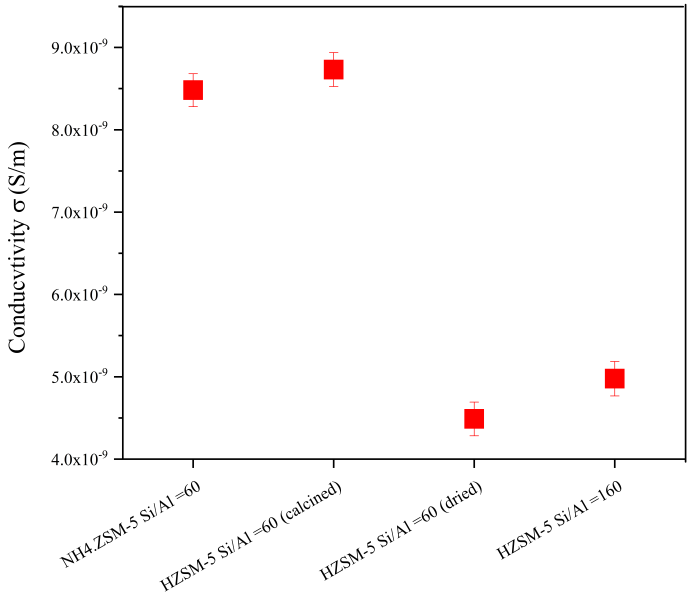


Figure 5.18: The microwave conductivity of zeolite samples.

When changing the framework of the zeolite, the (Si/Al =160) is exhibiting a lower conductivity comparing to (Si/Al = 60) as well as lower imaginary permittivity as it is proportional to conductivity. This can be attributed to the decrease in the Al content resulting in a reduced number of mobile cations. In addition, this would lead to an increase in the distance between the accessible hopping sites. On the other hand, the real permittivity value might be attributed to the water content within the zeolite.

Overall, zeolites contain exchangeable mobile cations that are weakly bonded to the framework. The dielectric properties of the zeolites can be adjusted by introducing the desired guest materials and ions. Thus, the electrical conductivity can be represented as a function of the number of current carriers and their mobility. The size and charge of the exchangeable cation, in addition to the size of the zeolitic framework and channels, can also influence the dielectric properties of the catalyst [57–60]. Dielectric measurements of iron oxide doped HZSM-5 catalysts will be presented in **Chapter 8**.

There are many factors that can determine the dielectric properties of a material. Besides the real permittivity ε' and the imaginary permittivity ε'' , the dielectric loss tangent is an important part of the dielectric characteristics of the material. Where the real permittivity describes the

ability of the material to be polarised in the electric field, and the imaginary permittivity measures the efficiency of converting the electromagnetic radiation into heat, the ratio of the real to the imaginary permittivity is called the dielectric loss tangent (tanδ). This important parameter defines the ability of a material to be heated by microwaves at a given temperature and frequency. This can be introduced by the following equation:

$$\tan\delta = \frac{\varepsilon''}{\varepsilon'} \tag{5.6}$$

Figure 5.19 - the dielectric loss tangent (tanδ) values of all utilised compounds in this study. It can be seen that the liquid nitrogen compounds are demonstrating the highest loss tangent (top corner graph), followed by the phenol with OH group. Among the sulphur compounds, the thiophene and the benzothiophene are exhibiting the highest loss tangent compared to the heavier sulphur materials. The paraffinic linear compounds illustrate low loss tangent; however, it is increasing slightly as a function of carbon atoms, whereas the paraffinic cylcocompounds have enhanced loss tangent values. Overall, liquid samples was found to have a better dielectric properties comparing to the solid samples from the same group of compounds.

Oil samples are varying in their ability to be heated by microwaves. In the case of pyrolysis oil, the measurements of the real permittivity and imaginary permittivity was found to be higher comparing to the bunker and crude oil due to its high loss nature. Between the heavy bunker and light crude oil, crude has a slightly higher loss tangent than the heavy bunker sample. As mentioned previously, heavy oil is very dense and viscous due to the high percentage of heavy aromatics and naphthenes compared to linear alkanes. It is also composed of high amounts of heavy fractions of nitrogen, sulphur, and oxygen, which render it less able to interact with microwaves. On the other hand, the presence of some light fractions of polar compounds influence its ability to be heated in microwaves to a greater extent than the paraffinic hydrocarbons. Moreover, the crude oil is very light compared to the bunker oil, which might indicate the large percentage of light factions compared to heavy oil. In addition, it has a shorter penetration depth of microwave comparing to bunker oil.

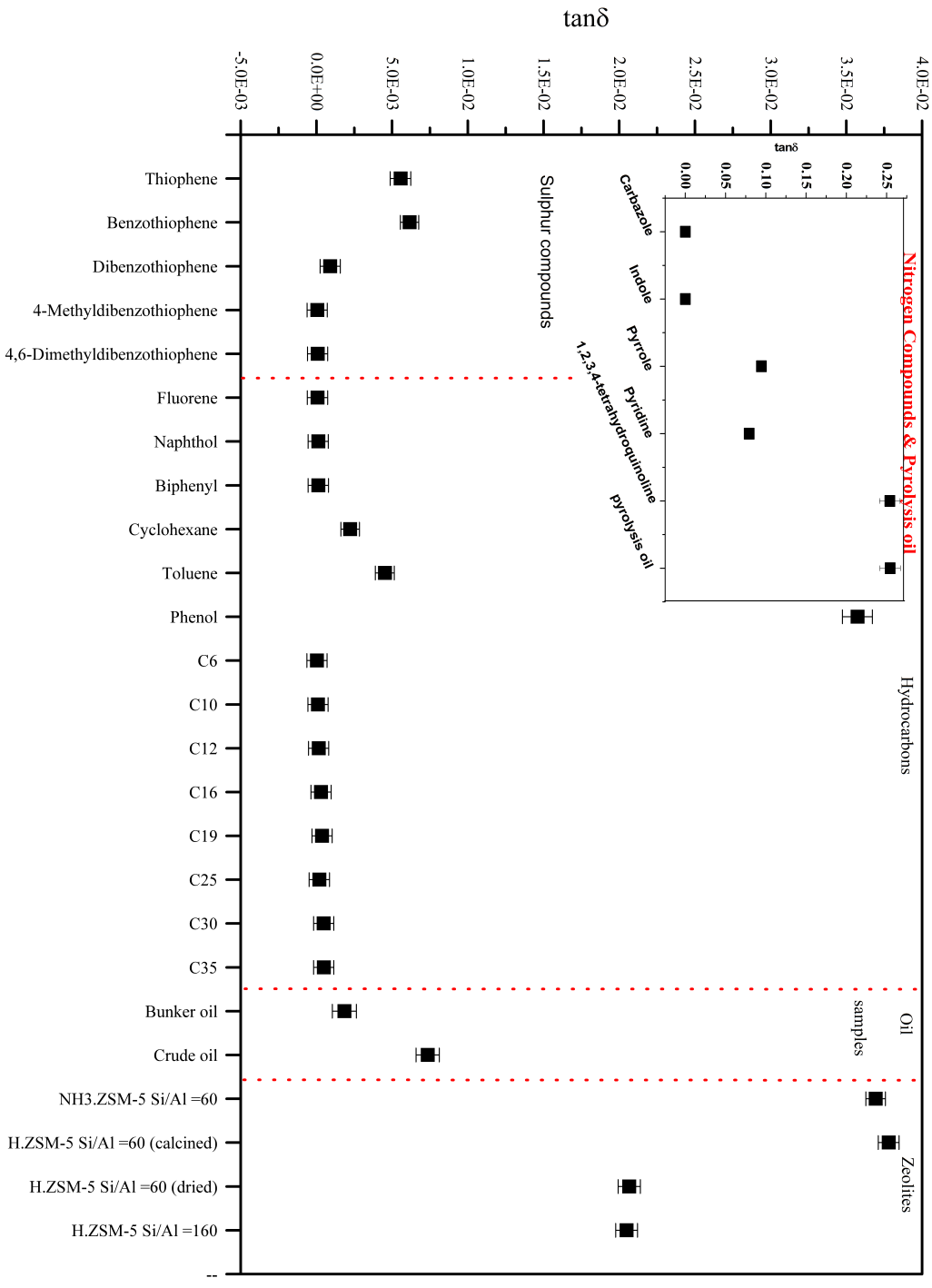


Figure 5.19: Library of dielectric loss tangent (tanδ) for a group of sulphur compounds, nitrogen compounds, cyclo and linear paraffinic compounds, heavy oil samples and zeolitic catalysts, nitrogen compounds are presented separately in the top corner as they are exhibiting higher loss value comparing to the rest of the compounds.

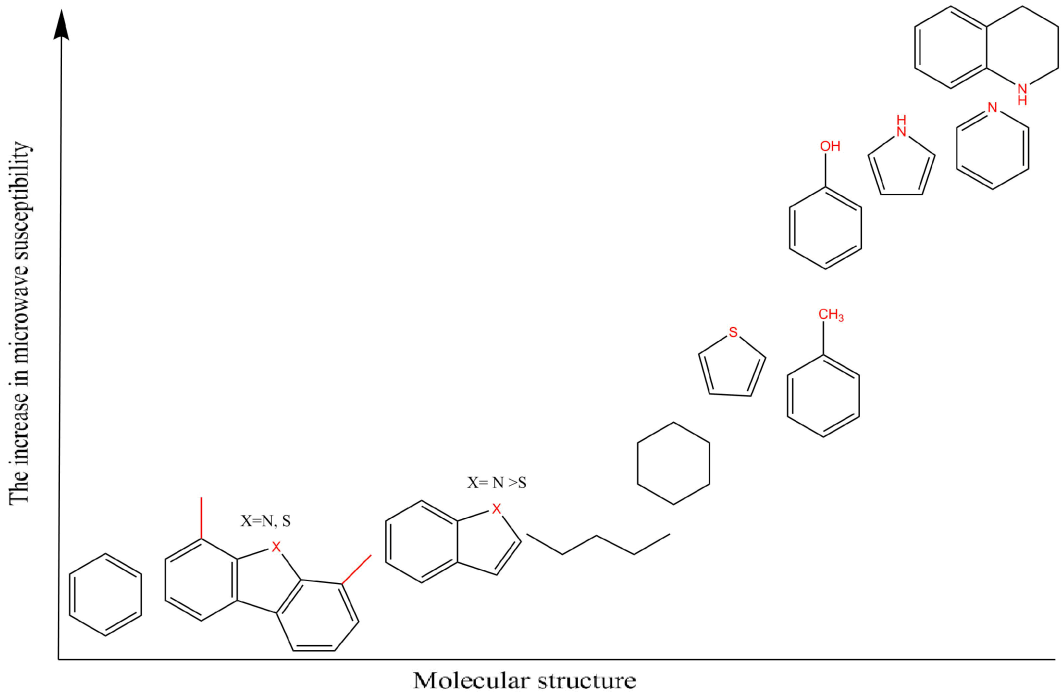


Figure 5.20: Overview of the increase in microwave susceptibility within the model compounds.

5.4 Conclusions and Future Work

In conclusion, the microwave heating of a material is a combination of several factors, such as the dielectric permittivity, conductivity and the applied field, in addition to temperature and material density.

In the case of solvent model compounds, the dipole moment of benzene is zero. However, the addition of substituents could result in a net dipole moment. This will have an effect on the dielectric properties as it increases intermolecular attractive forces and raises the boiling points as observed in the case of pyrrole and thiophene. It can be observed that the chemical behaviour is attributed to the heteroatoms and their effect on the dipole moment (i.e. a dipole of 1.8 D for pyrrole and a dipole of 0.5 D for thiophene). The difference observed between toluene and phenol

can be attributed to the OH group, which has a greater contribution to the dipole moment in comparison to the CH_3 group. The electronic polarisability might be the mechanism responsible for the low dielectric heating characteristic in the case of non-polar linear or cycloalkanes.

The dielectric study of the model compounds helps to optimise and understand the interaction between the heavy oil and microwaves. Additionally, the dielectric study of several oil samples helps to characterise the oil and defines its type based on the presence of various components and constituents, such as asphaltenes, or oxidised materials. The ionic conduction mechanism may also play a role in the heating of heavy oil and zeolite samples.

The dielectric properties of the oil samples indicated that both bunker and crude oil exhibit low dielectric properties compared to the pyrolysis oil. This can be attributed to the presence of heavy fractions of sulphur, nitrogen and hydrocarbon materials in case of the bunker oil. However, it could be slightly heated under microwave irradiation due to the presence of some charge carrying elements or ions. In the case of light crude oil, the large amount of non-polar hydrocarbon materials present is responsible for low dielectric properties. The higher dielectric properties of the pyrolysis oil was assigned to the water and oxygenated compounds content. This was confirmed by the chemical analysis of all the oil samples. Thus the cavity perturbation technique can give an insight into the oil properties, in addition to the required microwave system which can be used to conduct the desired oil processing reaction.

Exploring both real permittivity and imaginary permittivity properties of the material is very important not only for studying the material properties but also for designing catalytic materials. The real permittivity value provides information on the material polarisability, and the amount of energy that can be stored in a material. The imaginary permittivity value can provide information about the coupling efficiency of the materials with microwaves. The key is to achieve the best tuning of the utilised catalysts that can be modified with a good microwave absorber. The balance between these two values can be manipulated to achieve the best performance of a material for the required purpose.

For future work, further investigation of the materials properties using microwave resonant cavity under the magnetic field is recommended in order to explore the complete story of materials interaction with electromagnetic field.

Bibliography

[1] M. Faraday. *Experimental Researches in Electricity.* 11. Phil. Trans. R. Soc., London, 1838.

[2] G. Meurant. *Theory of Electric Polarization: Dielectrics in Static Fields.* Theory of Electric Polarization. Elsevier Science, 2 edition, 2012.

[3] O.F. Mossotti. *Memorie Mat*, volume 49. Fis. Modena, 1850.

[4] R. Clausius. *Die Mechanische W. Armtheorie*, volume II. Braunschweig, 1897.

[5] C.S. Helrich. *The Classical Theory of Fields Electromagnetism.* Springer Science & Business Media, 2012.

[6] P.Debye. *Phys.Z.* Number 97. 13, 1912.

[7] Y.Y. Akhadov. *Dielectric Properties of Binary Solutions.* Pergamon Press, Oxford, 1980.

[8] L. Sirdeshmukh D. Sirdeshmukh and K.G. Subhadra. *Micro- and Macro-Properties of Solids: Thermal, Mechanical and Dielectric Properties.* Springer Series in Materials Science. Springer Berlin Heidelberg, 2006.

[9] F. Kremer and A. Schonhals. *Broadband Dielectric Spectroscopy.* Springer Berlin Heidelberg, 2012.

[10] V.I. Gaiduk. *Dielectric Relaxation and Dynamics of Polar Molecules*, volume 8. World Scientific Publishing Co. Pte. Ltd., Singapore, 1999.

[11] R.H. Cole. Dielectric Polarization and Loss. *Annual Review of Physical Chemistry*, 11:149–168, 1960.

[12] P.J. Van Der Put. *The Inorganic Chemistry of Materials: How to Make Things out of Elements.* Springer US, 2013.

[13] K.L. Mittal. *Polyimides and Other High Temperature Polymers: Synthesis, Characterization and Applications*, volume 4. Taylor & Francis, 2007.

[14] R.J.D. Tilley. *Understanding Solids: The Science of Materials*. Wiley, 2013.

[15] A.A. Carey. The Dielectric Constant of Lubrication Oils. Technical report, Computational Systems Incorporated, 1998.

[16] R.E. Mark J. Borch, M.B. Lyne and C. Habeger. *Handbook of Physical Testing of Paper*, volume 2. Taylor & Francis, 2001.

[17] R.J. King W.L. James, Y.H. Yen and Forest Products Laboratory (U.S.). *A Microwave Method for Measuring Moisture Content, Density, and Grain Angle of Wood*. U.S. Dept. of Agriculture, Forest Service, Forest Products Laboratory, 1985.

[18] L.F. Chen, C.K. Ong, C.P. Neo, V.V. Varadan and V.K. Varadan. *Microwave Electronics: Measurement and Materials Characterization*. Wiley, 2004.

[19] M.J. Kennish. *Practical Handbook of Estuarine and Marine Pollution*. CRC Marine Science. Taylor & Francis, 1996.

[20] G.A. Olah and M. Arpad. *Hydrocarbon Chemistry*. Wiley, 2003.

[21] J.G.Speight. *The Desulfurization of Heavy Oils and Residua*. Science, 5 Nov 1999.

[22] A. Imtiaz. *Solid-State Microwave Heating for Biomedical Applications*. PhD thesis, Electrical and Electronic Engineering, Cardiff University, 2015.

[23] A. Porch, D. Slocombe, J. Beutler, P.P. Edwards, A. Aldawsari, T. Xiao, V. Kuznetsov, H. Almegren, S. Aldrees and N. Almaqati. Microwave Treatment in Oil Refining. *Applied Petrochemical Research*, 2:37–44, 2012.

[24] H.M. Heitzer, T.J. Marks, and M.A. Ratner. Computation of Dielectric Response in Molecular Solids for High Capacitance Organic Dielectrics. *Acc. Chem. Res*, 49:1614–1623, 2016.

[25] W.P. Pan, M.H. Mady and R.C. Miller. Dielectric Constants and Clausius-mossotti Functions for Simple Liquid Mixtures: Systems Containing Nitrogen, Argon and Light Hydrocarbons. *Aiche Journal*, 21(2):283–289, 1975.

[26] C. Gabriel, S. Gabriel, E.H. Grant, Edward, B.S.J. Halstead and D.M.P. Mingos. Dielectric Parameters Relevant to Microwave Dielectric Heating. *Chem. Soc. Rev.*, 27:213–224, 1998.

[27] L. Hao, L. Xifeng, Y Shuangjun, Y. Tianqi, Y. Zhi and Y. Wen. Prediction of Polarizability and Absolute Permittivity Values for Hydrocarbon Compounds Using Artificial Neural Networks. *Int. J. Electrochem. Sci.*, 9:3725–3735, 2014.

[28] J. Cuenca, E. Thomas, S. Mandal, O. Williams, A. Porch. Microwave Determination of sp^2

Carbon Fraction in Nanodiamond Powders. *Carbon*, 81:174–178, 2015.

[29] D.R. Lide. *1998 Freshman Achievement Award*. CRC Press LLC, 87th edition, 1998.

[30] J.G.Speight. *The Desulfurization of Heavy Oils and Residua*. Science, 1999.

[31] S. Otsuki, T. Nonaka, N. Takashima, W. Qian, A. Ishihara, T. Imai and T. Kabe. Oxidative Desulfurization of Light Gas Oil and Vacuum Gas Oil by Oxidation and Solvent Extraction. *Energy & Fuels*, 14(6):1232–1239, 2000.

[32] R.A. Abramovitch. *The Chemistry of Heterocyclic Compounds, Pyridine and Its Derivatives: Supplement*. The Chemistry of Heterocyclic Compounds. Wiley, 2009.

[33] Catalytic Compositions Useful in Removal of Sulfur Compounds From Gaseous Hydrocarbons, Processes for Making These and Uses Thereof, 2013.

[34] M.T. Klein, G. Hou, R. Bertolacini, L.J. Broadbelt and A. Kumar. *Molecular Modeling In Heavy Hydrocarbon Conversions*. Science, 2005.

[35] T. Banerjee and A. Ramalingam. *Desulphurization and Denitrification of Diesel Oil Using Ionic Liquids: Experiments and Quantum Chemical Predictions*. Elsevier Science, 2015.

[36] Mild Hydrodesulfurization Integrating Gas Phase Catalytic Oxidation to Produce Fuels Having an Ultra-low Level of Organosulfur Compounds, 2013.

[37] H. Li, Y. Chang, W. Zhu, W. Jiang, M. Zhang, J. Xia, S. Yin and H. Li. A DFT Study of the Extractive Desulfurization Mechanism by [BMIM]+[$AlCl_4$]-Ionic Liquid. *The Journal of Physical Chemistry B*, 119(19):5995–6009, 2015.

[38] J.A. Joule A.R. Katritzky, C.A. Ramsden and V.V. Zhdankin. *Handbook of Heterocyclic Chemistry*. Elsevier Science, 2010.

[39] H.S. Nalwa. *Handbook of Advanced Electronic and Photonic Materials and Devices: Semiconductors*, volume 1. Academic Press, 2001.

[40] R. Anantharaj and J. Jegalakshimi. Simultaneous Interaction Between Similar and Dissimilar Structures of Aromatic Sulfur and Aromatic Nitrogen Compounds with Imidazolium-based Ionic Liquid Using Quantum Chemical Method. *Asia-Pacific Journal of Chemical Engineering*, 10(6):904–922, 2015.

[41] Z.J. Shi. *Homogeneous Catalysis for Unreactive Bond Activation*. Wiley, 2014.

[42] D.D. Eley, W.O. Haag, B. Gates and Helmut Knozinger, editor. *Advances in Catalysis*, volume Volume 42. Academic Press, 1998.

[43] A.J. Bojarski et al. The Influence of Substitution at Aromatic Part of 1,2,3,4-tetrahydroisoquinoline on In Vitro and In Vivo 5-HT(1A)/5-HT(2A) Receptor Activities of Its 1-adamantoyloaminoalkyl Derivatives. *Bioorganic & Medicinal Chemistry*, 10(1):87 – 95, 2002.

[44] H. Qabazard M. Absi-Halabi, J. Beshara and A Stanislaus. *Catalysts in Petroleum Refining and Petrochemical Industries*. Studies in Surface Science and Catalysis. Elsevier Science, 1996.

[45] A. Chana, M.A. Concejero, M. Frutos, M.J. Gonzalez and B. Herradon. Computational Studies on Biphenyl Derivatives: Analysis of the Conformational Mobility, Molecular Electrostatic Potential, and Dipole Moment of Chlorinated Biphenyl: Searching for the Rationalization of the Selective Toxicity of Polychlorinated Biphenyls (PCBs). *Chemical Research in Toxicology*, 15:1514–1526, 2002.

[46] L.A. Pilato A. Gardziella and A. Knop. *Phenolic Resins: Chemistry, Applications, Standardization, Safety and Ecology*. Phenolic Resins: Chemistry, Applications, Standardization, Safety, and Ecology. Springer Berlin Heidelberg, 2013.

[47] H. Baba and S. Suzuki. Electronic Spectra and Hydrogen Bonding. I. Phenol and Naphthols. *The Journal of Chemical Physics*, 35(3):1118–1127, 1961.

[48] A. Demirbas. *Biofuels: Securing the Planet's Future Energy Needs*. Springer Science & Business Media, 2008.

[49] P. Kohl C. Case, T. Kikkawa and W.W. Lee. *Low-Dielectric Constant Materials III*. Materials Research Society Symposia Proceedings. Materials Research Society, 1998.

[50] S.A. Issaka, A.H. Nour, R.M. Yunus and A.H.Nour. The Heating Pattern of The Microwave Dehydrator for Treating Petroleum Crude Oils. *IJRET:International Journal of Research in Engineering and Technology*, 3:184–191, 2014.

[51] B.G. Terigar, S. Balasubramanian and D. Boldor. An Analysis of the Microwave Dielectric Properties of Solvent-oil Feedstock Mixtures At 300 - 3000 MHz. *Bioresource Technology*, 101(16):6510–6516, 2010.

[52] L. Chenhui, Z. Libo, P Jinhui, S. Chandrasekar, L. Bingguo, X. Hongying, Z. Junwen and X. Lei. Temperature and Moisture Dependence of the Dielectric Properties of Silica Sand. *Journal of Microwave Power and Electromagnetic Energy*, 3(47):199–209, 2013.

[53] R.J. Meredith and Institution of Electrical Engineers. *Engineers' Handbook of Industrial Mi-*

crowave Heating. Energy Engineering Series. Institution of Electrical Engineers, 1998.

[54] P.A. Jacobs L. Kubelkova, B. Wichterlova and N.I. Jaeger. *Zeolite Chemistry and Catalysis*. Studies in Surface Science and Catalysis. Elsevier Science, 1991.

[55] U. Simon and U. Flesch. Cation-Cation Interaction in Dehydrated Zeolites X and Y Monitored by Modulus Spectroscopy. *Journal of Porous Materials*, 6(1):33–40, 1999.

[56] Roque-Malherbe and M.A. Rolando. *The Physical Chemistry of Materials: Energy and Environmental Applications*. CRC Press, 2009.

[57] A. Szasz and J. Liszi. Dielectric Relaxation in Zeolites: Part III. Reduced Diagrams, A Tool For Separation Of Relaxation Domains. *Zeolites*, 11(5):517–520, 1991.

[58] M. Kraus, F. Kopinke and U. Roland. Influence of Moisture Content and Temperature on The Dielectric Permittivity of Zeolite NaY. *Phys. Chem. Phys.*, 13:4119–4125, 2011.

[59] S.M. Auerbach, K.A. Carrado and P.K. Dutta. *Handbook of Zeolite Science and Technology*. Taylor & Francis, 2003.

[60] E. Izci and A. Izci. Dielectric Behavior of the Catalyst Zeolite NaY. *Turkish Journal of Chemistry*, 31:523–530, 2007.

Chapter 6

STUDY OF DIELECTRIC PROPERTIES AT HIGH TEMPERATURES

Overview

The interaction between microwave energy and catalytic materials is governed by the dielectric properties of the sample. The real part of the permittivity (ε'- the dielectric constant) is related to energy storage within the material. The imaginary part (ε''- the dielectric loss) is related to energy conversion into heat. Both properties are influenced by material composition, moisture percentage, grain size and chemical and physical conditions of the material. The dielectric properties also depend on other parameters, such as the temperature, the frequency of radiation and the mass, volume and shape. Knowledge of the relationship between dielectric properties of the material as a function of temperature is essential for rationally developing heating and processing in a microwave cavity.

The application of microwave heating in catalytic and heavy oil processing has recently attracted high levels of interest from the petrochemical industry. Since permittivity is the fundamental property which defines a material susceptibility to absorb microwave energy, understanding how

the dielectric properties of a material changes during microwave heating is extremely important. In turn, this would help to facilitate deeper knowledge of the reaction path, as well as the device performance and the optimisation of energy parameters.

Several attempts to perform a temperature correction for dielectric measurements have been made using a rectangular mode [1, 2]. However, the use of a cylindrical cavity has more advantages to measure the temperature dependent properties for axial samples.

In this chapter, the dielectric properties of the heavy oil, and the HZSM-5 catalyst will be explored using cylinder cavity for high-temperature perturbation measurements. The resulting data from the heavy oil and catalysts will be compiled into thermogravimetric analysis as a function of temperature, to investigate the change in dielectric values correlated with samples decomposition and weight loss.

6.1 Microwave Measurement

6.1.1 Setup

The cavities used for this study are made of aluminium and copper respectively. They were fabricated in the mechanical workshop of the University of Oxford. The measurements were first operated using the aluminium; however, it was found that the cavity quality factor was dropping rapidly from 7,800 to 2,000 with significant difficulties in recovering the cavity for the next set of measurement. After several experimental tests and calibrations it was found that the high temperature measurements were preferably conducted using the copper cavity. Copper material was chosen for the cavity for these measurements in order to provide a better quality factor of 12,500 as it presents a higher heat and electrical conductivity and lower thermal resistance compared to aluminium [3]. It should be noted that the linear thermal expansion coefficient per degree for copper is $16.6\text{x}10^{-6}/^{o}\text{C}$ whereas the for aluminium it is $23\text{x}10^{-6}/^{o}\text{C}$ which is 35% higher in aluminium than copper [4]. However, the platinum which is more expensive has a linear thermal expansion of $9\text{x}10^{-6}/^{o}\text{C}$ is considered the best candidate for fabricating the cavity material for high temperature measurements [5]. A detailed description of the cavity sizing was given in **Section 4.1.**

The attached connectors to the cavity are SMA coaxial panel mount female jacks made of beryllium copper and plated with gold, with an impedance of 50Ω. A modification was made

to the connector where the Teflon® insulator material had been replaced with mica to hold the high temperature conditions. The coaxial cables were replaced with high temperature rigid coaxial cables purchased from Times Microwave Systems. The cables are 300 mm long, and fitted with SMA male connectors at both ends; these were also purchased from Times Microwave Systems. The connectors are YAG Laser welded to the stainless steel rigid cable outer jacket with glass-to-metal seals. The cables and connectors are customised to hold continuous operation performance up to 600°C. The cavity is placed in the central heating zone of a cylindrical furnace. Temperature is controlled by a Carbolite Eurotherm 2408 Temperature Controller. Figure 6.1 below illustrates the experimental setup for the high-temperature measurements.

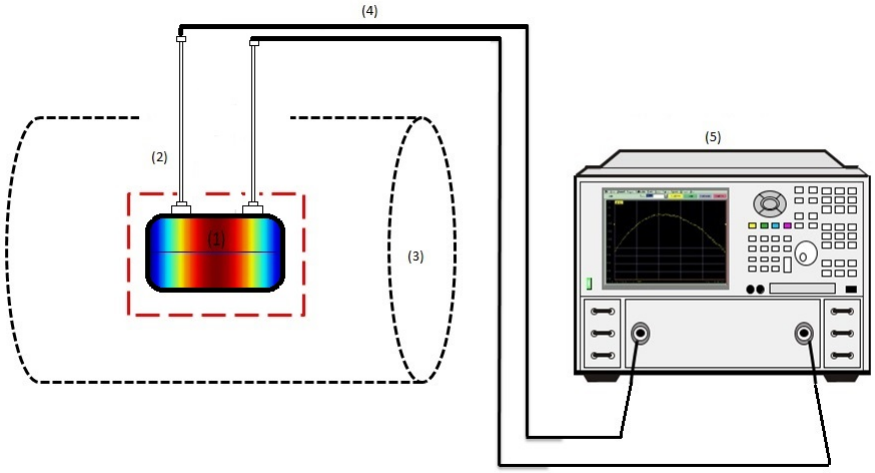


Figure 6.1: High-temperature dielectric measurements setup (1) Copper TM_{010} cavity showing the E-field distribution within in the centre simulated using finite element modelling COMSOL software (2) stainless steel rigid coaxial cables (3) Cylindrical furnace (4) Coaxial cables (5) Vector network analyser (VNA).

6.1.2 Procedure

The experimental approach is similar to the previously operated **(as shown in Section 5.2)** for the room temperature measurements. The perturbation cavity is equipped with a vector network analyser (VNA). The cavity was operated in the TM_{010} mode at a frequency of 2.45 GHz, and it

has an unloaded Q-factor value of approximately 12,500 at room temperature. The measurements of the background with an empty quartz tube at each temperature ramp are carried out to set up a reference of the procedure and thus allow to subtract the linear thermal coefficients of both cavity and quartz tube from the data. Each measurement has been conducted three times for reproducibility and validity purposes.

The samples were held in quartz tubes with a 2 mm inner diameter and a 4 mm outer diameter. The length of the tube was customised at 150 mm for safety purposes. A hole on top of the furnace was created to allow for easier placing of the sample into the centre of the cavity.

The measurements were taken for the heavy bunker oil sample and HZSM-5 with a Si/Al ratio of 60. Freshly prepared oil catalysts impregnated into HZSM-5, in addition to a sample of the same catalyst after microwave processing have also been examined.

An evaluation the volume loss in the heavy oil sample during the high temperature measurements was explored. This was done in order to account for the interfering factors to the permittivity values. The experiment was performed by measuring the volume loss of the heavy oil in cylinder heated in furnace up to 400°C. The volume was recorded to obtain the lost amount at each 100°C.

The impregnated catalyst was prepared by calcining the zeolite and introducing the dissolved heavy bunker oil in toluene to the zeolite catalyst. The mixture was mixed to ensure a correct dispersion of the oil into zeolite. The sample was then dried at 110°C for 48h.

The measurements were taken with the temperatures ranging from 20°C to 500°C except for the heavy oil sample was up to 400°C. The results documented the variation in the dielectric properties as a function of temperature.

The weight loss of the samples and change in compositions were analysed using TGA, whilst the dielectric properties were measured as the temperature was increased. The samples were heated at temperatures ranging from 50°C to 800°C at a rate of 10°C/min under a flow of oxygen at a rate of 100 mL/min. The TGA analysis was performed on the bunker oil, HZSM-5, impregnated fresh and spent zeolite catalysts.

6.2 Results and Discussion

The TM_{010} mode cylindrical cavity resonator was placed inside a temperature-controlled furnace to measure the resonance frequencies in addition to Q-factors at a temperature of up to 500°C. Figure 6.2 represents the change in Q_0-factor as a function of temperature. Experiment is performed on the empty cavity first to validate the approach before taking measurements and to track the shift in frequency as the temperature increases.

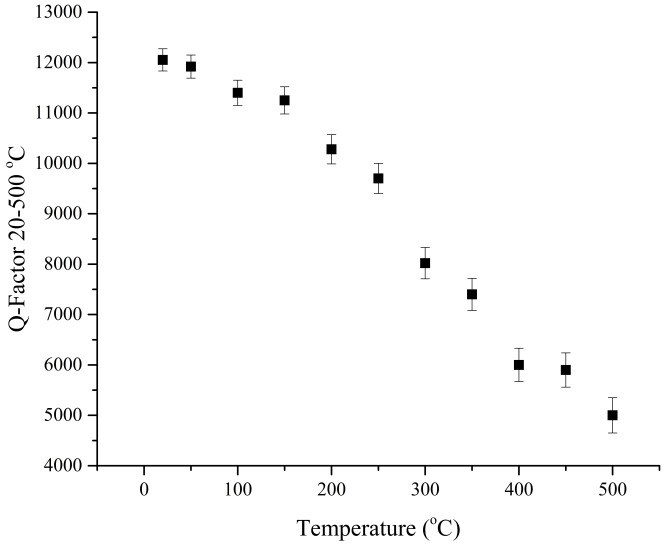


Figure 6.2: The Q-factor values of the unloaded copper cavity as a function of temperature.

At room temperature, the Q-factor loss of the empty cavity is only attributed to the copper electric conductivity. As the temperature increases, the quality factor decreases. The difference in Q-factor values as the temperature changes are tentatively attributed to copper oxidation processes. As the copper oxide is a dielectric material, it could result in a decrease of the Q-factor value as the temperature increases. This has been confirmed by blasting the cavity with high power sand grit blaster to remove the formed oxide layers. The Q-factor value of the unloaded cavity was found to increase to 8,000 as a result which is still considered as high quality factor for performing accurate

measurements.

In addition to the Q-factor tracking as a function of temperature, the TM_{010} mode frequency has been also recorded and the chased frequencies are presented in Figure 6.3.

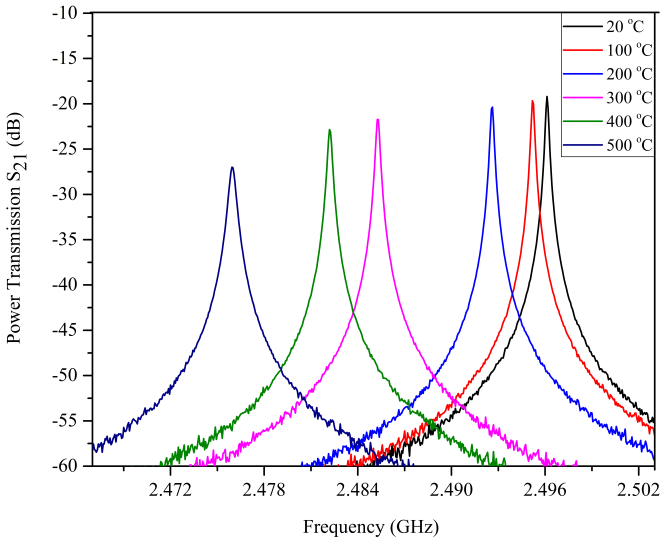


Figure 6.3: The shift in frequency to lower frequencies of the unloaded cavity as the temperature increasing.

It can be seen that the starting frequency of the TM_{010} mode is shifting towards lower frequencies as the temperature increases. The resonance frequency shifted from 2.49 GHz at room temperature to 2.47 GHz at the highest temperature. The reason behind this shift in frequency could be attributed to the linear thermal expansion of the copper cavity and the formation of oxide layers over the cavity. Thus the calculated permittivity values will be represented using the effective real permittivity (ε'_{eff}), and the effective imaginary permittivity (ε''_{eff}) due to the conflation of different factors related to the cavity itself. Also, it has been assumed that the cavity is a fixed volume.

For the tested sample of bunker oils, a separate experiment has been conducted in order to

estimate the change in volume as the temperature increases.

Overall, this type of process is found to be influenced by the thermal properties of the cavity and the sample.

6.2.1 Heavy Oil Sample

The dielectric properties of pure heavy bunker oil are examined using a perturbation technique at variable temperature. It should be taken into account that there are several factors contributing to the error of this measurement. Since the dielectric measurements are volumetric measurements, the volume loss is one of the factors that affects the obtained values. An experiment has been conducted in order to detect the change in oil volume according to temperature and its effect on the measurements.

Figure 6.4 represents the volume loss percent at variable temperatures. It can be seen that the change in volume is less than 3% at 300°C; however, it can reach 8% at 400°C. Thus, the change in volume above 300°C should be obvious and needs to be taken into account.

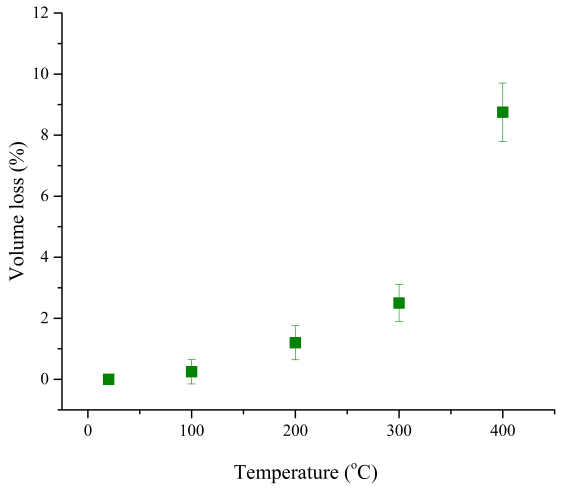


Figure 6.4: Experimental results for detecting the change in oil volume as the temperature increasing.

Additionally, the change in dielectric properties of the heavy bunker oil sample has been examined at variable temperatures. Figure 6.5 (a) illustrates the temperature dependent properties of a heavy bunker oil sample measured at the range from 20°C to 400°C. The real permittivity and imaginary permittivity are represented using the effective value (ε'_{eff}, ε''_{eff}), due to the interference of different factors to the overall dielectric properties in addition to the change in the sample itself.

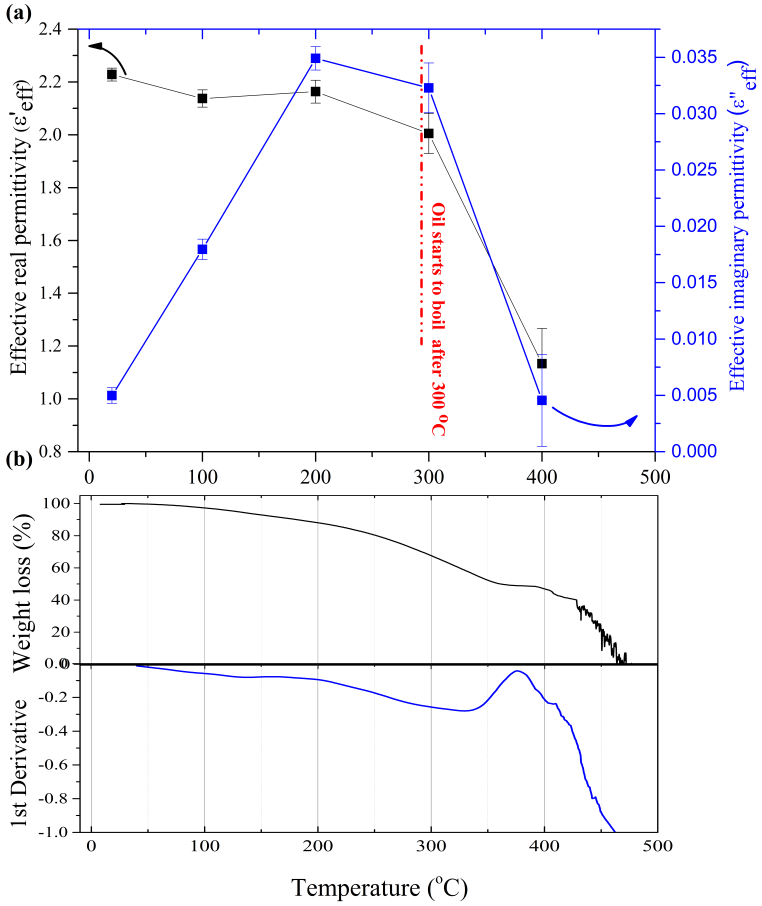


Figure 6.5: (a) The temperature dependent properties of heavy bunker oil using the TM_{010} mode (b) the TGA profile representing the weight loss of the heavy bunker oil with increasing temperature.

Figure 6.5 (a) shows a slight decrease in the real permittivity values of heavy bunker oil as

function of temperature. This small decrease might be correlated with the change in molar volume and the loss of light volatile compounds as the temperature increasing. However, as the temperature reaches the boiling point of the oil, a significant decrease in ε' can be observed, and especially for temperatures above 300°C.

Heavy oil can be considered as a multi-dispersion material of high molecular weight hydrocarbons, and heterocompounds including sulphur, nitrogen, oxygen and metals [6, 7]. The change in temperature dependent real permittivity can be attributed mainly to the change in viscosity with increasing temperature as a result of molecular rotation and random Brownian motion. Moreover, to the slight weight loss of the volatile material evaporation as the temperature increases.

The increase in temperature dependence on imaginary permittivity properties of heavy oil might initially be influenced by the dipolar rotation and movement of the molecules as result of the decrease in viscosity at higher temperatures within the heavy oil components.

Figure 6.5 (b) illustrates the thermogravimetric analysis (TGA) of the heavy oil sample. It can be seen that the weight loss of the heavy bunker oil sample begins at approximately 100°C and is complete at around 470°C as the heavy oil is fully decomposes. The TGA heating profile represents two different stages of weight loss. In the first stage, which is in the range of temperatures between 100 and 340°C, a broad peak can be seen. It indicates a weight loss of circa 50% involving the small water content and some of the lighter hydrocarbons. The second stage is in the temperature range of about 340-400°C with a 20% weight loss from heavier compounds, such as gasoline and kerosene. This is then followed by a sharp decrease and a total weight loss of the heavy oil sample as it decomposes [8].

It can be noticed that the real permittivity of the heavy oil was mainly affected by the change in the composition and weight loss of the samples, whereas the imaginary permittivity factor was mainly affected by the increase in temperature influencing the molecular rotations and the dipolar groups [9].

Dielectric properties can be determined by the charge distribution and thermal motion of the polar groups in the oil as it composed of a number of polar compounds.

As such, it can be seen that this contributes greatly towards an increase in the imaginary permittivity and loss tangent with an increase of temperature, (see Figure 6.6).

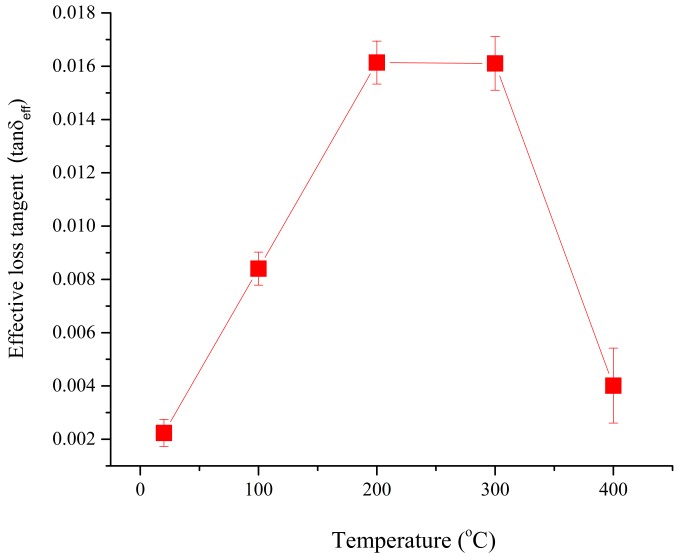


Figure 6.6: The temperature dependence of the effective loss tangent of the heavy oil.

6.2.2 HZSM-5 Zeolite

To produce the acidic zeolite, the fresh ammonium ZSM-5 zeolite was calcined according to the following equation:

$$NH_4\text{-ZSM-5} \xrightarrow{Heat} \text{H-ZSM-5} + NH_3$$

The dielectric measurements and the TGA analysis enables us to explore the changes in behaviour of the pure zeolite as a function of temperature.

In general, zeolites contain mobile cations which are weakly held to the neighbouring atoms compared to the framework ions. Thus, these ions are easily exchangeable and more mobile. In the calcined zeolite, protons are linked to the oxygen atoms leading to the formation of OH bridged groups (Brönsted acidity sites), which have been studied using IR, NMR and other spectrometric methods. [10, 11]. The exchangeable cations of zeolites are balancing the surface negative charge.

Thus, the polarisation mechanism which is related to real permittivity in this case and in any materials with mobile positive ions are due to the movements of cations and the hopping of charge carriers in the zeolite [12, 13].

Furthermore, the structure of the zeolites consists of pores, channels and cages of different shapes and dimensions, which in case of the HZSM-5 has a three-dimensional medium pore structure with an opening size of 5–5.5 Å . These channels allows for water trapping in the zeolite, which contributes by affecting the polarity of the zeolite thus the polarisation mechanisms of the zeolite.

The dielectric properties of the HZSM-5 were examined to follow the changes in sample behaviour with increasing temperature; measurements were correlated with the TGA profile. Figure 6.7 (a) represents the change in temperature dependence permittivity (ε'), (ε''), and (tanδ) with increasing temperature, whereas 6.7 (b) represents the change in TGA profile. Zeolites have a tendency to absorb moisture, therefore they trap water molecules within their cavities and channels. As mentioned above, the existence of water within the structure can contribute to the polarisation mechanism. However, the presence of the charge carrier cations can have a greater effect on the dielectric properties of the zeolite [14].

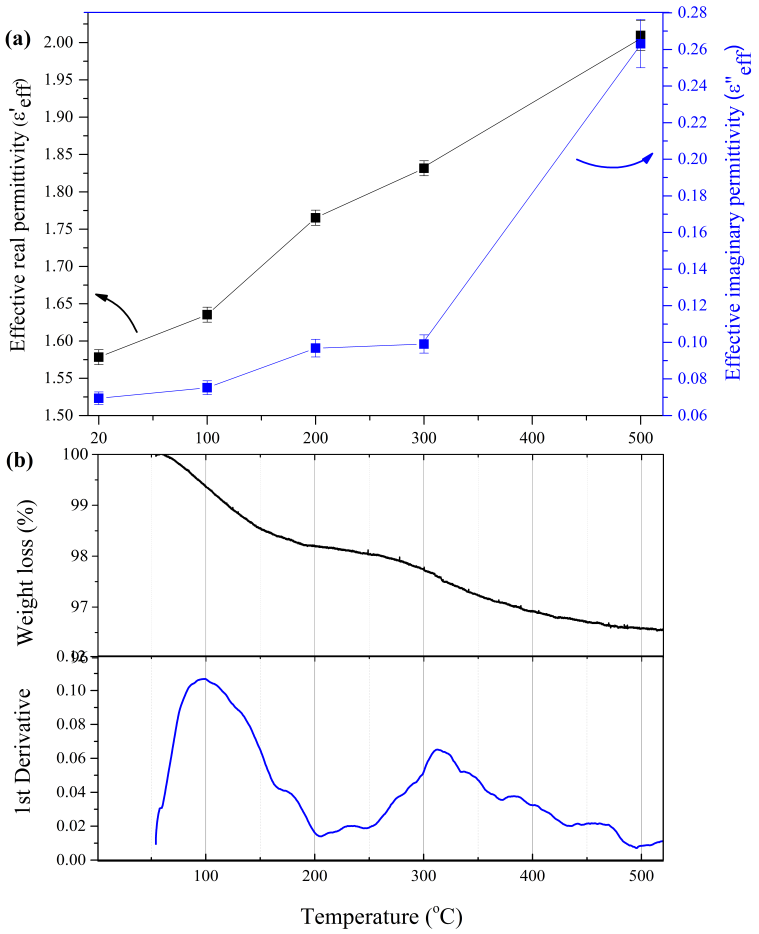


Figure 6.7: (a) the dielectric properties, and (b) the TGA profile of the HZSM-5.

The TGA profile in Figure 6.7 (b) illustrates two stages of weight loss the can be attributed mainly to the water thermo-desorption. The first process occurs at temperatures below 200°C from the release of the physically-adsorbed water from the zeolite. The second stage is represented as a broad peak with a total weight loss of around 1.5% indicating the removal of the coordinate water from the framework. The removal of water at different stages could be assigned to the different adsorption energies that link the water to the framework [15, 16].

Additionally, it can be seen that as the temperature increases the real permittivity increases as well. This suggests that the contribution of the water polarisation to the real permittivity is lower

than that of the charge carrier. In fact, the increase in temperature results in an increase in the motion of the charge carriers and thermal activation leading to higher values of (ε') . Although HZSM-5 zeolite shows a low real permittivity value at room temperature, this increase in permittivity should involve other factors than water polarisation which might be also related to the cavity effect factors.

The imaginary permittivity value was also found to increase with temperature. It can be seen that the imaginary permittivity values are exhibiting a slight increase up to 300°C; however, its increase became noteworthy at 500°C. A key point that the sensitivity of the ε'' is strongly associated the conduction mechanism [17].

Cavity perturbation technique is a sensitive tool to study the conductivity of low conductive materials. thus, the exploration of the change in microwave conductivity which gives an insight into the properties of the zeolite can be detected with increasing temperature. In addition the microwave conductivity measurements are associated with conductivity mechanisms (ionic and/or electronic), which is also strongly related to the imaginary permittivity values. Figure 6.8 shows the microwave conductivity of the HZSM-5 as a function of temperature. It can be seen that the conductivity increases a little between room temperature and 300°C, and the increase is more significant between 300°C and 500°C. There are two possible explanations behind the increase in temperature dependent conductivity above 300°C. The first is related to the sample thermal activation where the charge polarisation is increased at high temperature. This results in the migration of exchangeable cations (i.e. essentially the H^+ proton mobility) hopping between neighbouring Brønsted sites [13, 18–20]. The second explanation might be related to interference of the cavity effect at higher temperatures.

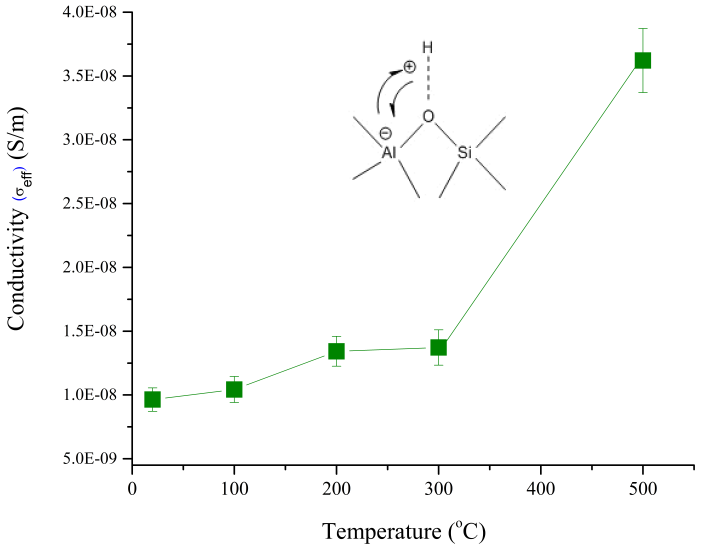


Figure 6.8: The microwave conductivity measurements of the HZSM-5 zeolite as a function of temperature.

The electrical microwave conductivity value is directly proportional to the imaginary permittivity value as shown in Figure 6.8. In addition to the dielectric loss tangent which represents the material susceptibility to be heated in microwave is illustrated in Figure 6.9. This behaviour corresponds to the suitability to interact with microwave which suggests that the interaction is increasing as the temperature increase.

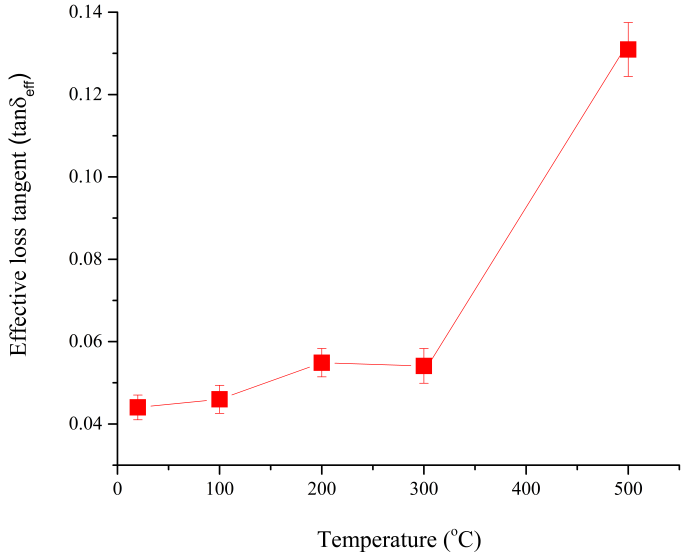


Figure 6.9: The change in the effective loss tangent of the HZSM-5 with increasing temperature.

6.2.3 Heavy Oil Impregnated into HZSM-5 (Fresh Sample)

The heavy oil impregnated HZSM-5 has been prepared by loading ~ 30 wt% of the oil was dissolved in toluene into zeolite. This have been done to insure a better dispersion of the oil into zeolite channels and cavities. The prepared catalyst is considered as a heterogeneous system, and it is composed of different dielectric systems, the zeolite, and the heavy oil. The polarisation mechanism in the case of heterogeneous systems can be attributed to the interfacial polarisation [14].

The general thermal processing of the heavy oil involves initially the removal of the gaseous products, then the light volatile liquids followed by the heaviest fraction products. The thermal cracking of the high molecular weight of hydrocarbons within the heavy oil into lighter fractions can result in a coke formation that started to form at temperatures above 400°C. Figure 6.10 (a) represents the change in dielectric properties of the fresh sample with increasing the temperature in the range of 20-500°C, whereas Figure 6.10 (b) illustrates the corporates TGA profile and indicates the weight loss and the change in catalytic composition.

The TGA profile of the heavy oil clearly illustrates the weight loss of the heavy oil, which can be distinguished over several processes. The first stage is falling in the range below 300°C, which

can be assigned to the water removal and processing of the volatile light materials. This feature corresponds to 10% of weight loss of the sample. The real permittivity of the oil/HZSM-5 zeolite at room temperature was found to be almost similar to the real permittivity of the heavy oil (ε' = 2.2) rather than the zeolite (ε' = 1.5). This indicates that the heavy oil dielectric properties would be the dominant mechanism at the early heating stage. At this stage, the corresponding real permittivity (ε') was found to be slightly decreased as a correspondent to the weight loss of the heavy oil.

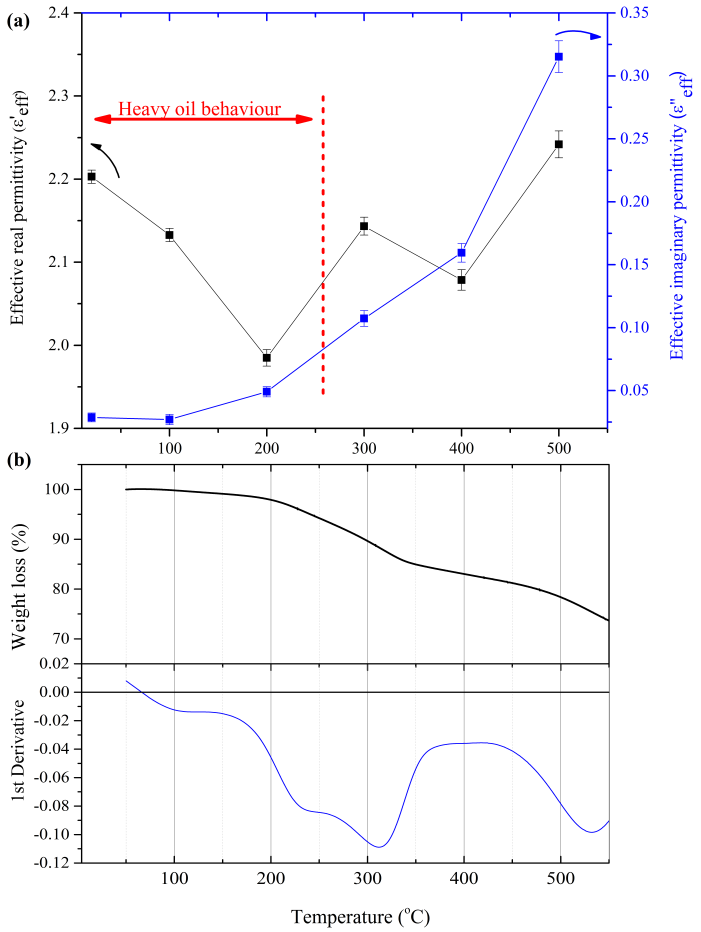


Figure 6.10: (a) the dielectric properties, and (b) the TGA profile of oil /zeolite pre-reacted (fresh) sample.

In the temperature range of 300-400°C, the observed weight loss can be attributed to the

cracking of heavier compounds, which corresponds to around 5% weight loss. In fact, in the temperature range of 20-400°C, the real permittivity value follows the same behaviour as the one of the pure heavy oil dielectric measurement in Figure 6.5 (a). Whereas around 400°C, in the thermal catalytic processing of heavy oil, the formation of coke started to occur and the amount of coke precursors increase with an increase in temperature. This can be the reason behind the re-increase in real permittivity value [9].

The formed coke can be considered a good electrical conductor. However, it is not as high as the carbon materials, such as carbon black and graphite. This can be assigned to the lower crystallinity of the coke compared to other conducting carbon species [21]. In general, the conductivity can be attributed to the delocalised π electrons. This value of conductivity can be increased under heating conditions [22], which can be clearly seen in Figure 6.11. The conductivity was found to be increased slightly with increasing temperature. However, during the coke formation at temperatures above 400°C, a noticeable enhance in conductivity can be observed [23, 24]. The increase in conductivity with temperature also showed a linear relationship with the imaginary permittivity and the loss tangent factor. (see Figure 6.11). This enhancement in susceptibility to interact with microwave can be attributed to the petroleum coke formation by the hydrogen abstraction from the hydrocarbons as shown in the following reaction:

$$C_nH_{2n+2} \longleftrightarrow nC + (n+1)H_2$$

As the dehydrogenation process occurs, the graphitic precursor formed will favour the formation of unsaturated carbons and increase in the ratio of sp or sp^2- over the sp^3- carbon forms [24, 25].

It is commonly understood that carbon materials are a strong microwave absorbent due to the presence of the delocalised π electrons. These π electrons play an important role in the microwave heating of carbons, since they are moving within a fixed region and cannot be fully coupled with the change in the microwave field. This, in turn, results in a dissipation of the absorbed energy in the form of heat [26].

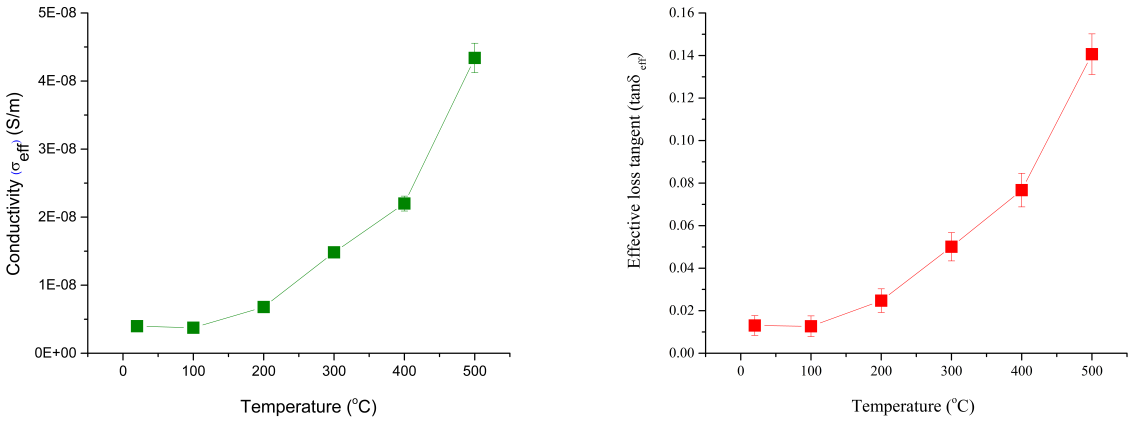


Figure 6.11: Microwave electrical conductivity (left) and loss tangent (right) of the impregnated zeolite with heavy bunker oil (fresh catalyst).

6.2.4 Heavy Oil Impregnated into ZSM-5 (Spent Sample)

The dielectric properties of the oil/zeolite spent sample after microwave processing of heavy bunker oil experiment have also been examined. The reaction was conducted at 550°C and the selectivity to hydrogen was found to be 80 mL of a total volume of 115 mL of the gas product. The reaction selectivity was mainly towards the gas formation. However, some of the unconverted liquids may remain in the catalyst. Reaction details will be presented in **Chapter 8**.

The reaction has been performed under microwave radiation at high temperatures. The Gas Chromatography analysis represents the high formation of hydrogen in the product, which can indicate a larger development of the coke precursor within the catalysis reaction.

The change in dielectric properties and the composition of the spent sample with increasing temperature is illustrated in Figure 6.12

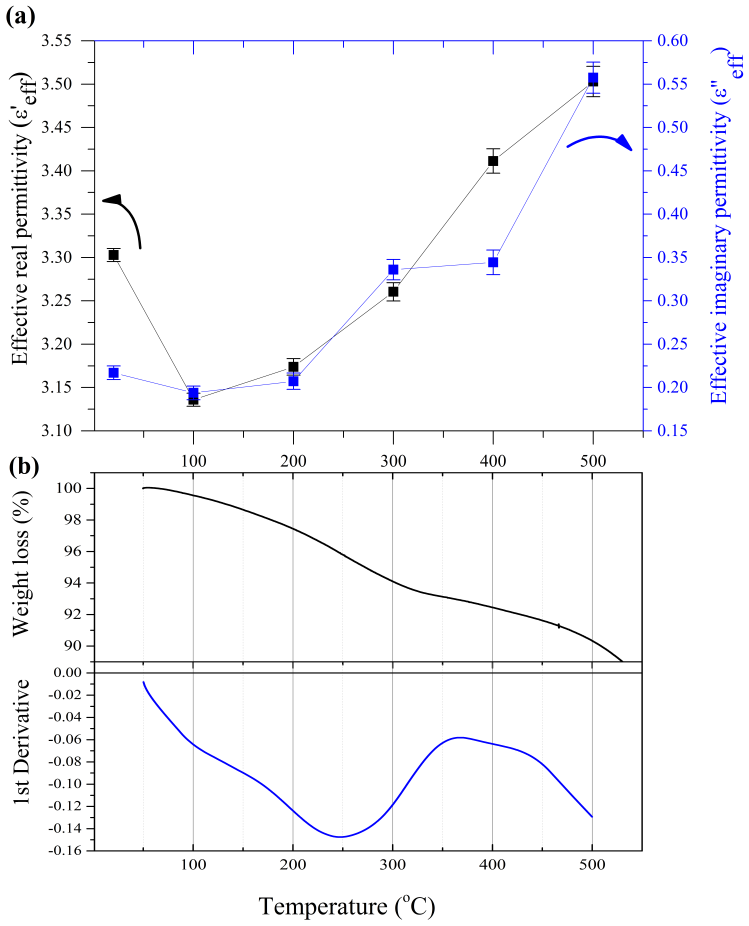


Figure 6.12: The dielectric properties (a) and the TG analysis profile (b), of the the oil/HZSM-5 spent catalysis.

The real permittivity of the spent sample, which starts with a real permittivity of $\varepsilon' = 3.3$, indicates the existence of an increase in the sp^2 carbon precursors within the catalyst. The TGA profile in Figure 6.12 (b) represents two stages of weight loss.

The first stage occurs at temperatures ranging from 50-300°C, where the lighter hydrocarbons can be lost. The corresponding weight loss is found to be ~ 6 wt%. Nonetheless, the equivalent real permittivity profile was found to show a decrease up to a temperature of 100°C indicating the loss of lighter hydrocarbons. Then a continuous increase up to 500°C can be assigned to the appearance of the carbon materials properties as a dominant contributor to the real permittivity value compared to the constant weight loss of the remaining unconverted materials. The second

stage of the TGA profile indicates a 4% weight loss at temperatures above 330°C that can be attributed to the removal of the heavier fractions of residual oil. The enhancement of the sample to be heated with microwave was found to increase with increasing temperature, which can also be observed in both Figure 6.13 and 6.14 where they represent an increase in conductivity and effective loss tangent with temperature respectively.

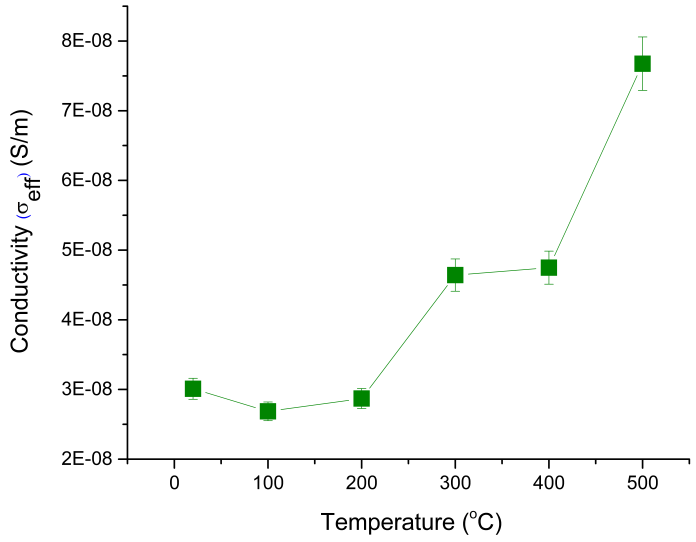


Figure 6.13: Electric conductivity of the impregnated zeolite with heavy bunker oil (spent) sample.

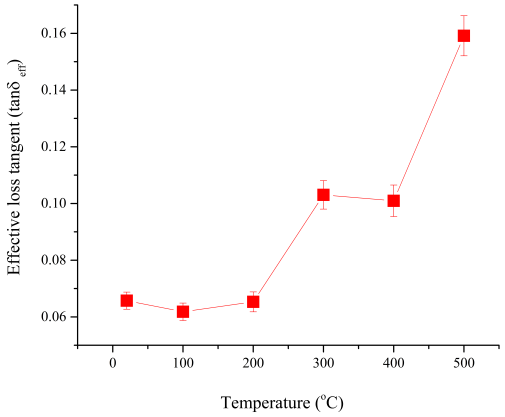


Figure 6.14: The change in loss factor value of the oil/HZSM-5 (spent) catalyst with increasing temperature.

6.3 Conclusions and Future Outlook

Dielectric measurement is known to be a useful tool to give an insight into materials properties. The research is aimed to establish whether the measurements of dielectric properties have provided important insight into this catalytic process. In this work, we were trying to present an experimentally-validated approach for detecting the change in dielectric behaviour of the catalyst as a function of temperature. A cavity perturbation system has been set-up to be able to evaluate the temperature dependence dielectric properties up to 500°C.

As this system has recently been established in the laboratory, the obtained measurements were presented as an effective value. The high temperature measurements is a challenging system due to the interference of different factors into permittivity values. The factors are related to the thermal expansion of the cavity, the formation of the copper oxide layers in and outside the cavity in addition to other uncounted factors related to the sample holder and the sample itself which needs to be taken into account when interpreting the permittivity values.

In order to understand the characteristics of the change in dielectric properties for heavy bunker oil and zeolite samples, the TG analysis has been correlated with each sample. As the parameters of the sample are continuously changing during the heating process, the results only represent

the influence of temperature on the weight loss and the change in chemical composition of the sample with the equivalent dielectric values and loss tangent factor behaviour. The zeolite sample permittivity values were found to be influenced by the polarisation mechanism of the zeolite sample for ε', and related to the conductivity mechanism (electron hopping) for ε'' in the framework of the zeolite.

In terms of the oil/zeolite catalysts (fresh and spent), the temperature-dependent dielectric measurements provide a different temperature profile, which may significantly alter the catalytic process and the rates of reaction. It can also be used to detect the catalytic activity and the potential behaviour under microwave conditions. As commonly accepted, carbon materials are strong microwave absorbers due to the presence of the delocalised π electrons. The change in dielectric behaviour of the samples indicates the formation of the sp^2- carbon species at high temperatures. As the microwave absorption is proportional to the increase in the sp^2- content over the sp^3-, a quantification detection of the sp^2- materials content could be achieved. As such, there might be potential to detect the catalyst activity, and estimate the coke content formation and development in catalysts as temperature changes.

In summary, I have presented herein the initial results from the high temperature measurements using the TM_{010} mode. Overall, there are some limiting factors contributing to the error of the measurements, since the reference background has been taken at each temperature. Thus for future experiments, higher order modes such as TM_{020} and TM_{110} will be used to perform more accurate high temperature measurements. Based on the fact that in the cavity, as the number of modes increases, the field maxima tend to move towards the edges of the cavity and the modes become less sensitive to the sample at higher order modes. Thus, a higher mode can be used to correct the systematic fluctuations as they are unaffected by the sample. Here, we have tried to conduct several experiments using this programme. However, it has been found that it needs more modification to be valid at temperatures higher than 300°C. One of the significant advantages of this method is that the measurements can be done *in situ* without the need to disturb the sample.

This can be developed to conduct the measurements at different ambient gases and elevated temperatures. In addition, it would be interesting to further evaluate the catalytic activity and deactivation over a wide range of heterogeneous catalysts.

Bibliography

[1] J. Krupka, K. Derzakowski, B. Riddle, and J. Baker-Jarvis. A Dielectric Resonator for Measurements of Complex Permittivity of Low Loss Dielectric Materials as a Function of Temperature. *Measurement Science and Technology*, 9(10):1751, 1998.

[2] B. Riddle, J. Baker-Jarvis, and J. Krupka. Complex Permittivity Measurements of Common Plastics over Variable Temperatures. *IEEE Transactions On Microwave Theory And Techniques*, 51:727–733, 2003.

[3] S.S. Eaton, G.R. Eaton and L. Berliner. *Biomedical EPR - Part B: Methodology, Instrumentation, and Dynamics.* Biological Magnetic Resonance. Springer US, 2006.

[4] R.M. German. *Particulate Composites: Fundamentals and Applications.* Springer, 2016.

[5] C.Y. Ho and R. E. Taylor. *Thermal Expansion of Solids.* ASM International, 1998.

[6] A. Hart. *Advanced Studies of Catalytic Upgrading of Heavy Oils.* PhD thesis, Chemical Engineering, University of Birmingham, 2014.

[7] F.J. Hein, D. Leckie, S. Larter and J.R. Suter. *Heavy-oil and Oil-sand Petroleum Systems in Alberta and Beyond.* AAPG Studies in Geology. American Association of Petroleum Geologists, 2013.

[8] A.T. Quitain, C.Y. Herng, S. Yusup, M. Sasaki and Y. Uemura. Conversion of Biomass to Bio-Oil in Sub- and Supercritical Water. *Biofuels - Status and Perspective*, 10:5772–59947, 2015.

[9] F. Huang, Fang B. Haoxi, P. Shaobo, P. Yunqiao and R. Arthur. The use of Combination of Zeolites to Pursue Integrated Refined Pyrolysis Oil from Kraft Lignin. *Sustainable Chemical Processes*, 2(1):1–11, 2014.

[10] M. Moliner. Direct Synthesis of Functional Zeolitic Materials. *ISRN Materials Science*, 2012:1–

24, 2012.

[11] M.A. Hussein, B.M.Abu-Zied and A.M. Asiri. Preparation, Characterization, and Electrical Properties of ZSM-5/PEG Composite Particles. *Polymer Composites*, 35:1160–1168, 2014.

[12] S.M. Auerbach, K.A. Carrado and P.K. Dutta. *Handbook of Zeolite Science and Technology*. Taylor & Francis, 2003.

[13] K. Praveena and S.R. Murthy. Dielectric Properties of Dehydrated Zeolites. *International Journal of Emerging Technology and Advanced Engineering*, 3(1):363–368, 2013.

[14] M.A. Rolando Roque-Malherbe. *The Physical Chemistry of Materials: Energy and Environmental Applications*. CRC Press, 2009.

[15] R. Roque-Malherbe, A.N. Costa-Hernandez, C. Rivera-Maldonado, F.N. Lugo-Alvarado and R. Polanco-Estrella. Study of the Adsorption Space of Modified Clinoptilolites. *Journal of Materials Science and Engineering*, 5:263–280, 2013.

[16] R.V. Ballmoos and G.T. Kerr. Silylations of H-ZSM-5. A TGA Study. In *Zeolites Synthesis, Structure, Technology and Application*, volume 24 of *Studies in Surface Science and Catalysis*, pages 307–318. Elsevier, 1985.

[17] M. Dietrich, D. Rauch, U. Simon, A. Porch, and R. Moos. Ammonia Storage Studies on H-ZSM-5 Zeolites by Microwave Cavity Perturbation: Correlation of Dielectric Properties with Ammonia Storage. *J. Sens. Sens. Syst.*, 4:263–269, 2015.

[18] L. Chenhui, Z. Libo, P Jinhui, S. Chandrasekar, L. Bingguo, X. Hongying, Z. Junwen and X. Lei. Temperature and Moisture Dependence of the Dielectric Properties of Silica Sand. *Journal of Microwave Power and Electromagnetic Energy*, 3(47):199–209, 2013.

[19] L. Rodriguez-Gonzalez , E. Rodriguez-Castellon, A. Jimenez-Lopez, and U. Simon. Correlation of TPD and Impedance Measurements on the Desorption of NH_3 from Zeolite H-ZSM-5. *Solid State Ionics*, 179:1968–1973, 2008.

[20] P.A. Anderson, A.R. Armstrong, P.D. Barker, M.J. Edmondson, P.P. Edwards, and A. Porch. rubidium Doped Zeolite rho: Structure and Microwave Conductivity of a Metallic Zeolite. *Dalton Trans.*, 7:3122–3128, 2004.

[21] D.D.L. Chung. Review: Electrical applications of carbon materials. *Journal of Materials Science*, 39:2645–2661, 2004.

[22] D.D.L. Chung. Review: Electrical Applications of Carbon Materials. *Journal Of Materials*

Science, 39:2645–2661, 2004.

[23] D. Salari, A. Niaei, J. Towfighi, P. Panahi and R. Nabavi. Investigation of Coke Deposition and Coke Inhibition by Organosulfur Compounds in the Pyrolysis of Naphtha in the Jet Stirred Reactor System. *Iranian Jurnal of Chemical Engineering*, 3(1), 2006.

[24] B. Jambor and E. Hajekova. Formation of Coke Deposits and Coke Inhibition Methods During Steam Cracking. *Petroleum and Coal*, 57(2):143–153, 2012.

[25] P. Broutin, F. Ropital, M.F. Reyniers and G.F. Froment. Anticoking Coatings for High Temperature Petrochemical Reactors. *Oil & Gas Science and Technology*, 54(3):375–385, 1999.

[26] J.A. Menendez, A. Arenillas, B. Fidalgo, Y. Fernandez, L. Zubizarreta, E.G. Calvo and J.M. Bermudez. Microwave Heating Processes Involving Carbon Materials. *Fuel Processing Technology*, 91(1):1–8, 2010.

Chapter 7

STUDY FOR CONTROLLING SINGLE-MODE APPLICATOR IN MICROWAVE HEATING REACTIONS

Overview

The effect of microwave parameters in a single-mode cavity system has been looked at in terms of case studies. In these studies, several materials such as carbon black, iron oxides, and HZSM-5 impregnated with decane were heated in a reactor. This allowed for a two-fold investigation. Firstly, various operating conditions in the microwave were modified (i.e. power level, ramping rate, and pulsing irradiation) to study the effect of the generated electromagnetic field within the catalyst bed. Secondly, studying the effect of physical properties (i.e. permittivity, particle size, and shape) on field absorption enhancements for optimising reaction conditions. The experiments were carried out in a single-mode applicator at a frequency of 2.45 GHz.

7.1 Introduction

In the past few decades, several industrial and scientific applications utilising microwave energy, ranging from food processing to medical treatment [1] have been investigated. Industrial uses of microwave vary from curing of polymer and composite materials to heating treatment of metal and semiconductor surfaces, in addition to plasma processing and pharmaceutical chemistry. Additional uses of microwave comprise the heating and processing of foods in commercial microwave ovens [2, 3]. Thus, microwave can be considered a well-developed technology, and single or multi-mode resonant cavities are used in most heating and processing applications. However, applicators have been developed continuously to examine more potential benefits of microwave heating applications [4].

A microwave applicator can be defined as the place where a given material is exposed to a microwave field in a controlled and safe environment. The interaction between the material and the microwave in this applicator can provide reliable and repeatable reactions [4–6]. Microwave applicators can be operated in either batch or flow system. In addition, the system can be modified to be operated under normal atmosphere. Moreover, it can be combined with a flow of hot air or steam depending on the required conditions and the desired products. The ambient conditions of the interaction -humidity, pressure, and vacuum- can vary depending on the design of the applicator. Overall, microwave reactor comprises the applicator, control systems, and a microwave system generator. However, what makes microwave design complex is the interaction between microwave energy and any given material, which changes as the properties of the material change [4]. Microwave systems must now meet new efficiency standards. In particular, microwave systems, applicators, and power oscillators have to meet new standards in energy efficiency, processing uniformity, and control of process cycles. The use of a single-mode cavity is one way to meet these standards.

In a multi-mode system, the material to be microwaved is randomly placed in the cavity and interacts with multiple resonant modes. In single-mode, however, the material is placed at a specific location where the highest intensity nodes for the desired frequency are found [7]. The single-mode cavity can be designed with required heating characteristics because its field distribution can be analytically determined. Nonetheless, it is still difficult to determine certain parameters

analytically. For example, the field pattern can deviate from the dominant mode if higher order modes are excited by how the material is loaded. However, there are ways to suppress these undesirable modes. The size of the aperture through which the waveguide system and the cavity are connected, can determine the impedance matching between the source and the cavity, and the amount of transferable power. Thus, the system's sensitivity to different parameters, (e.g. frequency, load position, or dielectric properties) can be determined [8].

Based on the application, the parameters in a designed single-mode applicator that need to be investigated can be classified into three different groups: 1) geometrical parameters, which are related to the physical dimensions of the applicator and reactor system; 2) materials parameters that are related to the dielectric properties of the tested sample and supporting structures; and 3) electrical parameters, which are related to the quality factor, resonant frequency, and coupling.

The aim of this work is to explore the heating behaviour of different materials (zeolite, carbon black, and Fe_2O_3) in a single-mode microwave applicator in well-defined E-field parameters. This will be conducted whilst modifying parameters, such as power level, ramping rate and samples grain size. Moreover, evaluating the effects of microwave heating rates on product distribution of zeolite material in relation to their possible heating mechanisms that might account in part for certain observations, such as product enhancement, would form the baseline for optimising reaction conditions for the modified heavy oil system.

7.2 Materials and Method

Three sets of particle sizes were examined from commercially-available (Sigma Aldrich) iron oxide (III) powders. The three particle size ranges are 50-100 nm, 125-250 μm, and 500-710 μm. The 500 μm particle size was further obtained by pressing and sieving.

A fresh HZSM-5 zeolite with a Si/Al=60 powder which was calcined at 550°C for 6h has been loaded with different percentages of carbon black. The carbon black which is a graphitised nano-powder with particle size below 500 nm (DLS) and purity above 99.95% based on trace metals analysis was purchased from Sigma Aldrich. Decane (Sigma Aldrich $\geq$ 99%) was chosen as a simple representative of the hydrocarbon cracking reaction to allow for further investigation and optimisation of the effect of microwave parameters on the product distribution. HZSM-5 was

calcined and impregnated with decane and left to dry at 60°C for 72 hours.

The microwave heating reactions were carried out in a 2 kW single-mode cylindrical cavity. The system specifications are described in detail in **Section 4.2.** During the heating experiments, samples were placed in quartz tubes with a 0.9 mm outer diameter and a 0.7 mm inner diameter on top of quartz wool. Tubes with the sample located in the middle were placed in the *E*-field of the maximum resonant cavity. The top of the reactor tube was attached to a Swagelok valve to allow for the flushing of the desired gas and to generate the required atmosphere (i.e. under argon). The top of the reactor tube was attached to a Swagelok valve to allow for the flushing of the desired gas and to generate the required atmosphere. The liquid trap had a side tube where the produced gas was flowing through to be further collected in an eudiometer cylindrical system. The formed products were then withdrawn after each reactor using a syringe and identified using gas chromatography. Finally, conventional infrared sensors have been used to monitor the temperatures of microwave-assisted reactions. However, the limitation of the IR pyrometer should be taken into account.

7.3 Result and Discussion

By studying the interaction between the microwaves and the catalysts, it was found that there are two main factors that control and monitor the degree of interaction: the effect of microwave parameters and the effect of samples properties.

The heating rate, the change in temperature with varying power, and the heat distribution inside the catalyst which affects the products formation all result from varying microwave system parameters. Samples properties include the catalytic dielectric characteristics, the metal loading, and the particle size of the catalyst when exposed to a well-defined, single-mode type of microwave field. However, it has been found that the value of the average dissipated power within a sample is related to both the applied electric field and its dielectric properties.

The equation 7.1 below, represents the amount of microwave power (P_{abs}) that can be dissipated within a dielectric materials of a volume V [9, 10]:

$$P_{abs} = 2\pi f \varepsilon_0 \varepsilon''_{eff} E^2_{rms} V \tag{7.1}$$

where $2\pi f$ is the angular frequency of the radiation,

ε_0 is the permittivity of free space

ε''_{eff} is the imaginary part of the effective permittivity

and E_{rms} is the root mean square of the electric field [11].

Thus, when modifying microwave parameters, the dielectric properties should remain constant to explore the effect of the applied electromagnetic field. On the other hand, different materials have different abilities to convert the electromagnetic field into heat, therefore the applied power needs to remain constant in order to verify the effect of dielectric properties.

7.3.1 Effect of Microwave Parameters

7.3.1.1 Microwave versus Conventional Heating

A hypothesis that explains electromagnetic effects in catalytic reactions is that the reaction rates in microwave irradiation can differ significantly from what is obtained through conventional convective heating [12, 13]. The concept of thermal and electromagnetic effect might contribute in explaining microwave rate enhancement in heterogeneous catalytic systems. Certain interactions occur between microwave energy and the material thus thermal processes occur when the heat is generated within the material [14, 15].

The first step towards verifying this electromagnetic field effect is to experimentally compare the conventional and microwave processing. The experiment was repeated for both cases; the first case was conducted under microwave irradiation, and the second one in a conventional cylindrical furnace with no applied microwave power. (Note that the variation in the heat distribution for both heating systems should be taken into account). Thus, to obtain fairly comparison conditions, rapid heating of thermal processing needs to be achieved. This can be done by placing the reactor tube in the furnace at the maximum required temperature of the reaction.

In the first experiment, the sample was irradiated in a 2.45 GHz microwave applicator. The quartz tube was filled with approximately 0.5 g of the tested sample. The system was flushed under Argon before the start of each experiment for approximately 10 minutes in order to create an inert atmosphere [16].

The sample was set to reach a temperature of 450°C. The power level was maintained for 30 minutes when the estimated temperature of 450°C was reached.

In conventional heating experiments (the second experiment), the target temperature cannot be achieved as quickly as the microwave set. Thus, the following procedures were applied. Using the same reactor tube configuration, the same amount of sample was placed in quartz tube which was then flushed under Argon. The cylindrical furnace was pre-heated up to 500°C. Then, the catalyst bed was directly placed in the centre heating zone of the furnace. The experiment was conducted for 30 minutes. The product distribution of gas composition was analysed for both reactions and this is illustrated in Figure 7.1.

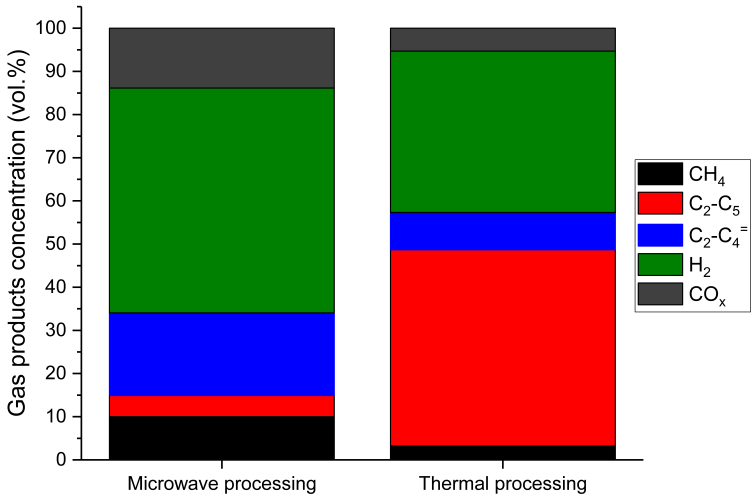


Figure 7.1: Comparison of the effect of thermal and microwave processing of decane over HZSM-5 zeolite on the individual vol.% of the gaseous products.

The gaseous composition of both GC detectors, the flame ionisation detector (FID) for hydrocarbon analysis and the thermal conductivity detector (TCD) for inorganic gases are presented below. Figure 7.2 shows the products from thermal cracking of the decane over zeolite, in compar-

ison to Figure 7.3, which shows the microwave cracking reaction before normalisation to exclude the dilution factors (Ar and N).

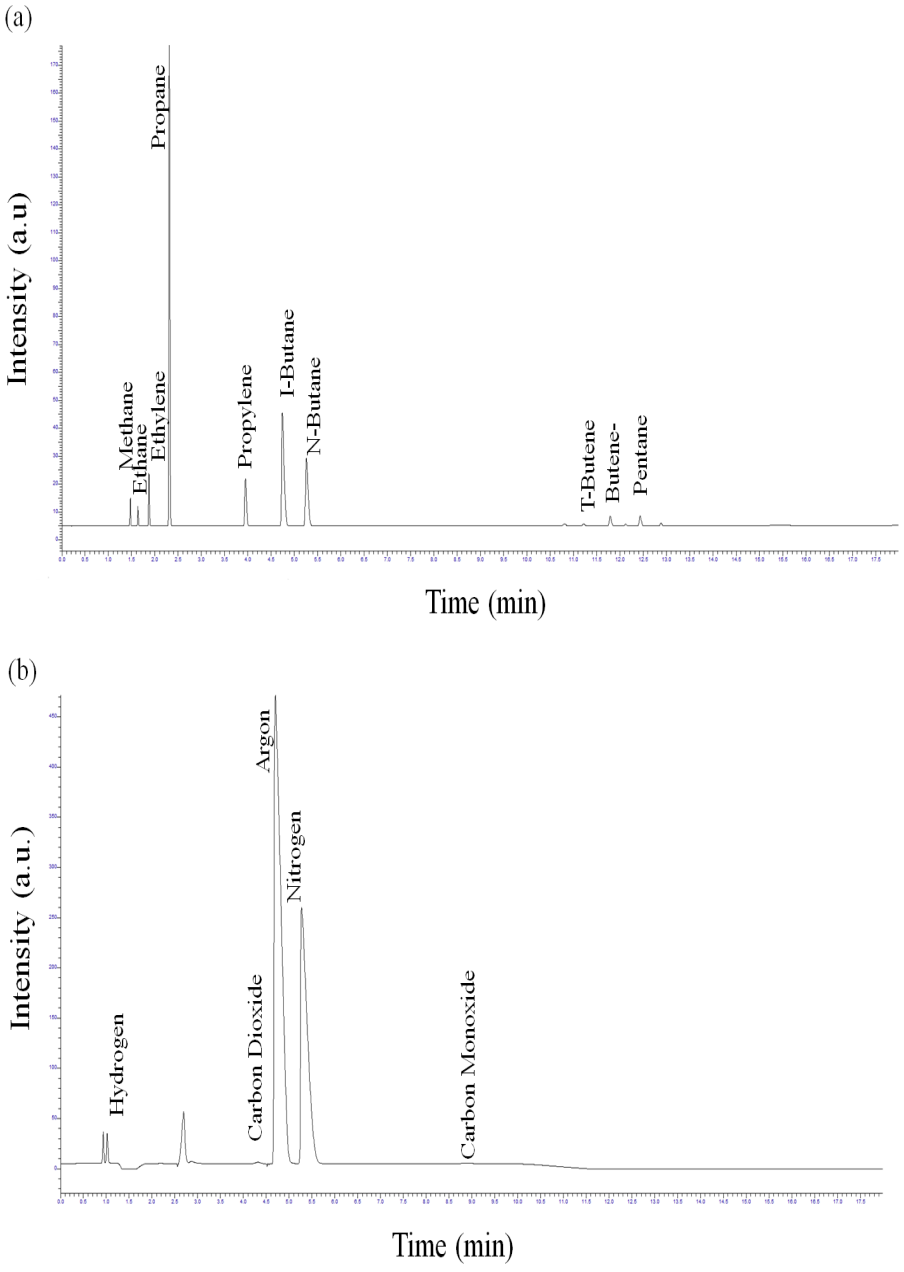


Figure 7.2: Chromatograph showing the gas products of the (a) FID channel specifically operated for hydrocarbon analysis and (b) TCD channel for general analysis of decane cracking over zeolite.

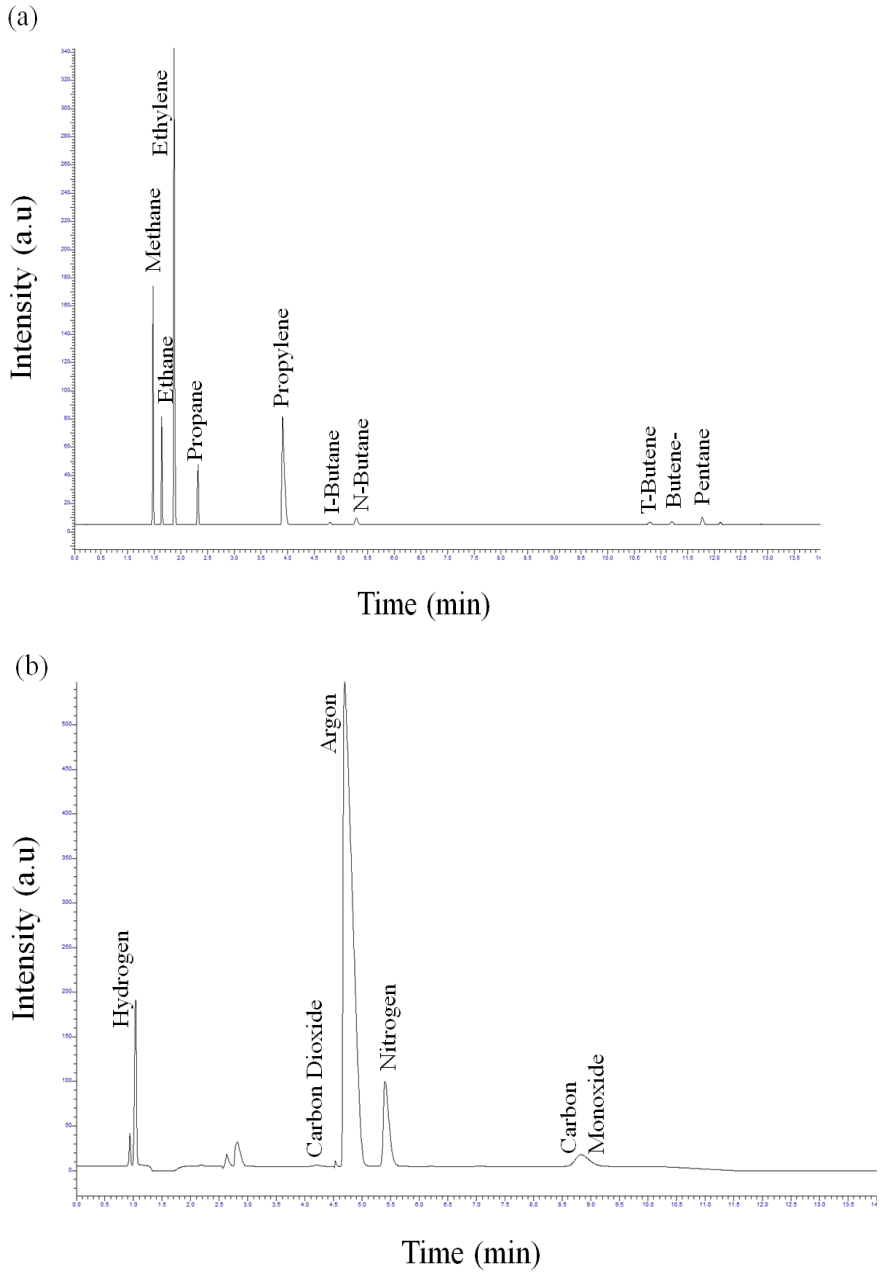


Figure 7.3: Chromatograph showing the gas products of the (a) FID channel specifically operated for hydrocarbon analysis and (b) TCD channel for general analysis from the microwave cracking of decane over zeolite.

A clear difference can be seen when comparing the gas compositions from both reactions. When a reaction is being conducted under microwave irradiation in a heterogeneous catalytic system, it typically experiences a reaction rate enhancement towards hydrogen and olefins production when compared to a conventional heating method under the same conditions [17].

It can be seen that microwave heating has a significant effect on the produced gases. The faster heating rate of microwave heating was confirmed by the presence of a high-value product. From the graph, the vol.% of CH_4, $C_2 - C_4^=$, and H_2, were found to be higher in the microwave system than in the conventional one. This represents a better production for a potentially high-value chemical feedstock. The higher percentage of the hydrogen obtained from the microwave irradiation is likely to be formed via a radical mechanism. This means that the selectivity of the target products will be significantly directed towards more cracking of the olefins, producing hydrogen and coke formation as shown in the reaction below [18]:

$$C_nH_{2n+2} \longleftrightarrow nC + (n+1)H_2$$

Figure 7.4 indicates the concentration level of the light olefins (C_2–$C_4^=$) in the microwave and thermal processing. In the microwave system, it can be seen that the olefin (C_2–$C_4^=$) production is almost doubled with 19 vol.%, than the thermal processing which is 8 vol.%.

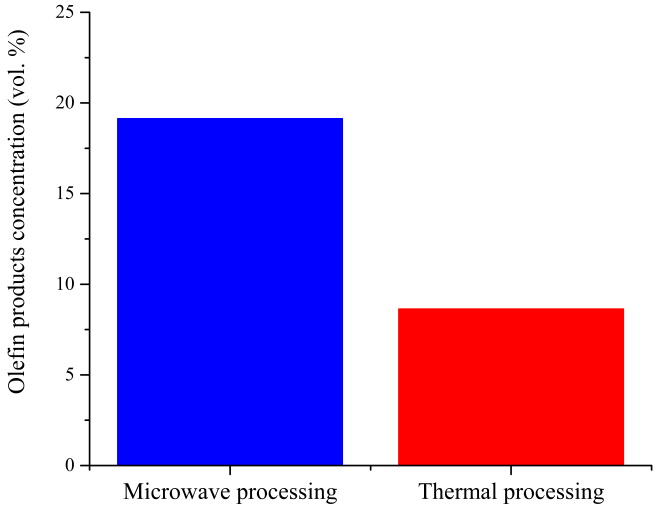


Figure 7.4: Effect of thermal and microwave processing of decane/ZSM-5 cracking on the vol.% of the olefins fractions C_2–$C_4^=$, illustrating a clear increase in the olefin production under microwave compared to the thermal method.

The outcome of the experiments is that microwave heating can significantly increase the production of H_2 and olefins compared to conventional thermal treatment. With conventional methods of heating, certain chemical reactions take hours to complete, but they can be completed in minutes with microwave irradiation. Moreover, in some cases, microwave heating can lead to chemical reactions that could not occur with conventional heating [19].

7.3.1.2 Power Input Level

This experiment was carried out to illustrate the effect of power level on the amount of energy absorbed by a fixed amount or volume of sample. This will help to evaluate and balance the microwave level needed to achieve the desired temperature for such a reaction. This can be done by directly comparing the changes in sample temperature as a function of increased input power. (Note that freshly-calcined HZSM-5 catalyst has been used in this study).

Figure 7.5 illustrates different heating profiles of zeolite samples under different applied power. It can be seen that the temperature is proportionally increasing with the power input. The rate of

temperature increase is changing remarkably with the power level, which plays important roles in product distribution of a reaction system. It can be seen that the initial dielectric heating rate is nearly four times faster at a power of 500W than at 100W, where the rate is significantly increasing with irradiation [11].

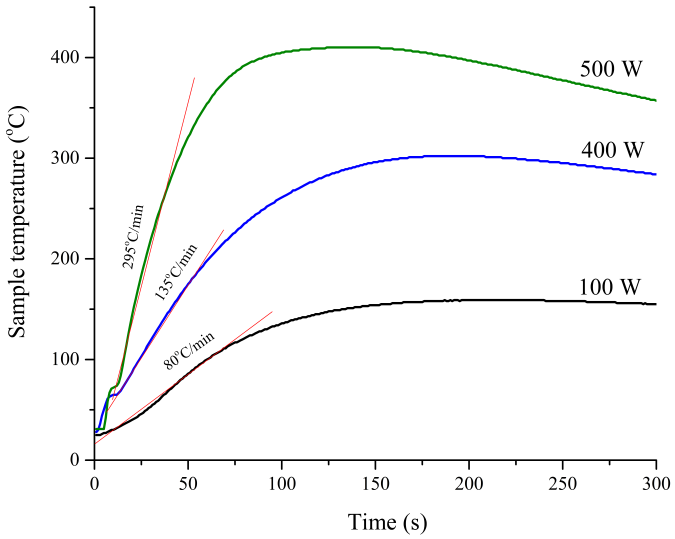


Figure 7.5: Effect of power level on the microwave heating behaviour of HZSM-5 representing the change in heating rate as the input power increases.

7.3.1.3 Heating Rate

One of the most important characteristics of microwave is the significant reduction in reaction time as a consequence of the ability to reach the target temperature in a short time. The irradiation energy is dissipated within the sample and the reaction temperature can be augmented by increasing the amount of microwave input. This results in an enhancement of the reaction at a higher heating rate.

This experiment evaluates the effect of the heating rate using microwave irradiation on the

product distribution of decane cracking over HZSM-5. Using the PID temperature control system, the experiments were conducted at different heating rates but reaching the same target temperature. The technical details of the PID controller in the microwave reactor are explained in **section 4.2.**

A quartz tube was filled with the same amount of decane/HZSM-5 sample in each run and placed inside the cavity, while an inert atmosphere was created in the reactor bed by flushing with argon for ten minutes. For the three experiments, the respective ramping rates were 50, 200, and 500°C/min, respectively. The target reaction temperature was 450°C. After completing the experiments, GC analysis was conducted on the gas products.

Figure 7.6 presents a typical gas distribution for all three experiments. It can be seen that the increase in H_2 volume% is associated with a decrease in CH_4. The dehydrogenation reaction is influenced by the heating rate leading to an increase in the H_2 content with an increase in the ramping rate. As such, raising the ramping rate in the upgrading process is the preferred pathway to increasing the percentage of hydrogen produced.

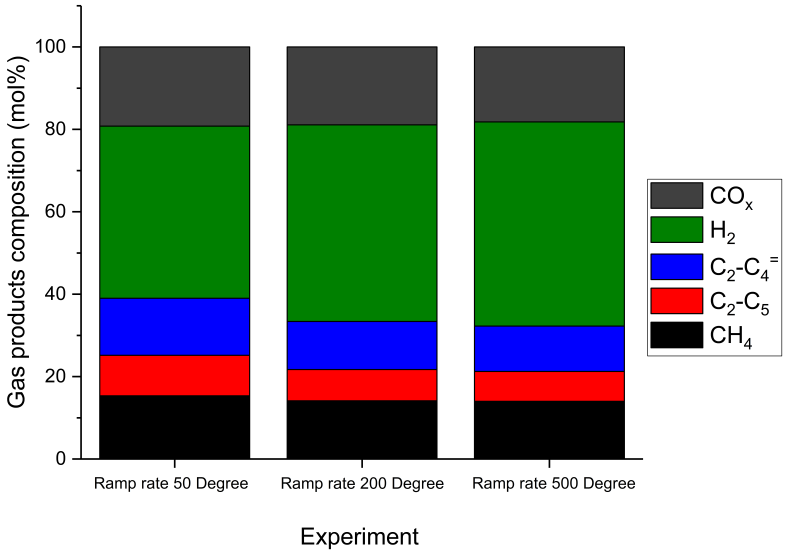


Figure 7.6: Comparison of the products distribution at different heating rates of the decane/HZSM-5 cracking reaction (50, 200, 500°C/min).

7.3.1.4 Microwave Power Delivery Using Pulsing and Continuous Irradiation

Output power control is one of the most important features in the microwave applicator. This section investigates the differences between two types of microwave power delivery to the sample on the product distribution in a decane cracking reaction. The pulse modulated and continuous microwave heating mode were applied to a decane/HZSM-5 sample in a fairly comparable similar conditions.

The temperature profile and the absorbed power pattern by the sample during the irradiation process are illustrated for the continuous and pulsing modes in both Figures 7.7 and 7.8, respectively.

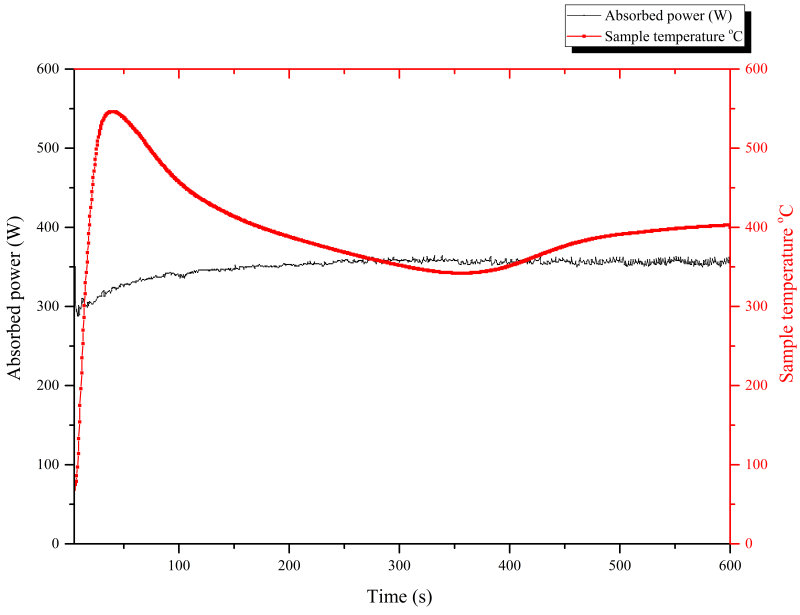


Figure 7.7: The absorbed power and heating profile in a continuous irradiation mode for decane cracking over HZSM-5 reaction.

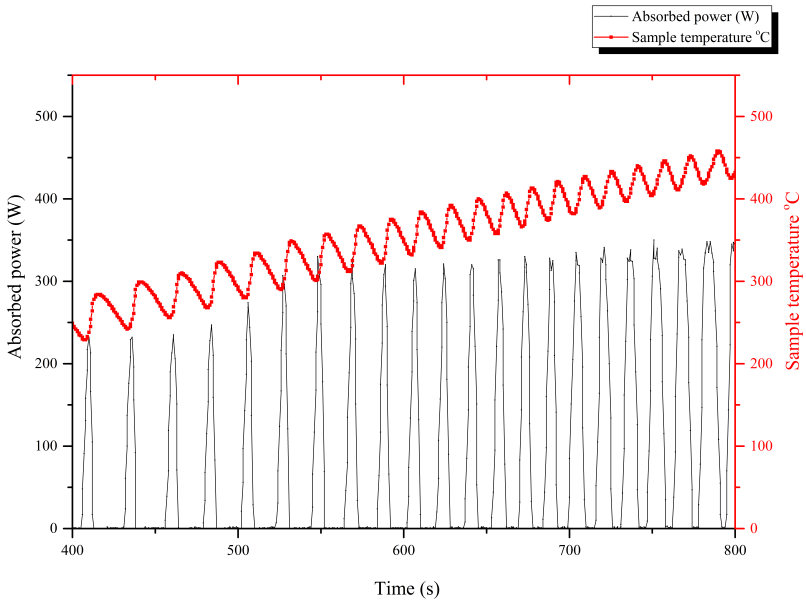


Figure 7.8: The absorbed power and heating profile in a microwave pulse modulated irradiation and a duty cycle of 20% of decane over HZSM-5 cracking reaction.

The previously examined high temperature measurements **(Section 6)** indicated that the dielectric properties of the samples are changing upon the catalytic decomposition. During the reaction, the samples heat up due to the molecular rotation, and the dielectric permittivity changes as the temperature rises. Subjected to microwave pulsing, the samples partially cool down when the power is turned off. When the power is turned on again, the absorption will then differ. This continuous change in electric field direction leads to molecular rotation in the interaction between microwaves and the dielectric sample. The effect of reaction rates enhancement on the products distribution are compared between the two heating approaches and the gas distribution for both experiments are shown in Figure 7.9.

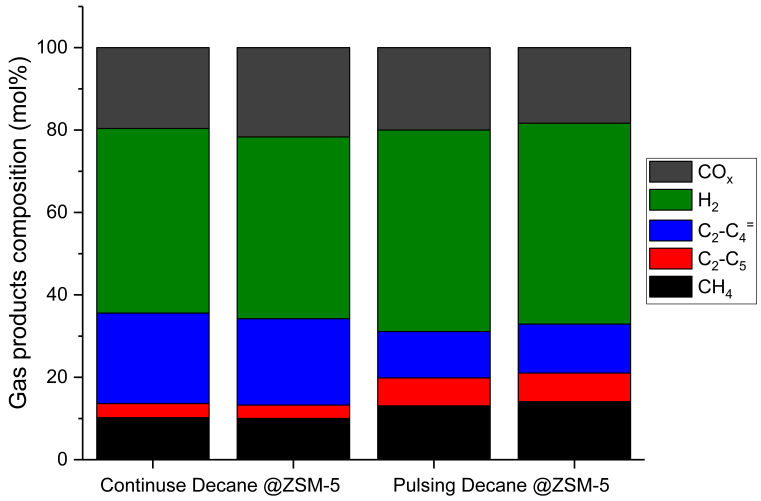


Figure 7.9: Product distribution of decane/HZSM-5 cracking under pulsing vs. continuous microwave irradiation.

When the microwave irradiation is being pulsed to the sample, the resultant electric field that would deliver to the sample corresponds to the duty cycle factor. When the irradiation is switched on, the same amount of power is applied in a short time, which results in a higher electric field being delivered to the sample. It can then be concluded that there is no significant difference in the product distribution for both operation modes. However, the produced hydrogen is slightly higher in the case of the pulsed-irradiation reaction. The amount of produced hydrogen is still remarkably high for both reactions; however, the slight difference between the two modes might indicate a contribution of the electromagnetic field effect. In addition, Figure 7.10 illustrates that the continuous irradiation tends to facilitate the olefin production over the pulsing reaction.

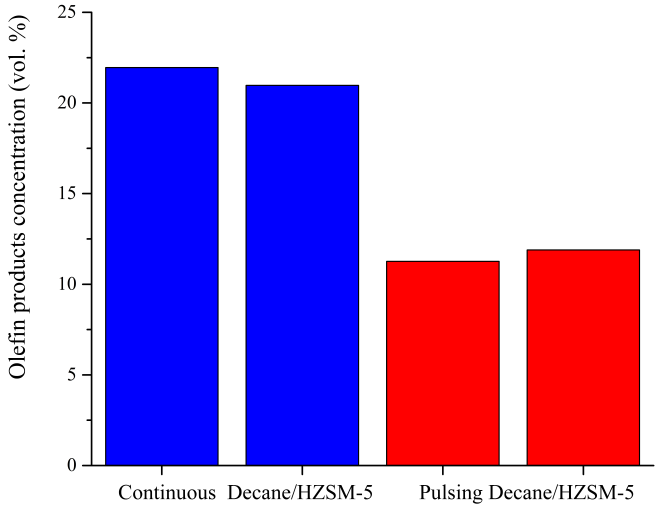


Figure 7.10: Comparison of the olefin distribution of decane/HZSM-5 cracking under pulsing and continuous irradiation.

On the catalytic processing of decane under microwave irradiation, the hydrogen production increased with increasing the input power. This can be attributed to dehydrogenation reaction which is activated under the severe reaction condition. It was found that the continuous irradiation mode favoured the C-C breakage, whereas the pulsing mode favoured the C-H breakage.

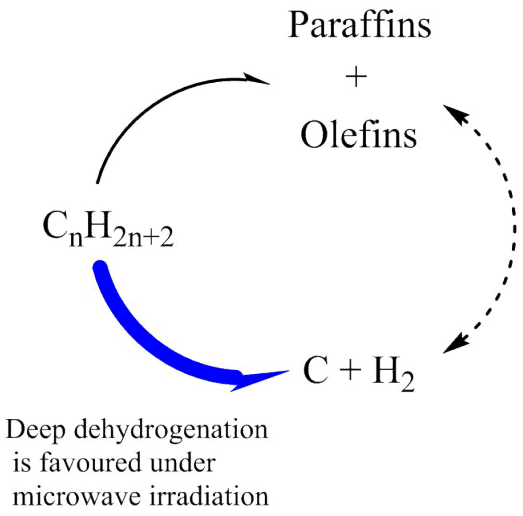


Figure 7.11: Model of general hydrocarbon cracking process, where the reaction favours the breakge of C-H over C-C under micorwave irreadiation compared to the theraml process where the oppisit case is ocurring.

Occurring of electromagnetic effects might be the reason behind the different temperature distributions within the samples. Having microwave absorbers additives in the catalytic system would lead to localised electric field and "hot spot" formation within the samples. This might lead to remarkable differences in temperature gradients between the pulsed-power and the continuous-power irradiation. Further investigations of the nature of the pulsing parameters, such as duty cycles, targeted temperature would be beneficial to evaluate the nature of microwave thermal and non-thermal effects [20].

7.3.2 Effect of Sample Parameters

This study aimed to determine the effect of the particle size on microwave absorption. The effect of microwave absorption on particle size is varying upon the nature of the sample, whether it is a metallic particle attached to the support, or dielectric metal oxides having two separate behaviours [21]. The experiments explored the potential of microwave absorption of iron oxide as a representative of the materials to be introduced in zeolite for heavy oil cracking reactions. The optimal condition of the microwave heating of an iron oxide catalyst sample will be presented by examining an Fe_2O_3 powder sample. The microwave absorptivity has been estimated by looking at

the heating profile of three different particle sizes. The three particle sizes are 50-100 nm, 125-250 μm, and 500-710 μm, which have been compressed into pellets, ground and sieved to the desired size. The sample tube was placed at the positions of the maxima of the E-electric field in a 2.45 GHz single-mode microwave cavity [22, 23].

In Figure 7.12, a comparison of the microwave heating of the three iron oxide samples as a function of particle size can be observed.

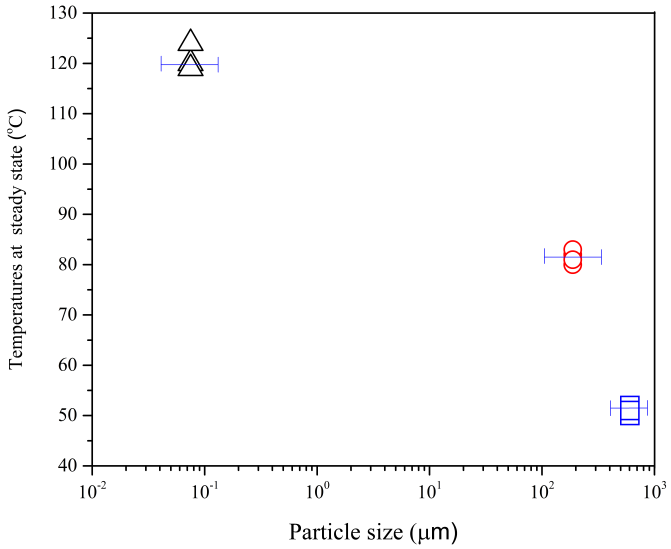


Figure 7.12: The effect of varying particle size on the heating behaviour of Fe_2O_3 in a microwave applicator at fixed applied power. The particles distribution was in the range of 50-100 nm, 125-250 μm, and 500-710 μm.

It can be seen that the samples show a greater temperature increase as the particle size of the iron oxide decreases. This is due to the change in surface area per unit volume of particle size [24, 25]. Assuming that both samples are exposed to the same electric field intensity and the material properties remain constant between the three powders, we would suggest a better coupling of the microwaves to the micron sized Fe_2O_3. Other studies [22] have noted a similar trend in temperature increase due to a decrease in particle size. Decreasing the particle size increases the

ratio of surface area to volume, which in turn increases the effective surface area of the sample, leading to an increased microwave absorption. Moreover, a decrease in particle size also decreases the volume of air voids in the compact. This, in turn, increases the effective conductivity of the compact. Ultimately, this increases the induced current density in the compact and thus increases microwave absorption.

Another way of enhancing the microwave selectivity and improving the sample heating is to introduce microwave absorbers into the catalytic system. Several microwave-absorbing materials have been reported and one of these materials is referred to as carbon black [26]. Experiments were then conducted to compare the HZSM-5 catalyst with different carbon loading percentages at a fixed input power. As such, 1, 3, and 5 wt% of carbon black have been loaded into the HZSM-5 zeolite. The experiments have been carried out in the same conditions and at the same microwave power level [27].

Figure 7.13 shows an increase in heating profile as the carbon loading increases within the sample.

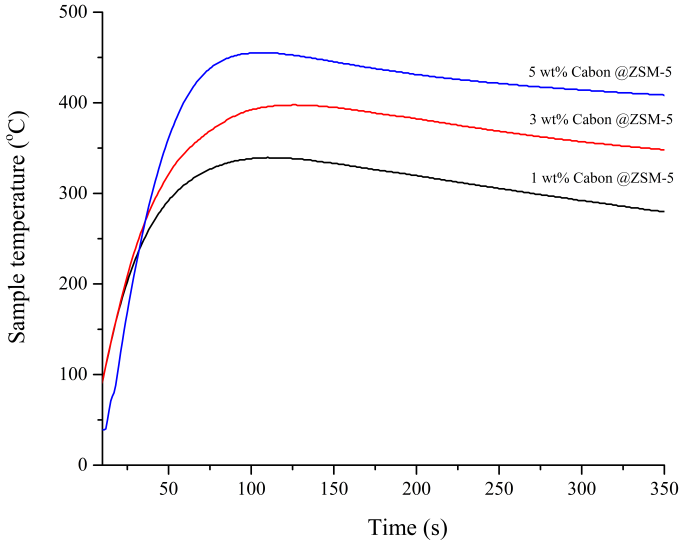


Figure 7.13: Variation in heating profiles of different carbon black loading over zeolite at fixed applied power.

This linear increase in heating is a representation of the increase in the dielectric loss of the material, which indicates the effect of permittivity on the material interaction with microwave. Moreover, it is essential to note the importance of the dielectric measurements before processing samples in a microwave system [28]. Usually, this type of selective heating takes place in a heterogeneous reaction system composed of different reactants, resulting in non-homogeneous energy dissipation and temperature gradients. The transfer of heat moves to be localised at the high absorbing area to form hot spots, and leaving the surrounding area to be the zones of lower temperatures. As the materials rapidly reach thermal equilibrium, hot spots disappear when the heat conduction rate is high between these different zones. Steady-state hot spots might exist and raise the rate of chemical reactions within those areas in systems in which heat transfer is slow. One explanation for the significant acceleration of reaction rates in microwave heating is the presence of meso- or microscopic hot spots. These spots are outside of the measurement range and could not be detected by the IR pyrometer [27].

Hot spots, or localised electric field, account for some reaction rate enhancement. Moreover, various heating effects have led to the acceleration of chemical reactions by microwave heating. It could be the selective heating due to the presence of microwave dielectric effects at the boundary between different mixtures of reactants. Additionally, it might be a rapid temperature ramping of the reaction system caused by the large microwave power input that affected the microwave dielectric heating [19].

One theory holds that only a purely thermal effect exists as a different temperature regime. A second theory holds that there are also electromagnetic effects. For example, there might be molecular interaction of substrates with the microwave field or a shifting reaction equilibrium. Such effects would explain the enhancement of reaction rates. In early studies, when results were not explainable in terms of temperature differences, researchers posited non-thermal effects. This is no longer the case because of the preference for dielectrically-heated reactions and improved temperature measuring methods suitable for microwave conditions. Three phenomena account for reported thermal effects: hot spot formation, selective heating, and high heating rate [15, 27].

7.4 Conclusions and Future Work

Comparison experiment between the microwave and thermal cracking of decane over HZSM-5 under the same possible conditions was conducted. The obtained results indicated a clear difference in the product distribution of both reactions. The remarkable difference was found in the hydrogen concentration which was higher in the case of microwave. Also the olefins concentration was found to be doubled in the microwave reaction. The results illustrated some unique selectivity in the microwave cracking reaction that could not be achieved in the thermal one. The outcome of this experiment encouraged us to proceed to the studies of heavy oil cracking reaction over different modified zeolites in the next chapter.

The further experiments described herein have provided a simple overview of the single-mode applicator parameters. This study has been conducted in order to optimise the conditions for microwave processing reactions. Using the illustrated applicator with controlled power output/reflected/dissipated enables to investigate the effects of different parameters on the reaction the system. It could be seen that changing the applied power can affect the dissipated power within the material, resulting in higher heating rates. Moreover, using the PID controlling system allows monitoring the heating rate and examining its effect on the product distribution in decane cracking over zeolite. By rapidly heating a multi-component material, it can be possible to selectively heat certain components based upon their dielectric properties which is a significant characteristic of the microwave heating over the conventional heating. Increasing the heating rate leads to a temperature differential between specific components and the bulk temperature. These might be the potential reason which leads to the benefits over conventionally-heated systems.

Microwave single-mode applicator is a highly versatile technology, thus it would be interesting to introduce additional modifications that enable more processes and parameters to be investigated, as there are significant opportunities for improving this applicator. Introducing a flow system to the reactor is important opportunity to increase the products yields. Moreover, as the applicator is operated under the TM_{010}, the heating process can be conducted under a uniformly-produced electric field. It would be possible with the versatile design of the reactor system to apply different applicators based on the desired activation field and mode. Since the materials behave differently in the E-field and the H-field [21]. It would be of high interest to investigate the effect of the electric

field of the microwave, as well as the magnetic field of the microwave.

More exploring on the product distribution between microwave and thermal processing might differ significantly in the case of enhancing the catalysts with microwave absorbing materials from the same catalysts in absence of additives.

Also further investigation on the pulsing feature needs to be conducted as it is a recently-installed feature. Different duty cycles, frequencies, and applied power density can be examined in order to assess the interaction between the field and the material. In addition, performing the reaction under controlled low temperatures and a highly applied field might have an insight into the separation of the thermal activation and the field activation of catalysts. The electromagnetic effect is difficult to detect due to the strong interface between the thermal heating and electromagnetic field, which makes it hard to be observed in practical studies. However, manipulating the single-mode applicator features and improving the system might help in giving a possible explanation and separation of both effects.

Bibliography

[1] Z.Z. Fang. *Sintering of Advanced Materials*. Woodhead Publishing Series in Metals and Surface Engineering. Elsevier Science, 2010.

[2] J. Benford, J.A. Swegle and E. Schamiloglu. *High Power Microwaves*. Series in Plasma Physics. CRC Press, 2nd edition, 2007.

[3] M.A. Surati, S. Jauhari, K.R. Desai. A Brief Review: Microwave Assisted Organic Reaction. *Arch. Appl. Sci. Res.*, 1(4):645–661, 2012.

[4] National Research Council (U.S.). Committee on Microwave Processing of Materials: An Emerging Industrial Technology. *Microwave Processing of Materials*. Publication NMAB. National Academies Press, 1994.

[5] J.D. Moseley. Microwave Synthesis in Process Chemistry Method, Scale and Scope. *Chemistry Today*, 27(2), 2009.

[6] J.D. Moseley and E.K. Woodman. Energy Efficiency of Microwave- and Conventionally Heated Reactors Compared at Meso Scale for Organic Reactions. *Energy Fuels*, 23:5438–5447, 2009.

[7] M. Mehdizadeh. *Microwave/RF Applicators and Probes: For Material Heating, Sensing, and Plasma Generation*. Elsevier, 2015.

[8] N. Yoshikawa, and E. Ishizuka, and S. Taniguchi. Heating of Metal Particles in a Single-Mode Microwave Applicator. 47:898–902, 2006.

[9] D.O. Hayward X. Zhang and D.M.P. Mingos. Microwave Dielectric Heating Behavior of Supported MoS_2 and Pt Catalysts. *Industrial & Engineering Chemistry Research*, 40(13):2810–2817, 2001.

[10] A.C. Metaxas and R.J. Meredith. *Industrial Microwave Heating*, volume 1 of *Energy Engineering Series*. P. Peregrinus, 1983.

[11] X. Zhang and D.O. Hayward. Applications of Microwave Dielectric Heating in Environment-related Heterogeneous Gas-phase Catalytic Systems. *Inorganica Chimica Acta*, 359(11):3421–3433, 2006. Protagonists in Chemistry: Professor D.M.P. Mingos.

[12] C.O. Kappe. Microwave Dielectric Heating in Synthetic Organic Chemistry. *Chem. Soc. Rev.*, 37:1127–1139, 2008.

[13] D.M.P. Mingos and D.R. Baghurst. Applications of Microwave Dielectric Heating Effects to Synthetic Problems in Chemistry. *Chem. Soc. Rev.*, 20:1–47, 1991.

[14] C.O. Kappe. Controlled Microwave Heating in Modern Organic Synthesis. *Angewandte Chemie International Edition*, 43(46):6250–6284, 2004.

[15] A. de la Hoz, A. Diaz-Ortiz, and A. Moreno. Microwaves in Organic Synthesis: Thermal and Non-thermal Microwave Effects. *Chemical Society reviews*, 34(2):164–78, February 2005.

[16] M.A. Herrero, J.M. Kremsner and C.O. Kappe. Nonthermal Microwave Effects Revisited: On the Importance of Internal Temperature Monitoring and Agitation in Microwave Chemistry. *The Journal of Organic Chemistry*, 73(1):36–47, 2008.

[17] Z. Chemat-djenni, B. Hamada and F. Chemat. Atmospheric Pressure Microwave Assisted Heterogeneous Catalytic Reactions. *Molecules*, 7(12):1399–1409, 2007.

[18] S.S. Lam, A.D. Russell, C.L. Lee, S.K. Lam and H.A. Chase. Production of Hydrogen and Light Hydrocarbons as A Potential Gaseous Fuel From Microwave-heated Pyrolysis of Waste Automotive Engine Oil. *International Journal of Hydrogen Energy*, 37(6):5011–5021, 2012. Optimization Approaches to Hydrogen Logistics.

[19] Z. Ying-Jie and C. Feng. Microwave-assisted Preparation of Inorganic Nanostructures in Liquid Phase. *Chemical reviews*, 114(12):6462–555, 2014.

[20] B. Fu and M.C. Hawley. Comparative Study of Continuous-power and Pulsed-power Microwave Curing of Epoxy Resins. *Polymer Engineering & Science*, 40(10):2133–2143, 2000.

[21] A. Porch, D. Slocombe and P.P. Edwards. Microwave Absorption in Powders of Small Conducting Particles for Heating Applications. *Phys. Chem. Chem. Phys*, 15:2757, 2013.

[22] Y. Yokoyama M. Hayashi and K. Nagata. Effect of Particle Size and Relative Density on Powdery Fe_3O_4 Microwave Heating. *Journal of Microwave Power and Electromagnetic Energy*, 44(4):198–206, 2010.

[23] C.A. Crane, M.L. Pantoya, B.L. Weeks, M. Saed. The Effects of Particle Size on Microwave

Heating of Metal and Metal Oxide Powders. *Powder Technology*, 256:113–117, 2014.

[24] V. Poponin and A. Ignatov. Local Field Enhancement in Star-like Sets of Plasmon Nanoparticles. *Journal of the Korean Physical Society*, 47:S222–S228, 2005.

[25] A. Mondal, A. Shukla, A. Upadhyaya, and D. Agrawal. Effect of Porosity and Particle Size on Microwave Heating of Copper. *Science of Sintering*, 42:169–182, 2010.

[26] J.A. Menendez, A. Arenillas, B. Fidalgo, Y. Fernandez, L. Zubizarreta, E.G. Calvo and J.M. Bermudez. Microwave Heating Processes Involving Carbon Materials. *Fuel Processing Technology*, 91(1):1–8, 2010.

[27] T. Durka. Microwave Effects in Heterogeneous Catalysis: Application to Gas-solid Reactions for Hydrogen Production. Master's thesis, Chemical Engineering, Warsaw University of Technology, 2013.

[28] W.C. Conner and G.A. Tompsett. How Could and Do Microwaves Influence Chemistry at Interfaces. *J. Phys. Chem. B,*, 112:2110–2118, 2008.

Chapter 8

MICROWAVE-ASSISTED HEAVY OIL UPGRADING

Overview

This chapter describes the experimental catalytic processing of heavy oil using a microwave-assisted reactor. The gaseous products were analysed and the change in catalyst integrity during the catalytic process was studied. A model is presented for batch and continuous flow conditions which acts as a guide for potential users, and may be used for future industrial research and development activities.

8.1 Introduction

The petroleum refining industry contributes significantly to the economies of the world oil market [1, 2]. It provides the basic raw materials for the chemical industry. Oil refining matters in hydrogen and light olefins, such as ethylene, propylene, and butylene. They are the basic building blocks of the petrochemical industry [3]. The conversion of hydrocarbons into light olefins is an important industrial process as light olefins are valuable starting chemicals widely used in the production of several high value materials, such as plastics and polyolefins (e.g. polyethylene, polypropylene and their co-polymers) [4–6].

The global demand for energy is increasing, and this presents significant challenges for industry. These challenges result from the high competitiveness within the refining sector. Moreover, there are some environmental stringent regulations resulting in an increase in the operating costs of refineries [7].

One of the possible solutions to overcome these problems is to enhance the petrochemical process by applying alternative energy sources which can reduce the energy cost and improve the quality of the products and increase their value [8].

Microwave radiation has been studied as an unconventional energy source for different applications in the petrochemical process [9–11]. It has been used to heat dielectric and non-dielectric materials in many processes; for example, during the reduction of metal oxides, the drying, the synthesis, the heating of materials, the production of active carbon, and the regeneration of spent carbon [12].

Microwave heating has also been applied for the pyrolysis of biomass, coal, and other organic wastes. The processing of these materials requires mixing with a good microwave receptor as they are very poor microwave receptors and cannot be heated directly to high temperatures at commonly used microwave frequencies [13, 14].

This chapter describes the heavy oil processing using microwave radiation generated in a bench top single mode applicators operating at frequency of 2.45 GHz. The reactor was described in detail in **Section 4.2.** Microwaves with a high frequency are generated by an oscillating electric field. This oscillation is selective which could result in various interactions between the catalyst and the heavy oil. Only part of the applied power is absorbed by the sample and some power is lost as the utilised catalysts are not perfect microwave absorbers. Several studies have been conducted to utilise microwaves as alternative energy source in the petrochemical industry. The catalytic cracking of heavy oil into light products has been investigated and the results are described in this chapter. The experiments are based on the catalytic process using different metal-doped zeolites under a fixed applied power and a controlled inert atmosphere. The gaseous product distribution of the heavy oil impregnated into different metal oxide zeolites is also presented. The morphological changes of the catalyst and support under microwave heating reactor has been studied and analysed.

8.2 Experimental

8.2.1 Catalyst Preparation

The catalytic properties of heterogeneous catalysts are significantly influenced by preparation procedures, as well as by the properties of the raw materials. The choice of a particular procedure for the preparation of a specific catalyst is dependent on the preferred chemical and physical characteristics of the final composition. Catalysts have been prepared using the impregnation method, which is carried out by loading the impregnating solution that contains the catalyst with an active metal cation to fill the pores of the zeolite and then mixed with a glass rod. HZSM-5 was loaded with 5, 10, and 20 wt.% of each of the following metal oxide: lanthanum (III), iron (II/III), and cobalt (II/III). The loaded catalyst was prepared and dried at 110°C for 24 hours and then calcined at 550°C for 6 hours under atmospheric conditions to obtain a final form of metal oxide in the zeolite.

The next step was introducing the (bunker) heavy oil -provided by Saudi Aramco- into the modified zeolite, using a similar impregnation method. The objective of this preparation method is to use prepared catalysts under microwave radiation with a high level of activity, selectivity, and stability. The impregnation method involved exposing a dry support with an extra amount of solution of the impregnate as a way of saturating the pores of the support material. During this process, heavy oil is loaded to the zeolite. As a result, the concentration of the support does not only depend on the concentration of the solution and pores volume. But it also depends on the concentration and/or the type of the adsorbing sites that are found on the surface. As such, the larger molecules cannot enter the pores and will deposit only on the outside surface, resulting in a non-homogeneous distribution. To achieve a good disposition of the oil, the build-up of local concentration gradients should be avoided through an efficient mixing process carried out simultaneously using a slow addition of the solvent solution.

The preparation process for the pure and modified zeolite which was impregnated with heavy oil consists of the following steps. The first step involves the dehydration of the zeolite at temperature of 550°C for 6 hours. Then the dehydrated sample was preserved in a round bottom sealed flask in order to prevent the introduction of moisture. In order to achieve a final loading of 25 wt.% of heavy oil into zeolite, the necessary amount of oil was dissolved in toluene and added to the zeolite HZSM-5 using a separation funnel that was slowly opened to allow for the solution to mix with

the zeolite. The slurry obtained was subsequently heated to a temperature of 120°C overnight, for toluene evaporation and dryness. Different metals loaded onto zeolite HZSM-5 (Si/Al = 60) have also been prepared in this way.

8.2.2 Experimental Setup

Experiments were conducted in batches, and 1.0 g of the prepared sample has been used in each experiment. The zeolite/heavy oil sample was put in the reactor quartz tube and placed in the microwave cavity resonator. The quartz reactor tube has an internal diameter of 9 mm, a wall thickness of 1 mm, and a catalyst bed length of 40 mm. The gas produced in the process was collected in an eudiometer tube over an aqueous solution, and after the reaction was complete, the gas compositions were determined using GC.

The procedure for a complete single reaction for the system involves the flushing of the reactor bed with argon for 15 minutes to create an inert atmosphere. Then, a fixed microwave power was applied for 30 minutes to complete the reaction period. Finally, the gaseous products trapped in the cylindrical tube were withdrawn and analysed by GC at the end of the process.

The spent sample was subjected to a washing procedure using toluene extraction to remove the residual and unconverted oil. In the following step, the sample was placed in 40 mL of toluene at 80°C for 3 hours under stirring, then filtered and dried overnight at 105°C in air. Further analysis and characterisation were conducted over the initial and the spent washed samples using XRD and TG analysis. SEM and TEM were also used to study the change in morphology of some of the fresh and spent washed zeolite samples. The dielectric properties of some of the catalysts before and after reaction were also evaluated.

The catalyst used for each reaction was weighed before and after heating. It should be noted that obtaining a good mass balance of (>95%) is quite limited with such a system due to the utilisation of a small amount of the catalyst (1.0 g), which is loaded with 25 wt.% of oil. This would result in only a very small amount of the liquid product being collected in the liquid trap and some would remain on the reactor walls. In practical terms, the minimum amount of oil that is required for product analysis of petroleum fractions is above 1.0 g. In addition, the precise temperature of the reactor bed in such systems is limited by the accuracy of the IR pyrometer.

Products from each run involved some gas remaining in the cylinder, residual carbon/coke

formed over the catalyst, and the liquid product. The liquid product has three components, one is directly collected from the liquid trap after each condensation, another is the one that has remained on the tube walls, and yet there is some liquid product that is trapped by quartz wool in the reactor bed. The calculations of the material balance can be found in **Appendix C.**

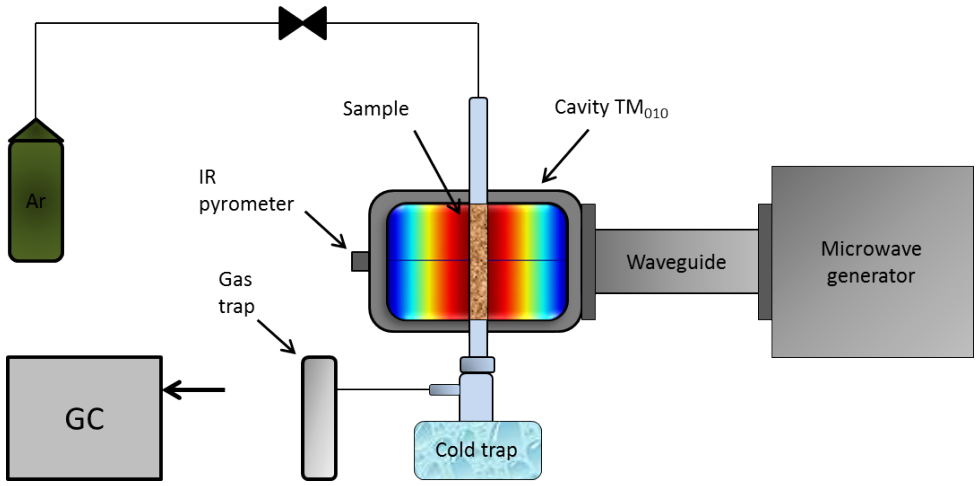


Figure 8.1: Schematic representation of the experimental setup.

8.2.3 Gas Chromatography (GC)

The gaseous products (C_1–C_5, C_2–$C_4^=$, H_2, CO and CO_2) were analysed by a gas chromatograph (A Perkin-Elmer Clarus 580 GC). The capillary column is 50 m long × 320 μm. The TCD temperature is 200°C and the helium carrier gas was set at a flow rate of 40 mL/min. The temperature of the FID was set at 250°C and the flow rates of H_2 and air were 45 mL/min and 450 mL/min, respectively.

8.2.4 Dielectric Measurements

Cavity perturbation methods have been used to study the dielectric properties of the catalysts. The dielectric measurements were performed at room temperature in TM_{010} mode at 2.49436 GHz (in practice). The measurement of each sample was performed a minimum of three times and the

average values were used. The measurement was introduced in details in **Section 5.2.**

8.2.5 X-Ray Diffraction (XRD)

XRD patterns of the catalysts were obtained for the fresh and the spent samples using the PW 3040/60 PanAnalytical Xpert Pro diffraction system with a monochromatic CuK_{α} source, operating at 40 keV and 30 mA from 5° to 60° in 2θ.

8.2.6 Thermogravimetric Analysis (TGA)

Thermaogravimetric experiments were carried out to monitor the weight loss during the catalytic process, and to study and evaluate the coke formation in the spent catalysts during the reaction process under microwave irradiation. The analyses were performed using a TGA (Perkin Elmer STA6000) instrument. The samples were placed in an alumina crucible preformed with a heating rate of 10°C/min up to 950°C under air flow 100 mL/min.

8.2.7 Scanning Electron Microscopy (SEM)/ Transmission Electron Microscopy (TEM)

The change in morphology of the coked samples was studied on the fresh and spent washed catalysts. It has been examined using a Field Emission Scanning Electron Microscopy (JSM - 7100F) and a high-resolution transmission electron microscopy (JEOL 3000F) field emission gun instrument.

8.3 Results and discussion

8.3.1 Heavy Oil Processing using HZSM-5 Catalyst

Microwave-assisted catalytic cracking has been applied to a sample of heavy oil over a zeolite impregnated sample in order to investigate the feasibility of undertaking the reaction under microwave conditions and evaluating the possibility of enhancing and accelerating such chemical reactions. In such systems, the reaction may reach the desired temperature more efficiently and more speedily than a conventional heating method.

Approximately 25 wt.% of heavy oil was impregnated into HZSM-5 zeolite. Figure 8.2 illustrates the typical heating profile for the oil/HZSM-5 reaction. It can be seen that the temperature increases rapidly from room temperature to ± 100°C in less than 100 s. The IR pyerometer indicates the change in the temperature of the external surface of the catalyst during the reaction. The recorded heating profile shows the temperature (T) versus time (t) with heating rate of 300°/min. The maximum reaction temperature of nearly 450°C was achieved in less than 2 minutes.

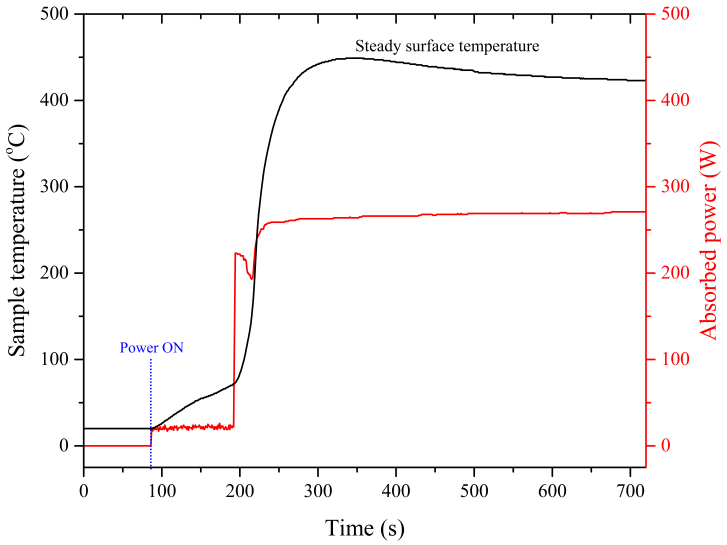


Figure 8.2: Microwave heating profile of HZSM-5 impregnated with 25 wt.% of heavy oil during the microwave cracking reaction.

As the reaction temperature increased, the cracking of the heavy oil over zeolite support occurred, resulting in lighter gaseous products. The gaseous products that were obtained from the cracking of heavy oil at 450°C over HZSM-5 were H_2, CO, CO_2, C_1 to C_5 alkanes, and C_2 to C_4 alkenes. In this section, the produced gases in different metal loading experiments are presented in terms of absolute volume instead of relative magnitude of vol.% concentration. This is due to the fact that there was no significant difference in the concentrations of gas products compositions.

However, the produced volume of gas was found to vary significantly with each run. However, the gas compositions of vol.% can be found in **Appendix B**.

The light hydrocarbon gases are very important and they can be used as a chemical feedstock. For instance, methane can be used as a feedstock in hydrogen production via steam reforming and ethane can be cracked to produce hydrogen and ethylene. However, due to the small amounts of the impregnated oil and the catalyst, the amount of produced liquid was not sufficient for GC/MS analysis[15].

Figure 8.3 provides a column-chart which illustrates the volume of the gases produced. H_2 (82 mL), CH_4 (10.2 mL), C_2-C_5 (1.4 mL), C_2-$C_4^=$ (7 mL), and COx (11.2 mL) were the primary gases produced in the microwave processing process.

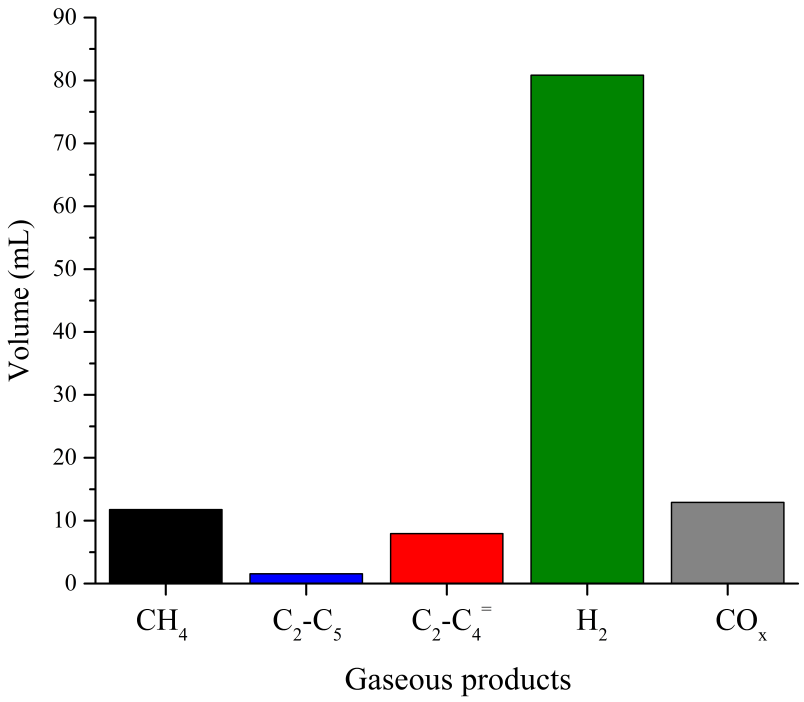


Figure 8.3: The volume of the gaseous products resulting from the heavy oil cracking over HZSM-5 zeolite.

The gaseous distribution from obtained from the GC analysis are illustrated in Figure 8.4. It shows the compositions results from both the flame ionisation detector (FID) for hydrocarbon analysis and the thermal conductivity detector (TCD) for hydrogen and other inorganic gases. It can be seen from the figure, the large peaks of ethylene and propylene comparing to the equivalent paraffins in addition to the large intensity of the hydrogen peak compared to other gases.

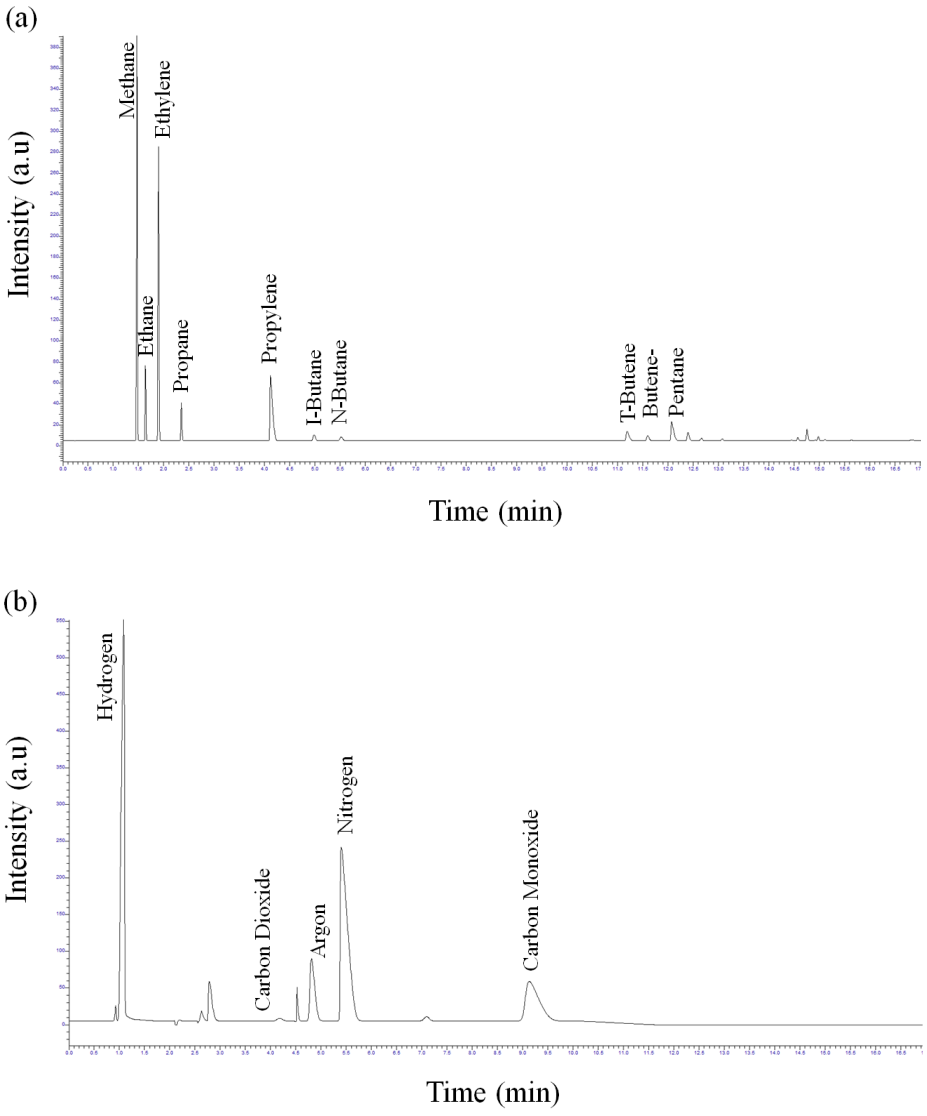


Figure 8.4: Chromatograph showing the gas products of the (a) FID channel and (b) TCD channel from the heavy oil cracking over zeolite.

The composition of the gases produced from heavy oil cracking using microwave radiation could be interpreted using different mechanisms. The catalyst is heated directly under microwave irradiation, which leads to it reaching the reaction temperature faster. On the other hand, the reactor walls are still at a lower temperature than the catalyst. In such a heterogeneous system where there

is an interface between the zeolite solid catalysts and the impregnated heavy oil, this would lead to significant temperature gradients within the system. In addition, the formation of hotspots is a distinct possibility. The high electric fields associated with microwave field would result in highly localised super-heating spots within the catalyst. High temperatures at the hotspots especially if they are in contact with heavy oil may favour the gasification reactions and the formation of the hydrogen. The formation of light gaseous products (i.e. C_1-C_5), is likely associated with a thermal cracking reaction of heavy oil. This phenomenon is different when the heat is flowing from the walls to the reactor and the sample. This would give the possibility for the volatile compounds generated to undergo secondary reactions and react in the gas phase. Other proposed possible justifications could be related to the microwave processing itself that is associated with non-desired effects arising from the electromagnetic fields generated by the microwave radiation.

As seen in Figure 8.1, H_2 was the major component of the gaseous products with 82 mL being formed. The results indicated that the cracking of heavy oil using microwave heating could be a potential source for the production of H_2-rich fuel gases. The ideal gas law was applied to calculate the mass of each component at standard conditions (25°C: 1 bar); in addition, the residual carbon and produced liquid have been estimated as the the liquid is composed of both products and unconverted oil. The mass balance closure of the reaction indicates a 3% deviation. The calculations are provided in **Appendix D.** The results of the product distribution calculations are presented in Table 8.1 and they are based on the overall amount of products. The weights of H_2, CO_x, CH_4, C_2-C_5, and C_2-$C_4^=$ are calculated in grams. Thus, the distribution of weights appears significantly different from that of the volume due to the very light mass of H_2.

Table 8.1: The product distribution (wt%) of the heavy oil cracking over unmodified HZSM-5 zeolite.

Product	Oil/HZSM-5
liquid (wt. %)	86.2
H_2(wt. %)	1.7
CH_4 (wt. %)	2.0
olefins (wt. %)	2.8
paraffins (wt. %)	7.1
gas volume (mL)	115
the coke content by TGA (wt. %)	9.4 ±1.0

The XRD patterns of the pristine and the spent catalysts are presented to examine the change in crystallinity of zeolite after the microwave radiation. Figure 8.5 indicates that the sample still exhibit the typical ZSM-5 structural characteristics however a slight decrease in zeolite crystallinity appears in the pristine sample after microwave irradiation. This can be observed from the decrease in intensity in the zeolite main crystallinity peaks between at 2θ = 22-25° [16]. On the other hand, the slight increase in the low-angle XRD intensities might be attributed to the removal of any extra-framework in side the zeolite channels with microwave heating [17].

The spent zeolite samples illustrates a clear decrease in zeolite characteristics which suggests the coke disposition and formation of amorphous carbonaceous materials over the zeolite surface and maybe disposition of carbonaceous materials within the zeolite channels.

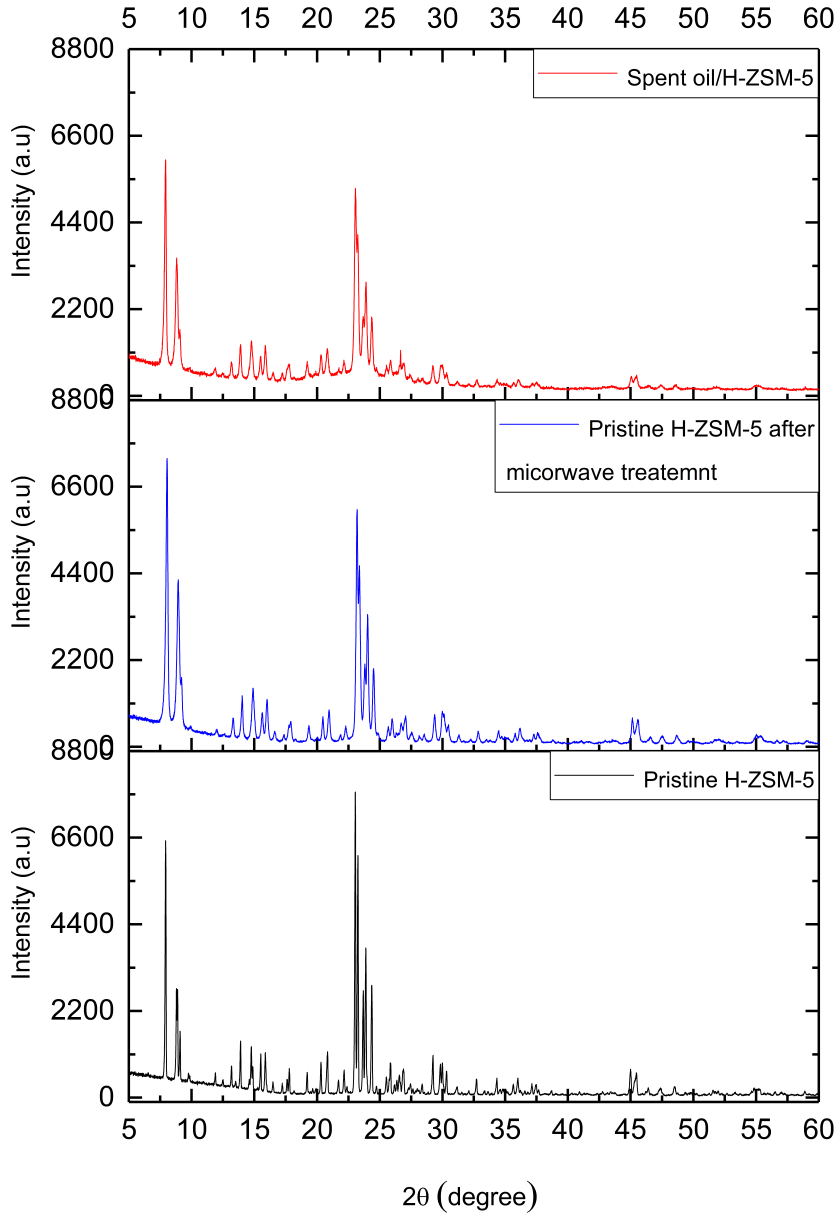


Figure 8.5: XRD patterns of the pristine HZSM-5 before and after microwave irradiation compared to the spent oil/catalyst after microwave irradiation at 450°C.

To evaluate the change in dielectric properties of the sample after microwave processing, the

cavity perturbation technique has been performed on the tested catalyst. Figure 8.6 represents the change in dielectric properties of the oil/HZSM-5 fresh, spent and after toluene washing samples.

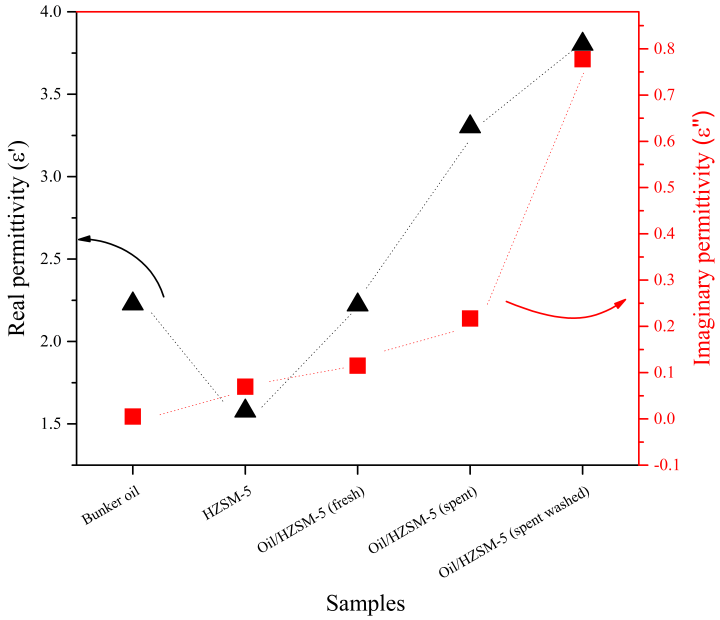


Figure 8.6: Change in dielectric properties of the HZSM-5/oil sample before and after the microwave reaction.

The measurements shows that the heavy bunker oil has higher real permittivity comparing to zeolite, and zeolite has slightly higher imaginary permittivity than the oil. However, when impregnating the oil into zeolite, it can be seen that the real permittivity of the fresh sample is adopting the heavy oil real permittivity value and imaginary permittivity value is closer to the pure zeolite value.

After the microwave processing it can be seen that the spent catalysts have gained higher imaginary permittivity and real permittivity compared to the fresh samples. This can be attributed to the coke formation within the sample after reaction. As the spent sample is composed of different carbonaceous materials with possible sp^2- hybridisation, this would give rise to the dielectric properties of the sample. This might be the reason behind the steady microwave absorption even

after deactivating the catalyst as these carbon material can be a good microwave absorber. This can be confirmed by the increase in dielectric properties of the spent washed sample. After removing all the residual materials and the unconverted oil, the increase in permittivity value is noteworthy.

Figure 8.7 shows the SEM micrographs for the fresh and the coked samples, which were separated from the liquid products and washed with toluene. Both samples are almost similar before and after, although it is possible to observe some agglomerated particles and loss in zeolite crystallinity after microwave reaction. This indicates that the zeolite catalyst has outstanding stability under the applied microwave conditions.

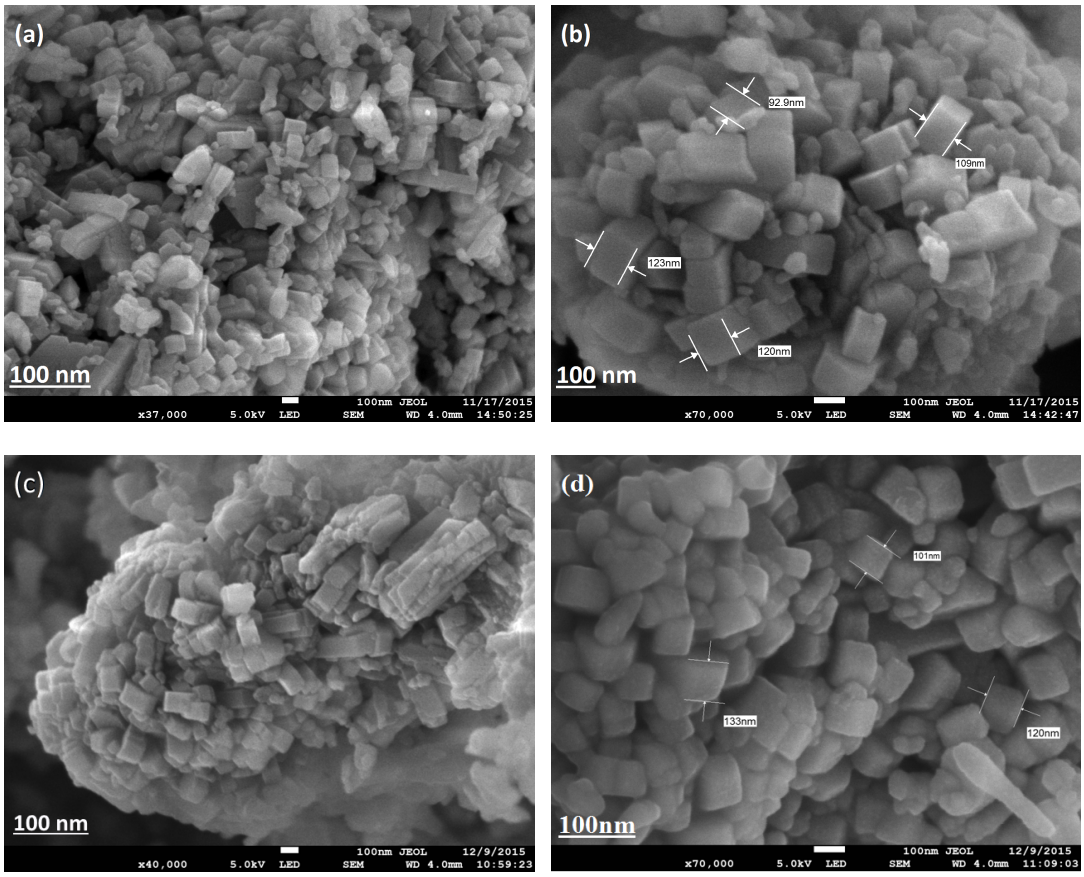


Figure 8.7: SEM images (a,b) of the pristine HZSM-5 before reaction, (c,d) spent sample after washing with toluene indicating some particle aggregation and loss in crystallinity after microwave treatment.

8.3.2 HZSM-5 Catalyst Impregnated with Transition Metal Oxides

The Impregnation of Iron Oxide into HZSM-5

Great efforts have been conducted to enhance the shape selectivity of the zeolite by modifying the distribution of its acid sites. This has been done by introducing some alkali metals, alkaline earth metals [18, 19], and transition metals [20]. Transition metal oxide catalysts were found to be active in promoting hydrocarbon cracking since the late 1960s. Iron is considered one of the non-toxic cheap transition metals and it is found to be fully effective in thermal processing reactions [21–23]. HZSM-5 zeolite has been doped with different levels of iron to examine the product distribution of the heavy oil cracking under microwave radiation as iron oxide is a very effective microwave absorber.

HZSM-5 has been prepared with three different loading levels of iron oxide (5, 10, and 20 wt.%) and two of the XRD patterns before adding the oil are presented in Figure 8.8. There is no obvious difference between the XRD patterns of the pure HZSM-5 and the Fe modified 5 wt.%, and 20 wt.% HZSM-5. The two patterns of the doped samples exhibit the characteristic diffraction peaks of the structure of MFI topology, which are appearing at 2θ = 7.9°, 8.8°, 23.1°, 23.9°, and 24.4°. There is almost no reflection observed in the iron oxides for the 5 wt.% of FeO_x/HZSM-5. However, intensity of the low angle XRD peaks was found to be reduced due to the loading of the iron oxide particles within the zeolite pores. In addition, other portion of the iron oxides were found to be deposited over the zeolite surface resulting in a clear decrease in zeolite crystallinity diffraction peaks. In the pattern for 20 wt.% FeO_x/HZSM-5, it can be seen that in addition to the reduction of the peaks intensity, some of the peaks can be assigned to the iron oxide particles which might be the spinel phase of Fe_3O_4 [24]. In general, all patterns indicate the crystallinity of the prepared samples and the iron oxide species in the two zeolites are well dispersed. However, in the 20 wt.% Fe, iron oxide species are formed on the external framework of the zeolite.

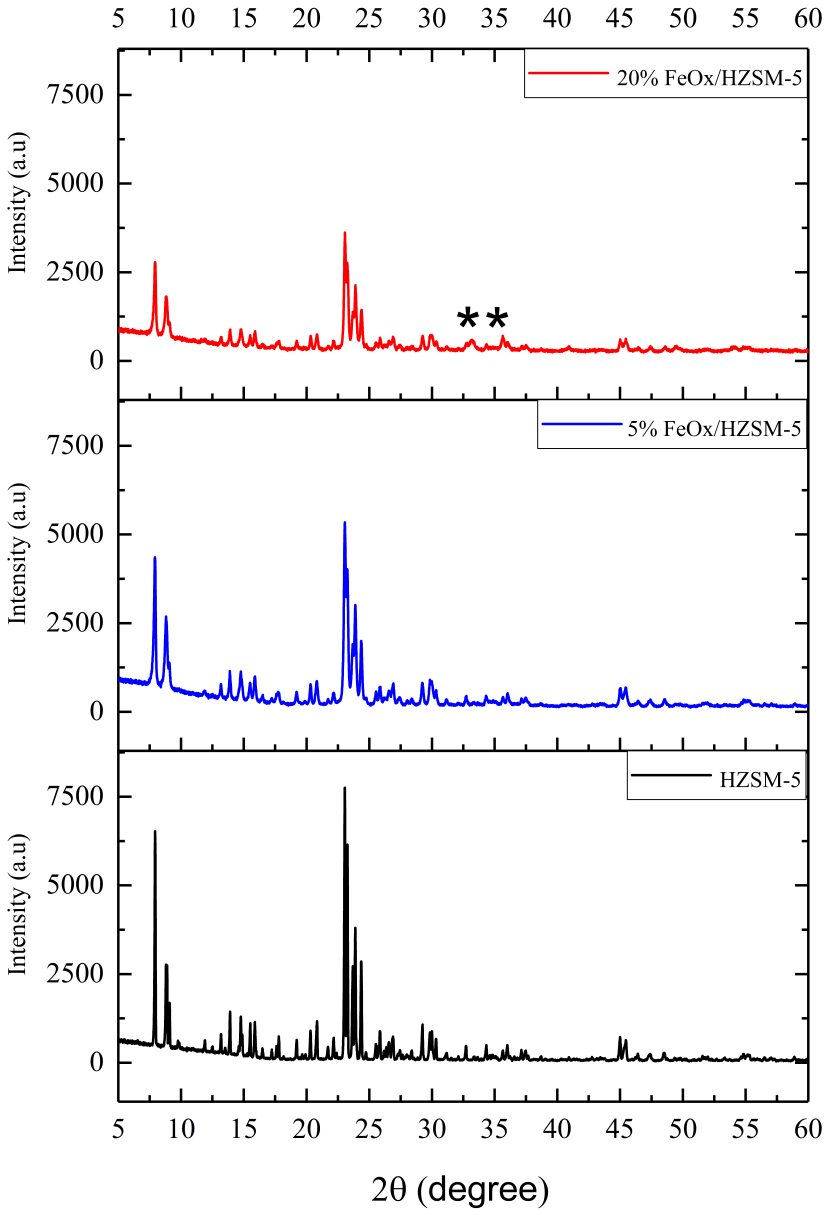


Figure 8.8: XRD patterns of different samples HZSM-5, 5 wt % FeO_x/HZSM-5, and 20 wt% FeO_x/HZSM-5, (*) indicates the presence of the iron oxide species.

Three different iron loadings impregnated with heavy oil have been irradiated with microwave

and processed under the same conditions. The results of the gas product volumes showed in Figure 8.9.

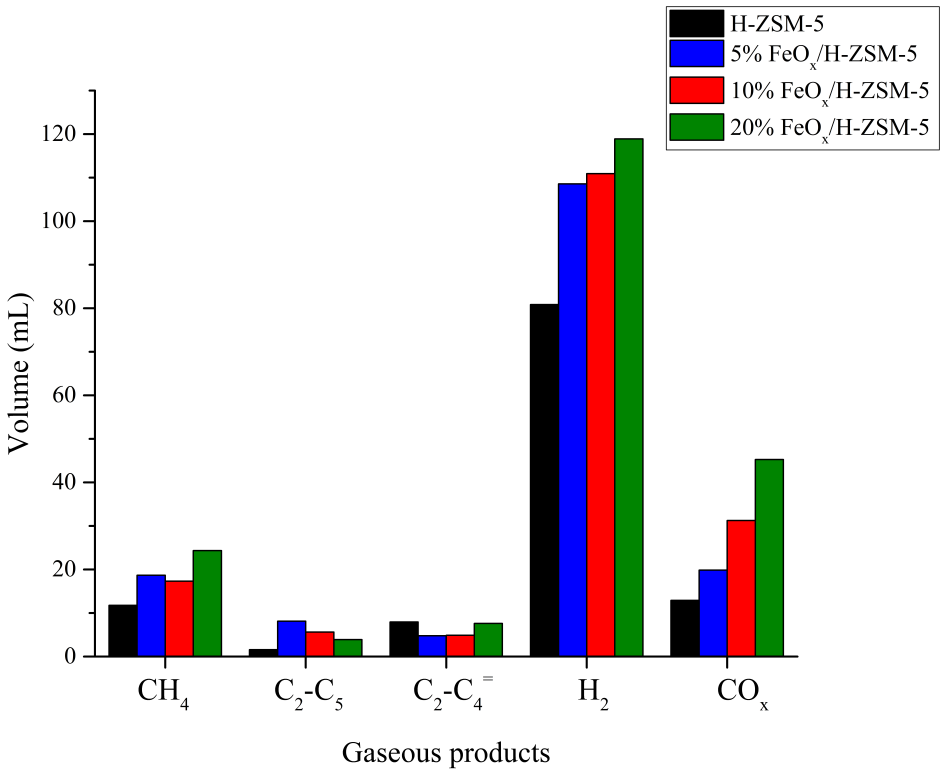


Figure 8.9: The volume of the produced gas from the heavy oil cracking over different iron loadings into HZSM-5 catalysts in comparison to the cracking over the parent HZSM-5.

From Figure 8.9, it can be seen that the gases produced contained the light hydrocarbons in addition to H_2 and CO_x. Similar to the pure zeolite, the volume of the H_2 appears to be the most significant product from this reaction. In addition, the volume of hydrogen seems to increase with the iron oxide doping level.

The increase in hydrogen concentration could be attributed to the formation of the hotspot within the catalyst. Nevertheless, the produced hydrogen was expected to be more than what obtained due to the partial consumption of hydrogen upon the reduction of some of the iron oxides. It is also noted an increase in the CO_x concentration compared to the pure zeolite reaction.

The temperatures of the cracking reactions were determined by the IR pyrometer, and they were found to be circa 450, 580, and 490°C for the three catalysts, respectively. As the infrared pyrometer is only detecting the surface temperature, it should be taken into account that the actual temperature of the catalyst may be higher than that observed. Iron oxide is considered a good microwave absorber, as most metal oxides. This results in a selective heating over the irradiated catalyst. As the electric field becomes concentrated over the iron particles, a thermal gradient and a hot spot phenomenon can be generated. The importance of hot spot effects for heterogeneous catalysts under microwave radiation has been proposed by a number of research groups [25–27]. It has been suggested that hot spot formation within the catalyst may influence not only the rate of the reaction but also shift the equilibrium. The hot spots are formed because of the variation in the dielectric properties of the catalyst under the electromagnetic fields. Thus, the temperature of the metal or metal oxide particle is higher than both the average temperature of the catalysts support and the catalyst bed.

Unfortunately, under such drastic conditions the zeolite catalysts may be quickly deactivated, as a result of coke formation and deposition of carbonaceous residues in the zeolite channels and pores [28]. Figure 8.10 shows a schematic of the dehydrogenation and the associated coke formation mechanism.

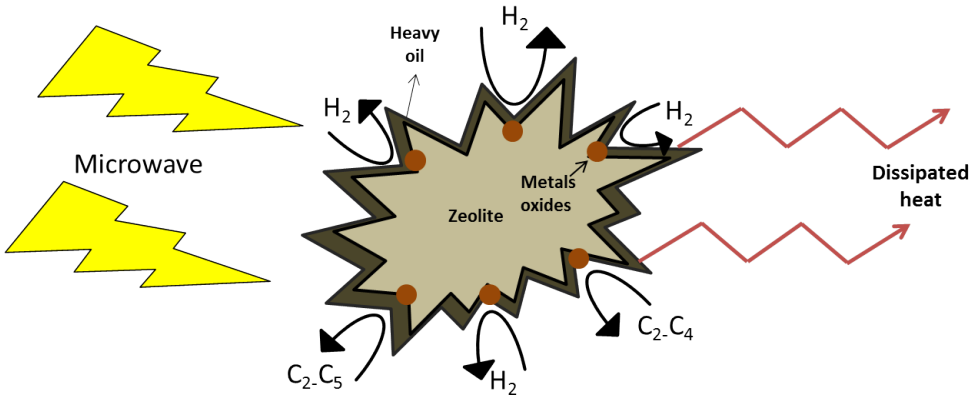


Figure 8.10: The dehydrogenation and coke formation mechanism under microwave irradiation.

The product distribution are illustrated in Table 8.2.

Table 8.2: Product distribution (wt.%) of HZSM-5 modified zeolite with iron oxide.

Product	5 wt.% FeO_x/HZSM-5	10wt.% FeO_x/HZSM-5	20wt.% FeO_x/HZSM-5
liquid (wt. %)	86.0	74.0	74.0
H_2 (wt. %)	3.7	6.0	6.0
CH_4 (wt. %)	5.2	7.5	9.0
olefins (wt. %)	3.0	4.6	6.0
paraffins (wt. %)	6.7	7.0	4.0
gas volume (mL)	160	170	200
the coke content by TGA (wt. %)	12.7 ±1.0	11.3 ±1.0	11.1 ±1.0

XRD patterns of the spent FeO_x/HZSM-5 samples are presented in Figure 8.11. It can be seen that the zeolite spent catalysts are exhibiting a huge decrease in crystallinity as the iron oxide loading increases. Also, it is noteworthy the formation of carbon materials and iron carbide due to the reduction of iron oxide to metal iron resulting in a release of CO_x.

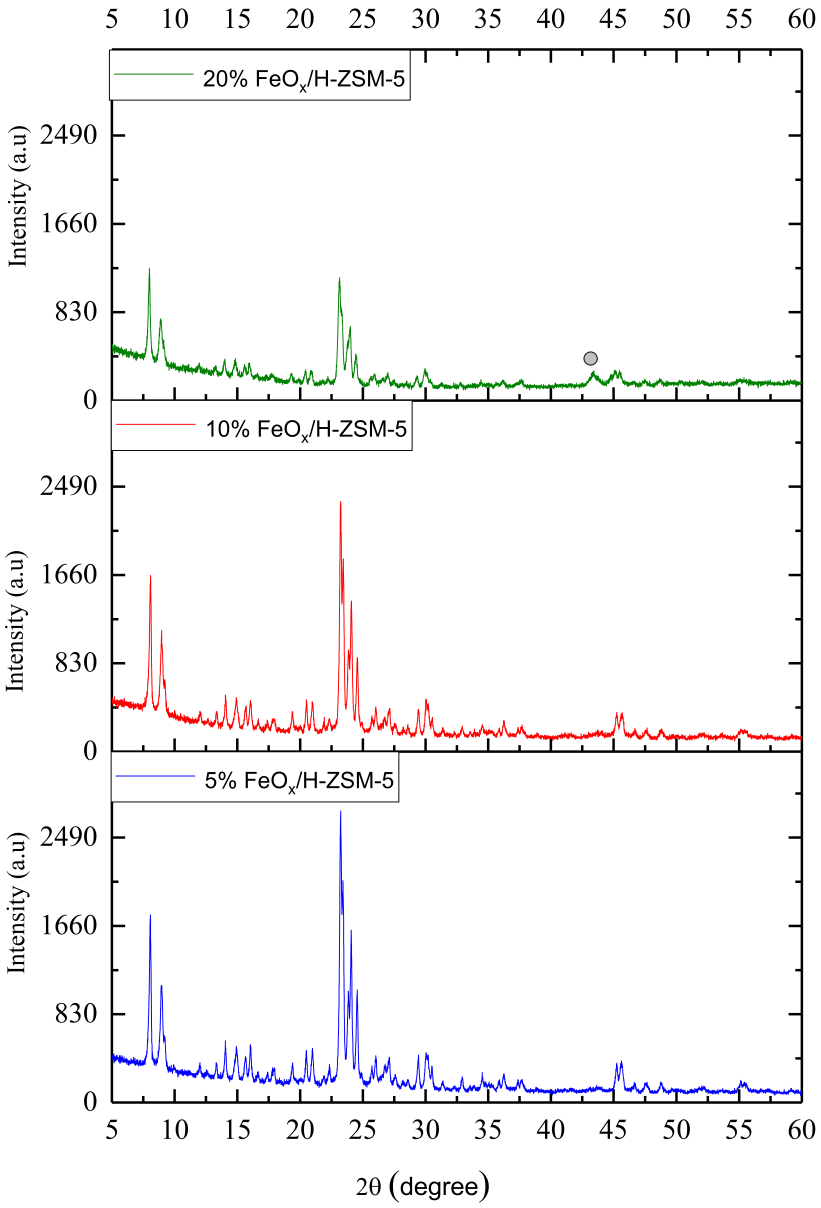


Figure 8.11: XRD patterns of different iron/zeolite spent catalyst after microwave irradiation, the (o) might be attributed to the iron carbide peaks.

In order to evaluate the change in morphology of the catalysts properties before and after reac-

tion they have been investigated using electron microscopy techniques, and dielectric measurements have been conducted. Figure 8.12 summarises the real permittivity and imaginary permittivity measurements for the catalysts before and after the catalytic process for the three loading levels.

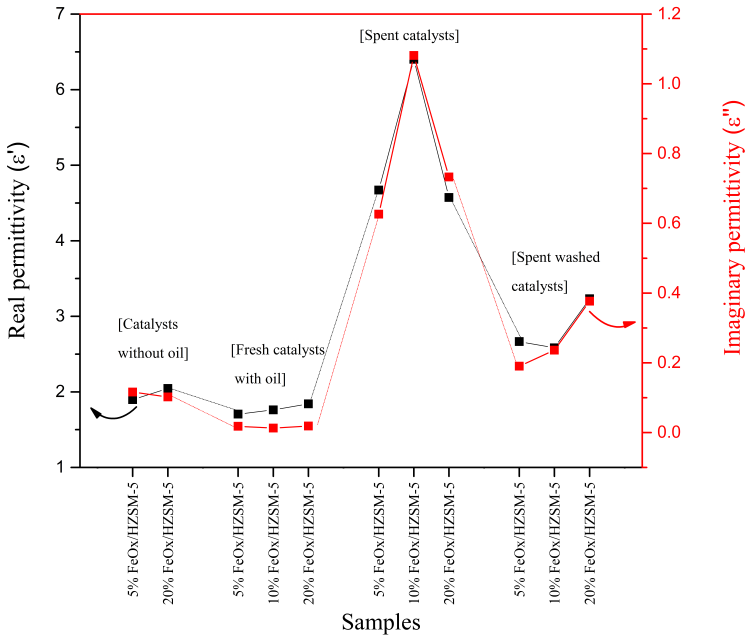


Figure 8.12: Dielectric properties of the fresh and spent catalysts for the 5, 10, 20 wt.% FeO_x/HZSM-5.

It can be seen that the spent catalysts exhibit significantly higher dielectric properties compared to the fresh samples and the spent washed catalysts. This indicates the formation of carbonaceous materials as the cracking reaction occurs.

The increase in hydrogen production accompanies coke formation. However, the amount of produced coke is not always associated with the increase in dielectric properties of the spent catalyst. The dielectric properties seem to be associated with the higher reaction temperature. As the temperature increases, more cracking and dehydrogenation is taking place leading to the formation of more of the sp^2– and sp- carbon materials. In this system, it can be challenging to relate the dielectric properties to the amount of formed coke from the TGA. In conclusion, the type and the

location of coke on the catalyst are fundamental properties that depend on the process conditions.

TGA analysis has been carried in air in order to obtain the amount of weight loss in the iron/HZSM-5 catalysts. The thermogravimetric analysis profiles are presented in Figure 8.13.

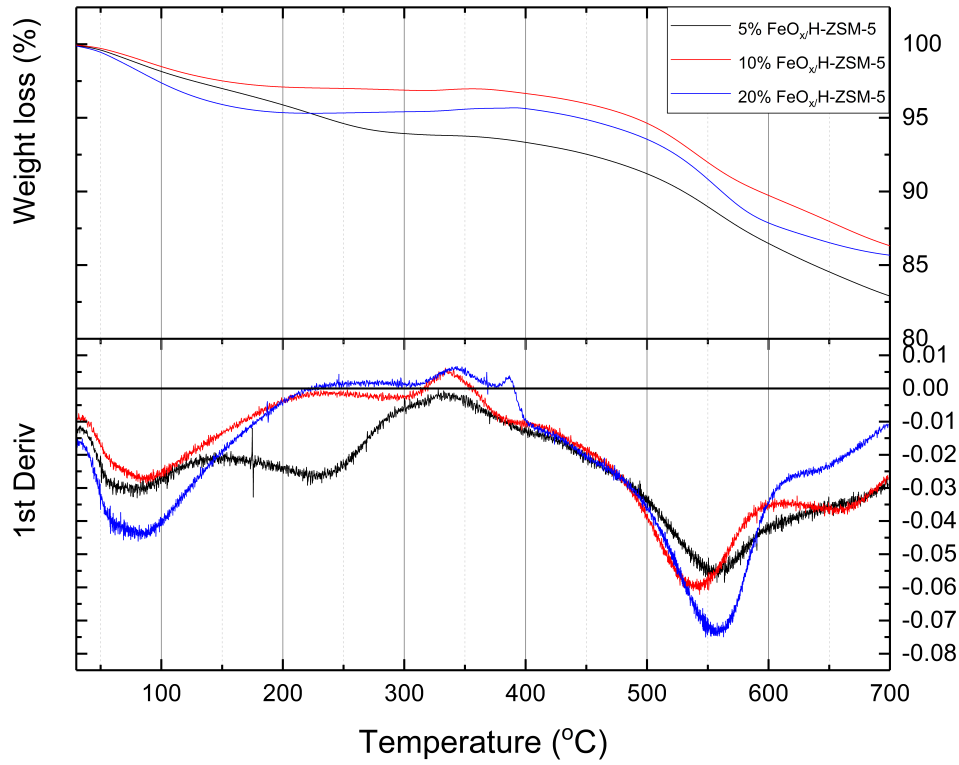


Figure 8.13: TGA profiles of the spent FeO_x/HZSM-5 catalysts before toluene washing.

The amount of deposited coke was determined from the TGA profile of the spent samples after toluene washing, (**see appendix C**) as the difference in weight loss above 400°C illustrates the region where coke deposits occurred.

The change in morphology of the 20 wt.% FeO_x/HZSM-5 spent sample has been characterised using SEM and TEM techniques. The first sample is the one that was heated at 490°C. The other was treated at a temperature higher than 800°C.

Figure 8.14 represents the SEM of the spent catalysts treated at different microwave levels.

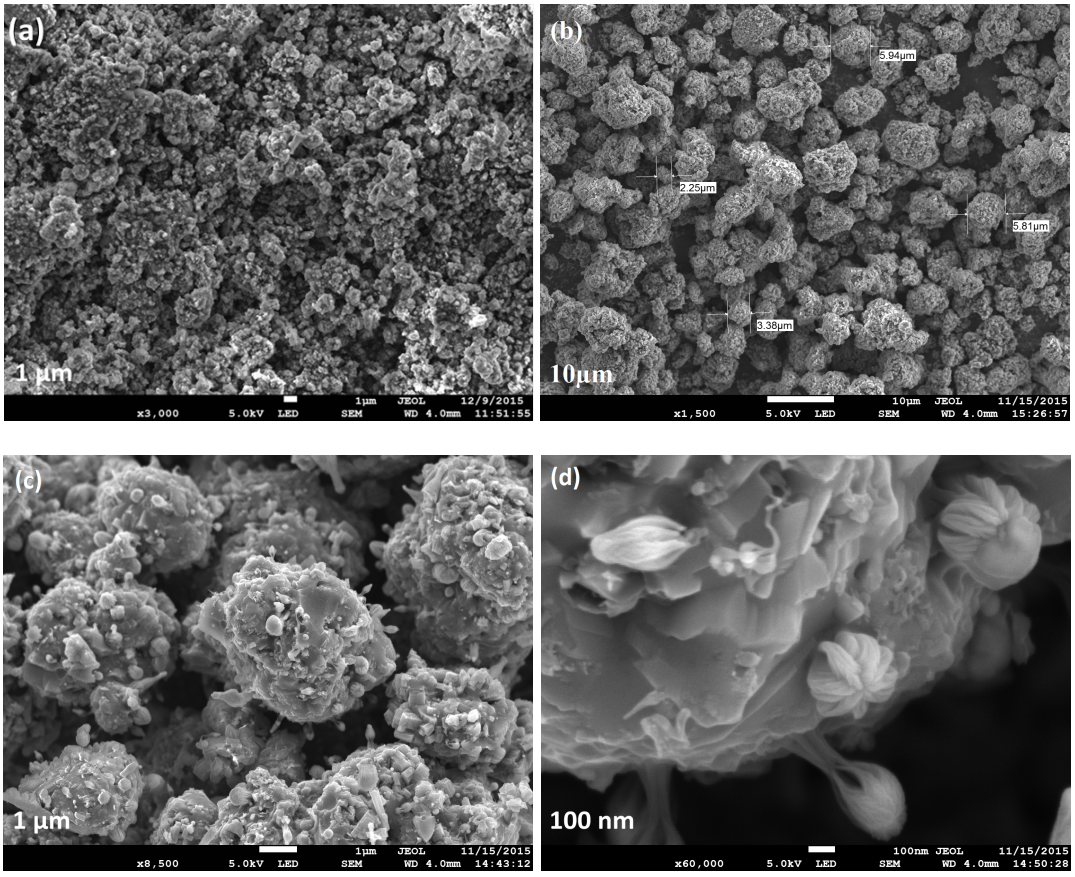


Figure 8.14: SEM images from the 20 wt% of FeO_x/HZSM-5-heavy oil samples treated at (a) and (b) 490-500°C, (c) and (d) around 900-1000°C.

Both samples exhibit particle agglomeration following microwave radiation. However, the sintering is more pronounced in the second sample where higher temperatures were achieved. This might be assigned to the formation of localised higher temperatures resulting in hot spot formation where aggregation is appearing. Additionally, some other particles can be formed on the surface of the flower shaped-aggregated particles. Iron incorporation into HZSM-5 at the high temperatures and applied microwave power could result in a crystallisation process and might produce strongly uniform and clean crystal grown of high silica HZSM-5 zeolite.

The TEM images shown in Figure 8.15 indicate significant change between both samples. The first sample shows particles aggregation as well as a formation of carbonaceous materials, which appears mostly to have an amorphous structure. The beginning of the formation of carbon nanotubes can also be observed. The reduction results in metallic iron and the formation of iron carbides in the spent catalyst [29]. The second sample clearly show carbon nanotubes formed over the iron particle.

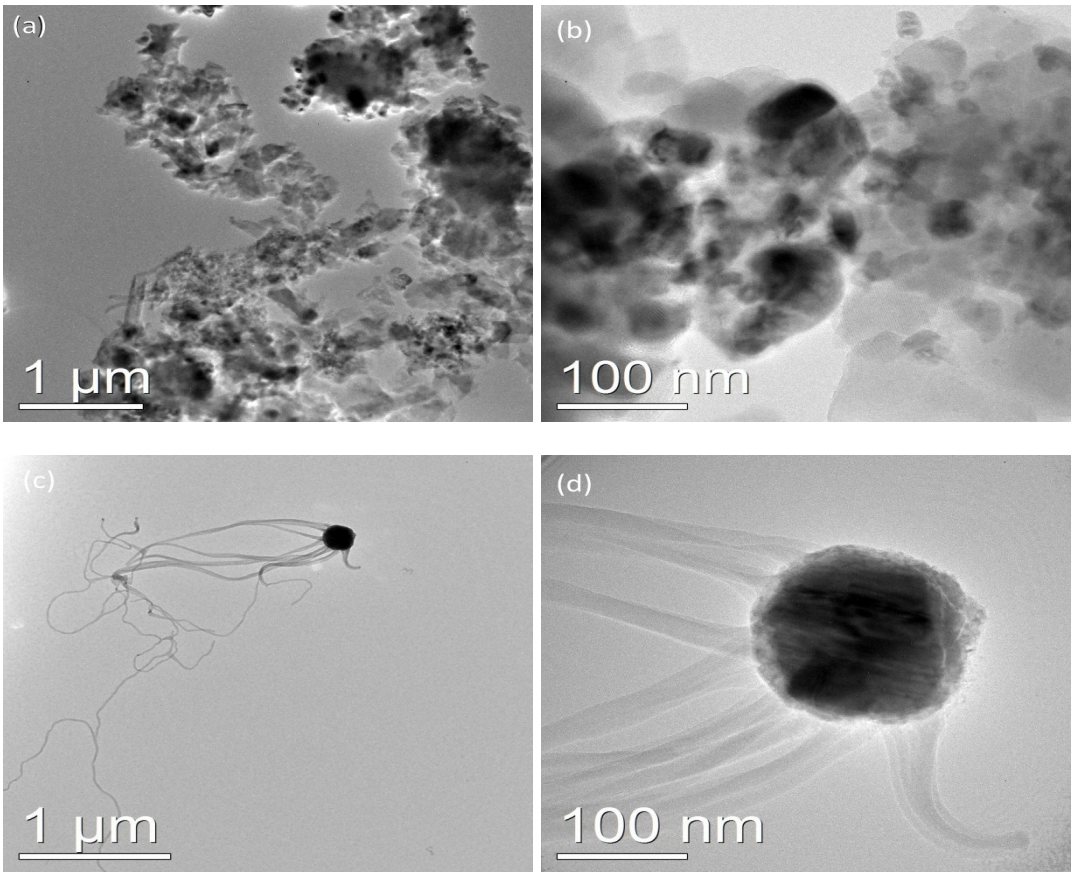


Figure 8.15: TEM images of the 20 wt% of FeO_x/HZSM-5-heavy oil samples (a) and (b) treated at 490-500°C, (c) and (d) showing the core-shell structure of the iron-zeolite surrounded by the carbon nanotubes of treated at 900-1000°C.

The Impregnation of Cobalt Oxide into HZSM-5

The impregnation of cobalt into zeolite has been studied extensively. Two different forms of cobalt species and cobalt oxide particles, at least, can be formed over the external surface and in the channels of the zeolite. The cobalt oxide species might demonstrate different catalytic activity in addition to magnetic properties, especially those impregnated with higher cobalt content [30–32].

Three different loading levels of cobalt have been impregnated into zeolite to be examined for heavy oil cracking under microwave irradiation. The prepared catalysts have been characterised using XRD before adding the heavy oil.

The XRD patterns in Figure 8.16 represent the incorporation of cobalt oxide into HZSM-5 and are compared with pure HZSM-5. It can be seen that all the characteristic peaks of the ZSM-5 catalysts are observed in both cobalt modified catalysts. However, the intensity was slightly reduced in the cobalt doped patterns. This decrease in crystallinity can be attributed to the cobalt particles present inside the zeolite pores.

Cobalt oxide, Co_3O_4, may also be identified when the XRD pattern is compared to the pure HZSM-5. Diffraction peaks at $2\theta = 31.3^o$, 37.2^o, 44.8^o and 59.8^o are characteristic of the presence of the cobalt oxide which might be indication of theCo_3O_4 spinel phase. These peaks become stronger in the case of 20 wt.% Co/HZSM-5 which might be attributed to the presence of more cobalt oxide particles, which can be indicated by the clear grey colour of the calcined catalyst.

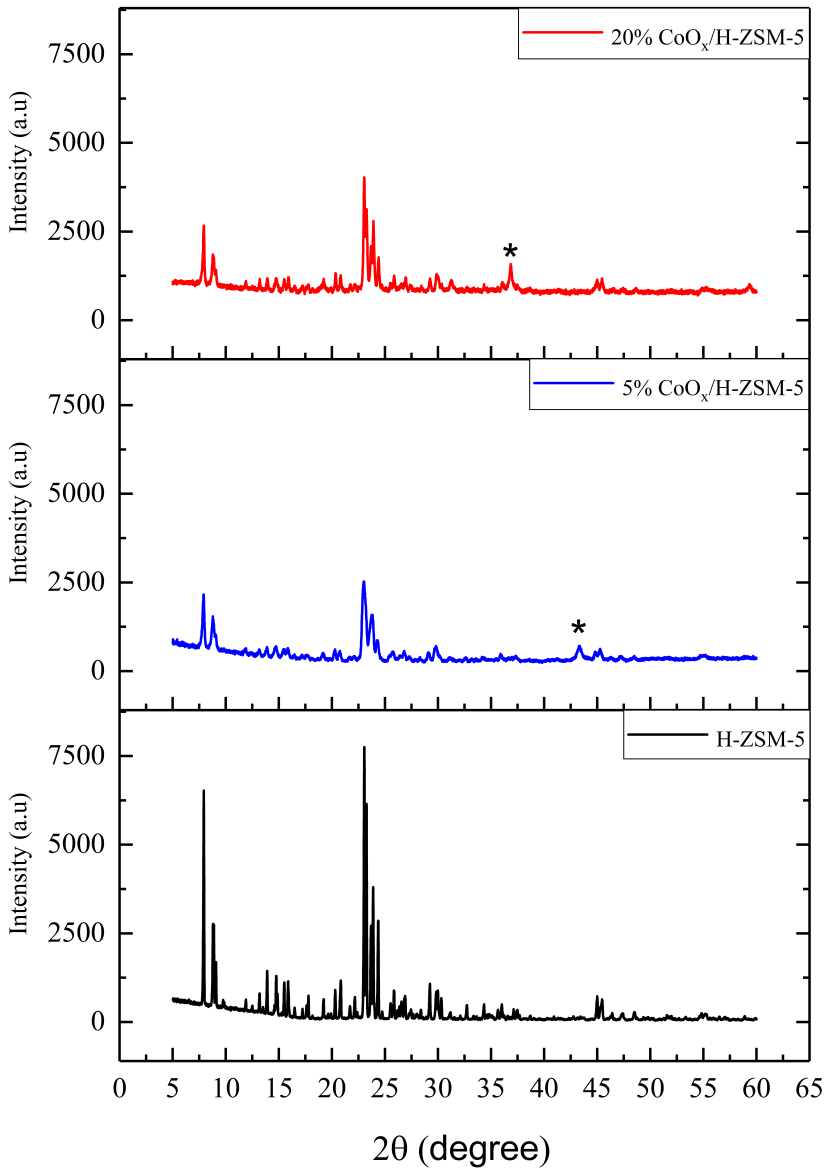


Figure 8.16: XRD analysis of 5 wt.% and 20 wt.% CoO_x/HZSM-5, (*) indicates the presence of the cobalt oxides species

The cobalt catalysts have been impregnated with 25 wt.% of the heavy oil and placed in the

microwave reactor. Figure 8.17 represents the gas products volume for the three different-doping levels of cobalt oxide into HZSM-5 catalysts. The catalytic cracking of heavy oil over 5, 10, 20 wt.% of CoO_x/HZSM-5 were examined under microwave radiation. The results indicate that the products distribution was directly affected by the temperature and the type of metal loading in the catalysts.

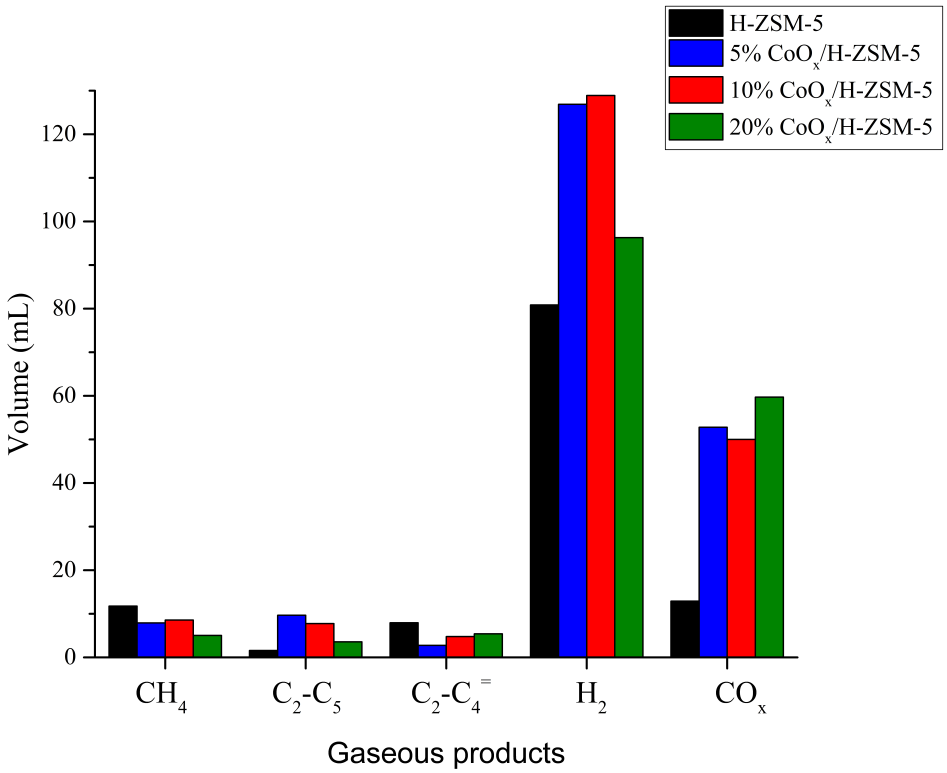


Figure 8.17: Volume of different gas compositions produced from the heavy oil cracking reaction over CoO_x/HZSM-5 catalysts with different loading of cobalt and 25 wt% of heavy oil.

It can be seen that the catalytic activity to produce hydrogen increases as the metal loading increases. This can be attributed to the rise of the active sites on the catalysts. Nevertheless, for a higher metal loading, i.e. 20 wt.% of cobalt, a noteworthy decrease can be observed, which may be attributed to some sort of catalytic deactivation resulted from overloading of metal that blocks the active site on the catalyst.

It has been found that the cobalt is a great microwave absorber even at a lower microwave power. In general, metal oxides, such as ferrites and cobalt materials are exhibit some magnetic loss in the microwave region which is induced by the electron spin resonance [33]. Thus, they can be used as microwave additives to the solid catalysts to enhance their dielectric heating. This can be assigned to the presence of magnetite Fe_3O_4 and Co_3O_4, but not Fe_2O_3 and Co_2O_3 as they are not magnetic materials [34].

The high tendency of the metal particles to absorb microwave results in the formation of hot spots, which could be effective during H_2 production. Under these severe conditions, more cracking of light gases can be noticed. In addition, slightly higher hydrogen volume was produced in comparison to the iron apart from the 20 wt.%. Some of the hydrogen could be consumed during the reduction of the cobalt oxide particles resulting in more formation of the CO_x as the metal loading increases. It suggests that a great deal of energy could be saved when doping the zeolite with cobalt oxide. However, the reaction system, when operating at this high temperature, is not favouring the formation of olefins. Also, under high temperatures, the catalyst would be deactivated rapidly.

The products distribution of the CoO_x/HZSM-5 catalysts are presented in Table 8.3.

Table 8.3: Product distribution (wt%) of HZSM-5 doped with different levels of cobalt oxides.

Product	5wt.% CoO_x/HZSM-5	10wt.% CoO_x/HZSM-5	20wt.% CoO_x/HZSM-5
liquid (wt.%)	73.6	78.0	94.0
H_2(wt.%)	7.1	6.0	1.5
CH_4 (wt.%)	3.5	3.0	0.6
olefins (wt.%)	2.8	4.2	1.6
paraffins (wt.%)	12.9	8.4	1.3
gas volume (mL)	200	200	170
the coke content by TGA (wt.%)	10.1 ±1.0	9.8 ±1.0	6.7 ±1.0

Figure 8.18 illustrates the XRD patterns of the spent catalysts after microwave irradiation. It is clear that the zeolite structure is losing considerable amount of crystallinity due to the formation

of amorphous coke materials. Metallic cobalt can also be observed, which indicates he reduction of cobalt oxide and the noted release of CO_x.

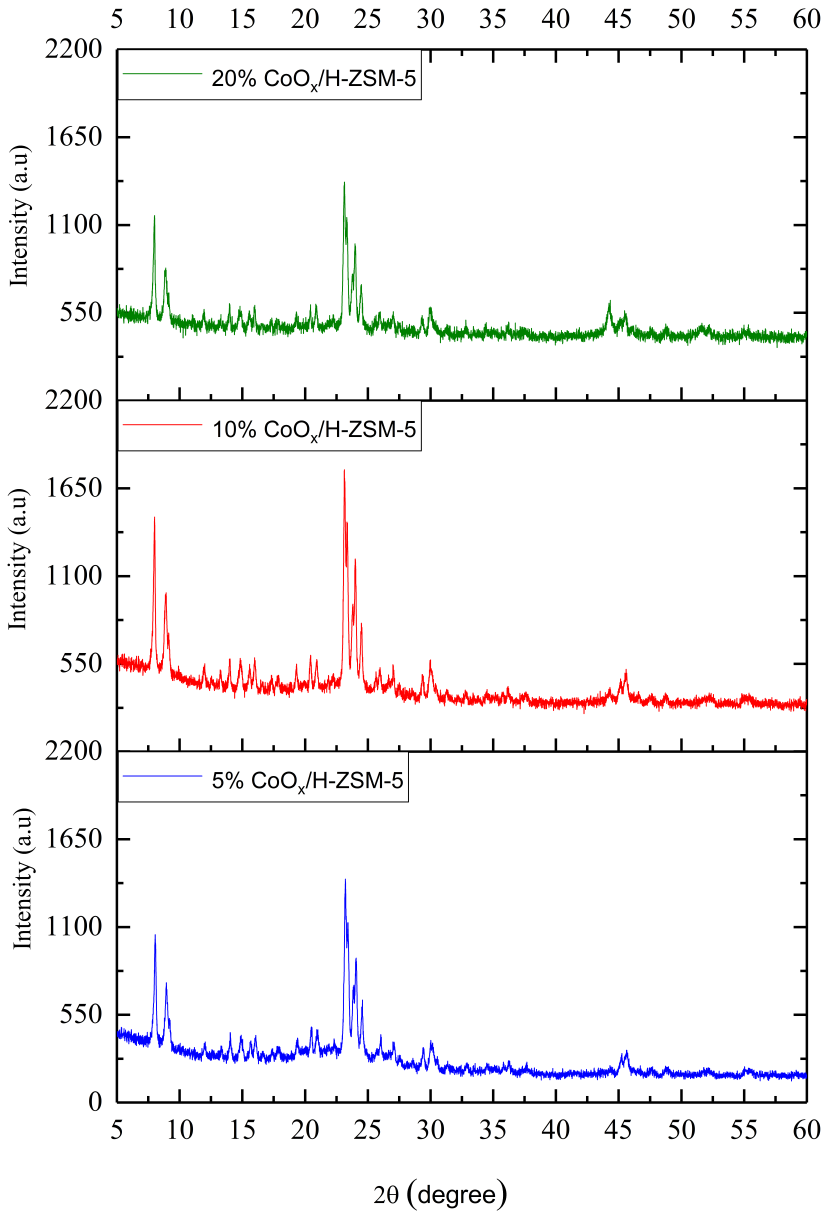


Figure 8.18: XRD pattens of the spent cobalt samples, illustrating a clear decease in the peaks intensity as result of coke formation

8.3.3 The Impregnation of Lanthanum Oxide into HZSM-5

Rare earth metals have been found to be effective catalysts in the petrochemical industry, and particularly in catalytic cracking [35]. They can affect the acidity, structure and catalytic performance of the HZSM-5 zeolite. Wang *et al.* have investigated the catalytic performance of rare earth modified HZSM-5 for light olefins production [36]. The results imply that rare earth doped HZSM-5 catalyst can remarkably increase the selectivity of light olefins; thus, decreasing the yield of aromatics in the catalytic cracking of butane. Moreover, in thermal reactions, it has been found that the role of lanthanides on alumina support can enhance the thermal stability and catalytic properties of the catalysts [37].

Thus, lanthanum has been impregnated into HZSM-5 zeolite to examine the cracking reaction of heavy oil under microwave conditions. Figure 8.19, represents the XRD patterns for the unmodified and the lanthanum-loaded HZSM-5 catalyst.

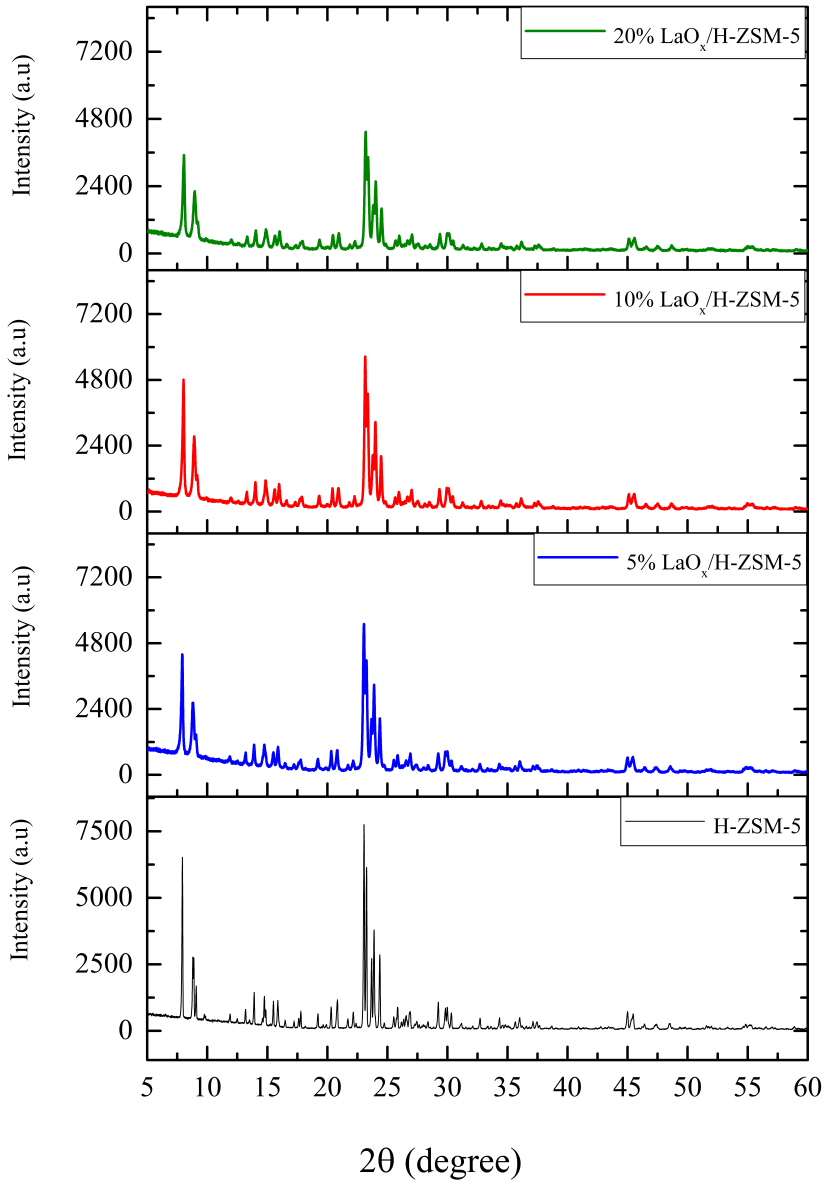


Figure 8.19: The XRD patterns of the parent HZSM-5 and the LaO_x/HZSM-5 with three different loading levels of lanthanum.

All patterns look very similar, which indicates that there is no significant loss of the zeolite

structure or crystallinity. However, the intensity of the peaks between (2θ = 8° - 28°) which are considered the main characteristic of the HZSM-5 zeolite have slightly decreased in the lanthanum-doped form of the zeolite. Generally, the XRD low-angle HZSM-5 peaks intensities are sensitive to the presence of particles inside the channels, which are the La^{3+} species that entered the pores during the impregnation process. It should be considered that the La^{3+} cations have an average diameter of 0.119 nm, which is smaller than the pore size of the HZSM-5 as the structure of the zeolites consists of pores with an opening size of 5–5.5 Å [38]. However, not all of the lanthanum species could have entered the zeolite channels. Some lanthanum oxides species are located on the external surface of HZSM-5 zeolite. Overall, the XRD cannot detect the particles that are smaller than 3 nm [39, 40].

The peak intensity of the modified zeolite are found to be decreased less in the case of the 10% by weight loading of LaO_x/HZSM-5 followed by 5 wt.% of lanthanum, whereas the highest decrease can be seen in the 20 wt.% LaO_x/HZSM-5. This suggests that the metal-zeolite interaction could affect the crystallinity of the zeolite. Moreover, the higher metal oxide dispersion is in 10 wt.% LaO_x/HZSM-5, which results from the greater interaction with the zeolite [41].

The microwave assisted reactor was utilised in the heavy oil processing experiments operated in batch mode. The obtained mass balance of the three systems were kept at 97%. The volume of the gaseous product obtained from heavy oil cracking over different loading levels of lanthanum into zeolite is shown in Figure 8.20.

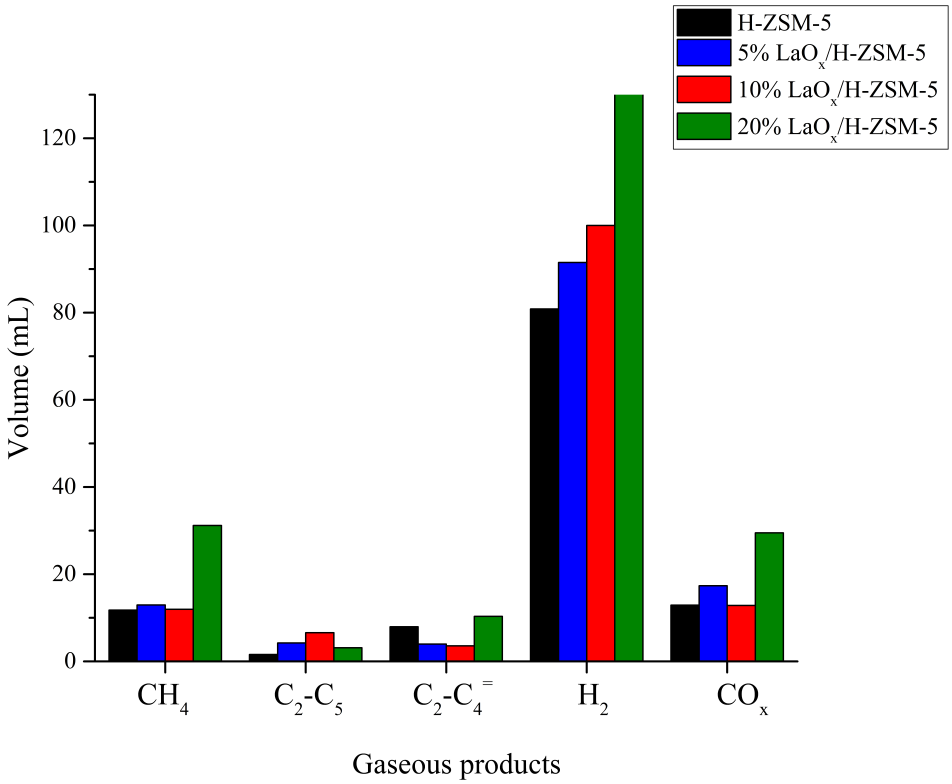


Figure 8.20: The volume of the produced gas composition from the catalytic processing of 25 wt% of heavy oil over 5, 10, 20 wt% of LaO_x/HZSM-5 compared with the pure zeolite.

The illustrated results of the gas products resulting from the heavy oil cracking over different LaO_x/HZSM-5 were increasing with the lanthanum oxide loading. The average temperatures of the reaction bed were in the range of 400°C for the three cracking processes. However, the local temperature of some of the micro-regions could be higher than the detected temperature, due to the formation of hot spots. The three modified zeolites show a large volume of hydrogen; however, is it slightly less than the transition metal oxide case, followed by methane, then light-olefins (ethylene, propylene, and butene), and light paraffins (ethane, propane, butane, and pentane). The remarkable result of this reaction is the high hydrogen concentration. The hydrogen volume in a presence of metal appears to be higher than that of the unmodified HZSM-5 cracking reaction.

The products selectivity of the cracked heavy oil reaction over LaO_x/HZSM-5 catalysts are presented in Table 8.4.

Table 8.4: Product distribution (wt%) of the heavy oil cracking reactions over La oxide modified HZSM-5.

Product	5 wt.% LaO_x/HZSM-5	10 wt.% LaO_x/HZSM-5	20 wt.% LaO_x/HZSM-5
liquid (wt.%)	78.0	74.0	71.7
H_2(wt.%)	5.6	6.3	7.4
CH_4 (wt.%)	6.4	6.2	10.7
olefins (wt.%)	3.1	3.9	7.1
paraffins (wt.%)	7.2	10.0	3.0
gas volume (mL)	130	135	250
coke content by TGA (wt.%)	9.1 ±1.0	9.3 ±1.0	11.6 ±1.0

XRD patterns of the spent oil/LaO_x/HZSM-5 samples are illustrated in Figure 8.21. Overall, it can be seen that all the peaks are exhibiting an obvious loss in zeolite crystallinity after microwave treatment, moreover, to the coke formation over the catalysts.

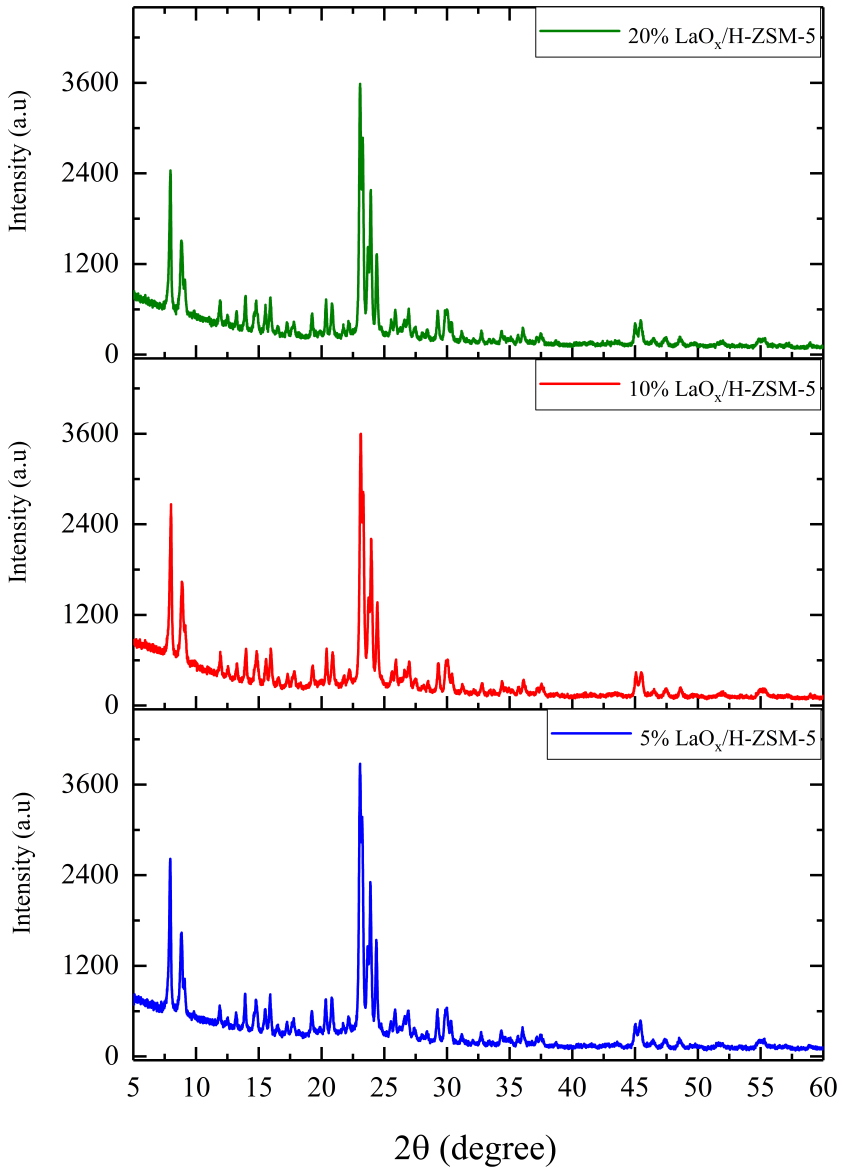


Figure 8.21: XRD patterns of different LaO_x doping levels into zeolite after microwave cracking reaction of heavy oil.

Overall, in such a single mode applicator where the field is concentrated at a certain point,

higher average reaction temperatures could be reached [14]. This high applied electric field can be correlated with possible polarisation mechanisms of some metallic additives into zeolite catalysts, which can significantly accelerate the dielectric heating and results in some localised heating that can influence the hot spot formation and thus the decomposition processes. Furthermore, this high electric field could be associated with plasma generation and field ionisation which might contribute to the decomposition processes as well.

8.3.4 Enhanced Batch Reactor System for Catalytic Activity Evaluation

A significant portion of the discussion above has been devoted to the utilisation of a microwave-assisted reactor. In order to examine the catalytic activity under microwave process, the batch reactor has been modified to allow the gas products to be collected at different stages of the reaction.

Iron oxide modified HZSM-5 with three doping levels of 5, 10, 20 wt.% of impregnated heavy oil zeolites have been produced under microwave radiation. The experiments were conducted under the same applied microwave power. The performance of the three FeO_x/HZSM-5 is presented in Figure 8.22.

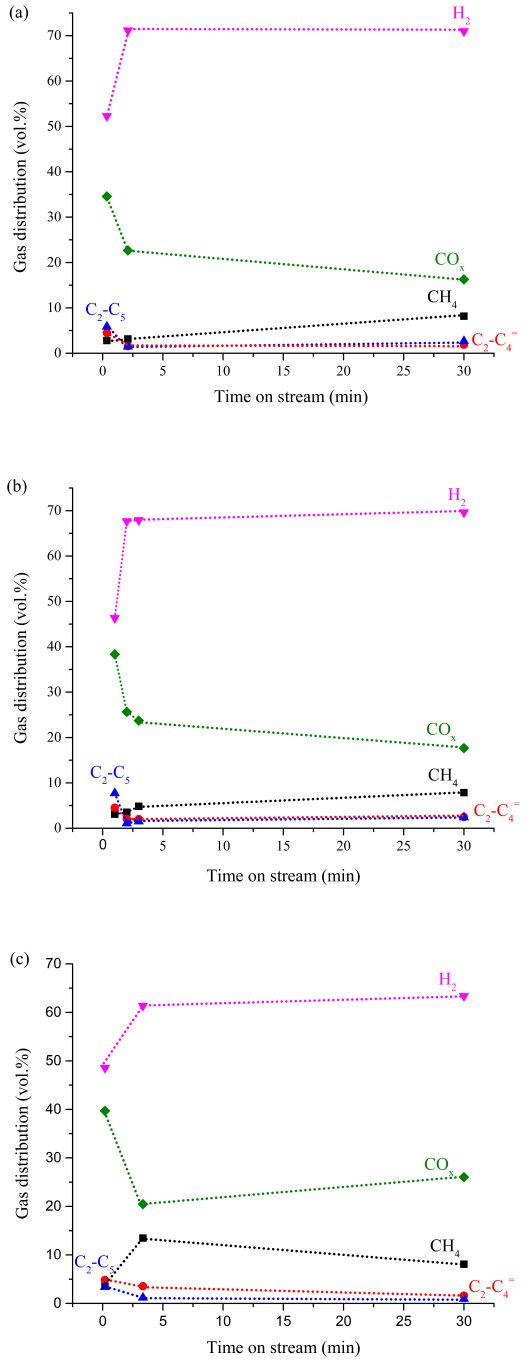


Figure 8.22: Evaluation of the gas compositions for the (a) 5 wt%, (b) 10 wt%, (c) 20 wt% of FeO_x/HZSM-5 heavy oil impregnated samples under batch operation conditions as a function of time on stream at 450°C.

The analysis of the gaseous products shows that the collected samples were composed of H_2, CO_x, CH_4, $C_2 - C_5$, and $C_2 - C_4^=$. The concentrations of the components are shown above. It was noticed that as the temperature increases, the hydrogen concentration increases as well. Also, the reaction path favours the production of hydrogen in the first minute of reaction time. The rapid production of the hydrogen is generally associated with coke formation and catalyst decomposition. However, it can be seen that the hydrogen concentration is fairly steady over the 30 minutes of the reaction time. The amount of light olefins and paraffins are found to decrease as the reaction temperature increases. On the other hand, the concentration of methane is found to increase slightly with time, which can indicate a possible C-C cracking taking a place within the system. A continuous flow system would enable more detailed examination of the catalytic activity and deactivation process.

8.3.5 Adopting a Continuous Flow System into Microwave Reactor

Significant efforts have been applied into this microwave system and this system has been developed to the several configurations during the previously stated experiments. The great motivation behind these steps was to examine the simulation of the scale-up of the furthest processes. As an initial experiment of this system, a crude oil has been processed instead of the heavy oil due to the advantages of simplicity in handling and pumping.

The system has been purged with argon for 15 minutes to perform the reaction under inert atmosphere. The reactor has been equipped with a pump that continuously feeds the crude oil into the system. The microwave radiation started when the catalyst reached the desired reaction temperature before the oil pump was turned on. This meant that the crude oil travelled down to the pre-irradiated hot catalyst. The gas products were collected at different times and analysed using GC. The heavier products would accumulate in an ice cold trap and analysed using GC/MS. After completing the reaction, the mass balance error deviation was found to be 4%. Figure 8.23 shows the modified microwave reactor with the flow system for cracking reactions.

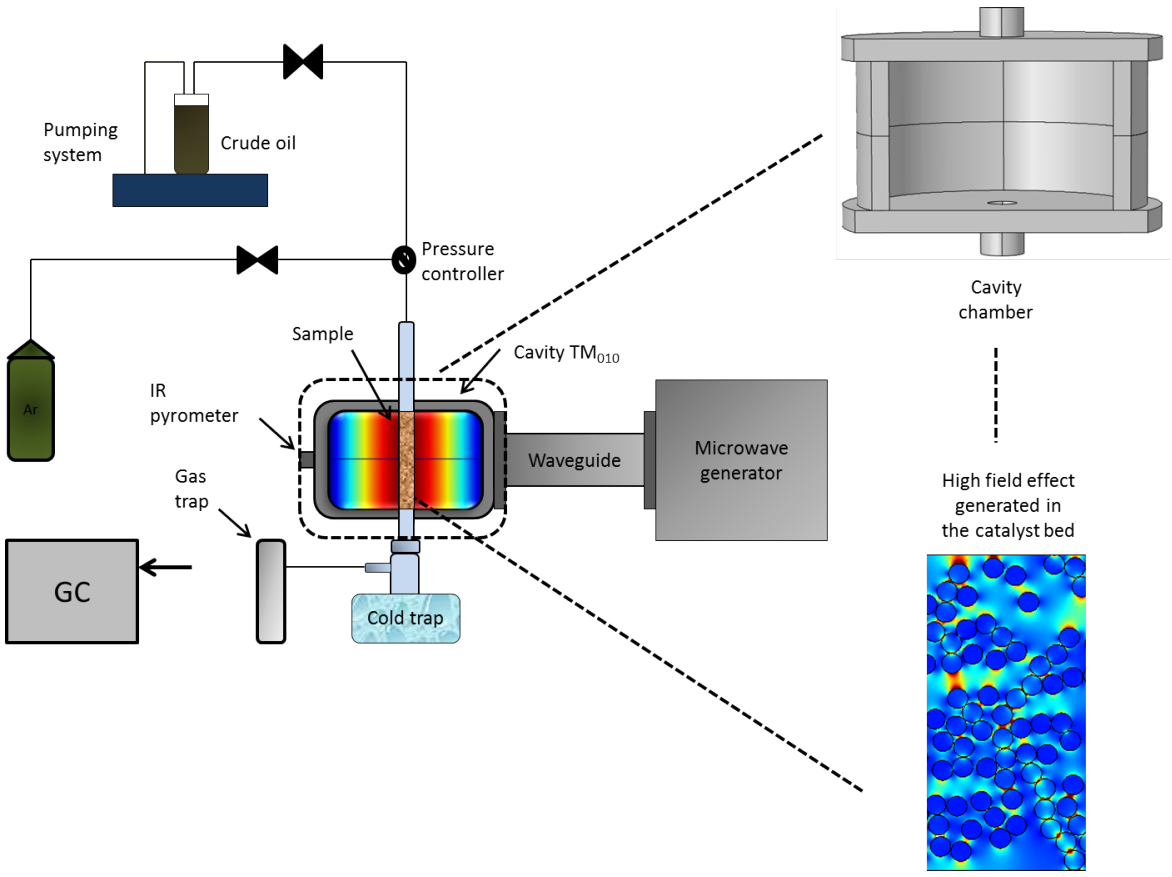


Figure 8.23: Schematic design of the continuous flow system representing a COMSOL simulated high field distribution of the generated electromagnetic field in the catalyst bed.

The 20 wt.% of iron oxide modified HZSM-5 zeolites has been heated up to 450°C before pumping the crude oil. The flow of oil was set to 0.1 mL/min for a reaction time of 20 minutes. The performance zeolites in the catalytic cracking of crude oil and the gaseous concentration are presented in Figure 8.24.

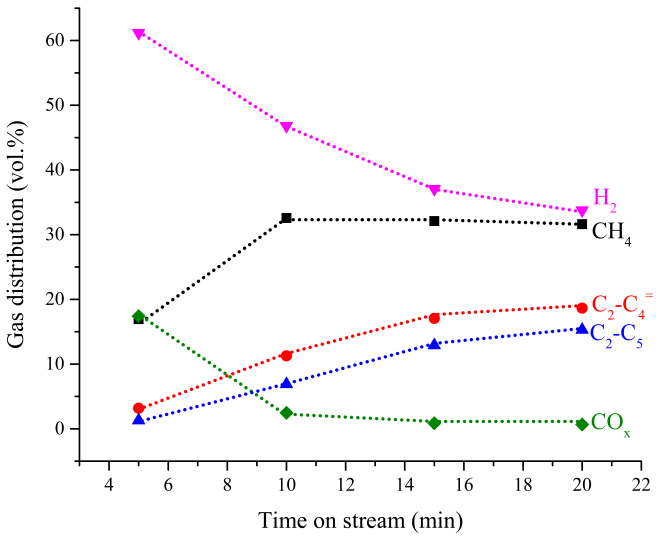


Figure 8.24: Gas composition of the proceed crude oil over 20 wt% FeO_x/HZSM-5 under continuous flow operation conditions.

The results indicates that there is a significant change in catalytic activity and selectivity when the batch and continuous flow systems are compared. The concentration of total light olefins ($C_2 - C_4^=$) and paraffins is found to increase with time. The hydrogen concentration shows the opposite trend as it starts with fairly high concentration (similar to the one from the batch system) and decreases as the reaction goes on. This indicates that the C-C bond breaking is favoured more over the C-H bond breaking with time. This might be attributed to the formation of more coke that blocks the active sites on the zeolite in addition to the metal oxide particles.

There might be several factors that can explain the differences in reaction path and products behaviour between the two systems. In the batch reactors, a small amount of heavy oil is deposited on the sample, as large volumes make the reaction difficult to proceed effectively. On the other hand, with the flow system it is more efficient to treat a larger amount of feedstock. This allows for the collection of the produced liquid materials which are presented in Figure 8.25. The products are generally classified according to their carbon number into six groups: gases, gasoline (C_6–C_9), kerosene (C_7–C_{13}), gas oil (C_{14}–C_{20} and C_{21}–C_{35}), and heavy oil (C_{36}–C_{44} and above C_{45}). It can

be seen from Figure 8.25 that the main products are falling in the gasoline to diesel range.

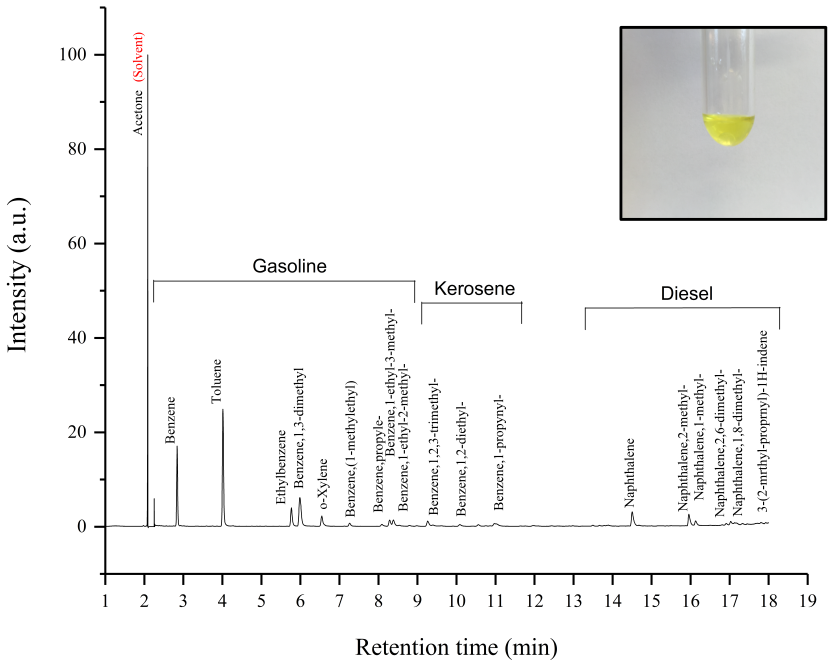


Figure 8.25: Qualitative analysis of the GC–MS data for the collected liquid product of the processed crude oil under microwave irradiation, the top corner image shows the liquid product obtained after completing the reaction.

The configurations of the reactors have two different contact times between the oil and the catalysts, which is markedly larger in the batch system. This also might have an influence of the cracking behaviour of the oil over zeolites.

Both systems show a good concentration of certain products. If hydrogen or olefins are desired then the required system can be operated. Although, the methane concentration appears very high in comparison to the batch system, and the production of hydrogen seems to decrease with reaction time.

The flow system was found to be more complex in microwave processing due to the extra

momentum transfer of the microwave energy to heat the liquid/solid mixture. Moreover, it can be difficult to process solids and highly viscous liquids.

Lastly, the continuous flow system can save some of the time which could be spent in a simple batch system when scale-up processes are taken.

8.4 Conclusions and Future Work

Microwave processing of heavy oil using a bench-top single-mode applicator has been demonstrated in this chapter. The microwave reactor has gone under several development stages from batch to continuous flow mode. The main focus is to conduct and explore the product distributions resulting from the heavy oil cracking over different modified zeolites under microwave radiation.

Zeolites in general were found to be good catalysts for cracking reactions due to their acidic nature. Impregnating zeolites with transition and rare earth metals oxides may enhance their acidic characteristics and introduce more active transition metal catalytic sites [41].

From the conducted experiments, the GC results of heavy oil cracking showed that the amount of produced hydrogen was significantly high and overall it increases as the metal loading increases. This suggests that the C-H bond breaking dominates under microwave irradiation. The highest hydrogen volume was achieved using 20 wt.% of LaO_x/HZSM-5 at an apparent temperature of 400°C. The dehydrogenation process is associated with deposition of coke and rapid deactivation of the catalysts.

HZSM-5 doped with transition metals (Fe, Co) oxides were found to be a good microwave absorber due to the magnetic properties of the oxides. The highest concentration of CO_x was found in both iron and cobalt catalysts which increases as the metal loading increases in the zeolite due to the partial reduction of the metal oxide to metal and metal carbide.

Overall, the IR pyrometer showed a range of reaction temperatures between 350 and 600°C which is the surface temperature of the detected area of the catalyst bed. However, it is believed that the microwave radiation of heterogeneous catalysts results in localised heating and formed hot spots in the catalyst bed. The temperature of these hot spots should be higher than the temperature observed in the pyrometer. The formation of hot spots in the catalyst could be the reason behind the dehydrogenation reaction and high catalytic decomposition. Moreover, the applied electric

field might result in surface polarisation of the metallic particles within the catalyst. This can be readily observed in transition metal doped zeolite compared to the pure or La-doped HZSM-5 where the dielectric heating is significantly enhanced and where the ionised field could contribute to the decomposition processes.

The product distribution of the time on stream reactions showed that the highest concentration of the hydrogen is being produced within less than 5 minutes of the reaction time. On the other hand, the methane formation starts at a low concentration and increases with time indicating that the favoured mechanism of bond breaking is the C-H bond followed by the C-C bond as time increases. The selectivity for both light olefins and paraffins was found to decrease with time.

Under continuous flow of crude oil, the highest concentration of hydrogen is produced during the first 5 minutes of the reaction and it clearly decreased with time. Also, most of the CO_x is being produced at the beginning of the reaction and it decreased to even lower concentration with time. On the other hand, the methane, light olefins and paraffins concentrations are found to increase as the reaction goes on which is the opposite case for batch system for olefins and paraffins.

The dramatic difference between the products distribution using batch and continuous flow could be attributed to secondary cracking reactions that take place in the continuous flow and led to the production of heavy compounds. These heavy compounds are influencing the formation and growth of coke molecules inside the zeolite porous structure. Moreover, the contact time between the catalyst and the heavy oil might have an effect on the observed differences in chemical composition between the two reactor systems.

The development of the continuous flow microwave-assisted reactor is an important step to the industrial scale-up of the process. More catalysts and experiments need to be conducted under flow conditions before moving to any scale-up stage. Temperature detecting of the reactor bed needs to be replaced with more accurate systems that allow for measuring the catalyst and the hot spot temperatures.

Bibliography

[1] C. Difiglio. Oil, Economic Growth and Strategic Petroleum Stocks. *Energy Strategy Reviews*, 5:48–58, 2014.

[2] H. Tahmassebi. OPEC and ASIA: The Changing Structure of the Oil Market Crude Oil and Product Value Differentials: Historical Perspective and Outlook. *Energy*, 11:343–359, 1986.

[3] H. Konno, R. Ohnaka, J. Nishimura, T. Tago, Y. Nakasaka, and T. Masuda. Kinetics of the Catalytic Cracking of Naphtha Over ZSM-5 Zeolite: Effect of Reduced Crystal Size on the Reaction of Naphthenes. *Catalysis Science and Technology*, 4:4265–4273, 2014.

[4] S.A.P. da Motaa, A.A. Mancioa, D.E.L. Lhamas, D.H. de Abreua, M.S. da Silvaa, W.G. dos Santos, D.A.R. de Castroa, R.M. de Oliveira, M.E. Araujoa, Luiz E.P. Borges, and N.T. Machado. Production of Green Diesel by Thermal Catalytic Cracking of Crude Palm Oil (Elaeis Guineensis Jacq) in a Pilot Plant. *Journal of Analytical and Applied Pyrolysis*, 110:1–11, 2014.

[5] M. Greavesb A. Harta and J. Wood. A Comparative Study of Fixed-bed and Dispersed Catalytic Upgrading of Heavy Crude Oil Using-CAPRI. *Chemical Engineering Journal*, 282:213–223, 2015.

[6] Y. Zhang, D. Yu, W. Li, S. Gao and G. Xu. Bifunctional Catalyst for Petroleum Residue Cracking Gasification. *Fuel*, 117:1196–1203, 2014.

[7] J.G. Seebold, R.T. Waibel, and T.L. Webster. Control Refinery NOx Emissions Cost-Effectively. *Hydrocarbon Processing*, 11:55–59, 2001.

[8] C. Lee, and J. Chih-Ju. Using Low Energy-Consuming Microwave Technology to Regenerate High Carbon-Containing Pt Catalyst. *Canadian Center of Science and Education*, 3:41–47, 2014.

[9] J. Salimon, N. Salih and E. Yousif. Industrial Development and Applications of Plant Oils and

Their Biobased Oleochemicals. *Arabian Journal of Chemistry*, 5:135–145, 2012.

[10] H. Shang, Y. Liu, J. Shi, Q. Shi and W.I Zhang. Microwave-Assisted Nickel and Vanadium Removal from Crude Oil. *Fuel Processing Technology*, 142:250–257, 2016.

[11] C. Lucas-Torres, A. Lorente, B. Cabanas and A. Moreno. Microwave Heating for the Catalytic Conversion of Melon Rind Waste into Biofuel Precursors. *Journal of Cleaner Production*, pages 1–11, 2016.

[12] O. Muraza, A. Abdul-lateef, T. Tago, A.B.D. Nandiyanto, H. Konno, Y. Nakasaka, Z.H. Yamani and T. Masuda. Microwave-Assisted Hydrothermal Synthesis of Submicron ZSM-22 Zeolites and their Applications in Light Olefin Production. *Microporous and Mesoporous Materials*, 206:136–143, 2015.

[13] B. Hascakir, C. Acar, and S. Akin. Microwave-Assisted Heavy Oil Production: An Experimental Approach. *Energy & Fuels*, 23:6033–6039, 2009.

[14] A. Stonoga, V. Silva, R. Weinschutz, C. Yamamoto and L. Jr. Catalytic Cracking of Light Gas Oil Using Microwaves as Energy Source. *Fuel*, 106:632–638, 2013.

[15] N. Mo and P.E. Savage. Hydrothermal Catalytic Cracking of Fatty Acids with HZSM-5. *ACS Sustainable Chemistry & Engineering*, 2:88–94, 2014.

[16] Hongchuan Xin, Arjan Koekkoek, Qihua Yang, Rutger van Santen, Can Li and Emiel J. M. Hensen. A Hierarchical Fe/ZSM-5 Zeolite with Superior Catalytic Performance for Benzene Hydroxylation to Phenol. *Chem. Commun.*, 24:7590–7592, 2009.

[17] B. Thomas, B.B. Das, and S. Sugunan. Rare Earth Exchanged (Ce^{+3}, La^{+3} and Re^{+3}) H-Y Zeolites as Solid Acid Catalysts for the Synthesis of Linear Alkyl Benzenes. *Microporous and Mesoporous Materials*, 95:32–338, 2006.

[18] D. Goto, Y. Harada, Y. Furumoto, A. Takahashi, T. Fujitani, Y. Oumi, M. Sadakane, and T. Sano. Conversion of Ethanol to Propylene Over HZSM-5 Type Zeolites Containing Alkaline Earth Metals. *Appl. Catal. A: Gen*, 383:89–95, 2010.

[19] C. Mei, P. Wen, Z. Liu, H. Liu, Y. Wang, W. Yang, Z. Xie, W. Hua and Z. Gao. Selective Production of Propylene from Methanol: Mesoporosity Development in High Silica HZSM-5. *J. Catal.*, 258:243–249, 2008.

[20] D.R Dubois, D.L. Obrzut, J. Liu, J. Thundimadathil, P.M. Adekkanattu, J.A.Guin, A. Punnoose and M.S. Seehra. Conversion of Methanol to Olefins Over Cobalt-,manganese- and

Nickel-incorporated SAPO-34 Molecular Sieves. *Fuel Process. Technol.*, 83:203–218, 2003.

[21] N. Rahimi and R. Karimzadeh. Catalytic Cracking of Hydrocarbons Over Modified ZSM-5 Zeolites to Produce Light Olefins: A Review. *Applied Catalysis*, 398:1–17, 2011.

[22] S. Jiang Y. Yan and H. Zhang. Catalytic Wet Oxidation of Phenol with Fe-ZSM-5 Catalysts. *RSC Adv.*, 6:3850–3859, 2016.

[23] M. Rostamizadeh and F. Yaripour. Bifunctional and Bimetallic Fe/ZSM-5 Nanocatalysts for Methanol to Olefin Reaction. *Fuel*, 181:537–546, 2016.

[24] X. Lia, B. Shena, and C. Xu. Interaction of Titanium and Iron Oxide with ZSM-5 to Tune the Catalytic Cracking of Hydrocarbons. *Applied Catalysis A: General*, 375:222–229, 2010.

[25] S. Horikoshi, M. Kamata, T. Mitani, and N. Serpone. Control of Microwave-Generated Hot Spots Part IV. Generation of Hot Spots in Dispersed Catalyst Particulates and Factors That Affect Catalyzed Organic Syntheses in Heterogeneous Media. *American Chemical Society*, 53:14941–14947, 2014.

[26] X. Zhang and D.O. Hayward. Applications of Microwave Dielectric Heating In Environment-related Heterogeneous Gas-phase Catalytic Systems. *Inorganica Chimica Acta*, 359(11):3421–3433, 2006. Protagonists in Chemistry: Professor D.M.P. Mingos.

[27] X. Zhang, C. Lee, D. M. P. Mingos, and D. O. Hayward. Oxidative Coupling of Methane Using Microwave Dielectric Heating. *Applied Catalysis A: General*, 249:151–164, 2003.

[28] D. Mores, J. Kornatowski, U. Olsbye, B.M. Weckhuysen. Coke Formation During the Methanol-to-Olefin Conversion: In Situ Microspectroscopy on Individual H-ZSM-5 Crystals with Different Bronsted Acidity. *Chem. Eur. J*, 17:2874–2884, 2011.

[29] Th. Bein, G. Schmiester, and P. A. Jacobs. Characterization of a New Iron-on-Zeolite Y Fischer-Tropsch Catalyst. *The Journal ofPhysica1 Chemistry*, 90:4851–4856, 1986.

[30] L.B. Pierella, C. Saux, S.C. Caglieri, H.R. Bertorello and P.G. Bercoff. Catalytic Activity and Magnetic Properties of Co-ZSM-5 Zeolites Prepared by Different Methods. *Applied Catalysis*, 347:55–61, 2008.

[31] H.R. Bertorello, L.B. Pierella, P.G. Bercoff, C. Saux and J.P. Sinnecker. Magnetic Behavior of Co Clusters Embedded in A Zeolite Matrix. *Physica B: Condensed Matter*, 354:137–140, 2004.

[32] C. Chupin, A.C. van Veen, M. Konduru, J. Despres and C. Mirodatos. Identity and Location of Active Species for NO Reduction by CH_4 Over Co-ZSM-5. *Journal of Catalysis*, 241:103–114,

2006.

[33] Z. Shi, J. Zhang, D. Gao, Z. Zhu, Z. Yang, Z. Zhang, and D. Xue. Magnetic Resonance of the $NiFe_2O_4$ Nanoparticles in the Gigahertz Range. *Nanoscale Research Letters.*, 8:1–5, 2013.

[34] S. Horikoshi and N. Serpone. Role of Microwaves in Heterogeneous Catalytic Systems. *Catalysis Science and Technology*, 4:1197–1210, 2014.

[35] M. Weihe, M. Hunger, M. Breuninger, H.G. Karge and J. Weitkamp. Influence of the Nature of Residual Alkali Cations on the Catalytic Activity of Zeolites X, Y, and EMT in their Bronsted Acid Forms. *Journal of Catalysis*, 198:256–265, 2001.

[36] W. Xiaoning, Z. Zhen, X. Chunming, D. Aijun, Z. Li and J. Guiyuan. Effects of Light Rare Earth on Acidity and Catalytic Performance of HZSM-5 Zeolite for Catalytic Cracking of Butane to Light Olefins. *Journal of Rare Earths*, 25:321–328, 2007.

[37] L. Zhang, J. Gao, J. Hu, W. Li, J. Wang. Lanthanum Oxides-Improved Catalytic Performance of ZSM-5 in Toluene Alkylation with Methanol. *Catalysis Letters*, 130:355–361, 2009.

[38] M. Moliner. Direct Synthesis of Functional Zeolitic Materials. *ISRN Materials Science*, 2012:24, 2012.

[39] Y. Zhang, Y. Zhou, H. Liu, Y. Wang, Y. Xu and P. Wu. Effect of La Addition on Catalytic Performance of PtSnNa/ZSM-5 Catalyst for Propane Dehydrogenation. *Applied Catalysis*, 333:202–210, 2007.

[40] W. Huang, F. Gong, M. Fan, Q. Zhai, C. Hong and Q. Li. Production of Light Olefins by Catalytic Conversion of Lignocellulosic Biomass with HZSM-5 Zeolite Impregnated with 6 wt. % Lanthanum. *Bioresource Technology*, 121:248–255, 2012.

[41] J. K. Basu D. Ghosal and S. Sengupta. Application of La-ZSM-5 Coated Silicon Carbide Foam Catalyst for Toluene Methylation with Methanol. *Bulletin of Chemical Reaction Engineering and Catalysis*, 10:201–209, 2015.

Chapter 9

CONCLUSIONS AND FUTURE WORK

9.1 Conclusions

The goal of this research was to develop a basic, fundamental understanding of the interaction of microwave with heavy oil and an efficient process for heavy oil cracking in order to produce hydrogen high value light hydrocarbons. The process brings the advantages offered by microwaves by enhancing dielectric heating of both heavy oil and catalysts. We here found that one of the main characteristics of microwave heating over conventional heating is the selective heating within catalysts, which can lead to lowering the process energy [1], in addition to the enhancement in reaction rate and product selectivity [2]. Figure 9.1 highlights the differences from the heat generated in a bulk material between thermal and microwave sources.

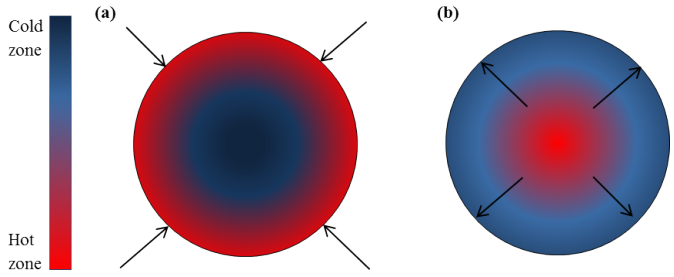


Figure 9.1: Comparison between (a) thermal heating and (b) microwave heating, where heat is transferred from the atmosphere to the bulk material in thermal heating and generated from the centre of the material in microwave heating.

The successful development of microwave technology has recently found its way to the petrochemical industrial application. However, the main challenge to be overcome in the heavy oil processing industry, besides overcoming the environmental regulations, is to balance the unstable market conditions. The current world demand for olefins and liquid fuels has steadily grown year on year. On the other hand, the fraction of the heavy oil is gradually increasing compared to the lighter ones. Moreover, microwave application applied to petrochemical processing has attracted significant research as an alternative technology for unconventional approaches.

Evaluating the dielectric properties of the processed materials is required before conducting any microwave reactions. This helps to understand and design the required catalytic properties for the desired reaction.

The cavity perturbation technique was conducted at room temperature using an aluminium cylindrical cavity at TM_{010} mode and frequency of 2.49 GHz. The measurements were performed on three types of oil samples and many other naturally-occurring model compounds in the heavy oil. The results clearly show that heavy oil exhibits low permittivity compared to the crude and pyrolysis oil. This can be attributed to the presence of large numbers of heavy fractions of alkanes, sulphur and nitrogen compounds.

Moreover, dielectric measurements were conducted on HZSM-5 zeolites. It was found that the moisture and the Si/Al ratio have an influence on the zeolite permittivity. Both heavy oil and zeolite showed low dielectric properties. However, this can be enhanced by introducing a good

microwave absorber. Later, the set up was modified to be performed at a high temperature in order to evaluate the change in dielectric properties of the heavy oil and zeolite as temperature increases. The high temperature measurement was conducted on heavy oil and zeolite samples within a copper cavity that was designed especially for this study. A correlation was observed between the change in dielectric properties and samples properties as a function of temperature. Generally, as the samples decompose and more coke is formed, the microwave suitability increases. Figure 9.2, illustrating the dielectric measurement at room temperature using cavity perturbation technique.

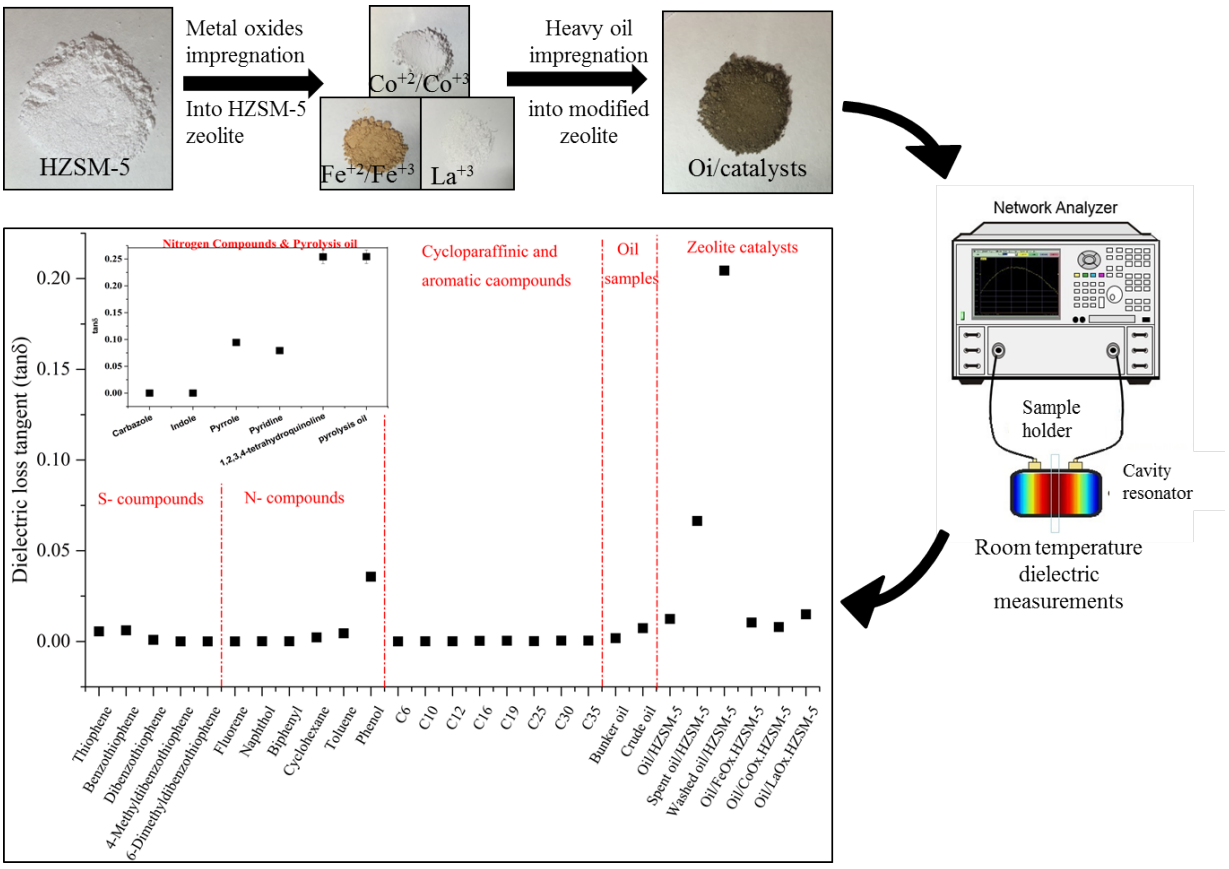


Figure 9.2: Schematic diagram summarising the performed dielectric measurements accompanied with the explored library of dielectric properties of the model compounds, oil samples, and zeoltic materials.

The next step was to design a microwave reactor that efficiently performs the cracking reactions. A bench-top single-mode applicator was designed for microwave dielectric heating experiments. The set up and parameters of the system were first evaluated by processing the decane over HZSM-5 zeolite. The first experiment was conducted to compare the thermal and microwave cracking of decane over zeolite under the same reaction conditions. It was found that there is a clear difference in product distribution resulting from both catalysts. Importantly, the main highlight was the larger hydrogen concentration and the double amount of olefins in microwave system comparing to the thermal one. Thus, the microwave system parameters were investigated to optimise the desired reaction conditions. Two factors were evaluated; the first was the parameters related to the microwave applicator, such as the input power level, heating rate, pulsing and continuous radiation. The second is related to the sample itself, such as the particle size and the dielectric properties.

The single-mode applicator was finally used to process the heavy oil over zeolite in a batch system. The implied catalysts were pure zeolite in addition to metal-doped HZSM-5. The main highlight of the products of the batch system was the high hydrogen concentration. The rapid hydrogen production was found to be influenced by either the electromagnetically-generated hotspots within the catalyst or the high-field effects which contribute to plasma generation. In addition, it was found that the HZSM-5 zeolite is a good catalyst for oil cracking to lighter compounds, and the volume of the produced gas was found to be larger when the zeolite is doped with different metals oxides. Study of zeolite doped with different iron oxides showed that the reaction under microwave conditions favours the breakage of the C-H bond rather than the C-C bond, which might be attributed to the differences in the C-X (X = H, C) bond polarisability. Hydrogen production from heavy oil has led to the discovery of successful hydrogen production from wax under microwave irradiation and it offers a new safe material for efficient hydrogen storage [3]. Figure 9.3 shows a diagram summarising the heavy oil cracking process using microwave assisted reactor.

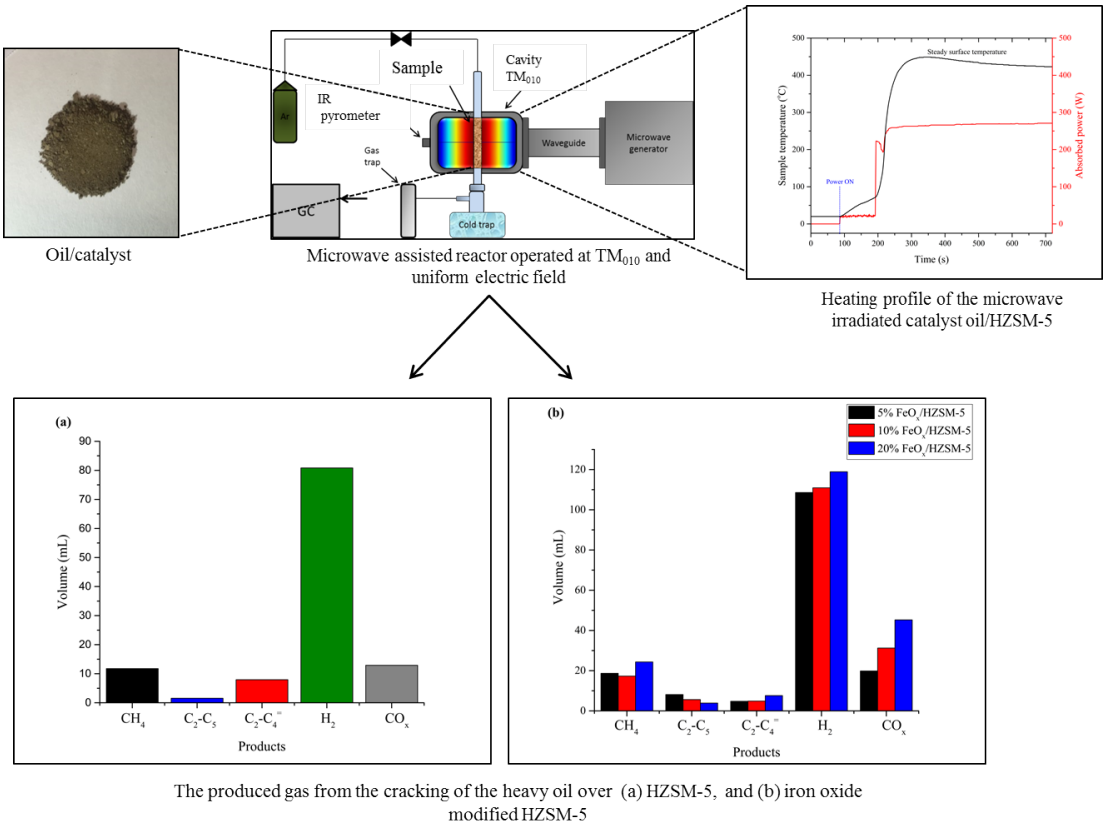


Figure 9.3: Schematic diagram represents the catalytic cracking process of heavy oil over pure and modified zeolites, the result indicated an enhanced hydrogen production in case of metal oxide doping compared to the non-modified zeolite.

The microwave applicator was then developed to perform a continuous flow of the crude oil under microwave radiation. Under the same previously operated conditions, it was found that there is a clear difference in product distribution between the batch and flow system. The flow system was found to be a better procedure to produce olefins compared to the batch. However, the hydrogen concentration appeared to decrease with time. This provided an opportunity to make a comparison study between two different systems. However, the flow system results were the initial results and need to be further investigated.

Despite the results presented by microwave cracking of heavy oil, the use of this technology in

this field has not been extensively investigated. In addition, there is a debate behind the reaction rates enhancement, whether it is attributed to the selective dielectric heating or the high heating rates, or a combination of these factors in addition to other undefined specific effects, such as bond activation. Nevertheless, it is clear that microwave heating does result in different thermal heating profiles compared to conventional techniques and this is of significant value.

9.2 Future Work

9.2.1 High Temperature Dielectric Measurements

In order to achieve greater accuracy of the measurements at high temperature, an improvement of the system needs to be undertaken. Higher order modes, such as TM_{020} and TM_{110} need to be introduced, as they will carry out more accurate high-temperature measurements (the field is less sensitive to the sample at higher modes). Thus, a higher mode can be used to correct the systematic fluctuations as they are unaffected by the sample. This would be helpful when conducting the experiments at temperatures higher than 500°C. Moreover, the measurement system could be improved to perform the experiments in different reaction conditions and variable atmospheres.

9.2.2 Microwave Single Mode Applicator

Several modifications can be introduced to the microwave single-mode applicator that allows for more investigations of the parameters and catalytic processes. For the electromagnetic field effect, additional exploring of the pulsing feature needs to be conducted as it is a recently-installed feature with different catalytic systems to be tested. A very powerful electromagnetic field can be produced from pulsing the radiation as it is generating very short but intense waves within hundreds of nanoseconds. This could be a significantly important way to drive the reactions into different pathways.

Other important parameters, such as varying the duty cycles, frequencies, and applied power density could be examined with different catalytic systems in order to evaluate the interaction between the field and the material. In addition, the installed PID temperature controller would allow performing the reaction under specific conditions, such as low temperatures and under a

highly applied field. This feature might be able to provide the ability to separate the thermal and microwave field effect on catalysts, which is one of the major controversial points in microwave reaction systems.

As the microwave reactor is versatile in its design, it could be possible to exchange the applicator based on the desired activation field and mode. The reactor is carried out under the TM_{010} mode and an uniformly-produced electric field. It would be interesting to explore the reactions under the magnetic field as the materials behave differently in the E-field and the H-field.

In terms of reaction system modifications, a flow system has been introduced with an oil-pumping system, which was a great opportunity to examine the potential difference between two different systems. However, it still requires more modifications for an enhanced performance. Introducing a flow system is a great chance to simulate the industrial systems and to help increase the product yields.

9.2.3 Purification of the Produced Hydrogen

Since the processed heavy oil contains circa 2% in weight of sulphur, the produced hydrogen under microwave radiation can also be incorporated with H_2S. Thus, the hydrogen separation process is required and the purification processes are applied in refineries by mixing the produced gas mixture with amine-cantoning solution, which would lead to the scrubber of hydrogen. Another method for separating the hydrogen sulphide consists in introducing sodium hydroxide to react with H_2S as H_2S will be dissolved to form sodium bisulfide and sodium sulphide [4]. H_2S can also be easily converted into FeS or CuS by introducing Fe or Cu powder or sorbents in the reaction system [5].

Other small quantities of CH_4 and compounds of higher molecular weight are mixed with the produced hydrogen. The membrane separation method is considered an effective way for hydrogen purification [6].

9.2.4 Catalyst Configuration and Regeneration

One of the potential configurations of the catalyst is to develop the system to be operated as a fluidised bed reactor where the catalyst mixture (oil/zeolite) can be moved continuously and completely passed through the heating zone in the cavity. This would allow for the flexibility

in introducing the catalyst and might help increase the number of products. However, the large produced amount of carbon materials can be considered one of the drawbacks of this process. Nevertheless the spent catalyst can be regenerated continuously to simulate a FCC catalytic process. Here below are provided some outlines about the potential applications of the produced coke:

- Catalysts could be gasified to produce syngas.
- Recycling of the catalyst by reduction and reloading metals which might be useful for carbon-based catalysts, as the generated carbon can enhance the microwave absorption susceptibility.
- The formed carbon nanotubes could be extracted from the spent catalysts and this might give rise to a possible way of generating CNTs.

9.3 Scaling Up Considerations

One of the biggest challenges in microwave systems for chemical reactions is the possibility of scaling-up the system directly with keeping all the previously-optimised parameters in the small scale. There are several points which need to be taken into account that can affect the transformation from laboratory to industrial scale as shown below.

Penetration depth: which is defined as the distance from the surface of the microwaved object to the point where microwave power dropped to 1/e of the applied power. Since the microwave heating is a volumetric process, the increase in reactor size would result in a change of the microwave absorption by the sample, which needs to be maintained to avoid losing many of the benefits of microwave heating.

Reproducibility: to achieve a good reproducibility between different microwave scales, the accurate control of reaction temperature is essential. Moreover, the reaction pressure is another important factor. Both factors could have a significant effect on the reaction rate and products as the increase in reaction temperature will provide a rise in pressure. Thus, it was required to install the PID-temperature controller to the system.

Frequency of operation: for the scaled up applicator, the system would operate at lower frequencies (such as ~900MHz, in accordance with ISM standards) [7]. It is important to maintain the mode of operation, (i.e. the field distribution within the applicator).

The design of a 900 MHz microwave applicator is presented in Figure 9.4. It should be noted that the 900 MHz cavity can be run on both batch and flow systems.



Figure 9.4: The initial design of the larger scale cavity operated at 900 MHz.

Last but not least, the scaled-up process required microwave equipment with enhanced process control, in addition to safety, which is the main factor for a successful application of the desired system.

Bibliography

[1] J.D. Moseley and E.K. Woodman. Energy Efficiency of Microwave- and Conventionally Heated Reactors Compared at Meso Scale for Organic Reactions. *Energy Fuels*, 23:5438–5447, 2009.

[2] J.D. Moseley. Microwave Synthesis in Process Chemistry Method, Scale and Scope. *Chemistry Today*, 27(2), 2009.

[3] S. Gonzalez-Cortes, D.R. Slocombe, T. Xiao, A. Aldawsari, B. Yao, V.L. Kuznetsov, E. Liberti, A.I. Kirkland, M.S. Alkinani, H.A. Al-Megren, J.M. Thomas, and P.P. Edwards. Wax: A Benign Hydrogen-storage Material that Rapidly Releases H_2-rich Gases Through Microwave-assisted Catalytic Decomposition. *Nature, Scientific Reports*, accepted: 28 September 2016.

[4] H. ter Maat, J.A. Hogendoorn, and G.F. Versteeg. The Removal of Hydrogen Sulfide from Gas Streams using an Aqueous Metal Sulfate Absorbent :Part I. The Absorption of Hydrogen Sulfide in Metal Sulfate Solutions. *Separation and Purification Technology*, 43:183–197, 2005.

[5] Z. Li and M. Flytzani-Stephanopoulos. Cu-Cr-O and Cu-Ce-O Regenerable Oxide Sorbents for Hot Gas Desulfurization. *Ind. Eng. Chem. Res.*, 36:187–196, 1997.

[6] S. Adhikari and S. Fernando. Hydrogen Membrane Separation Techniques. *Ind. Eng. Chem. Res.*, 45:875–881, 2006.

[7] R.J. Meredith. *Engineers' Handbook of Industrial Microwave Heating*. Institution of Electrical Engineers, 1998.

APPENDICES

Appendix A

THE CHEMICAL PROPERTIES OF MODEL COMPOUNDS AND HEAVY OIL

A.1 1-Model compounds

Table A.1: The Physical Properties of the linear hydrocarbons bought from Sigma Aldrich

Sample	Chemical formula	Density[g·cm^{-3}] at 20 °C	Purity %
Hexane	C_6H_{14}	0.659	≥ 99
Decane	$C_{10}H_{22}$	0.730	≥ 99
Dodecane	$C_{12}H_{26}$	0.749	≥ 99
Hexadecane	$C_{16}H_{34}$	0.773	≥ 99
Nonadecane	$C_{19}H_{40}$	0.786	99
Triacontane	$C_{30}H_{62}$	0.810	98
Pentatriacontane	$C_{35}H_{72}$	0.813	98

Table A.2: Sulphur Compounds

Sample	Molecular weight	Company	Purity %
Thiophene	84.14	Sigma Aldrich	≥ 99
Benzothiophene	134.20	Fluka	≥ 95
Dibenzothiophene	184.26	ACROS	99
4-Methyldibenzothiophene	198.28	Sigma Aldrich	96
4,6-Dimethyldibenzothiophene	212.31	Sigma Aldrich	97

Table A.3: Nitrogen Compounds

Sample	Molecular weight	Company	Purity %
Carbazole	167.2	Sigma Aldrich	≥ 95
Indole	117.15	Sigma Aldrich	99
Pyrrole	67.09	Sigma Aldrich	98
Pyridine	79	ACROS	≥ 99
1,2,3,4-tetrahydroquinoline	133.19	Alfa Aesar	99

Table A.4: Cycloparaffinic and Aromatic Compounds

Sample	Molecular weight	Company	Purity %
Fluorene	166.2	Alfa Aesar	≥ 98
Naphthol	144.17	Sigma Aldrich	≥ 99
Biphenyl	154.2	ACROS	99
Cyclohexane	84.16	Sigma Aldrich	≥ 99
Toluene	92.14	Sigma Aldrich	≥ 99
Phenol	94.1	Sigma Aldrich	≥ 99.5

A.2 2-Oil samples analyses

A.2.1 Bunker oil

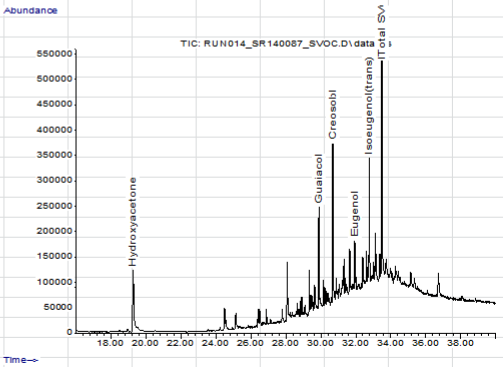
Analysis of light fractions	
C	84.020 wt%
H	11.220 wt%
S	4.750 wt%
Density	0.91g mL−1

A.2.2 Crude oil

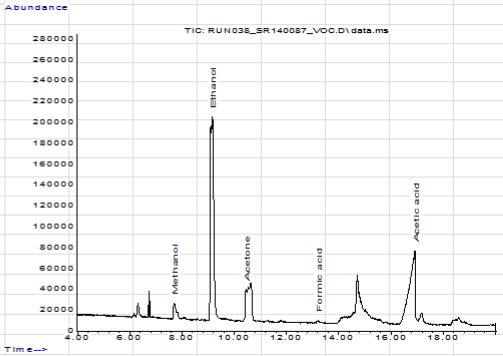
Analysis of light fractions	
C	84.160 wt%
H	12.700 wt%
S	3.140 wt%
Density	0.86 g mL−1

A.2.3 Pyrolysis oil

Feedstock name	Py-oil
Analysis of light fraction, wt%	
Water	**28.00**
TAN (mgKOH/g sample)	**71.50**
C	**40.000**
H	**8.160**
O	**51.840**
Density	1.16
GC-MS analysis	
	mg/g
Isoeugenol(trans)	1.4
2,6-Dimethoxy-phenol	<0.5
Eugenol	<0.5
Creosol	1.4
Guaiacol	1.3
Phenol	<0.5
Furfural	<0.5
Catechol	1.1
Levoglucosan	10
Benzene	<0.5
Toluene	<0.5
Ethylbenzene	<0.5
m+p Xylenes	<0.5
o-Xylene	<0.5
1, 3, 5-Trimethylbenzene	<0.5
1,2,4-Trimethylbenzene	<0.5
Naphtalene	<0.5
Total Alkanes	ND
Total SVOCs	230
Tetralin	<0.5
Decalin	<0.5
Hydroxyacetone	8.6



	mg/g
Ethyl formate	<0.5
Acetic acid	27
Formic acid	3.2
Ethylacetate	<0.5
Methylacetate	<0.5
Acetone	1.8
Ethanol	53
Furan	<0.5
Methyl formate	<0.5
Methanol	12



Appendix B

PRODUCT DISTRIBUTION IN VOL.%

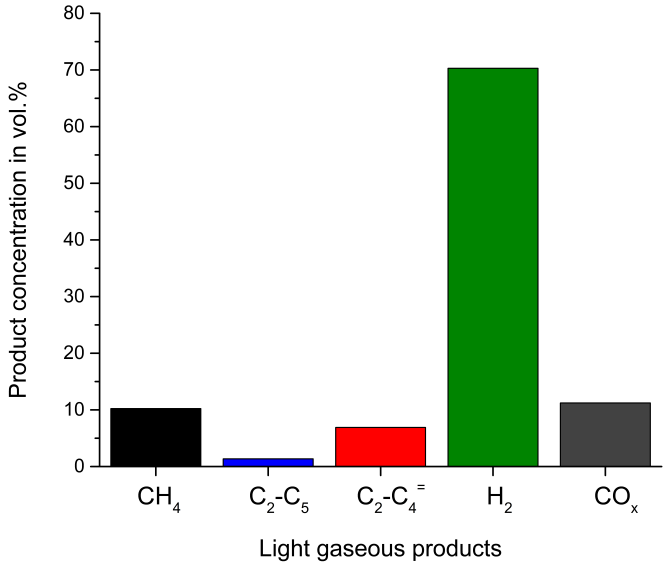


Figure B.1: Gas composition of heavy oil cracking over HZSM-5 zeolite in vol.%

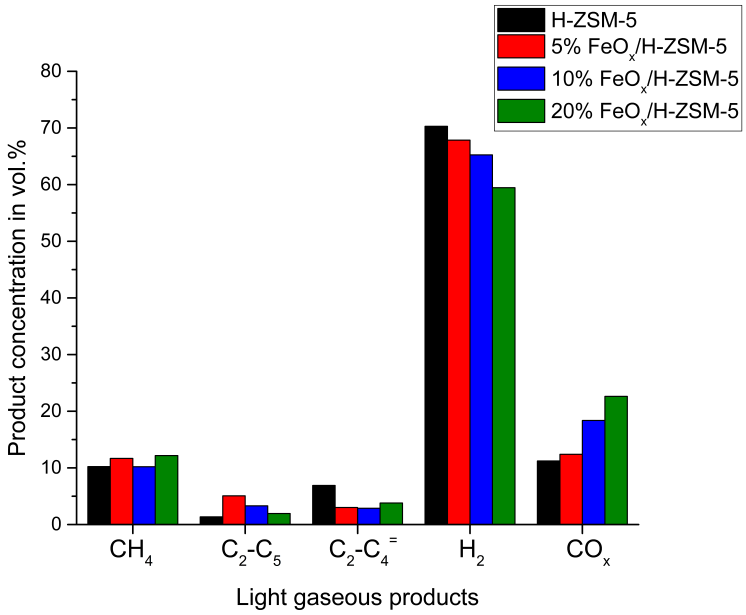


Figure B.2: The gas composition concentration in vol.% of the heavy oil cracking over different iron loadings into HZSM-5 catalysts in comparison to the parent HZSM-5

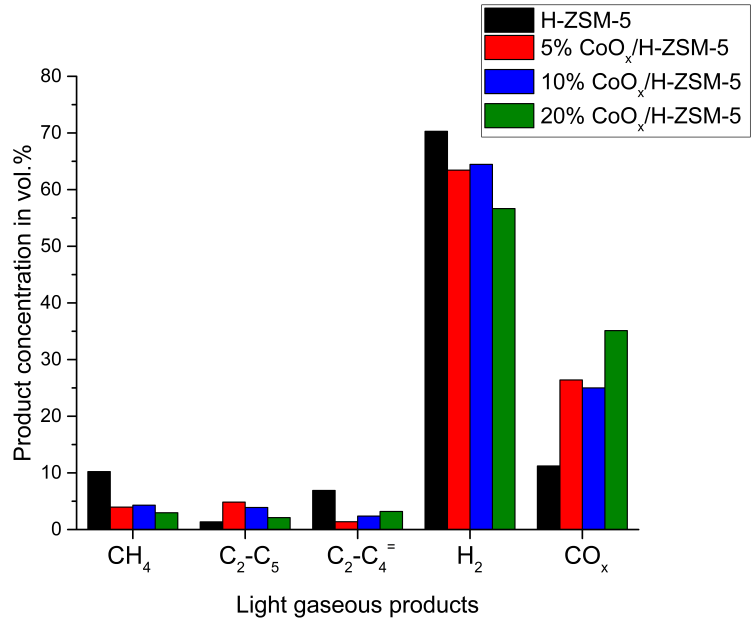


Figure B.3: Gas composition of the heavy oil cracking reaction over Co/HZSM-5 catalysts with different loading of cobalt and 25 wt% of heavy oil

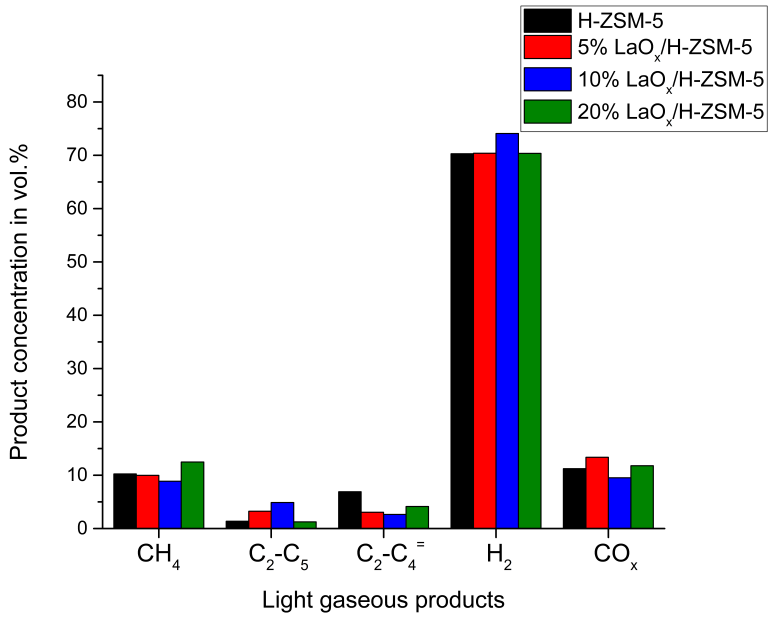


Figure B.4: Typical analysis of gas composition of a catalytic processing 25 wt% of heavy oil over 5, 10, 20 wt% of La @ HZSM-5 compared with the pure zeolite

Appendix C

TGA ANALYSIS FOR COKE CONTENT

The coke content is calculated based on the amount of weight loss above 400°C in the spent washed samples.

1-FeOx/ZSM-5

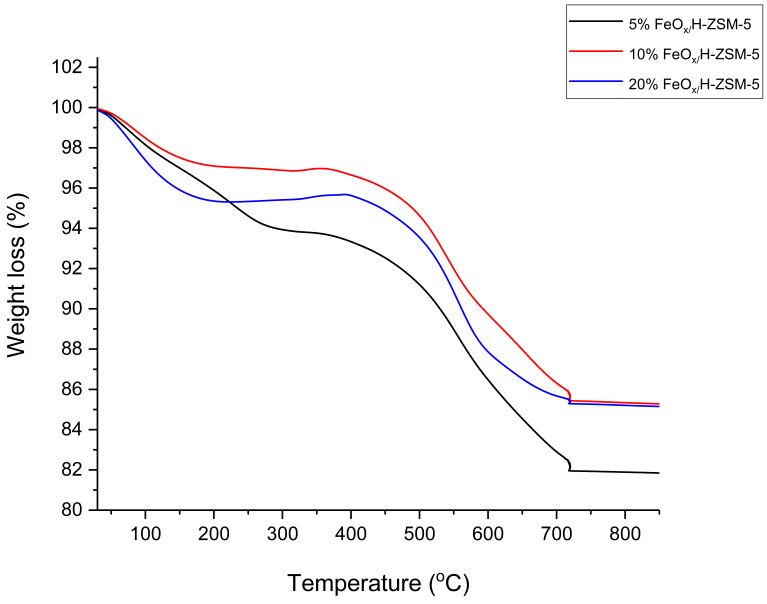


Figure C.1: The TGA profile of the spent sample after toluene washing for the 5, 10, 20 wt.% FeOx/ZSM-5

2- CoOx/ZSM-5

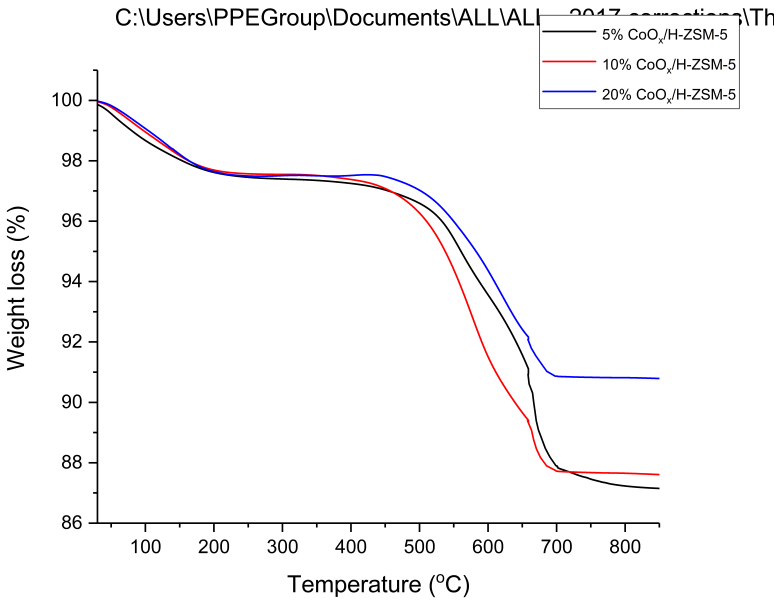


Figure C.2: TGA plot of the cobalt spent catalysts CoOx/ZSM-5

3- LaOx/ZSM-5

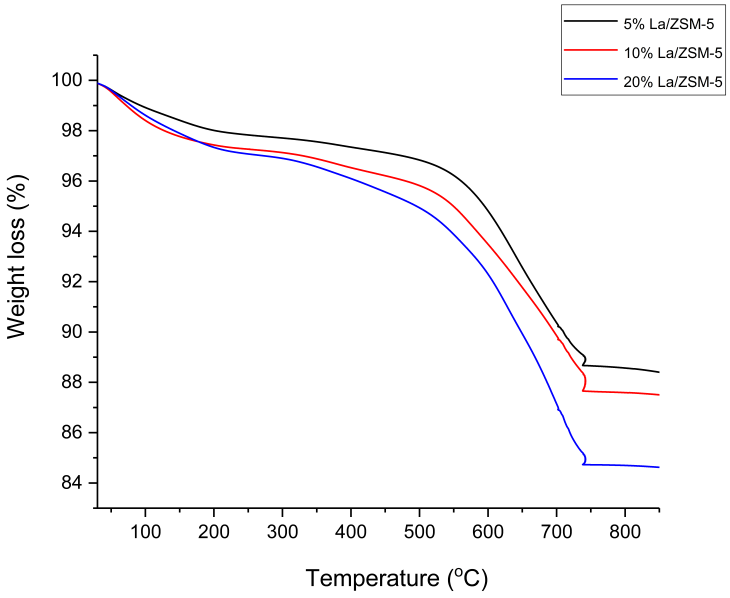


Figure C.3: TGA analysis of the LaOx/ZSM-5 spent samples

Appendix D

CALCULATIONS

D.1 Mass balance calculations

Mass of gas = (mass of tube before reaction - mass of tube after reaction) - mass of liquid in bottom trap

Mass of liquid = mass collected from (liquid trap+quartz wool+tube wall)

Mass of residual solid= mass of catalyst-(mass of gas+mass of liquid)

$$\text{Mass balance\%}=\frac{\text{residual solid+mass of liquid+}\sum mi\text{total mass of gas (from the GC)}}{\text{mass of sample}}$$

D.2 Error calculations

The percentage error and standard error calculations:

$$\text{RelativeError}=\frac{\text{AbsoluteError}}{\text{MeasuredValue}}$$

$$\sigma s\text{ample} = \sqrt{\frac{1}{N-1}\sum_{i=1}^{N}(x_i-\bar{x})^2}$$